“Co-crystallisation of Active Pharmaceutical Ingredients”

Vijay Kumar Srirambhatla

Thesis Submitted for the Degree of Doctor of Philosophy.

Heriot-Watt University

Institute of Chemical Sciences

December 2014

Abstract

In the thesis presented here, novel co-crystals of two active pharmaceutical ingredients (APIs), i.e. paracetamol and furosemide are presented. Co-crystals are molecular complexes in which two or more components are held together through non-covalent interactions. The work on co-crystals was aimed to investigate and identify robust hydrogen bonds and primary structural motifs which can be used to predict the solid-state assembly in related molecular complexes.

The Database mining based on retro-synthetic approach followed by co-crystal screening using mechano-chemical and crystallisation methods in conjunction with high-throughput powder X-ray analysis led to the discovery of four novel co-crystal forms of paracetamol. The study shows that a balance between the retrosynthetic approach and database screening of supramolecular synthons provides a useful approach for targeted co-crystal synthesis.

The ability of charge transfer hydrogen bonding interaction to drive the assembly of molecules in co-crystals was investigated. This led to the synthesis of a series of isostructural host-guest complexes of furosemide. It has been discovered that charge transfer interaction drives the crystal packing arrangement in presence of other hydrogen bonding interactions.

The ability of two component physical mixture to form ternary co-crystals has been investigated. Systematic synthesis with careful selection of components based on simple geometric principles led to the discovery of a series of ternary co-crystals stabilised through a novel two-dimensional hydrogen-bonded network, which serves a prototype for a new family of ternary co-crystals. This has enabled a targeted approach for the selection and synthesis of new ternary co-crystals with control over symmetry and gross structural features. The study demonstrates that networks that maintain their dimensionality and integrity provide a degree of predictability in the crystal packing arrangements in the solid state.

Acknowledgements

I take this opportunity to express my sincere gratitude to my supervisor Prof. Anthony Vivian Powell and my co-supervisor Dr. Arno Kraft for their constant support and guidance throughout the course of this study.

I wish to thank my industrial collaborator, Dr. Stephen Watt from Solid Form Solutions for allowing me to use their thermal instruments.

Support from the Scottish Funding Council and Heriot-Watt University is greatly acknowledged.

Finally, I would like to thank all my lab mates in the Solid State Chemistry Group.

Table of Contents

Chapter 5: A Robust Two-Dimensional Hydrogen-Bonded Network for the Predictable Assembly of Ternary Co-crystals.

Chapter 6: Conclusions and Further Work.

List of Abbreviations

AIM – Atoms in molecules

APIs – Active pharmaceutical ingredient

NCEs – New chemical entities

CCF – Co-crystal formers

OX – *S*-oxiracetam

RH – Relative humidity

NFLX – Norfloxacin

R&D – Research and Development

1D, 2D, 3D – One, two and three dimensional

PXRD – Powder X-ray diffraction

SXRD – Single crystal X-ray diffraction

ATR - Attenuated total reflectance

IR – Infrared

DSC – Differential scanning calorimetry

TGA – Thermogravimetric analysis

CSD – Cambridge Structural Database

CIF – Crystallographic Information File

PAC – Paracetamol

BPEA – 1,2-bis(4-pyridyl)ethane

BPEE – 1,2-di(4-pyridyl)ethylene

Cyclam – 1,4,8,11-tetraazacyclotetradecane

DMSO – Dimethyl sulphoxide

FUR – Furosemide

IM – Imidazole

PIP – Piperazine

BIPY – 4,4’-bipyridyl

Chapter 1: Introduction.

1.1. Introduction

Intermolecular interactions in molecular crystals are responsible for the extraordinarily specific way in which molecules interact to form a highly ordered crystalline material. These intermolecular interactions referred to as molecular recognition events are significant features of biological and chemical systems. The ensemble of intermolecular interactions ultimately defines the physical properties and reactivity of any given solid. Therefore understanding the intermolecular interactions has attracted interest from scientists in various disciplines, ranging from solid-state chemists to protein crystallographers, theoreticians and crystal engineers. A better understanding of the intermolecular interactions is imperative for efficient co-crystal synthesis. This introduction chapter will discuss the types of intermolecular interactions, outline the use of dimensional solids in the context of the crystal engineering challenges, in particular co-crystals, explain the relevance of co-crystals in the pharmaceutical industry and provide examples related to enhancing the properties of pharmaceutical compounds.

1.2. The nature and types of intermolecular interactions

All molecules possess the potential for some type of intermolecular interactions.[1] When two atoms or molecules come together, the interactions between them could be attractive or repulsive depending on the mutual orientation of the two molecules. When these interactions are attractive they contribute to the stability of the molecules. However, the interaction between two atoms is not always attractive; it becomes repulsive after a certain distance and the curve of the interaction energy follows the Morse-like shape curve. In the literature, for molecular crystals, there are many classifications of intermolecular interactions.[2] An intermolecular interaction consists of the following energy components (1) exchange-repulsion; (2) electrostatic interactions; (3) polarisation interactions; and (4) dispersion interactions. The interactions can be represented in an analytical form and are interdependent on each other to a certain extent. The intermolecular interactions relevant to the work presented here can be classified into

1. *Ionic bonds.*
2. *Hydrogen bonds.*
3. *van der Waals interactions.*
4. *Halogen bonding.*
5. *π–π interactions.*

1.2.1. Ionic bonds

Ionic bonds are observed in molecular crystals in which at least one of the components possess a net charge. The simplest case involves two atoms with opposite signs, such as $X^+\cdots Y^-$ bond. The prototypical example is the NaCl crystal containing $Na^+\cdots Cl^-$ interactions. Ionic bonds also exist in crystals where only one of the species involved possesses a net charge while the other is a neutral component; examples of such types are the ion-solvent interactions. These interactions are characterised as charge-induced hydrogen bonds.[3] In ionic bonds, the total interaction energy is dominated by the electrostatic term. In ion-ion interactions, the total interaction energy is dominated by the charge-charge term, while in ion-neutral interactions the total interaction energy is dominated by the charge-dipole or charge-quadrupole terms, depending on the nature of the neutral species involved.

1.2.2. Hydrogen bonds

1.2.2.1. Discovery of the hydrogen bond

The influence of the hydrogen bond was observed in gaseous, liquid and solid state long before it was identified and given a name. A literature survey of the late 19th and early 20th century shows references which, in retrospect, could be perceived as evidence of hydrogen bonding. The terms *Nebenvalenz* (near valence) and *innere Komplexsalzbildung* were used by German chemists Werner[4], Hantzsch[5] and Pfeiffer[6] to describe both inter- and intramolecular hydrogen bonds.

According to Linus Pauling, the concept of the hydrogen bond can be attributed to M. L. Huggins, as well as W. M. Latimer and W. H. Rodebush. Latimer and Rodebush[7] published a paper which contained the statement that "the hydrogen nucleus held by two octets constitutes a weak bond". In a paper entitled the Electronic Structure of Atoms, Huggins[8] stated that "a positively charged kernel containing no electrons in its valence shell (i.e. H^+) reacting with an atom containing a lone valence pair can form a weak bond".

In the late 1920s and early 1930s crystal structures of $NaHF_2$[9], urea[10], and NH_4F_2 began to appear but nothing was mentioned about hydrogen bonding. None of the authors used the term hydrogen bond in their original publications. It was Pauling in 1931 who wrote a general paper on the nature of chemical bond, where he possibly for the first time used the term hydrogen bond. This paper was the precursor to his famous book *Nature of the Chemical Bond*[11] where he introduced the concept of hydrogen bonding to the chemical world. He noted

that “under certain conditions an atom of hydrogen is attracted by rather strong forces to two atoms instead of only one, so that it may be considered to be acting as a bond between them”. This he called the hydrogen bond.

1.2.2.2. Definition of hydrogen bond

Hydrogen bonds are of fundamental importance in chemistry and biology. The hydrogen bond usually lies in the energy range between covalent bonds and van der Waals interactions. The weakest of the hydrogen bonds are difficult to be distinguished from the van der Waals interactions, while the strongest of hydrogen bonds are energetically stronger than some of the weak covalent bonds. Therefore, in molecular crystals there exists a continuum of energy going form covalent bonds to hydrogen bonds to van der Waals interactions. An intermolecular interaction *X*-*H*···*A* is called a hydrogen bond if (1) it constitutes a local bond and (2) *X*-*H* acts as a proton donor to *A*. The *X*-*H* group is called the proton donor and the *A* is called a proton acceptor. In this definition the hydrogen bond is in principle viewed as an incipient proton transfer reaction. The above definition incorporates the acid-base properties of the donor *X*-*H* and acceptor, *A* groups. This definition of a hydrogen bond excludes the van der Waals contacts, agostic interactions and does not set a threshold value for an interaction to be called a hydrogen bond, provided the above two conditions are satisfied. In the simplest case, the donor interacts with one acceptor. However, complex situations like bifurcated and trifurcated hydrogen bonds arise when one donor is hydrogen-bonded to two or three acceptor groups, or an acceptor is bonded to more than one donor group. Theoretically a hydrogen bond is possible between two, three or more acceptors. However, in practice hydrogen bonds with more than three acceptor groups are rarely observed experimentally due to steric hindrance.

The above definition of a hydrogen bond requires the evidence for the existence of a bond between the *H*···*X* groups. Identifying the evidence for the existence of a bond is at times problematic, especially in cases involving weak interactions. One criterion for the existence of a bond is based on atoms in molecules theory (AIM).[12] The AIM theory requires the molecule to be energetically stable and must possess at least one critical point between the atoms. This method of ascertaining the existence of a bond requires some computation on the experimentally observed structures. Other, readily available criteria for the existence of the bond are based on analysing the geometrical features of the hydrogen bond and these provide evidence directly from the structure.

Evidence of intermolecular bond directly from crystal structures:

1. The evidence for the existence of intermolecular bonds is based on empirical observations. This criterion is based on the electrostatic nature of the *X-H···A* hydrogen bond, the dipole *X-H* donor group prefers to align with the negative acceptor group *A* so as to minimize the interaction energy. Ideally the interaction energy will be at a minimum when the angle made by the *X-H···A* interaction is close to 180^{o}. The tendency of the angle made by the *X-H···A* interaction to be close to 180^{o} is considered as a criterion for the evidence of a strong hydrogen bond and can be readily measured in any crystal structure.
2. The evidence of an intermolecular bond can be obtained by measuring the percentage contraction from the van der Waals cut off radii. The shorter the *H···A* distance in *X-H···A* interactions, the greater the percentage contraction of van der Waals cutoff radii. It must me mentioned that hydrogen bonds possess long range distances and in some cases especially weak interactions like C-H···O and C-H···N the H···O/N distance can be greater than the sum of van der Waals radii. In such cases, other complementary criteria must be considered.
3. Evidence of the presence of an intermolecular hydrogen bond can also be obtained from spectroscopic data. For example, the presence of a hydrogen bond manifests itself with a decrease in the value of X-H stretching frequency (ν_{X-H}) in the infrared spectrum when compared to a free X-H bond; this is called a red-shifted hydrogen bond. At this place it is appropriate to mention that in some unconventional hydrogen bonds an increase in the X-H stretching frequency is noticed when compared to a free X-H bond. These are called blue shifting hydrogen bonds.
4. In cases where the above criteria do not give concrete proof, especially in interactions involving weak C-H···O and C-H···N contacts, evidence for the existence of intermolecular interactions can be obtained by calculation and inspection of Hirshfeld surfaces. The Hirshfeld surfaces provide direct visual evidence for the existence of the hydrogen bonds. An *X-H···A* interaction is represented by a different colour on the calculated Hirshfeld surface. Strong interactions have intense red colours, while weak interactions are represented as light colours.

The factors that determine the existence of a bond are also the properties of the hydrogen bonds. In addition to the above factors, one of the important properties of hydrogen bonds is cooperativity. Accordingly, the energy of a series of *m* interlinked hydrogen bonds is larger than the sum of the *m* isolated hydrogen bonds. Functional groups, like the alcohols which can

act simultaneously as donors and acceptors form extended chains or rings in which the individual hydrogen bonds enhance each other's strength due to mutual polarisation.
In addition to these, in suitable π–systems, charge flow due to polarised hydrogen bonds increases the strength of the hydrogen bonds, which are referred to as charge assisted hydrogen bonds.

1.2.2.3. Types of hydrogen bonds

Given the importance of the hydrogen bonds in organic crystal engineering, these are divided into three categories based on their strength. The three categories as suggested by Jeffrey are (a) strong (b) moderate and (c) weak hydrogen bonds.[2] Hydrogen bonds which have an interaction energy between 4 to 14 kcal mol^{-1} are referred to as moderate hydrogen bonds. The hydrogen bonds that have the interaction energy stronger than 14 kcal mol^{-1} are called strong hydrogen bonds, while the ones that have the interaction energy less than 4 kcal mol^{-1} are called as weak hydrogen bonds. Table 1.1 shows the three different types of hydrogen bonds as proposed by Jeffrey.

Strong hydrogen bonds are sub-divided into three types based on the nature of the donor-acceptor groups, these are (a) neutral···neutral hydrogen bonds, formed between the donor and acceptor groups possessing no net charge and the dominant electrostatic term is made up of dipole-dipole interactions; (b) charge···charge hydrogen bonds, here the dominant electrostatic term is the stronger charge-charge component; (c) neutral···charge hydrogen bonds, in which the electrostatic component is dominated by the charge – dipole term.

Moderate hydrogen bonds are generally formed between neutral donor and acceptor groups, *i.e.* of the type O-H···O and N-H···O interactions. These hydrogen bonds have an interaction energy that lies between 4-14 kcal $mole^{-1}$. In these hydrogen bonds, the donor atoms (*X*) are more electronegative relative to hydrogen and the acceptor *A* atoms have lone-pair unshared electrons in a *X-H···A* hydrogen bond. These are the most common type of hydrogen bonds found in nature and are also called *normal* hydrogen bonds.

Weak hydrogen bonds are formed between weak donors and strong acceptors (eg. C-H···O=C), between strong donors and weak acceptors (N-H···Ph, O-H···Se) and between weak donor–weak acceptors (C≡C-H···C≡C) groups and possess interaction energy less than

4 kcal mol^{-1}. The first systematic study on C-H···O interactions was done by Sutor in 1962.[13] Sutor assumed van der Waals distance in a H···O contact to be 2.6 Å and repeatedly observed very short C-H···O distances in theophylline (d = 2.25 Å), caffeine (d = 2.12 Å) and uracil (d = 2.20, 2.27Å). She called these interactions as C-H···O interactions which were a subject of debate for a long time and is historically called the Sutor–Donohue controversy.

Table 1.1: Types of hydrogen bonds.

	Strong	Moderate	Weak
Interaction type	Strongly covalent	Mostly electrostatic	Electrostatic/dispersion
Bond lengths (Å) H···A	1.2 – 1.5	1.5 – 2.2	> 2.2
Lengthening of X-H (Å)	0.08 – 0.25	0.02 – 0.08	<0.02
X-H versus H···A	X-H~H···A	X-H<H···A	X-H<<H···A
X···A [Å]	2.2-2.5	2.5-3.2	>3.2
Directionality	Strong	Moderate	Weak
Bond angles [^{o}]	170-180	>130	>90
Bond energy [kcal/mol]	15-40	4-15	<4
Effect of crystal packing	Strong	Distinctive	Variable
Relative IR shift $\Delta\nu_{X-H}$ [cm^{-1}]	25%	10-25%	<10%

1.2.3. van der Waals interactions

Van der Waals interactions form the extreme end of the attractive forces between molecules. Weak attractive forces between uncharged atoms or molecules are collectively referred to as van der Waals forces. These forces arise from the electrostatic attraction of the nuclei of one molecule for the electrons of a different molecule. The repulsions between the electrons and the nuclei of the two molecules counteract the electrostatic attractions, but there is always a small net attractive force. Van der Waals forces are short-range forces, that is, they are only significant when the molecules are very close to one another. There are two types of van der Waals forces: dipole-dipole interactions and London (or dispersion) forces.

1. Dipole-Dipole Interactions: These interactions arise because of the electronegativity

property of the atoms, molecules become polar which gives rise to a net dipole moment. The net dipole moment of a molecule is the resultant of the vector addition of the individual bond dipoles in the molecule. The larger the dipole moment of a molecule, the greater the dipole-dipole interactions between molecules.

2. London or Dispersion forces: A fluctuating dipole moment in one atom induces a temporary dipole moment in a nearby atom in such a way that there is a net attraction between the two rapidly fluctuating dipoles. This attractive force between a pair of rapidly fluctuation dipoles whose electronic motions are correlated is called the London dispersion force, named after Fritz London. The strength of the dispersion force depends on how easily the electron cloud of the atom or molecule can be distorted or polarized.

1.2.3.1. Distinction between weak hydrogen bond and van der Waals interaction

The difference between a weak hydrogen bond and van der Waals interaction can be understood by analysing different types of C-H···O interactions. It is well recognised that C-H groups can act as weak hydrogen bond donors. The C-H donor strength depends on the hybridisation of the carbon atom involved and follows the trend C(sp)-H > C(sp^2)-H > C(sp^3)-H. While the bonds formed by acidic C-H groups (alkynes) are moderately strong, those that involve weakly polarised C-H groups are much weaker.

The main structural feature that distinguishes hydrogen bonds from van der Waals interactions is the directionality of the hydrogen bonds. The hydrogen bonds tend to exist in linear geometry or close to linear geometry whereas van der Waals contacts are isotropic.

The angular characteristics of the weak C-H···O hydrogen bonds are retrieved from Cambridge structural database (CSD), for those involving C(sp)-H, C(sp^2)-H, C(sp^3)-H in conjunction from data with those for van der Waals contacts of the type C-H···H-C. The details are given in Table 1.2. Table 1.2 shows the gradual decrease in the directionality of C-H···O interactions with decreasing C-H polarisation, but is still clearly different from the perfectly isotropic C-H···H-C contacts.

Table 1.2: Data showing difference between C-H···A hydrogen bonds and C-H···H-C contacts.

Contact type	Mean (H···A) (Å)	Mean X···A(Å)	Mean X-H···A(^{o})
HC≡C−H···O=C	2.360(4)	3.312(2)	152.0(2)
2HC=CH_2···O=C	2.670(1)	3.561(2)	143.1(1)
2HC−CH_3···O=C	2.761(6)	3.590(7)	137.1(7)
2HC−CH_3···H−C	2.500(2)	3.246(4)	128.6(3)

1.2.4. Halogen bonding

The term "halogen bond refers to an attractive interaction between a halogen atom *X* and an atom or a group of atoms in different molecules(s), where there is evidence of bond formation".[14] Analogous to hydrogen bonding interactions, energetic and directional behaviours are observed in halogen bonding interactions.

To understand halogen bonding, we should consider the anisotropic distribution of electron density around the halogen atom as shown in Figure 1.1. It is observed that for the halogen bonds chlorine (Cl), bromine (Br) and iodine (I) a positive electrostatic potential develops on the outer surface of the halogen atom, centered along the intersection of the covalently bonded C-X axis, while there is a negative electrostatic potential throughout the halogen atom. The positive electrostatic potential is referred to as a "σ–hole". The presence of the positive regions on halogen atoms is responsible for the halogen atoms acting as lone pair acceptors in molecular crystals. The term halogen bonding refers exclusively to the ability of halogen atoms to act as electron acceptors. It must be mentioned that organofluorine almost never acts as a hydrogen bond acceptor.[15]

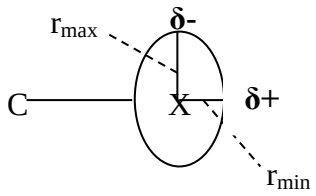

Figure 1.1: Anisotropic distribution of electron density around the halogen atoms. The halogen atom shows a negative electrostatic potential and maximum radius along the equatorial region and positive electrostatic potential and minimum radius along the polar region.

All halogen···halogen interactions show directional preferences. These directional preferences of halogen···halogen interactions are divided into two types

(a) type-I ($\theta_1 = \theta_2$) and

(b) type-II[16] ($\theta_1 = 180^o$ and $\theta_2 = 90^o$) (Scheme 1.1), where θ_1 and θ_2 are the C-X···X-C angles (X = Cl, Br, I).

Type-I interactions (scheme 1.1(a)) symmetrical interactions, and occur whilst possessing a crystallographic inversion centre in crystal structures. Type-II interactions (scheme 1.1(b)) are unsymmetrical halogen···halogen interactions and usually occur around a screw axis or glide plane and are explained using the anisotropic model presented above. It has been observed that the possibility of formation of type-II interactions increases as the halogen atom becomes more polarisable, i.e. moving down the group from chlorine to iodine.[17] It has been recently noticed that X···X contacts in hexachlorobenzene (C_6Cl_6) and its isostructural analogues (C_6Br_6 and C_6I_6) cannot be grouped into either of the above two types. The packing arrangement in these crystal structures is governed by using the trimer motif shown in scheme 1.1(c).[18] The trimer motif is known to act as a supramolecular synthon.[19]

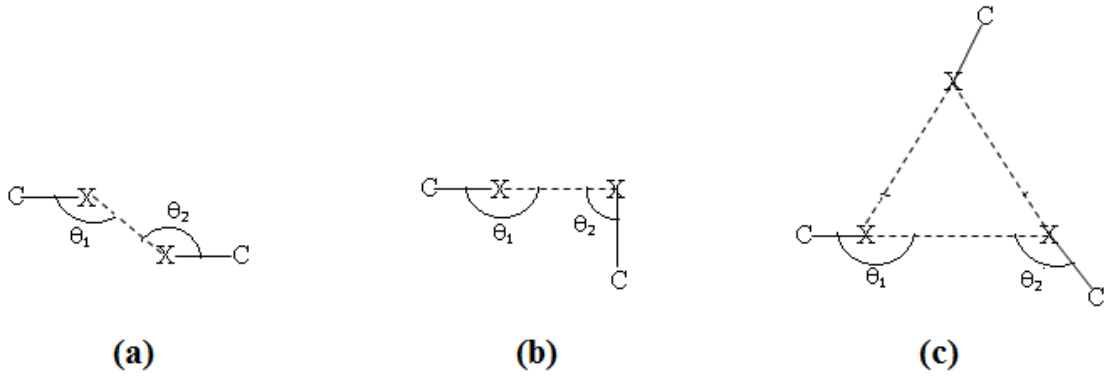

Scheme 1.1: Halogen···halogen interactions, (a) type –I and (b) type – II (c) the trimer synthon

1.2.5. π–π interactions

Non-covalent interactions between aromatic moieties play a significant role in determining the structure and properties of molecular assemblies in Chemistry, Biology and Material Science. The π–π interactions constitute one of the important classes of non-covalent interactions.

In a given molecule more than one type of π–π interaction can exist. Understanding the nature of π–π interactions in substituted benzene rings is fundamental in crystal engineering and material science. π–π interactions in substituted benzene rings occur in various geometries

shown below (Figure 1.2). Typically the aromatic rings are arranged in a face–to–face (sandwich configuration) or an offset face–to–face[20] (parallel - displaced) geometry (Figure 1.2), or slipped by a certain angle (α) (Figure 1.3). However, structures that are near–sandwich configurations are observed in some crystal structures. Another common interaction motif between benzene rings is the edge-to-face or perpendicular (T-shaped) configuration. Intermediate configurations between parallel and perpendicular-type configurations are frequently observed in chemical/biological systems.

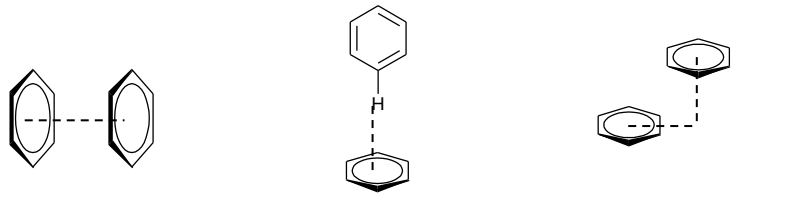

Figure 1.2: Prototypical π-π configurations observed in benzene dimers.

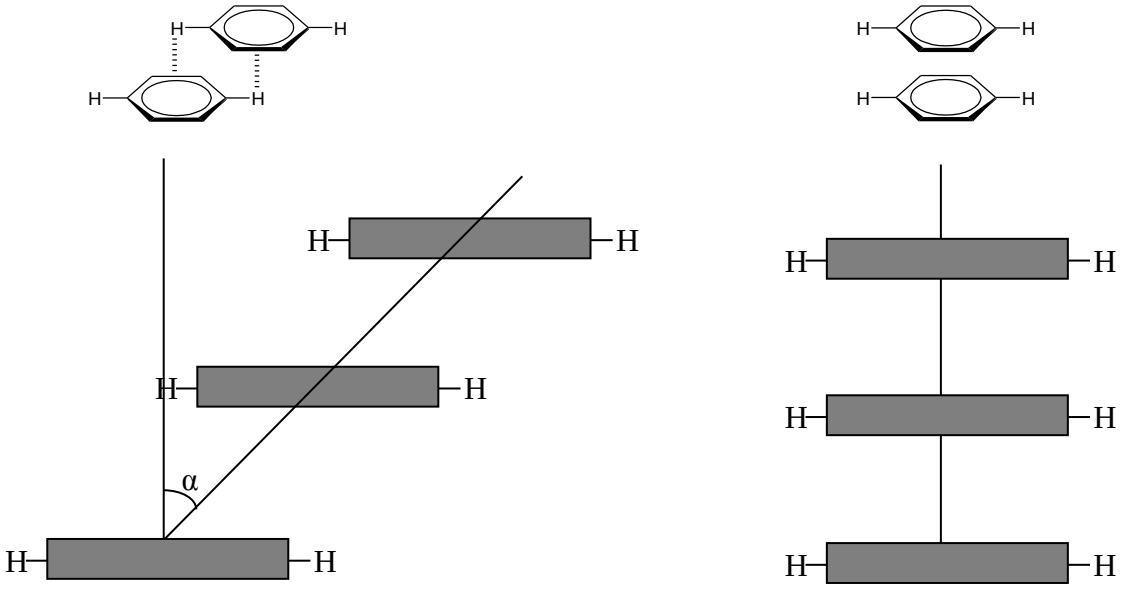

Figure 1.3: Face-to-face/center-to-edge with a slip angle (α) (left) and face-to-face/center-to-center (right) geometries in aromatic systems.

An electrostatic model of the nature of π–π interactions in substituted aromatic rings was proposed by Hunter and Sanders.[21] In this model, for each contributing carbon atom in the π system, Hunter and Sanders placed a +1 charge at each carbon nucleus and a -1/2 charge above and below the plane of aromatic ring, representing the π–cloud. According to Hunter

and Sanders model, the electron–withdrawing substituents reduce the negative quadrupole charge from the negatively charged π–clouds, favouring the formation of parallel displaced face – to – face and/or sandwich configurations. While the electron donating groups increase the negative charge of the π–cloud, which may favour the formation of a T-shaped configuration. These rules for stacking interactions prevailed until sophisticated computations were available. Theoretical calculations on mono–substituted benzene dimers indicated that both the electron-withdrawing and electron-donating groups increase the attraction between the benzene rings leading to the formation of a sandwich-type orientation. It is noticed that the attraction is due to the strong attractive London dispersion term contributing to the interaction energy, which overcomes the repulsive/unfavourable electrostatic term leading to the formation of a sandwich type orientation.[22,23] When the two electron clouds overlap, the diffuse electron clouds do not repel each other as compared to the point charges. The electron-to-nucleus attraction terms slightly outweigh the sum of electron to electron and nuclear to nuclear repulsion terms leading to the formation of a sandwich orientation in substituted benzene rings.

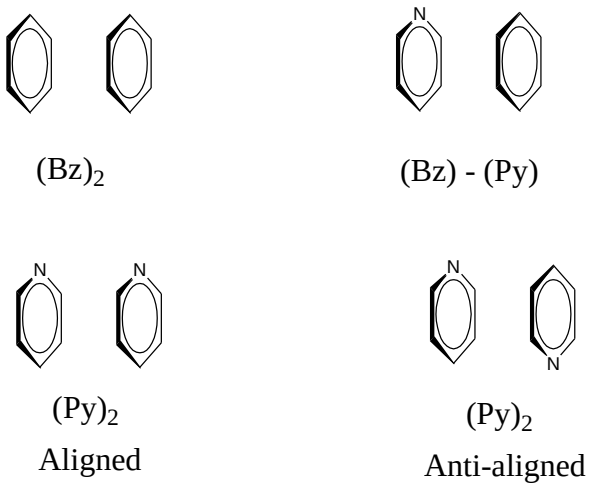

Figure 1.4: Sandwich configurations of the benzene, benzene-pyridine, and pyridine dimmers.

Many naturally occurring aromatic heterocyclic compounds possess at least one heteroatom in the π system. There can be four possible configurations in a system containing one benzene and one pyridine. These systems generally form the sandwich geometries shown in Figure 1.4. From the possible sandwich geometries, the anti-aligned pyridine dimer is the most stable configuration while the aligned pyridine dimer is the least stable geometry in the sandwich arrangement. This is due to the dipole-dipole interactions that exist between the aligned

pyridine dimers. Theoretical calculations have shown that the electrostatic term is attractive for all the four model sandwich complexes shown in Figure 1.4 with the benzene-pyridine sandwich geometry being the most stable. It has been noticed that the dispersion term, while being favourable for the formation of the benzene dimer, is the least favourable for the pyridine dimer, with values for benzene-pyridine combination falling in between. More theoretical calculations are required in order to understand the interactions between substituted pyridine moieties. The other types of π–π interactions i.e. the cation–π and anion–π are not of interest to the thesis presented here and hence are not mentioned.

Arene–arene interactions between various substituted aromatic rings represent an important class of supramolecular synthon in organic crystal engineering. These synthons have been extensively used for the design and synthesis of molecular complexes. Arene–arene interactions in cooperation with other interactions such as hydrogen bonding interactions are used for the synthesis of supramolecular architectures.[24]

1.3. Supramolecular synthon

The term "synthon" was first coined by E. J. Corey in 1967 in an article entitled "General methods for the construction of complex organic molecules".[25] A synthon is described as an identifiable design element and incorporates both geometric and chemical recognition features of the molecules. Desiraju extended the term synthon in the supramolecular context and called it a supramolecular synthon which is defined as "*structural units within supermolecules which can be formed and/or assembled by known or conceivable synthetic operations involving intermolecular interactions".*[26] Examples of some supramolecular synthons commonly studied in supramolecular chemistry are shown in Scheme 1.2.

The association of supramolecular synthons uniquely defines a crystal structure. Supramolecular synthons can be used in a retrosynthetic approach to predict the crystal packing arrangements in related crystal structures. The retrosynthetic process for predicting the crystal packing arrangement effectively involves analysing a number of related crystal structures and identifying supramolecular synthons in which a given functional group or combination of functional groups can participate. While some synthons are sufficiently dominant and may invariably occur in the presence of a particular functional group, it is challenging to identify and reproduce combinations of supramolecular synthons in related crystal structures. This happens because of the following reasons.

1. Since all the hydrogen bonding/ intermolecular interactions are weak, a small increase in the molecular functionality will increase the number of possible and competing supramolecular synthons very quickly.
2. Structural interference from remote molecular functionalities may be fickle and unpredictable.
3. The final and perhaps the most difficult to handle is the interference from the hydrocarbon residue, though this hydrocarbon core is generally considered not to be a functional group in molecular chemistry, it is known to exhibit supramolecular functionality by participating in non-covalent interactions.

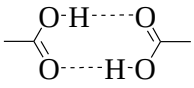

acid-acid homosynthon

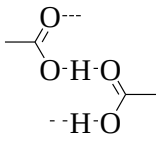

acid-acid catemer

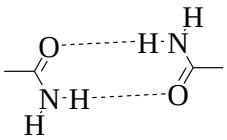

amide-amide homosynthon

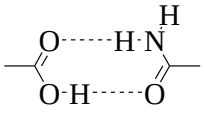

acid-amide heterosynthon

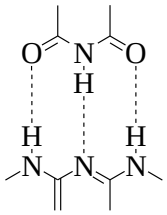

triply hydrogen bonded synthon

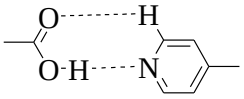

two point acid-pyridine synhton

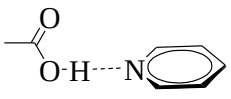

single point acid-pyridine synthon

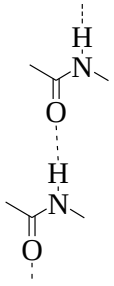

chain motif
in amides

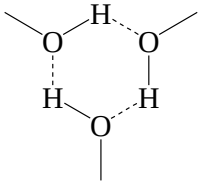

ring motif in alcohols

Scheme 1.2: Commonly occurring supramolecular synthons.

1.3.1. Types of synthons

Supramolecular synthons can be divided into two distinct categories:

Supramolecular homosynthons (Scheme 1.2) that are composed of identical complementary functional groups also referred to as self-association motifs. Examples are carboxylic acid dimers, amide dimers, etc.

Supramolecular heterosynthons (Scheme 1.2) composed of different but complementary functional groups such as acid-amide, acid- pyridine, etc. It is quite well documented that some of the supramolecular heterosynthons are preferred over the corresponding supramolecular homosynthons.

1.4. Graph-set analysis of intermolecular interactions

Analysis of hydrogen-bonded networks in molecular solids may be achieved using graph sets.[27] The analysis of hydrogen bonding networks is based on the fact that complex hydrogen bonding networks can be reduced to combinations of simple patterns. The simple patterns observed in molecular crystals are designated as chains (**C**), rings (**R**), intramolecular hydrogen-bonded patterns (**S**), and other finite patterns (**D**) (Scheme 1.3). The hydrogen bonds in molecular crystals are described by these pattern designators followed by a subscript representing the number of hydrogen–bond donors (**d**), and a superscript representing the number of hydrogen bond acceptor groups (**a**), while the number of participating atoms are represented by a number **n**, within parentheses as (**n**).

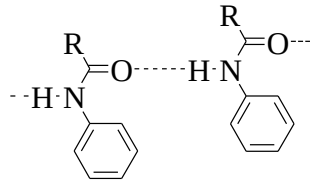

1 **C(4)**

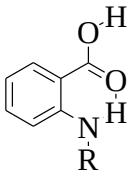

2 **S(6)**

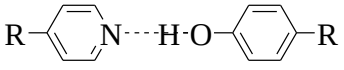

3 **D**

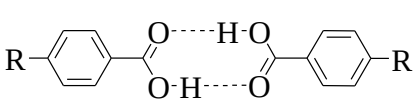

4 $\mathbf{R^2_2(8)}$

Scheme 1.3: Pattern designators in hydrogen-bonded systems.

Based on the number and complexity of the hydrogen-bonded network present in a crystalline

compound different pathways of graph set analysis can be followed. These are unitary, binary, ternary or higher levels of graph set analysis. In the thesis presented here the unitary level of graph analysis are used.

1.5. Crystal engineering

Crystal engineering of molecular solids is concerned with the rational design of functional molecular solids.[28] Co-crystal synthesis is imperative for effective crystal engineering and vice versa. The term crystal engineering was first introduced by Pepinsky in 1955.[29] The concepts of crystal engineering have been applied by chemists, solid-state chemists in particular, theoreticians, crystallographers, and protein crystallographers. Schmidt was amongst the first to implement the concepts of crystal engineering to organic solid-state photochemistry.[30] Thomas while reviewing organic solid-state photochemical reactions noted that the reactivity of organic compounds in the solid state is governed by the molecular orientation and stacking sequences in the crystal structures.[31] The term crystal engineering is defined as "the understanding of intermolecular interactions in the context of crystal packing arrangements and utilisation of such understanding in the design and synthesis of new solids with desired properties". Crystal engineering depends on the use of non-covalent interactions to assemble molecules in the solid state; an effective control of non-covalent interactions is required for effective crystal engineering. Initially, crystal engineering work focussed on systems containing purely organic compounds, which in recent years has been extended to inorganic systems. Drawing an analogy between intermolecular bonds and covalent bonds, Lehn noted that an intermolecular bond in a supermolecule is analogous to a covalent bond in a molecule.[32] Following this argument, Dunitz stated that "a crystal is a supermolecule par excellence".[33] This statement in essence states that a crystal represents a higher level of complexity when compared to molecules with the crystallisation process being the supramolecular reaction. The ability to build crystal structures from the molecular structures would therefore require a complete understanding of the crystallisation process. Understanding the crystallisation process is the ultimate aim of crystal engineering, this would then allow the prediction of crystal structures from molecular structures and the synthesis of higher order crystals. The rational synthesis of higher order crystals is necessary if we are to ever understand the enormously complex molecular recognition process in biological systems. Understanding intermolecular interactions in terms of molecular recognition units lies at the heart of crystal engineering.

1.5.1. Molecular assemblies formed by intermolecular interactions

One of the principal challenges in crystal engineering or molecular co-crystal synthesis is to predict the crystal structure and property of molecular solids from the molecular structure of the constituent components.[34] In this context, molecular solids stabilised through predefined solid state structures can find important applications for developing new solids. Predefined molecular structures are usually conceived though hydrogen bonding interactions. Many design strategies for the synthesis of molecular complexes or co-crystals are based on utilising the complementary nature of hydrogen bonding interactions.[35] Combinations of hydrogen bonding interactions can lead to the formation of a wide variety of molecular assemblies. These can be categorized into 0D, 1D, 2D and 3D molecular architectures, host guest assemblies and appendage structures. The hydrogen bonding interactions in these complexes can be homomeric or heteromeric and involve neutral or charge-assisted interactions. These networks can serve as modules in the design and synthesis of molecular materials. In addition, robust supramolecular modules significantly reduce the number of possible solid-state packing motifs.

1.5.2. Appendage structures

Appendage structures are formed in systems containing more than one component. In these structures, one component forms a hydrogen-bonded network, to which the other component is appended through hydrogen bonding interactions without being part of the network formed by the first component. The simplest examples of appendage structures is the complex formed by formic acid with hydrogen fluoride.[36] The structure shows chains of hydrogen-bonded formic acid molecules to which H-F molecules are appended through F-H···O and C-H···F hydrogen bonds (Scheme 1.4).

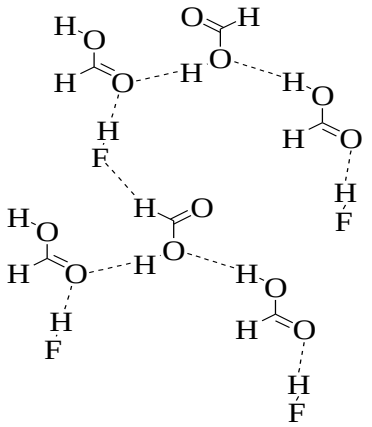

Scheme 1.4: Structure of formic acid····hydrogen fluoride.

1.5.3. Zero-dimensional networks

Molecular complexes are said to have zero–dimensionality when the components in a crystal are hydrogen-bonded to from a discrete group. Molecular complexes stabilised though zero-dimensional networks are observed in systems containing one two and three component systems.

Zero-dimensional hydrogen-bonded networks in unitary systems:

Benzoic acid is a prototypic example of a solid stabilised though a homomeric zero-dimensional network. The carboxylic acid groups form a cyclic $\mathbf{R_2^2}(8)$ motif through two O-H···O interactions (Scheme 1.5).

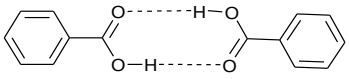

Scheme 1.5: Hydrogen bonding in benzoic acids.

Zero-dimensional hydrogen-bonded networks in binary co-crystals:

An example of a zero-dimensional hydrogen-bonded network in a binary system is shown in Scheme 1.6. The co-crystal contains two components, cinnamic acid (A) and isonicotinamide (B).[37] The two components arrange in an A-B-B-A arrangement to form a discrete zero-dimensional network. The supermolecule is stabilised through acid-pyridine and amide-amide supramolecular synthons (Scheme 1.6). The robustness of the network is demonstrated by the synthesis and structure solution of a series of binary co-crystals stabilised through acid-pyridine and amide-amide supramolecular synthons, suggesting that it is an example of a high-yielding supramolecular reaction.

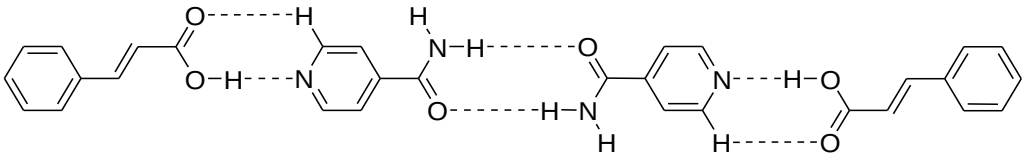

Scheme 1.6: Discrete zero-dimensional network observed in co-crystals of cinnamic acid and isonicotinamide.[37]

Zero-dimensional hydrogen bonding network in ternary co-crystals:

Ternary co-crystals were synthesised from known supramolecular synthons using the Scheme 1.7.[38] The rationale for the synthesis of ternary co-crystals is based on the findings of Etter and Frankenback,[39] where they noticed that the best hydrogen bond donor will preferentially hydrogen bond to the best acceptor. An extension of this observation is that the second best

donor preferentially hydrogen bonds to the second best acceptor. This preference of donors and acceptors has been tested and proved by synthesising and analysing a series of ternary co-crystals.[38]

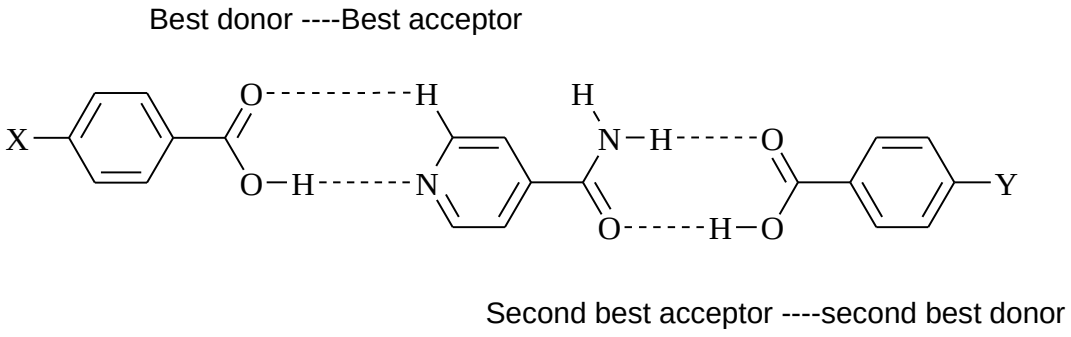

Scheme 1.7: Rationale for the construction of ternary co-crystals.[38]

1.5.4. One-dimensional hydrogen-bonded networks

The simplest one–dimensional (1-D) hydrogen-bonded networks formed by molecular solids are wires, chains, tapes or ribbons. One dimensional hydrogen-bonded networks are observed in many unitary and binary systems.[40] The requirement for forming a one-dimensional hydrogen-bonded network is that its components should be able to form two hydrogen bonds. These can be homomeric or heteromeric hydrogen bonds.

The formation of robust 1-D hydrogen-bonded aggregates in a series of nitro-anilines was reported by Panunto *et al.*[41] The nitro-anilines arrange in the solid state via head-to-tail hydrogen bonding interactions between the amino donors and nitro acceptors (Scheme 1.8) to form one-dimensional chains. In these structures the hydrogen bonding pattern clearly contains chains with rings as links. The hydrogen bonds are symmetrically independent. The bifurcated hydrogen bonds at the unitary level can be represented by the $\mathbf{R}_1^2(4)$ motif. The chain pattern is designated by the complex binary notation $\mathbf{C}_1^2(8)$. This notation does not uniquely describe the pattern in these crystals. In such cases, where the pattern is described as "chain of rings" the notation $\mathbf{C}_1^2(8)[\mathbf{R}_1^2(4)]$ is used. In this notation the ring description is appended in square brackets to the chain description.

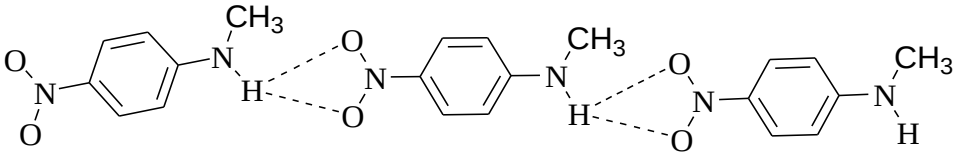

Scheme 1.8: One-dimensional network in nitro-anilines.

An example of 1-D wires are the binary molecular complexes formed between the dications of 1,2-bis(2'-tetrahydropyrimidyl) ethane and terephthalate and isophthalate dianions (Figure 1.5).[42] Robust one dimensional tapes are observed in the 1:1 co-crystals of 5,5-diethylbarbituric acid and substituted tris(amino)pyrimidines (Scheme 1.9).[43] The presence of the bulky substituents on the pyrimidine groups prevents the formation of 2-D layers in favour of rosette network.

1.5.5. Two-dimensional hydrogen-bonded networks

Two–dimensional molecular networks based on hydrogen–bonding interactions are formed by components containing three or more hydrogen bonding functionalities. The networks formed can be either homomeric (formed between identical molecules) or heteromeric (formed between different components). The formation of planar two-dimensional hydrogen bonding networks leaves a void space in crystal structures. However, the voids in crystal structures are interpenetrated by symmetrically equivalent 2-D hydrogen-bonded networks. The interpenetration occurs in order to maximise packing. The prototypical example of a homomeric two-dimensional network is pure trimesic acid (1,3,5-benzenetricarboxylic acid).[44]

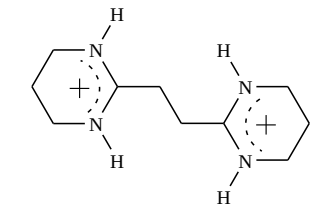

1,2-bis(2'-tetrahydropyrimidyl)ethane

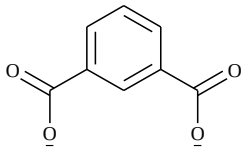

isophthalate

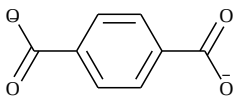

terephthalate

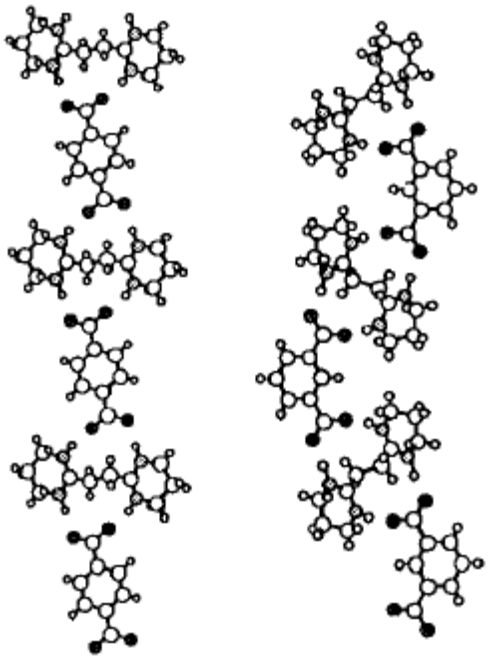

Figure 1.5: Molecular diagrams of dications of 1,2-bis(2'-tetrahydropyrimidyl) ethane and terephthalate and isophthalate dianions and the corresponding crystal structures showing the formation of 1-D wires.

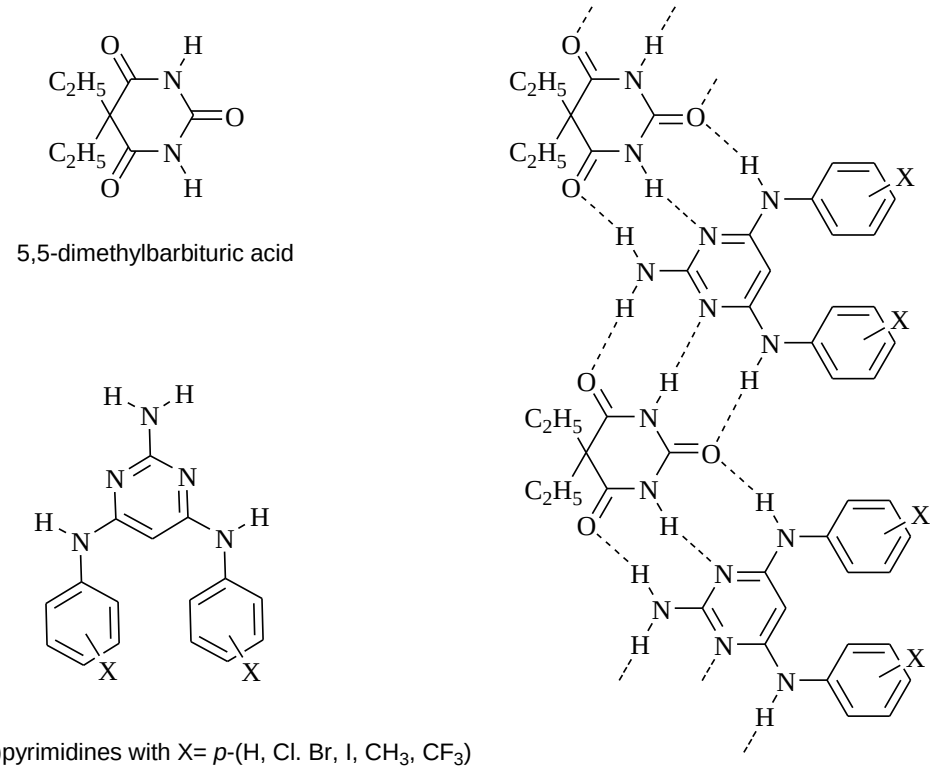

Scheme 1.9: One-dimensional tapes observed in co-crystals of 5,5-diethylbarbituric acid and substituted tris(amino)pyrimidines.

Trimesic acid crystallises through hydrogen bonds between the carboxylic acid groups to form a two-dimensional honey comb structure (Scheme 1.10). The voids formed by the two-dimensional arrangement are interpenetrated by other symmetry-equivalent networks. However, recently crystals of trimesic acid without interpenetration of two-dimensional networks leading to the formation of 1-D channels were isolated form a solution of diethyl ether in presence of pyrene molecules.[45,46] The pyrene molecules act as guests by occupying the channels formed by the trimesic acid molecules.

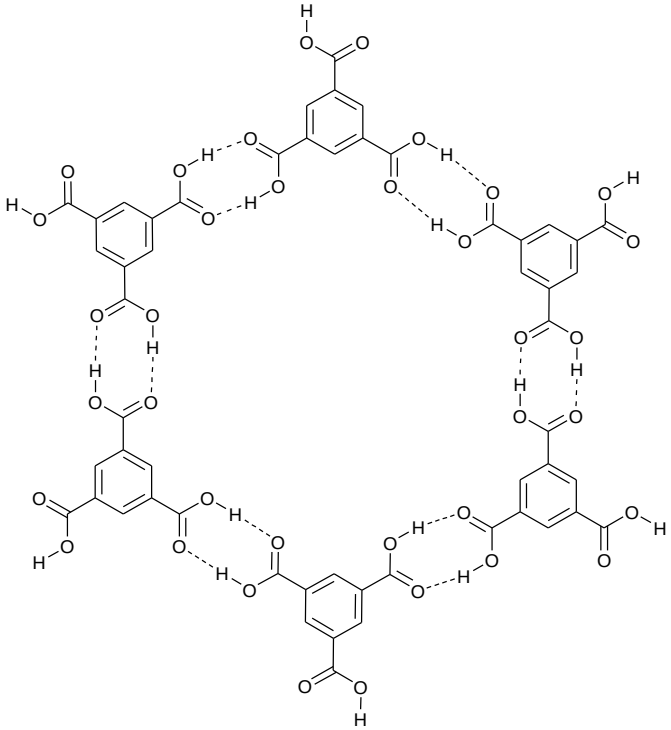

Scheme 1.10: Two-dimensional honeycomb arrangement in the crystal structure of trimesic acid.

An early example of a robust two-dimensional hydrogen-bonded network in molecular crystals is reported by Gong *et al*[47] in a series of substituted sulphamide molecules. The rationale for the synthesis is based on utilising the geometry of the tetrahedral shaped sulphamide group. It is noticed that despite the different size and nature of the substituents the robust two-dimensional hydrogen-bonded network (Scheme 1.11) prevailed in all compounds. A 2-D network formed by the sulphonamide groups arranges around a plane with the substituents hanging above and below the plane resulting in the formation of a three-dimensional crystal organised through van der Waals interactions.

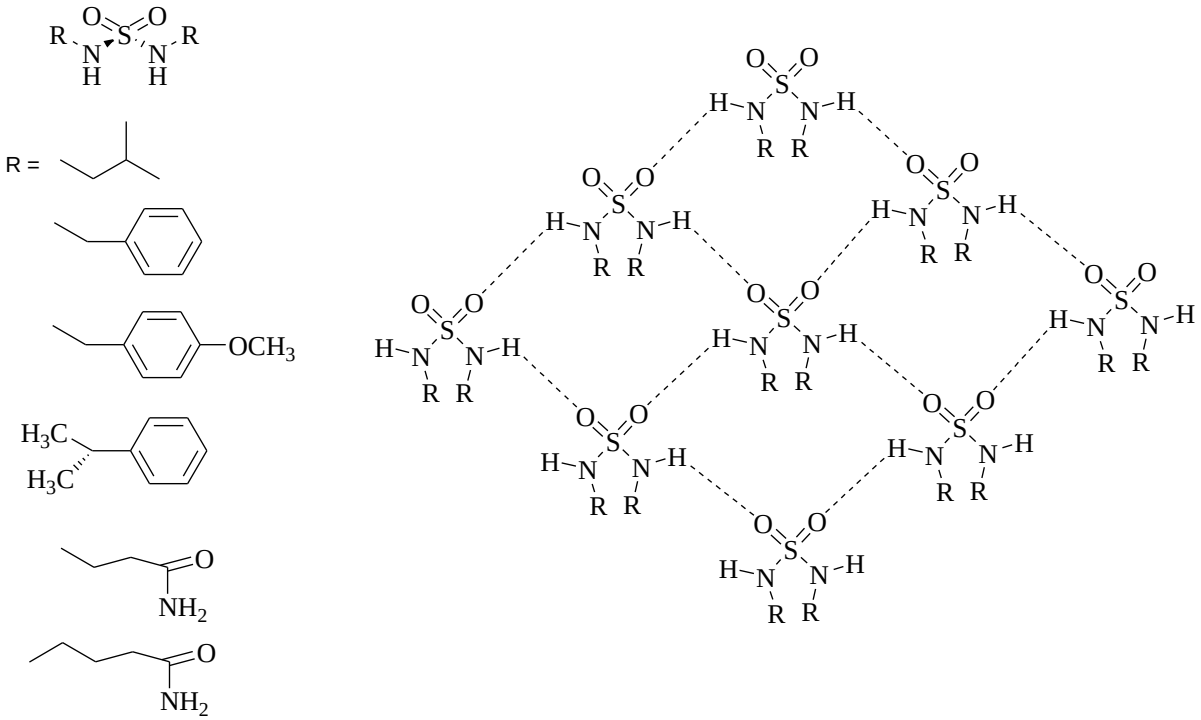

Scheme 1.11: Robust two-dimensional network in related sulphamide molecules.[47]

1.5.6. Three dimensional hydrogen-bonded networks

Molecular crystals with 3-D networks are intriguing due to the fundamental and practical issues. Three-dimensional molecular networks are structurally similar to inorganic zeolites. While the zeolite networks are stabilised through strong metal-oxygen bonds, 3-D open framework molecular networks are not very stable due to the relatively weak nature of non-covalent interactions. In addition, the formation of 3-D open network structures requires the molecules to possess empty space, which is against the principle of close packing. However, three-dimensional molecular networks can be stabilised by trapping suitable guest or solvent molecules thereby restricting interpenetration of symmetry-equivalent networks. The early examples of such hydrogen-bonded molecular networks are adamantane-1,3,5,7-tetracarboxylic acid[48] and methanetetracarboxylic acid (Scheme 1.12).[49] Both compounds form diamondoid networks though hydrogen bonding between the carboxylic acid groups.

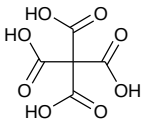

methanetetracarboxylic acid

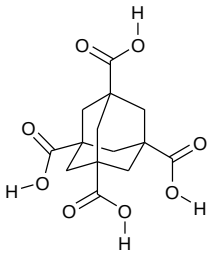

adamantane-1,3,5,7-tetracarboxylic acid

Scheme 1.12: Molecular diagrams of methanetetracarboxylic acid and adamantane-1,3,5,7-tetracarboxylic acid.

Both structures possess pseudo-tetrahedral topologies. Topologically similar diamondoid networks are observed in crystal structure of tetrakispyridone (Scheme 1.13).[50]

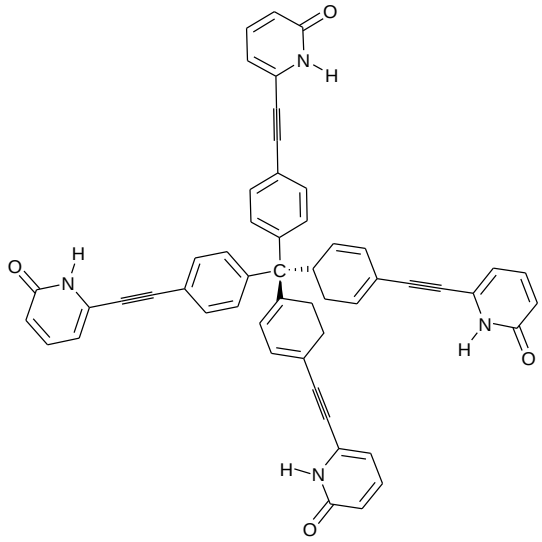

Scheme 1.13: Molecular structures of tetrakispyridone, compound exhibiting diamondoid networks.

1.5.7. Three-dimensional hydrogen bonding networks in binary systems

Topologically similar adamantoid networks are observed in 1:1 complexes of diamines and quinones.[51] The rationale for the synthesis of co-crystals is based on the complementary hydrogen bonding nature of alcohols and amines. The formation of a 1:1 complex is driven by the 50% increase in the number of hydrogen bonds observed in the individual components of alcohols and amines. The molecular complexes of *p*-phenylenediamine, benzidine with hydroquinone and 4,4'-dihydroxybiphenyl form super-diamond lattices through the formation

of O-H···N hydrogen bonds. The super-tetrahedral lattice formed by these linear dialcohols and linear diamines is shown in Figure 1.6.

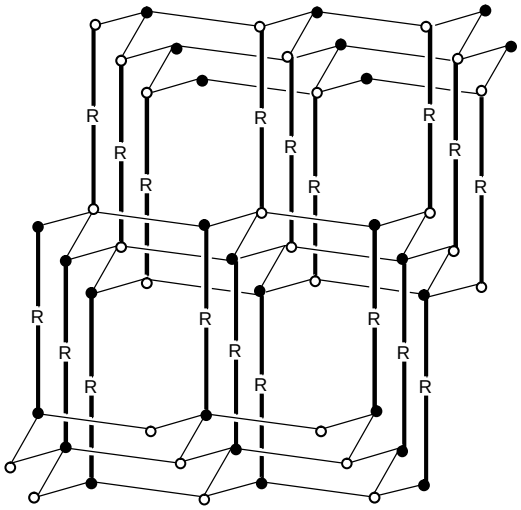

Figure 1.6: Super-tetrahedral lattice observed in molecular complexes of dialcohols and diamines.

1.5.8. Host-guest assemblies

Host-guest assemblies are the complexes that are composed of two or more molecules or ions held together in a unique structural relationship by non-covalent forces.[52] A necessary requirement to classify complexes as host-guest assembly is that the host and the guest are distinguishable from one another. Generally in a host-guest assembly, the larger component forms an array which includes the guest molecules. In host-guest complexes two different types of arrangements are observed.

1. The tunnel type inclusion complexes.[53]
2. The clathrate type host-guest arrangement.[54]

In the first type the guests are included in the tunnels formed by the host molecules and can be in mutual contact with one another. In the second type the guest molecules are separated from one another while being included in the cages formed by the host molecules.

In both the tunnel and clathrate types, the interactions between the host compounds can be divided into two types: (i) in which the host molecules interact through directional hydrogen-bonding interactions; (ii) complexes in which the host molecules interact through non-directional van der Waals interactions. Similar types of interaction can be observed between the host and the guest molecules. In host-guest assemblies, the host network can be made up of one or two components with other components occupying the guest positions.

1.5.8.1. Tunnel type inclusion complexes with directionally bonded hosts

The first among the tunnel type inclusion complexes are the crystalline adducts formed by urea.[55] Urea forms crystalline hexagonal complexes with a series of homologous *n*-paraffins[32] and rhombohedral complexes[56] with other bulkier guests. However, depending on the crystallisation conditions, urea forms both hexagonal and rhombohedral complexes with certain guests. Examples of guests which form hexagonal inclusion complexes with urea include[57] *n*-paraffins, alcohols, ketones, ethers, thioethers, esters, carboxylic acids. Rhombohedral inclusion complexes of urea are less common when compared to the hexagonal structure types. Dioxane, trioxane, acetone, 2,15-dimethylhexadecane, 2,18-dimethylnonadecane and 2,19-dimethyleicosane are among the guest molecules which form rhombohedral inclusion complexes with urea. Thiourea[58] and selenourea[59] form isostructural rhombohedral complexes similar to that of urea, with guest molecules such as *n*-paraffins, alcohols, ketones and halogen-containing compounds.[60] The structures of the inclusion complexes of urea are based on forming a hexagonal cross-section with the urea molecules forming four hydrogen bonds between the N-H and C=O groups. The structure types of compounds formed though directional interactions are called tectons.[61]

One example of a molecular tecton formed though hydrogen bonding interactions is the structure shown in Scheme 1.14. The results demonstrate that the 3-D porous hydrogen-bonded network remains intact upon exchange of the guest molecules.

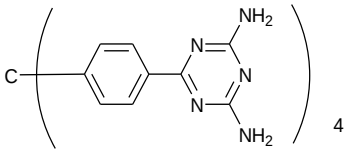

Scheme 1.14: Molecular structure of a compound forming a hydrogen-bonded framework.

1.5.8.2. Tunnel type inclusion complexes with van der Waals bonded hosts

There are many examples of channel type inclusion complexes formed by cleft and tweezer shaped molecules. Deoxycholic acid (DCA) is an example of a cleft molecule. 2,6-Dimethylbicyclo[3.3.1]nonane-*exo*-2,*exo*-6-diol and Trogers base (Scheme 1.15) are examples of tweezer shaped molecules which form inclusion complexes with different guest molecules.

2,6-dimethylbicyclo[3.3.1]nonane-2,6-diol

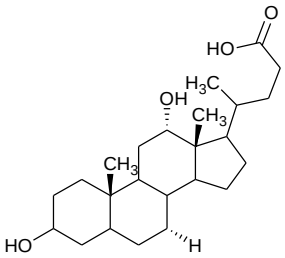

deoxycholic acid

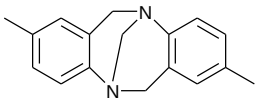

Trogers base

Scheme 1.15: Molecular structures of 2,6-dimethylbicyclo[3.3.1]nonane-2,6-diol (a), deoxycholic acid (b), Trogers base (c).

DCA forms orthorhombic, tetragonal and hexagonal inclusion complexes with a variety of guests which include organic acids, aliphatic and aromatic hydrocarbons, alcohols, alkaloids, and methyl orange. The host network in these complexes is stabilised through van der Waals interactions. In addition to the DCA molecules, some substituted bicyclo[3.3.1]nonane compounds form host networks which are stabilised through van der Waals interactions. The molecular shape of the substituted bicylco[3,3,1] compounds is suitable for the molecules to form supramolecular inclusion channels type structures.[62] Based on these biclyclic molecules, analogous compounds like Trogers base have emerged as a valuable building block for the construction of a number of chiral host systems for molecular recognition studies.[63]

1.5.8.3. Tunnel type two-component host network

Robust tunnel type inclusion complexes resulting from two-component host-networks are rare. The 1:1 co-crystal of caffeine and succinic acid forms a host network in which different guest molecules occupy the void space to form a host-guest assembly as shown in Figure 1.7. The structure determined by single crystal X-ray diffraction shows that the caffeine and succinic acid molecules form layers held together though O-H···O, O-H···N and pairs of C-H···O hydrogen bonds. The channels are occupied by the different guest molecules existing in stoichiometric or non-stoichiometric ratios.[64]

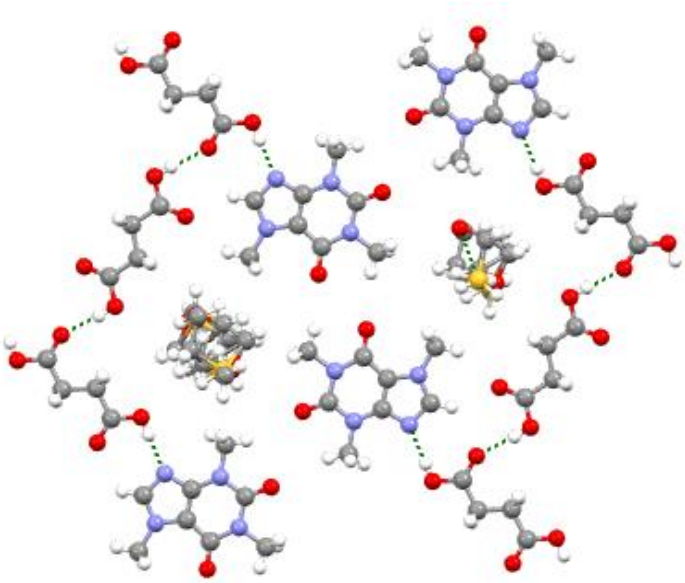

Figure 1.7: Host-guest arrangement in a caffeine–succinic acid co-crystal.[62]

1.5.8.4. Clathrate inclusion compounds

The term clathrate was coined by H. M. Powell in 1948.[65] Clathrates are molecular complexes formed by host molecules which pack in crystal structures such that they leave cavities between them. The cavities produced by the host molecules are occupied by guest molecules. In clathrate structures the guest is entirely enclosed in a framework formed by the host molecules. These molecular complexes can be divided into three types depending on the type of interaction observed between the host molecules.

1. Directionally hydrogen-bonded hosts: The complexes formed by hydroquinone (quinol) belong to this category of clathrate complexes. There are three known polymorphs of quinol (α, β, γ). Among the three polymorphs only the β-polymorphic arrangement is known to form clathrate type complexes. The β-quinol clathrates are structurally isomorphous but are known to crystallise in three space groups depending on the guest molecules and the interactions between them. The guest molecules enclosed by the β-quinol clathrates include Ar, Kr, Xe, HCOOH, CO_2, HBr, C_2H_2, CH_4, SO_2, etc.
2. Host networks formed by a combination of van der Waals interactions and hydrogen bonds: Host networks formed by phenol and related compounds belong to this class of clathrates. The crystals formed by the phenol clathrate networks crystallise in the rhombohedral space group $R\bar{3}$, containing small guest molecules like HCl, HBr, HI, H_2S, SO_2, CO_2, etc. In addition to the phenol molecules, Dianin's compound is known

to form clathrate complexes with many organic compounds Scheme 1.16.

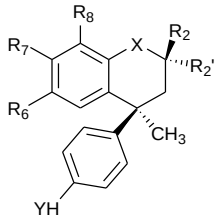

Scheme 1.16: Molecular structure of Dianin's compound. (R_2, R_2', R_6, R_7, R_8 are CH_3 or H. While X and Y can be O or S).

3. Van der Waals linked hosts: Tetraphenylene (Scheme 1.17) is known to form clathrate complexes with dioxane, pyridine, CCl_4, benzene, $CHCl_3$ and acetone as guests.

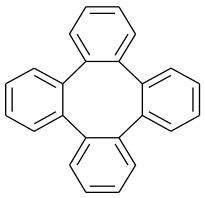

tetrabenzo[a,c,e,g] cyclooctatetraene

Scheme 1.17: Molecular structure of tetraphenylene.

1.6. Co-crystals or molecular complexes in the context of the pharmaceutical industry

Co-crystals represent a well-known class of compounds termed addition compounds,[66] organic molecular compounds,[67] mixed binary molecular crystals,[68] molecular complexes[69] or solid-state complexes.[70] Prototypical examples of co-crystals in the literature were reported as early as 1844 and 1893.[71,72] While co-crystals have been known for some time, to date there is no consensus between various research groups on the definition of what constitutes a co-crystal (Table 1.3). One agreed commonality is that all co-crystals are crystalline materials comprised of at-least two different chemical components, i.e. co-crystals are analogous to multi-component crystals. However, there is no consensus on what constitutes a component and this can be drastically different, ranging from neutral to ionic species involving solids, liquids and gases states.

In this thesis, the term co-crystal will imply the following criteria:

1. A multi-component crystalline material existing in a definite stoichiometry.
2. The components in the crystal are held together through neutral hydrogen bonding or other non-covalent interactions.
3. To differentiate a co-crystal from solvates or pseudo polymorphs, we use the concepts of

crystal engineering, i.e. if the molecular complex containing the solvent molecule or molecules is assembled through known or conceivable molecular recognition events then we consider it to be a co-crystal rather than a solvate. In cases where the molecular complex containing the solvent molecule is one isolated case obtained as a serendipitous result of crystallisation, in such cases we consider the crystal as a solvate rather than a co-crystal.

Table 1.3: Various definitions of a co-crystal reported in the literature:

Author	Definition of a co-crystal	Ref.
Bond, A.	"synonym for multi-component molecular crystal"	[73]
Aakeroy, C. B.	"compounds constructed from discrete neutral molecular species, made from reactants that are solids at ambient conditions and are present in definite stoichiometric amounts"	[74]
Nangia, A.	"multi-component solid-state assemblies of two or more compounds held together through by any type or combination of intermolecular interactions"	[75]
Stahly, G. P.	" a molecular complex that contains two or more different molecules in the same crystal lattice"	[76]
Childs, S. L.	" crystalline materials made up of two or more components, usually in a stoichiometric ratio, each component being an atom, ionic compound, or molecule"	[77]
Jones, W.	" a crystalline complex of two or more neutral molecular constituents bound together in the crystal lattice through noncovalent interactions, often including hydrogen bonding"	[78]
Zaworotko, M. J.	"are formed between molecular or ionic active pharmaceutical ingredient (API) and a co-crystal former that is solid under ambient conditions"	[79]

1.6.1. Pharmaceutical co-crystals

It is well-known that properties of materials (crystalline or amorphous) are fundamentally dependent on the molecular arrangement within the solid. Altering the molecular arrangement or intermolecular interactions within a solid, with or without introducing new molecular species/component can and usually does affect the properties of that particular solid material.

Hence co-crystals or multi-component crystals represent one strategy to alter the physical and chemical properties of pharmaceutical compounds. Given the importance of active pharmaceutical ingredients (APIs) and new chemical entities (NCEs), in terms of their intellectual property it is perhaps surprising that only in recent years have crystal engineering strategies been implemented in the pharmaceutical industry. In addition, co-crystallisation represents an alternative to drug product formulation.

Pharmaceutical co-crystals are multi-component crystals containing at least one component which is an API or NCE. Generally a pharmaceutical co-crystal consists of an API and a co-crystal former (CCF). Analogous to the salts and polymorphs, co-crystals also alter the properties of the active ingredient. Properties of APIs that are of importance in the pharmaceutical industry include melting point, solubility, chemical stability, dissolution profile, hygroscopicity, bioavailability, and mechanical properties. Current strategies to alter the chemical and physical properties of pharmaceutical compounds are based on co-crystallisation, salt formation, hydrate/solvate formation, screening and identification of different polymorphic forms and co-crystallisation of the API. While the strategies may be successful, no particular one offers a complete solution for property enhancement applicable to all APIs. Each API must be examined on a case by case basis based on the desired final property. The number of publications and reviews detailing the use of crystal engineering and supramolecular concepts applied to APIs is extensive and are continuing to increase.[80] Most commonly the publications are based on targeting a particular supramolecular synthon while using solid-state synthesis strategies to address the desired property enhancement of the API. In the beginning, examination of the API in terms of the number of hydrogen bond donor and acceptor groups,[81] the salt forming capability,[82] and the conformational flexibility is carried out. Based on the targeted property and the API, suitable co-crystal formers are selected while considering the toxicology profiles of the CCFs. However, to date, predicting the outcome of a particular co-crystal reaction is not possible until tested experimentally.[83] Examples of using co-crystals to enhance the properties of APIs are discussed here.

1.6.1.1. Hydrate formation

Co-crystals are supramolecular assemblies synthesised by targeting the hydrogen bonding ability of the functional groups in the API. Solvate or hydrate formation of an API also relies on the ability of the API to form hydrogen-bonding interactions. Therefore, when compared to a free API, a pharmaceutical co-crystal will have a reduced propensity for the formation of a

hydrate or solvate, thus stabilising the API. This however depends on the strength of the intermolecular interactions formed between the API and co-crystal former (CCF) when compared to the strength of the intermolecular interactions between the API and solvent molecule. An example of co-crystals stable to hydration is the co-crystal of carbamazepine with nicotinamide and saccharin. A purely anhydrous form of carbamazepine transforms into a dihydrate while the co-crystals of carbamazepine with isonicotinamide or saccharin do not form a dihydrate even after exposure to high levels of relative humidity.[84]

A similar study on caffeine-oxalic acid co-crystals shows that they do not transform to the hydrate form under high relative humidity.[85] An analogous study conducted on co-crystals of *S*-oxiracetam showed an improved hygroscopic stability compared to *S*-oxiracetam (ox). Oxiracetam is a nootropic drug used in the treatment of cognition disfunction. It is a racemic compound comprised of *S*-ox and *R*-ox enantiomers. It is noticed that the *S*-ox enantiomer is highly hygroscopic and transforms into a liquid when exposed to 85% relative humidity (RH) at 25 ^{o}C in three days. The co-crystals of *S*-ox with gallic acid and 3,4-dihydroxybenzoic acid are found to be stable at all RHs.[86]

Generally anhydrate forms of any drugs are more soluble in water when compared to the hydrate forms. In this context, norfloxacin is an exception, since its hydrate is more water soluble than the anhydrate.[87] In all the known hydrate forms of norfloxacin (NFLX),[88] it exists in a zwitterionic state when compared to the anhydrate form. The formation of a zwitterionic state in hydrated forms is responsible for the increased water solubility of NFLX hydrates when compared to the anhydrate form.

1.6.1.2. Chemical Stability

Co-crystals of pharmaceutical compounds are known to improve the stability of the active pharmaceutical ingredient. It has been noticed that, in the solid state, a single component carbamazepine polymorph undergoes photodegradation to form a cyclobutyl dimer as the main product. [89,90] It has been noticed that the degradation is possible only when the azepine rings of carbamazepine are within a distance of 4.1Å. This was confirmed by the synthesis of carbamazepine co-crystals in which the azepine rings are separated by more than 4.1Å, which prevented the photodegredation and thereby stabilises the API.

1.6.1.3. Dissolution rate

Dissolution rates of various pharmaceutical co-crystals have been reported. One of particular importance is itraconazole (an antifungal agent). Itraconazole has a very low water solubility

and is marketed in its amorphous form to increase bioavailability. Remenar *et al.* [91] synthesised and structurally characterised co-crystals of itraconazole. They demonstrate that the dissolution profiles of itraconazole co-crystals are comparable to the amorphous form and 20-fold higher when compared to the crystalline form of itraconazole.

1.6.1.4. Bioavailability

If co-crystals of any API are to be a viable alternative for a solid form of a drug, it is mandatory to study bioavailability. Two recently published articles have reported bioavailability studies conducted on co-crystals. McNamara *et al*. reported that a 1:1 co-crystal of 2-[4-(4-chloro-2-fluorophenoxy)phenyl]pyrimidine-4-carboxamide with glutaric acid had a dissolution rate 18 times higher than the pure API. Bioavailability studies revealed that the co-crystal attained approximately three times higher plasma concentrations for the same dose in dogs.[92] Another such example is the co-crystal of Amgen compound (AMG 517) with sorbic acid. The co-crystal is isolated by co-slurrying of AMG 517 with sorbic acid. The co-crystal exhibited better dissolution and bioavailability than the free API. Pharmacokinetic studies of the co-crystal revealed that only 30 mg/kg of the co-crystal were necessary to achieve similar plasma levels in rats, when compared to the 500 mg/kg dose needed for the free API.[93]

1.6.1.5. Co-crystals with improved solubility profiles

It is estimated that around 40% of the drugs on the market and around 70% of the new chemical entities are poorly water soluble. An improvement in the solubility of the drugs can enhance their bioavailability. Pharmaceutical co-crystals represent a strategy to enhance the solubility of the API. In this perspective, some recent examples of co-crystals with enhanced solubility compared to the APIs are discussed here. One such example is niclosamide.[94] Niclosamide is an anthelmintic drug used for the treatment of worm infection in humans and animals. It is practically insoluble in water and is usually formulated as a suspension. Pharmaceutical co-crystals of niclosamide with caffeine, urea, *p*-aminobenzoic acid, theophylline, nicotinamide and isonicotinamide were synthesised and structurally characterised. It was observed that among all the crystalline forms of niclosamide the molecular complex containing niclosamide-theophylline and acetonitrile showed the highest solubility, improved by six times when compared to that of the API.

The pharmaceutical industry at the moment is facing a crisis due to the combined effects of increased research and development (R&D) costs and a decreasing number of new chemical

entities being identified. In addition to this, a very high proportion of NCEs cannot be advanced to the next stage of the development process due to poor aqueous solubility. While co-crystals represent one possible strategy, new approaches are required to overcome the solubility issue. In cases where no acceptable co-crystal or salt form can be generated, the pharmaceutical industry is left with no option but to deliberately generate an amorphous form of a drug. Amorphous or partially crystalline forms of the drug candidates are known to have high aqueous solubility.[95] However, formulations containing amorphous forms are less stable when compared to the crystalline forms. Amorphous materials are less stable and often more reactive to process related techniques, which include milling, drying, compression and thermal stress.[96] In addition, there is always a significant risk that the amorphous form crystallises at a later stage.

1.7. Salts

Salt formation is used as the traditional approach in the pharmaceutical industry to alter the physical and chemical properties of APIs. It is estimated that more than half of the marketed drugs are administered as salts.[97] One major limitation for salt formation is that the API must possess a suitable ionisable site. In comparison, the co-crystallisation is targeted at the very nature of a compound being an API, i.e. the presence of external functional groups, regardless of possessing acidic, basic or ionisable functional groups. Examples in the literature are extensive where the salt forms of a drug are known to possess better solubility profiles compared to the API. One interesting example is lamotrigine,[98] which is an anticonvulsant drug and has low water solubility. A series of lamotrigine salts with dicarboxylic acids were generated and their aqueous solubility has been investigated. Since all the synthesised salts were isostructural, it could be concluded that the solubility was directly related to that of the precursor dicarboxylic acid.

1.8. Undesirable forms of APIs

While crystalline forms of any drug candidates may be potentially important, process related serendipitous isolation of polymorphs, solvates, amorphous forms and solid solutions are undesirable. In the subsequent sections, the potentially unstable forms of pharmaceutical crystals, and the transformations they undergo to enhance their stability, are highlighted. An

excellent review of potentially unstable pharmaceutical compounds and their effects on drug formulation is given by Shekunov and York.[99]

1.8.1. Polymorphism

An active pharmaceutical ingredient can exist in various solid forms and often show polymorphism.[100] Polymorphism is defined as the ability of a substance to exist in more than one crystalline form, with different arrangements and or conformations of the molecule in the crystal lattice.[101] Different polymorphs have divergent physical properties. In the context of the pharmaceutical industry, polymorphs can significantly alter the pharmacokinetic factors, such as rates of absorption, drug availability, and the resulting physiological concentrations.[102] In the context of polymorphism, McCrone noted that the number of forms known for each compound is proportional to the time and money spent in research of that compound.[103]

Polymorphs of a compound may be isolated under the same set of conditions; these are called concomitant polymorphs. In certain cases, specific crystallisation conditions including temperature and concentration may lead to the isolation of polymorphs. For example, two polymorphs of the drug sulphathiazole (II and III) can be crystallised from water, two other polymorphs (I and IV) are obtained from acetone, and only one (I) can be recrystallised from *n*-propanol.[104] In some cases, when the isolated polymorphic form is metastable, solid-state transformation from one polymorph to another may take place.[105] The time duration of these transformations can range from seconds to years. Hence the occurrence of a metastable form is particularly worrying for the pharmaceutical industry.

One such example is the serendipitous isolation of a polymorph of norvir, an HIV protease inhibitor. There was a serious shortage of the supply of norvir capsules due to the discovery of a new polymorph.[106] It is therefore necessary to understand the kinetic process of crystallisation for any drug candidate.

1.8.2. Solvates

The solvate form of a drug candidate provides another opportunity to modify the physicochemical properties due to their inherent capacity to alter the crystal structure.[107] However, a solvate or hydrate form may transform into anhydrous forms or into a solid form

containing non-stoichiometric amounts of solvent molecules, which affects the stability and crystallinity of the compound.[94] Therefore in the case of solvates it is therefore necessary to completely understand the stability of the form.

1.8.3. Chiral drugs

More than half of all marketed drugs are chiral.[108] In these cases the problems are associated with the enantiomeric purity of the drug. A chiral impurity incorporated into the crystal will alter the physicochemical properties of the crystalline material. In most cases the chiral compounds exists as a racemic mixture. However, the presence of a metastable racemic mixture must be avoided.[76]

1.8.4. Solid-state transformations

In some cases, during the shelf-life of a drug compound, it may undergo a solid-state transformation to a more stable form. The transformations may be photochemically-induced, thermally-induced, or the result of mechanical stress during compression.[109] Solid-state transformations of the compound alter the structure and hence the properties of the material. It is proposed that molecules undergo solid-state transformations if there are defects in the crystal structure or in cases involving intergrowths of two polymorphic compounds.[110] In such cases a thorough investigation must be conducted to understand the stability and transformation of the compound.

1.8.5. Solvent-mediated transformations

While solid state transformations are rare, solvent-mediated transformations of the drug compounds are common in the pharmaceutical industry. At almost every stage of the developmental process, pharmaceutical compounds come into contact with solvent molecules. The appearance and disappearance of a solvated form can and does hamper the development process. Therefore, a complete understanding of the kinetics and the mechanisms of solvent-mediated transformations is of practical importance.[111]

All of the above mentioned examples illustrate the instability and the transformations of pharmaceutical compounds under certain conditions. Different crystalline modifications can have a dramatic effect on the properties of the drug substance, in particular the toxicity, dissolution rate, and bioavailability. It is therefore imperative that the kinetic factors affecting

the crystallisation process are well understood in order to confer the polymorphic form of a pharmaceutical material.

Chapter 2: Experimental methods

2. Co-crystal synthesis

2.1. Mechano-chemical methods of co-crystallisation

The co-crystals presented in the thesis are initially synthesised through mechano-chemical process of co-crystallisation. Mechano-chemical reactions are solid–state reactions activated by grinding or milling. Mechano-chemical methods have in recent years gained importance for the synthesis of molecular complexes. The synthesis of molecular complexes requires the breaking and formation of intermolecular interactions stabilised through hydrogen bonds, halogen bonds, π–π interactions, and van der Waals interactions. Early investigations of solid state intermolecular reactions were carried by Etter[112,113] and Rastogi.[114] Etter investigated the reactions between solids stabilised through hydrogen bonding interactions. She demonstrated that co-crystals of molecular systems can be prepared not only by evaporation through solution but also by grinding together stoichiometric amounts of the components. Rastogi studied reactions between picric acid and naphthalene, phenanthrene, anthracene and naphthols in the solid state.[12] Molecular complex synthesis through mechanochemical routes has gained wide importance in recent years.[115] The process of grinding two or more molecular species and be done in two different ways,

1. Grinding in the presence of the solvent.
2. Grinding in the absence of solvent.

Mechanochemical synthesis of co-crystals requires simple equipment, often a mortar and pestle can suffice. Stoichiometric amounts of the APIs and the CCFs are ground using a mortar and pestle with or without the presence of a solvent component. In the thesis presented here, the solvent drop grinding method of co-crystallisation was followed. The polycrystalline materials obtained from the solvent drop grinding were then analysed by powder X-ray diffraction (PXRD).

2.2. Crystallisation from solution

In order to study the intermolecular interactions existing in a crystalline material it is essential to obtain diffraction quality crystals of the material. The crystals of the molecular complexes presented in the thesis were prepared by crystallisation from solution. The chemical purity and stability of the components is taken into consideration before crystallisation. A suitable concentration range of ≈ 5 wt % ≤ $X_{\text{crystalline material}}$ ≤ 30 wt% with respect to the solvent of

crystallisation was used to obtain diffraction quality crystals. The material for crystallisation is dissolved in a suitable solvent and allowed to crystallise isothermally by slow evaporation of the solvent. The crystals obtained were then analysed by X-ray diffraction techniques. Initially, all the molecular complexes were analysis by PXRD. Powder X-ray diffraction was performed to identify crystalline phase's different form the starting materials. The crystals for which the characteristic diffraction patterns of the starting materials were not present were then analysed by single crystal X-ray diffraction to confirm the co-crystal formation.

2.3. Powder X-ray diffraction

Generally, many materials with interesting properties can only be prepared as polycrystalline materials. In such a case powder X-ray diffraction is the only option to extract structure-related information for the material. A powder diffraction pattern is as a measure of the scattered intensity as a function of the Bragg angle. The powder diffraction pattern is a fingerprint of that particular material and is dependent on the structural features of the material. The structural features of crystalline materials or phases are manifested in powder diffraction pattern as Bragg reflections with each possessing specific intensity, peak shape and location.

The equation representing the interplanar distance as function of the unit cell parameters and miller indices, *h, k, l* for the triclinic system may be expressed as:

$$\frac{1}{d^2} = \left[\frac{h^2}{a^2 sin^2\alpha} + \frac{2kl}{bc}(cos\beta\, cos\gamma - cos\alpha) + \frac{k^2}{b^2 sin^2\beta} + \frac{2hl}{ac}(cos\alpha\, cos\gamma - cos\beta) + \frac{l^2}{c^2 sin^2\gamma} + \frac{2hk}{ab}(cos\alpha\, cos\beta - cos\gamma)\right] / (1 - cos^2\alpha - cos^2\beta - cos^2\gamma + 2cos\alpha\, cos\beta\, cos\gamma)$$

Expressions for other crystal systems can be derived from the above equation while considering the restrictions imposed on the unit cell parameters.

The experimental data obtained in a powder diffraction pattern is a one dimensional projection of the three dimensional reciprocal lattice, recorded as a function of the Bragg angle. Thus, in a powder diffraction pattern the directions are lost and only the lengths of the reciprocal lattice vectors are measured. While in a single crystal X-ray diffraction experiment, both the length and the direction of the reciprocal space are preserved. The loss of direction in a two-dimensional case is shown in the Figure 2.1.

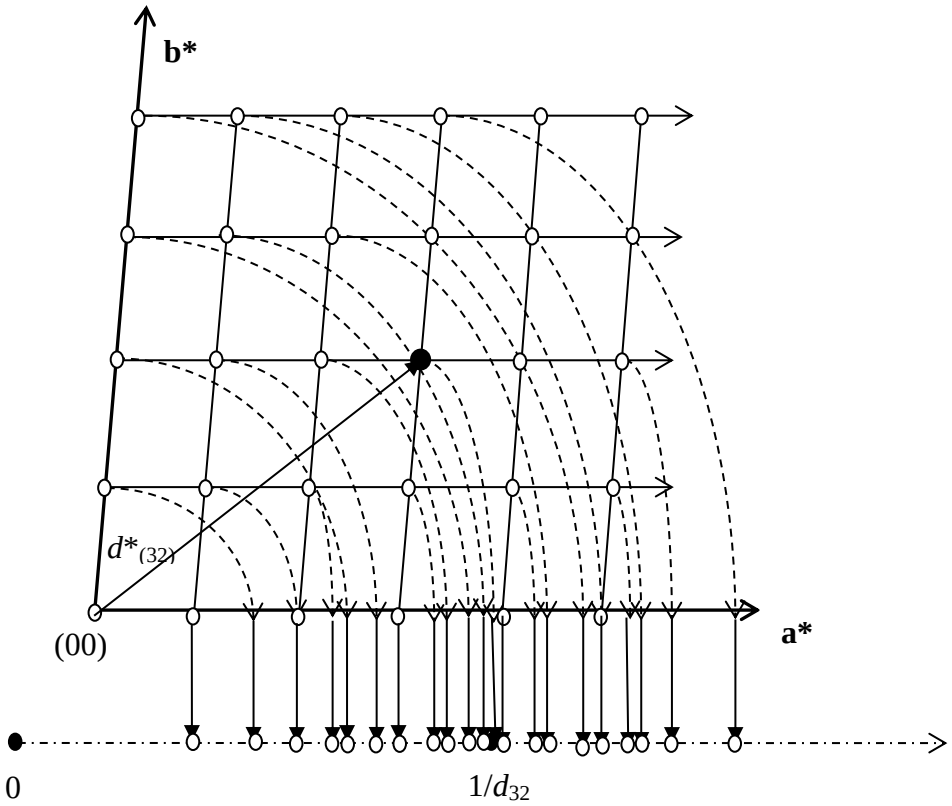

Figure 2.1: Illustration showing the projection of a 1-D reciprocal lattice (top) onto a 1-D (1/*d*) axis (bottom).

Reliability of indexing powder patterns: The reliability of indexing the peaks in a powder diffraction pattern is based on obtaining the minimum discrepancy between the observed *2θ* positions and the calculated *2θ* positions (obtained by assigned index triplets from the unit cell parameters). For N observed reflections, the reliability of indexing (ε) is given by he formula;

$$\varepsilon = \sum_{i=1}^{N} \left(2\theta_{hikili}^{obs} - 2\theta_{hikili}^{calc}\right)^2$$

where, *h, k, l* and *i* are integers.

Powder X-ray diffractometer

The powder X-ray diffraction data for polycrystalline materials presented in the thesis were obtained using the Bruker D8 Discover and Bruker D8 Advance diffractometers. The Bruker D8 diffractometer was used for phase identification of polycrystalline materials. The Bruker D8 Discover diffractometer, operates in transmission geometry with Cu Kα radiation (λ = 1.5418 Å) and fitted with a Göbel X-ray focusing mirror and a LynxEye linear detector. Finely ground samples of each of the products from co-crystal screening experiments were

contained in a 96-well plate. Data for each sample were collected over the angular range $4 \leq 2\theta/° \leq 50$, counting for 0.25 s at each 0.02019 increment of the detector position. The diffractometers used in the analysed are shown in Figure 2.2.

Figure 2.2: Bruker D8 Advance (left) and D8 Discover diffractometers used in this work.

Bruker D8 Advance diffractometer operates in Bragg-Brentano geometry and is fitted with a germanium crystal to allow only the Cu Kα1 (λ=1.54056 Å) radiation and possess a Lynxeye linear detector. The D8 Advance diffractometer is used when high resolution data were required for indexing the polycrystalline phases. Data were collected on finely ground samples over the angular range $5 \leq 2\theta/^{o} \leq 60$ at an increment of 0.01^{o} of the detector position with a counting time of 0.4 sec. Data collection was done using the zero background sample holders, which are made of single crystal silicon cut in such a way that the peaks corresponding to the silicon do not interfere with the sample over the 2θ range scanned.

The powder diffraction patterns of the polycrystalline materials were evaluated using the EVA[116] software package. Indexing of diffraction patterns and refinements of unit cell parameters against the powder diffraction pattern is done using the TOPAS software.[117]

2.4. X-ray diffraction

2.4.1. Background

X-ray diffraction is used to analyse the spatial distribution of electron density in crystalline compounds. An X-ray diffraction experiment is analogous to viewing an object at higher magnification using an optical microscope. In a typical optical microscope, the radiation scattered by an object is recombined using a lens allowing it to be viewed at higher magnification. In order to view the atomic arrangement one would need a radiation that is of the order of around 0.1nm. X-rays belong to that part of the electromagnetic spectra, which possess wavelengths of the order of 1Å. However, there is no known material that could focus the X-rays scattered by crystalline compounds, thus making it impossible to view atomic arrangement. The alternative method to study crystalline compounds is by the use of the phenomena of diffraction.

The interaction between X-rays and crystalline material is the interaction between an oscillating electric field of X-rays with the point charges in atoms and molecules. The oscillating electric field component of the electromagnetic radiation forces the electrons and protons to oscillate about their equilibrium positions. The oscillating point charges, according to theory of electromagnetic radiation, emit energy in the form of radiation with a frequency similar to that of incident wave.

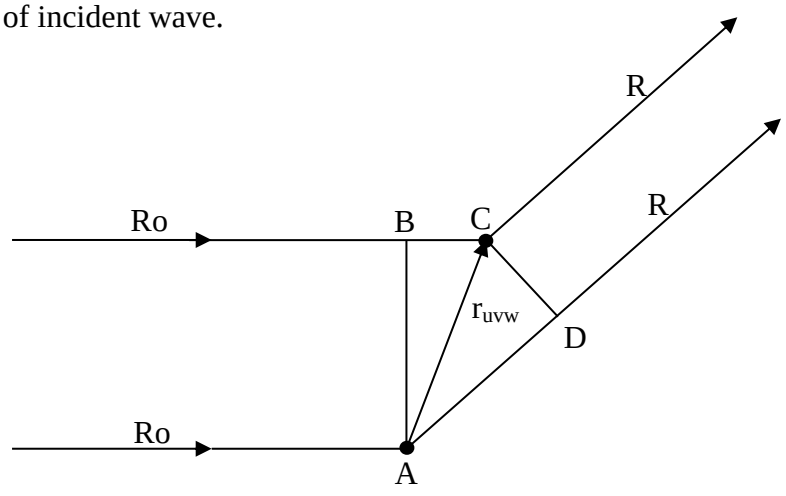

Figure 2.3: Scattering of point charges for the derivation of Laue diffraction conditions.

The X-rays being a part of the electromagnetic radiation can be represented in terms of plane waves with appropriate wave vectors. A crystal is assumed to be a periodic arrangement of atoms and molecules possessing a three-dimensional translational symmetry. In order to

explain the scattering from a crystal, it will be sufficient to consider two point charges A and C in three-dimensional lattice. The point charges A and C are assumed to be separated by a translational vector r_{uvw}, which is related to the non-collinear basis vectors a, b, c as $r_{uvw} = ua + vb + wc$; where *u*, *v*, *w* are integers. Considering, $\mathbf{R_o}$ and $\mathbf{R}$ to be the incident and scattered wave vectors from point charges A and C respectively (Figure 2.3). Considering constant wavelengths, the magnitudes of incident and scattered wave vectors will be identical.

$$|\mathbf{R}| = |\mathbf{R_o}| = \frac{1}{\lambda} \qquad \text{eq.}-(2.1)$$

The waves scattered from point charges A and C interfere with one another. The interference is constructive if the optical path difference is an integral multiple of the wavelength λ. From Fig. 2.3 the optical path difference (Δ) is given by

$$\Delta = AD - BC$$

$$= r_{uvw} \cdot \frac{\mathbf{R}}{|\mathbf{R}|} - r_{uvw} \cdot \frac{\mathbf{R_o}}{|\mathbf{R_o}|}$$

$$= \lambda\, r_{uvw} \cdot (S - S_o)$$

the condition for constructive interference therefore is

$$r_{uvw} \cdot \mathbf{k} = \text{integer},$$

Where, $\mathbf{k} = (\mathbf{R} - \mathbf{R_o})$ is called the diffraction vector in reciprocal lattice.

The eq. 2.1 can be written as

$$(ua + vb + wc) \cdot \mathbf{k} = \text{integer}$$

the above equation is equivalent to,

$$a \cdot \mathbf{k} = h, \qquad b \cdot \mathbf{k} = k, \qquad c \cdot \mathbf{k} = l \qquad \text{eq.}-(2.2)$$

The interference between the scattered waves to be constructive, the above three conditions have to be satisfied, where *h*, *k*, *l* are integers. These three conditions were discovered by Max von Laue and are named after him and are called Laue conditions.[118]

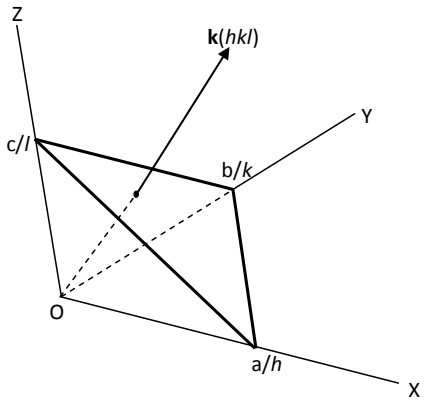

Figure 2.4: Geometrical interpretation of Laue's equations.

The Laue equations are represented geometrically by considering a plane with intercepts a/*h*,

b/*k*, and c/*l* along the three co-ordinate axis (figure 2.4). The interplanar distance (d_{hkl}) i.e. the distance from the origin to the plane in is the projection of the vector $\frac{\mathrm{a}}{h}$ on the direction of plane normal to it, if $\frac{\mathbf{k}}{|\mathbf{k}|}$ is a unit vector normal to $\frac{\mathrm{a}}{h}$, then the projection of the vector $\frac{\mathrm{a}}{h}$ on $\frac{\mathbf{k}}{|\mathbf{k}|}$ is simply the scalar product of the two vectors and is given by,

$$d_{hkl} = \frac{\mathrm{a}}{h} \cdot \frac{\mathbf{k}}{|\mathbf{k}|} = \frac{1}{|\mathbf{k}|} \qquad \text{(following from eq.(2.2))} \qquad \text{eq. – (2.3).}$$

If we consider 2θ to be the angle between the incident and scattered waves, for $|\mathbf{k}|$ we have

$$|\mathbf{k}| = |\mathrm{R}| \sin\theta + |\mathrm{R_O}| \sin\theta = \frac{2sin\theta}{\lambda}$$

From eq's (2.1) & (2.3), we have

$$\lambda = 2d_{hkl}\sin\theta$$

For a family of lattice planes having common factor *n*, the above equation can be written as

$$n\lambda = 2d_{h'k'l'}\sin\theta.$$

The above equation is called Bragg equation.[119] It is a simplest representation of Laue equations, in terms of known wavelength, a measurable scattering angle and the interplanar spacing of the (*hkl*) family of planes.

2.4.2. Structure factor and electron density

For a crystal containing N atoms, the equation for X-ray scattering is obtained as a Fourier transform of the electron density and is given by

$$F(\mathbf{k}) = \int \rho(r)\exp(2\pi i\, \mathbf{k} \cdot r). \qquad \text{eq.}-(2.4)$$

Where, $F(\mathbf{k})$ is called the structure factor corresponding to diffraction vector **k**,

k is related to the diffraction angle θ by $|\mathbf{k}| = 2\sin(\theta)/\lambda$,

and $\rho(r)$is the electron density at position r.

One of the principal aims for applying X-ray diffraction is to elucidate the internal structure of a material. In the above equation we have expressed the structure factor as a Fourier transform of electron density, while the inverse is also true it is not straightforward to calculate the electron density. The main reason is that in a X-ray diffraction experiment we measure a quantity proportional to the amplitude of the structure factor, *I*(*hkl*).

$$I(hkl) \propto |F(hkl)|^2$$

To compute the arrangement of electron density in a unit cell given by the formula,

$$\rho(xyz) = \frac{1}{V}\sum_{h=-\infty}^{\infty}\sum_{k=-\infty}^{\infty}\sum_{l=-\infty}^{\infty} F(hkl)\exp[-2\pi i(hx + ky + lz)]$$

the crystallographer must somehow deduce the values of *F*(*hkl*) from the intensities.

2.4.3. The phase problem

In order to determine the electron density ($\rho(xyz)$) within a unit cell, we must obatin the values of $F(hkl)$. In a diffraction experiment we measure a quantity proportional to the amplitude of structure factor. The relation between the available $|F(\mathbf{k})|$ and the desired $F(\mathbf{k})$ can be explained as follows and is termed the phase problem in crystallography.

The structure factor is a complex number and can be written in a general form as,

$$F(\mathbf{k}) = A(\mathbf{k}) + iB(\mathbf{k})$$

Where, $A(\mathbf{k})$ and $B(\mathbf{k})$ are the real and imaginary parts of the complex number $F(\mathbf{k})$. If $F(\mathbf{k})$ is considered as a vector in a complex plane, the square of its length is given by

$$|F(\mathbf{k})|^2 = F(\mathbf{k})\, F^*(\mathbf{k})$$

where $F^*(\mathbf{k})$ is the complex conjugate of $F(\mathbf{k})$.

The phase of $F(\mathbf{k})$, denoted as $\varphi(\mathbf{k})$, is the angle between the vector $F(\mathbf{k})$ and the real axis $A(\mathbf{k})$, as shown in the Argand diagram (Figure 2.5).

$A(\mathbf{k})$, $B(\mathbf{k})$ and $F(\mathbf{k})$ form a right angled triangle, in which

$A(\mathbf{k}) = |F(\mathbf{k})| \cos(\varphi(\mathbf{k}))$ and

$B(\mathbf{k}) = |F(\mathbf{k})| \sin(\varphi(\mathbf{k}))$.

Consequently,

$$I(\mathbf{k}) = |F(hkl)|^2.$$

Therefore, in a diffraction experiment by measuring the intensities, we are losing information on the phases.

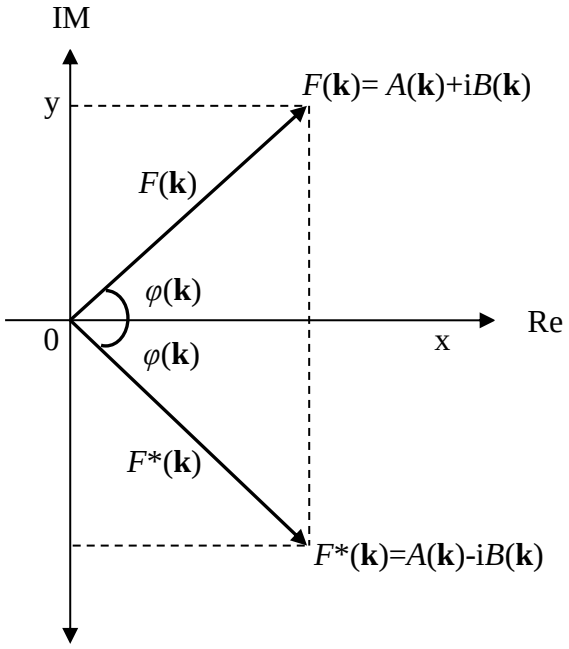

Figure 2.5: Argand diagram representing the structure factor F(**k**) as a complex number.

2.4.4. Solutions to the phase problem

Initial methods for crystal structure analysis of simple structures included extensive use of space-group symmetry and trial-and-error methods. The first systematic approach for structure determination was put forward by Patterson.

2.4.4.1. Patterson Method

The Patterson method[120,121,122] is an indirect method of solution to the crystallographic phase problem. The principle of Patterson methods is demonstrated easily by considering the diffracted intensities,

$$I(\mathbf{k}) \propto |F(\mathbf{k})|^2$$
$$= F(\mathbf{k})\, F^*(\mathbf{k})$$
$$= (\sum_{j=1}^{N} f_j \exp\ (2\pi i\ \mathbf{k}\,.\,r_j))\ (\sum_{k=1}^{N} f_k \exp\ (-2\pi i\ \mathbf{k}\,.\,r_k))$$
$$= \sum_{j=1}^{N}\sum_{k=1}^{N} f_j f_k \exp\ (2\pi i\ \mathbf{k}\,.\,(r_j - r_k))$$

Where,

N= total number of atoms in the unit cell,

f_j and f_k are the scattering factors of atoms j and k ,

r_j and r_k are the respective position vectors of atoms j and k and $\mathbf{k}$ is the diffraction vector.

The equation for electron density at a point r in crystal space can be written as

$$\rho(r) = \frac{1}{V}\sum_{\mathbf{k}} F(\mathbf{k}) \exp(-2\pi i\ \mathbf{k}\,.\,r)$$

The Patterson function $P(u)$ is the resultant function obtained from the Fourier synthesis of the above equation when $F(\mathbf{k})$ is replaced by $|F(\mathbf{k})|^2$ and is written as

$$P(u) = \frac{1}{V}\sum_{\mathbf{k}} |F(\mathbf{k})|^2 \exp(-2\pi i\ \mathbf{k}\,.\,u)$$

Where, u corresponds to the inter-atomic vectors $(r_j - r_k)$. The above equation is the same form of the electron density equation but without the term phase angle in the expression. The Patterson function can be calculated by the Fourier synthesis of $|F(\mathbf{k})|^2$.

2.4.4.2. Direct methods of estimating relative phases

These are based on the statistical methods for estimating the relative phases while considering that the electron density is never negative, and consists of isolated sharp peaks at atomic positions. The electron density map is calculated with the derived phases of the structure factors, without any prior structural knowledge. The structure factor equation can be written as,

$$F(\mathbf{k}) = \sum_{j=1}^{N} f_j\ (\mathbf{k}) \exp\ (2\pi i\ \mathbf{k}\,.\,r_j) = |F(\mathbf{k})| \exp[i\varphi(\mathbf{k})],$$

Where, r_j is the position vector of the j^{th} atom, $\varphi(\mathbf{k})$ is the phase of the structure factor corresponding to diffraction vector $\mathbf{k}$. From the above equation it can be seen that by shifting the origin by a vector p, there will be a change in the phase by an amount of $2\pi\mathbf{k}\,.\,p$. The new phase is given by $\varphi'(\mathbf{k})$ and is equal to $\varphi(\mathbf{k}) - 2\pi\mathbf{k}\,.\,p$.

Structure invariants:

$$\varphi'(\mathbf{k}) = \varphi(\mathbf{k}) - 2\pi\mathbf{k} \,.\, p$$

Considering linear combinations on both sides with integer coefficients $Z_{\mathbf{k}}$,

$$\sum_{\mathbf{k}} Z_{\mathbf{k}}\ \varphi'(\mathbf{k}) = \sum_{\mathbf{k}} Z_{\mathbf{k}}\, \varphi(\mathbf{k}) - 2\pi \,(\sum_{\mathbf{k}} Z_{\mathbf{k}}\mathbf{k}) \,.\, p$$

For a set of **k** vectors that are linearly dependent

$$\sum_{\mathbf{k}} Z_{\mathbf{k}}\mathbf{k} = 0$$

Then we have,

$$\sum_{\mathbf{k}} Z_{\mathbf{k}}\ \varphi'(\mathbf{k}) = \sum_{\mathbf{k}} Z_{\mathbf{k}}\, \varphi(\mathbf{k}).$$

The above equation shows that no matter by what vector the origin is shifted; there exists a set of phases whose linear combination is independent of the choice of origin. These phases are called structure invariants.

If we consider this in terms of single structure factor $F(\mathbf{k})$, one can deduce that the structure factor $F(\mathbf{k})$ is independent of the choice of origin when the vector $\mathbf{k}$=0.

When the product of two structure factors $F(\mathbf{k})$ and $F(\mathbf{l})$ is considered, the combined structure factor will be phase invariant when the vectors are arranged such that $\mathbf{k} = -\mathbf{l}$.

Similarly, when the product of three structure factors $F(\mathbf{k})$, $F(\mathbf{l})$ and $F(\mathbf{h})$ are considered, we can deduce that the product of the three structure factors $F(\mathbf{k})$, $F(\mathbf{l})$ and $F(\mathbf{h})$ will be independent of the choice of the origin, when the conditions $\mathbf{k} + \mathbf{l} + \mathbf{h} = 0$, or $\mathbf{k} = -(\mathbf{l} + \mathbf{h})$, are satisfied.

Structure seminvariants:

In structure invariants, the choice of the origin was completely unrestricted. However, in crystal structures, the origin of the unit cell is usually chosen at some symmetry element or intersection of symmetry elements, except for the space group *P*1. Therefore, depending on the space group, there exist certain linear combinations of phases whose values remain unchanged provided the changes are subject to space-group symmetry constraints. These phases are called structure seminvariants.

$$\varphi'(\mathbf{k}) = \varphi(\mathbf{k}) - 2\pi\mathbf{k} \,.\, p$$

From, the above equation, when p is an allowed translation vector for a particular space group, then the dot product $\mathbf{k} \,.\, p$ is an integer, in this case the phase is altered by a factor 2π, which is effectively unchanged. Such phases are called structure seminvariants.

The first attempts for determining phases of structure factor amplitudes were made by Harker and Kasper[123,124] and was based on Schwarz and Cauchy inequalities, which was later developed by Karle and Hauptman[125,126] considering the probability theory. Karle and Hauptman showed that the determinant of unitary structure factors is non-negative only if the electron density is non-negative at every point in the unit cell. A complete list of phase invariants and seminvariants for the 230 space groups were listed by Hauptman and Karle and are in a general form now listed in the *International Tables for Crystallography Volume B.*

Sayre equation: The Sayre formalisation[127] of phase determination for the structure factor amplitudes is based on two assumptions,

1. The crystal is composed of isolated identical atoms possessing identical displacement parameters and spherical symmetry,
2. A hypothetical crystal structure is considered for which the electron density is squared at each point.

Sayre's first relationship for diffraction vectors **H**, **K** and **H-K** holding the triplet relationship is given by

$$F_{\mathbf{H}} = \frac{f}{Vf^2} \sum_{\mathbf{K}} F_{\mathbf{K}} F_{\mathbf{H-K}}$$

From the above equation, it can be deduced that the phase of $F_{\mathbf{H}}$ is the equal to the phase of the summation on the right hand side, since the term $\frac{f}{f^2}$ called the shape factor term is a real and positive quantity.

2.5. Least-squares refinement

The structure obtained from Patterson method, direct methods or from any other structure solution method is an approximate structure and is not very precise in terms of the structural parameters. A more precise structure is required in order to understand the underlying chemistry of the compound. The more precise a given crystal structure, the better the values of the computed bond lengths and bond angles. The process of obtaining precise atomic coordinates from those obtained from an initial structure solution model is called refinement of the crystal structure. [128] The atomic positions *x*, *y*, *z* and the atomic displacement parameters of each atom are adjusted in a iterative process until a convergence is reached between the calculated $|F(hkl)|_c$ and observed structure amplitudes $|F(hkl)|_o$.

The best values of the atomic positions and displacement parameters are obtained when the difference (*D*) between the observed and calculated structure factor amplitudes is minimum.

$$D = \sum_{hkl} w_{hkl}[F(hkl)_o - F(hkl)_c]^2$$

where, w_{hkl} is the weight factor for each *hkl* reflections.

The refinement of the structure is considered to be complete when the changes in the individual parameters are no longer significant. The progress of refinement or the improvement in the agreement between $|F(hkl)|_o$ and $|F(hkl)|_c$ crystal structure is monitored by a term known as the residual index, **R** value, which is defined as

$$\mathbf{R} = \sum_{hkl} \left||F(hkl)_o| - |F(hkl)_c|\right| / \sum_{hkl}|F(hkl)_o|$$

The **R** value measures the precession of the results. A high value of **R** suggests that the structure is not likely to be the correct structure in terms of the assigned atoms.

2.6. Single crystal X-ray diffraction (SXRD)

In an X-ray diffraction experiment, diffraction quality crystal is selected by careful examination of the crystals under a polarising microscope. The selected crystal is mounted on the goniometer head (Figure 2.6(a)) whilst holding to a cryoloop fibre and is centered to a position on the diffractometer, at which all the axes of rotation (θ, χ, φ, ω) intersect. The X-rays generated from the X-ray source interact with the crystal and are measured by the detector as diffracted intensity.

A standard setting of single crystal X-ray diffractometer consists of (a) an X-ray generator fitted with a beam collimator and a monochromator, (b) a goniometer head, upon which the crystal to be analysed is mounted, (c) diffractometer circles (θ, χ, φ, ω), which allow the crystal to be rotated in different orientations, (d) a beam stopper, used to stop the direct beam that passes through the crystal, and (e) a detector, used to measure the diffraction peaks.

X-ray Sources:

The most common sources of X-rays available in a laboratory are conventional sealed X-ray tubes. Conventional sealed X-ray sources can be of two types, (a) sealed tubes and (b) rotating anode tubes. The X-rays used in the study were generated from a sealed X-ray tube. A sealed X-ray tube consists of a stationary anode coupled with a cathode, with both placed in a ceramic container sealed under high vacuum (Figure 2.6). Sealed X-ray tubes have very low efficiency (1%) since much of the energy of the accelerated electrons is converted into heat; hence the anode of the X-ray tube is continuously cooled by circulating cold water. A typical X-ray emission spectrum generated from a laboratory sealed tube is shown in Figure 2.6.

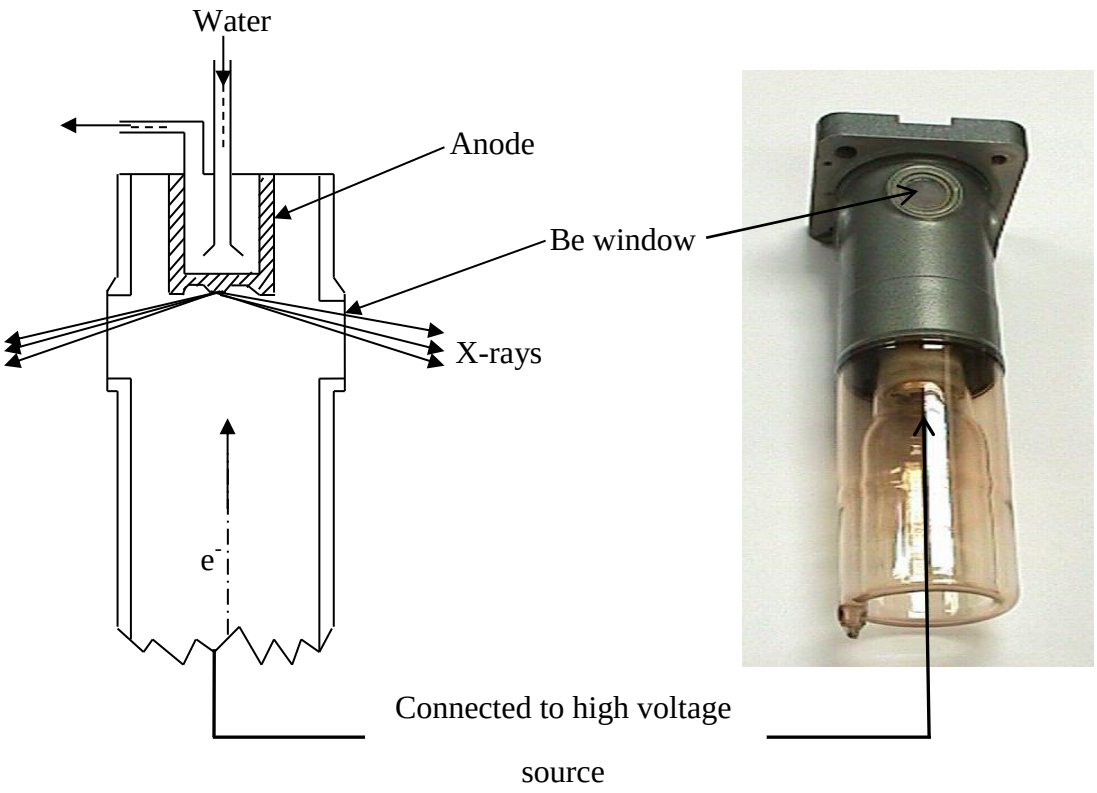

Figure 2.6: Schematic (left) and photographic (right) representation of a sealed X-ray tube

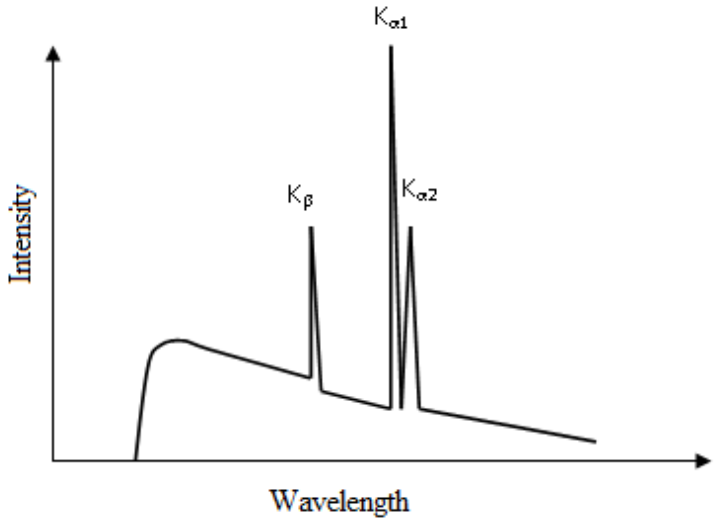

Figure 2.7: The X-ray emission spectrum generated from a typical sealed X-ray tube containing a copper anode.

Single crystal data collection for all the complexes reported here were performed using a Bruker Nonius X8-Apex2[129] CCD diffractometer, equipped with a graphite monochromatised Mo Kα X-ray source (λ = 0.710173 Å). An Oxford Cryosystems Cryostream was used to cool the crystals to 100 K prior to data collection. The data collection for most of the crystals presented here is done at 100 K to reduce the thermal vibrations.

Indexing, Data collection and structure solution:

Indexing of the reflections and the data collection was achieved using the automated software SMART. The indexing process involves recording at least 20 reflections at known values of θ, χ, φ, ω angles. These 20 or more reflections are arranged in an increasing order of magnitude of the diffraction vector. The three shortest non co-planar vectors are chosen as basis vectors of the reciprocal lattice and are arbitrarily assigned indices of 100, 010 and 001. By the method of approximation, the orientation matrix and the corresponding unit cell dimensions are obtained. The initial values of cell parameters are refined through least-squares refinement to obtain better values with standard deviations.

Based on the range of indices *hkl* observed in the indexing process and the wavelength of the radiation used, the intensity data collection is planned and executed automatically by the computer. The entire data set is then reduced by integration using the SAINT package. Lorentz and polarization corrections are applied to all the data, followed by correction for absorption using SADABS[130] programme. The space group symmetry of the crystals is determined by sorting the systematic absences using the XPREP programme. Crystal structures of the compounds were solved by direct methods using SHELXS[131] and are refined on full matrix by least-squares refinement process using values of F or F^2 in CRYSTALS.[132] All non-hydrogen atoms were refined with anisotropic displacement parameters.

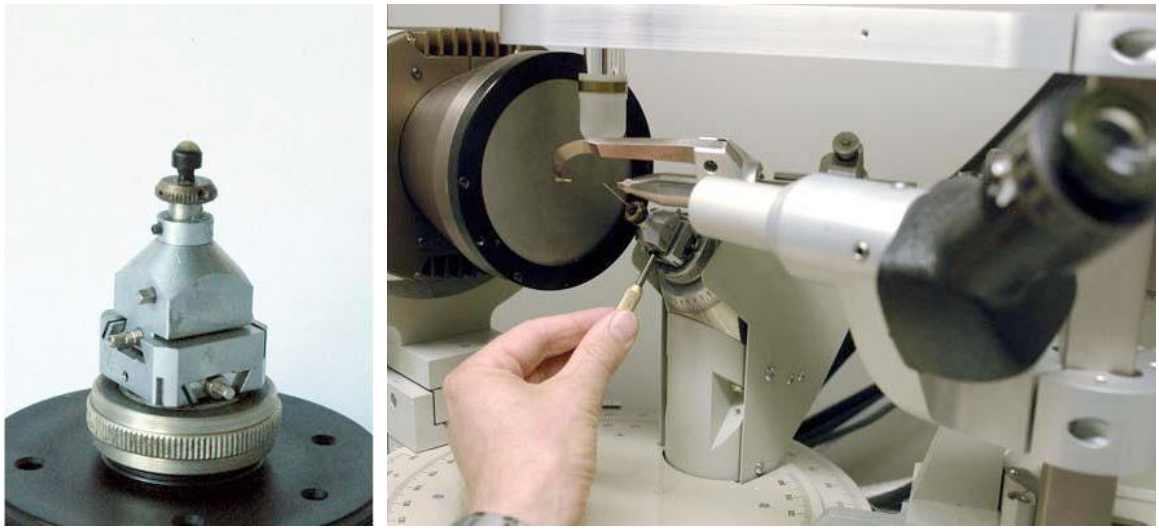

Figure 2.8: (a) Goniometer head (b) centering the single crystal on the diffractometer.

All non-hydrogen bonding hydrogen atoms were placed geometrically and refined with the isotropic displacement parameter fixed at 1.5 times Ueq of the atoms to which they are

attached. Hydrogens involved in hydrogen-bonding interactions were located *via* the difference Fourier map inspection and were refined isotropically.

2.7. Spectroscopic methods

2.7.1. Nuclear Magnetic Resonance (NMR)

The basic principle of NMR spectroscopy is based on the property of nuclei possessing spin. Any spinning nucleus will have an intrinsic nuclear spin quantum number, *I*. The most common nucleus for NMR studies, the proton, has a spin of 1/2. This spin half nucleus interacts with the external magnetic field by giving rise two energy levels, characterised by the quantum number '*m*'. In the case of spin half nuclei the two values of *m* are $-\frac{1}{2}$ and $+\frac{1}{2}$. The energy level with $m = +\frac{1}{2}$ is denoted by α and is termed "spin up". The energy level with $m = -\frac{1}{2}$ is denoted by β and is termed "spin down".

In any spectroscopic technique there are selection rules, in the case of NMR, the selection rule is that only the transitions that have a change in *m* value corresponding to ± 1 are allowed.

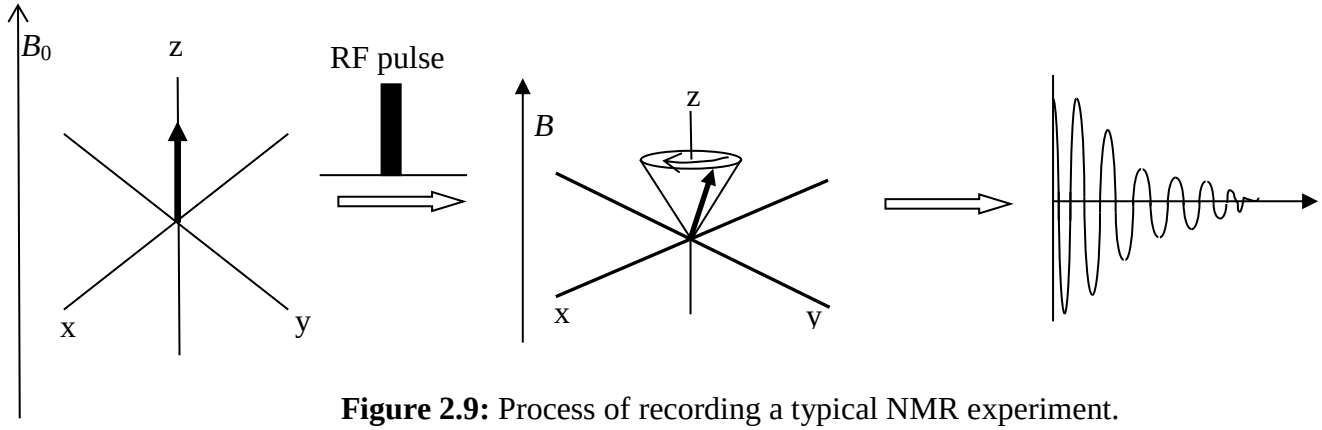

Figure 2.9: Process of recording a typical NMR experiment.

The typical NMR experiment is shown in Figure 2.9. On applying a radio frequency pulse, the bulk magnetisation vector under the influence of the external magnetic field precesses at a constant angle β to form a cone and is called Larmor precession.

If the external magnetic field strength is B_o, the frequency of the Larmor precession (ω_0) is given by

$$\omega_0 = -\gamma B_0,$$

in terms of frequency (ν_o) in Hertz,

$$\nu_0 = -\frac{1}{2\pi}\gamma B_0$$

Where, γ is the gyromagnetic ratio.

In a typical ^{1}H-NMR experiment, the sample under investigation is placed under the external magnetic field and allowed to equilibrate for a fixed amount of time, after which the radiofrequency (RF) power is switched on and a 90^{o} RF pulse is applied to the sample to rotate the bulk magnetization by 90^{o}. After the RF pulse is switched off, the induced current from the sample is recorded as a signal by the same RF coil wound around the sample in the xy-plane.

^{1}H-NMR spectra for all the molecular complexes studied here were recorded using a Bruker 300 MHz spectrometer after dissolving the compounds in DMSO-d_6. ^{1}H chemical shift values are reported on the δ scale.

2.7.2. Infrared spectroscopy

The infrared (IR) range falls in the region between the microwave and visible regions of the electromagnetic spectrum. It is divided into three regions; the near-, the mid- and the far-infrared regions. The mid-infrared region, possessing wavelengths approximately 4000–400 cm^{-1} is of importance to study the molecular vibrations in organic solids. For a given vibrational mode to be infrared active it must be associated with a change in dipole moment. Of the many vibrational modes in a molecule, only a few atoms have large displacements while the rest of the molecule is almost stationary. The frequency of such vibrations is characteristic for that particular functional group. The infrared spectrum of a compound is unique (except for enantiomers) to that particular compound and is used to identify that particular compound.

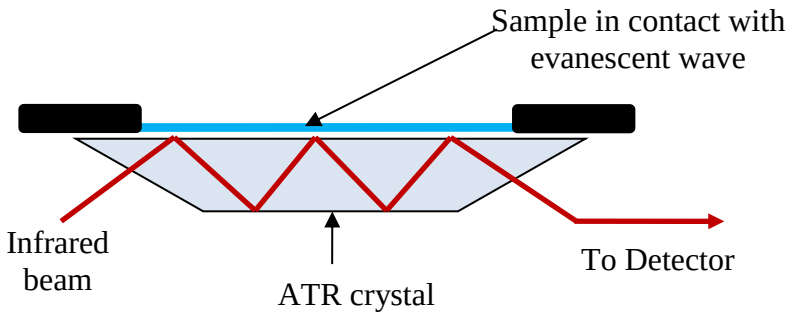

Figure 2.10: A multiple reflection ATR system.

Infrared spectroscopic data for all the molecular complexes presented in the thesis were recorded using a Perkin–Elmer 100 attenuated total reflectance (ATR) spectrometer operating under diffuse reflectance geometry. ATR is a technique where the sample to be analysed is

placed in contact with the internal reflection element or ATR crystal (Germanium crystal), acting as a sensing element allowing to record the spectrum of the sample. A typical ATR setup is shown in Figure 2.10. Prior to recording an IR spectra, the crystal is cleaned and background spectrum collected. The sample was then analysed by placing a pinch of the compound on the crystal area fitted with a pressure arm positioned exactly over the sample/crystal area. Force is then applied through the pressure arm on to the sample by pushing it into close contact with the crystal. The spectrum is recorded based on the total internal reflection property of the crystal resulting in the formation of an evanescent wave. The incident wave is passed through the crystal such that it reflects at least once from the internal surface of the crystal, in contact with the sample. The evanescent wave formed by the reflected beam extends into the sample which is recorded by the detector as spectrum of the sample in absorption bands.

2.8. Thermo analytical methods

2.8.1. Differential Scanning Calorimetry (DSC)

Working principle: During a typical DSC analysis, a test sample and the reference material are subjected to a programmed temperature change. Thermal energy is altered to the sample or the reference containers in order to maintain the sample and reference at the same temperature. The amount of thermal energy added is monitored in terms of thermal transitions.

The DSC data for all the compounds reported here were performed using a Seiko model DSC-6200 instrument. The samples were weighed into DSC aluminium pans, crimped with a pinhole in the lid and analysed over the temperature range 25–280 ^{o}C using a constant heating rate of 10 ^{o}C/min. The data were processed using Muse Measurement v.5.4 (Build 263) software.

2.8.2. Thermogravimetric Analysis

Thermogravimetric (TG) analysis provides a quantitative measurement of any weight changes associated with thermally induced transitions. It records directly the loss in weight as a function of temperature or time for transitions that involve dehydration or decomposition. Thermogravimetric curves are characteristic of a given compound or material due to the unique sequence of physical transitions that occur over definite temperature ranges. The rates

of these chemically induced transformations are often a function of the molecular structure. The changes in weights may involve physical or chemical bonds forming and breaking at elevated temperatures. These processes may involve volatile products or form reaction products that result in a change in weight of the sample.

For TG/DTA analysis, approximately 5 mg of material into an open aluminium pan and loaded into a simultaneous thermogravimetric/differential thermal analyser (TG/DTA) and held at room temperature. The sample was then heated at a rate of 10°C/min from 25°C to 300°C during which time the change in sample weight was recorded along with any differential thermal events (DTA) compared to the reference. Nitrogen was used as the purge gas, at a flow rate of 100 cm^3/min.

2.9. Cambridge Structural Database in crystal engineering

A large number of organic and organo-metallic crystal structures are organised and contained within the Cambridge Structural Database (CSD).[133] While there are other crystallographic databases,[134] CSD is suitably organised for crystal engineering studies. There are at present 577,833 structures in CSD[135] consisting of different classes of compounds, which include organic and organometallic compounds. The availability of large numbers of structural data in the form of crystallographic information files (CIFs) provides an effective way to extract information of how chemical compounds are arranged within in a crystal. The development of new tools for harnessing crystallographic information available in the CSD has allowed for effective crystal engineering.

The utilisation of CSD for crystal engineering studies focuses on features of crystal structures that are not immediately apparent for individual crystal structures. For example searches based on molecular symmetry, molecular connectivity, molecular geometry, supramolecular geometries and connectivity or any other supramolecular feature can be performed. A range of possible search options are available through the graphical interface *ConQuest*[136] software. The CSD analysis is performed using CSD v 5.23 (2012 release with Nov 2011 updates).

Chapter 3: Crystal engineering methods for the synthesis of paracetamol co-crystals

3.1. Introduction

Paracetamol (PAC), also known as acetaminophen is a widely used analgesic and antipyretic drug used in the treatment of fever, headaches, and other major aches and pains. It belongs to a class of drugs known as aniline analgesics. In its molecular structure (Scheme 3.1) paracetamol contains two conventional hydrogen bond donors, a phenolic O-H and the amidic N-H, and three acceptor groups, an amide oxygen, phenolic oxygen and amidic nitrogen. In the crystalline form, these hydrogen bond donor and acceptor groups arrange differently relative to the carbon backbone to form three known polymorphs of paracetamol. The first polymorph of paracetamol (form-I) crystallises in monoclinic system, the second (form-II) and the third (form–III) forms crystallise in orthorhombic system. Apart from the three known crystalline forms, paracetamol is also known to exist in an amorphous form. Amongst the three known crystalline forms, the monoclinic form-I (Figure 3.1) is the thermodynamically stable form and is the active ingredient in all the tablets containing paracetamol. In the crystal structure of paracetamol form-I, molecules are arranged in a herringbone pattern to form puckered hydrogen-bonded sheets (Figure 3.2). Due to the arrangement of the molecules in puckered hydrogen-bonded sheets, the molecules in form-I do not slip over one another upon compression. Therefore, paracetamol form-I requires a wet granulation step or addition of other binding agents called plasticisers prior to the tabletting process, adding significant cost to the production.[137] Considering the higher costs involved in the production of paracetamol, much of the research on paracetamol is focussed on (a) identifying facile methods for the crystallisation of form-II[138] and (b) identifying new crystalline polymorphic forms of paracetamol and (c) obtaining new co-crystal forms of paracetamol with better compression properties.

Paracetamol form-II crystallises in an orthorhombic crystal system with *Pbca* as the space group. It is a metastable form and is known to convert to form-I over time.[139] In its crystal structure the molecules arrange to form flat hydrogen-bonded sheets[140] (Figure 3.3) and it is therefore amenable to direct compression. While there are serious problems in isolating paracetamol form-II on an industrial scale[141], several research groups have recently reported specific methods for the selective crystallisation of paracetamol form-II. In this context, the article published by Thomas *et al.*,[142] is of particular importance. It is reported that in the presence of some co-formers (co-crystal forming agents) like substituted benzoic acids,

paracetamol form-II can be produced in 100% yield. In addition, it is also observed that altering the API:coformer ratio can have a significant effect on the yield of paracetamol form-II produced. Crystallisation of paracetamol with 4-aminobenzoic acid in a 4:1 mole ratio resulted in the isolation of a mixture of form-I and form-II, while crystallisation of paracetamol with 4-aminobenzoic acid in 1:1, 2:1 molar ratios resulted in a 100% yield of form-II. Interestingly, the form-II obtained by the above method in quantitative yield is stable up to one year. Earlier reports of obtaining paracetamol form-II were based on slow cooling of melts and *via* crystallisation from ethanolic solution when seeding technique is applied. While the melt crystallisation technique is not reproducible, the yield of form-II through crystallisation from ethanolic solution was reported to be very low (less than 30%) at optimised conditions of crystallisation.

The third polymorph of paracetamol (form-III), known for a decade,[143] is the most unstable form of paracetamol. While the structural information from single crystal X-ray diffraction still remains elusive, Marc-Antoine *et.al.* recently reported the crystal structure of this polymorph determined from powder X-ray diffraction methods.[144] The molecule crystallises in orthorhombic crystal system with *Pbca* as the space group. The authors also noticed a close relationship between the cell parameters of form-II and form-III. The cell dimensions of form-II and form-III are related in the following way: form-III a = form-II b, 2 $*$ form-III b = form-II c, and form-III c = 2 $*$ form-II a. The close relationship in the cell parameters of form-II and form-III is attributed to the fact that paracetamol molecules in both form-II and form-III arrange to form a two-dimensional hydrogen-bonded network (Figure 3.4). The difference in the two orthorhombic forms is due to the different orientations of the benzene rings with respect to the plane formed by the two-dimensional hydrogen bonding network.

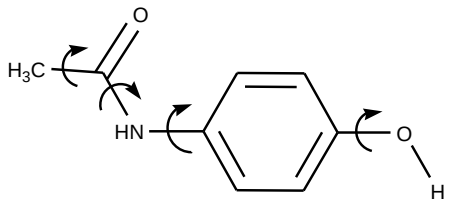

Scheme 3.1: Molecular structure of paracetamol, indicating rotational bonds.

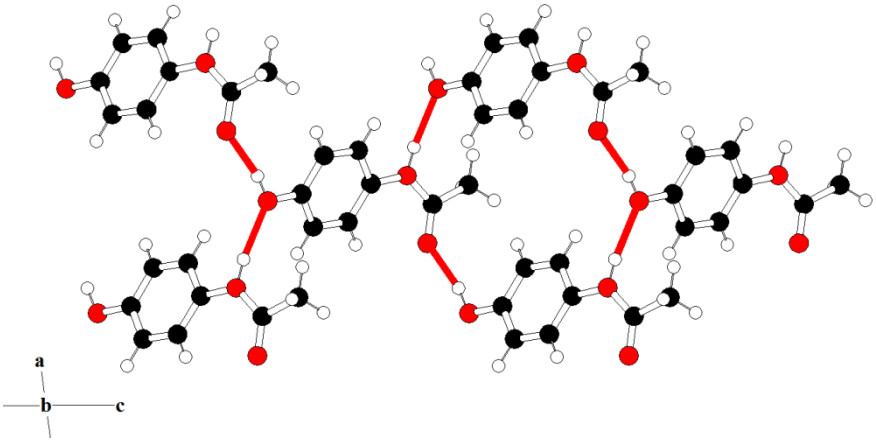

Figure 3.1: Packing arrangement of paracetamol form-I, viewed along '*b*'. Solid red lines represent intermolecular hydrogen bonds. Key: nitrogen, blue circles; oxygen, red circles; carbon, black circles; hydrogen, small white circles.

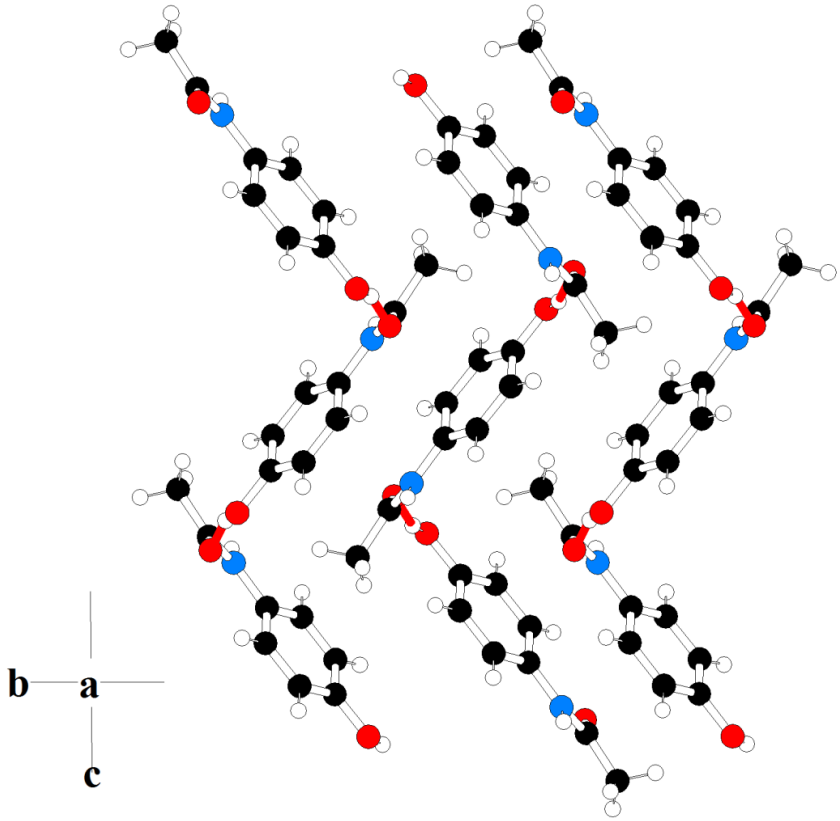

Figure 3.2: Packing arrangement of paracetamol form-I, viewed along '*a*'.

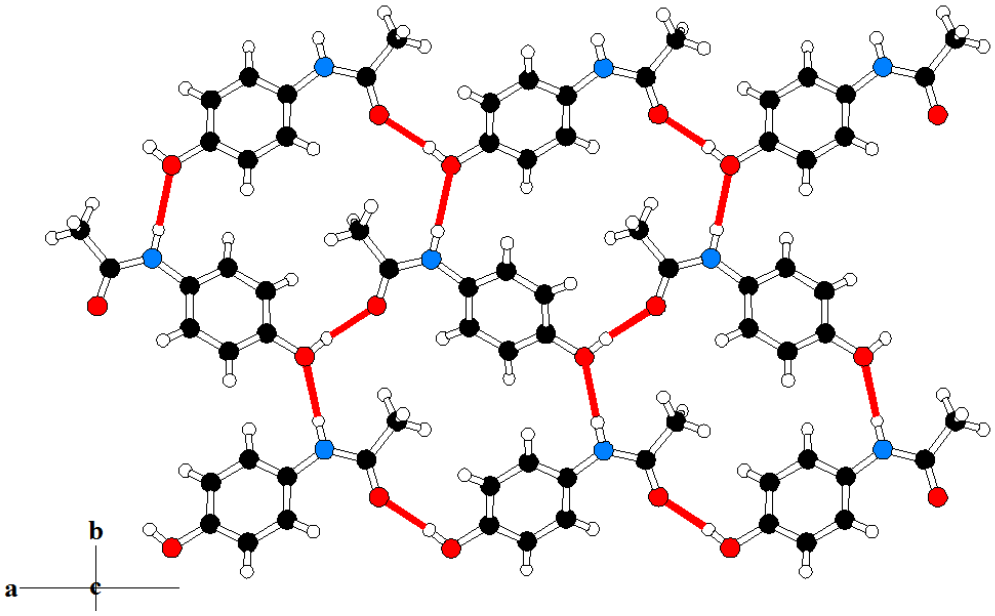

Figure 3.3: Packing arrangement in paracetamol form-II, viewed along '*c*'.

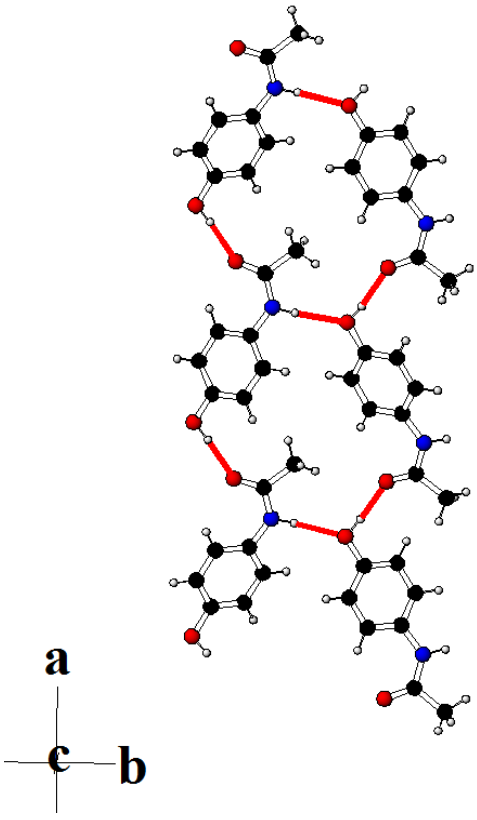

Figure 3.4: Packing arrangement in paracetamol form-III, viewed along '*c*'.

In-order to identify developable forms of paracetamol with better compression properties, several research groups have synthesised and structurally characterised multi-component crystalline forms of paracetamol involving *N,N'*-dimethylpiperazine, 4,4'-bipyridine, *N*-methylmorpholine, morpholine, 1,4,8,11-tetraazacyclotetradecane, 1,4-diazabicylco[2,2,2]octane, ethanol, water, piperazine and 1,4-dioxane as co-crystal formers (CCFs) or solvates.[145] In this context, the co-crystals of paracetamol published by Karki *et.al.* is of importance. Four new co-crystals of paracetamol with theophylline, oxalic acid, naphthalene and phenazine as co-crystal formers were synthesised and structurally characterised. These co-crystals are reported to have better compression properties when compared to that of paracetamol form-II.[146]

In the chapter presented here a crystal engineering-based method for the synthesis of new co-crystal forms of paracetamol is presented. Initially, the Cambridge Structural Database (CSD) was used as a means to identify potential CCFs; this was followed by co-crystal screening by mechanochemical crystallisation techniques to identify new co-crystals of paracetamol.

The crystal structures of both the paracetamol forms (form-I and form-II) possess identical hydrogen bonds between the pac molecules. In both form-I and form-II the phenolic O-H group of paracetamol acts both as a hydrogen bond donor and acceptor, thereby acting as a bridge between two other paracetamol molecules through N-H···O and O-H···O interactions.

While the hydrogen bonds formed in the two polymorphic forms are identical, the two crystalline forms of paracetamol differ in the manner in which the paracetamol molecules are arranged within the crystal lattice. Taking the hydrogen bond distance as the criterion, the strongest hydrogen bonds (Table 3.1) in both form-I and form-II are observed between the phenolic O-H group and the amide oxygen (d(H···O) = 1.77Å) resulting in the O-H···O hydrogen bonds. In addition to the O-H···O interactions, the N-H donors of paracetamol participate in N-H···O hydrogen bonds, where the phenolic oxygen acts as an acceptor. These interactions are weaker (d(H···O) = 2.00Å) compared to the O-H···O hydrogen bonds. In order to synthesise co-crystals of paracetamol, it is necessary to rearrange or replace the existing hydrogen bonds in the paracetamol with interactions from the CCFs. The CSD database search serves as a starting point to identify suitable co-crystal former molecules. Targeting the phenolic-OH group of paracetamol, the CSD search is conducted to identify a series of functional groups which form complementary hydrogen bonds with the phenolic-OH groups. Based on the functional groups identified from the CSD search, a series of molecules

possessing functional groups which can form complementary hydrogen bonds with paracetamol were selected for co-crystal screening (Scheme 3.2).

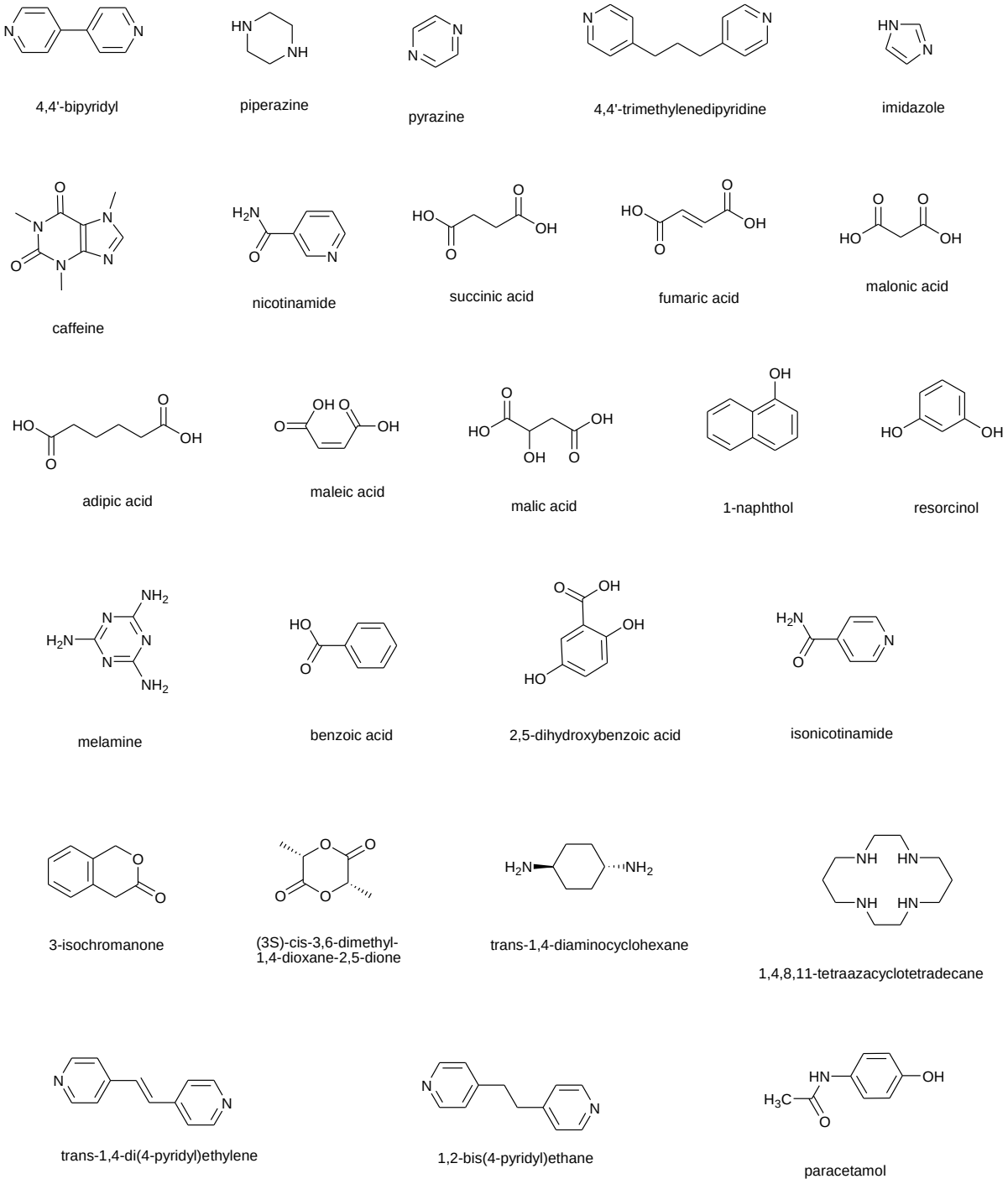

Scheme 3.2: Chemical structures of explored co-crystal formers and paracetamol.

Table 3.1: Geometric parameters of hydrogen bonds in crystalline paracetamol form-I.

	hydrogen bond	*d*(H···A) (Å)	*d*(D···A) (Å)	θ (^{o}) (D-H···A)	(H···A) vdW cutoff contraction (%)
Paracetamol	O-H···O=C	1.77	2.66(3)	166.1	36
Paracetamol	N-H···O	2.00	2.91(2)	163.8	26

3.2. CSD analysis

Potential co-crystal formers were identified by the CSD analysis using the CSD version 5.33 (November 2011) + 2 updates. In the CSD analysis, the following criteria were applied: 1. The search is restricted only to organic crystal structures for which the three-dimensional co-ordinates have been determined. 2. Crystal structures with $R \leq 7.5\%$ were only retained in the search. 3. Disordered structures, structures known to have errors and polymeric species were excluded from the search. The summary of the results from the CSD search are presented in Table 3.2. The database search was conducted by targeting the phenolic OH group of paracetamol. The results of the CSD search are divided into two categories: raw and refined. The raw search results represent the occurrence of particular functional groups in the presence of other functional groups. The refined search results represent the occurrence of that particular functional group with no additional functional groups in the immediate vicinity. From the search it is identified that there are 8009 crystal structures in the CSD database which contain at least one phenolic O-H moiety. These 8009 crystal structures could be stabilised through combination of supramolecular homosynthons and supramolecular heterosynthons depending on the functional groups present in the molecules.

Of the identified 8009 crystal structures 13% of them possess the O-H···O-H supramolecular homosynthon synthon while in the remaining crystal structures the phenolic O-H group participates in other supramolecular heterosynthons. The raw data of the CSD search reveals that the percentage occurrence of the O-H···N supramolecular heterosynthon in molecules containing phenolic O-H, aromatic nitrogen or amines is between 42-52%. In the absence of other functional groups the percentage occurrence of the O-H···N supramolecular heterosynthon increases to 54% and 64% respectively for pyridyl and amines functional

groups. In the case of structures containing the phenol and amide functional groups, the raw data indicates that the percentage occurrence of the amide···amide supramolecular homosynthon is predominant when compared to the occurrence of phenolic O-H···amide heterosynthon. However, the phenolic O-H···amide interactions are predominant in the refined data. In the crystal structures containing phenolic O-H and carboxylic acid groups, in both the raw and refined data the supramolecular heterosynthons formed between the phenolic O-H and carboxylic acid groups prevail over the acid-acid and OH···OH supramolecular homosynthons. The CSD data of crystal structures containing the phenol and amine functional groups indicate that the phenol-amine interactions formed through O-H···NH_2 supramolecular heterosynthons are more common when compared to the O-H···OH supramolecular homosynthons. In summary, the CSD data on crystal structures suggest that molecules containing phenol OH groups have a marked preference for the formation of supramolecular heterosynthons over supramolecular homosynthons.

Taking into consideration the percentage of occurrence of the supramolecular heterosynthons observed in refined searches, molecules containing at least one of the functional groups involving aromatic nitrogen, amides, carbonyl groups, carboxylic acids, and amines were selected as potential co-crystal formers (Scheme 3.2). Following the selection of potential co-crystal formers, experimental co-crystal screening was conducted using a solvent drop grinding technique of co-crystallisation.

In the solvent drop grinding screening process, stoichiometric amounts of the API (paracetamol) and each potential co-crystal former were ground together for *ca.* 5 min with a mortar and pestle in the presence of a solvent component (15 μl of solvent per 50 mg of starting materials). The grinding experiments were conducted in seven different solvent systems which included methanol, ethanol, acetonitrile, chloroform, *n*-propanol, tetrahydrofuran, and acetone. The solvents were chosen to contain at least one representative from each of the polar protic, polar aprotic, and nonpolar solvent categories. In addition, care was taken to include a wide range of dielectric constants, ranging from 4.8 to 37.5. The polycrystalline materials obtained from the solvent drop screening experiments were analysed by PXRD using a Bruker D8 Discover instrument. The details of the instrument are given in Section 2.3. Analysis by powder X-ray diffraction revealed that for critical PAC/CCF ratios, the reflections arising from the starting materials were absent when *trans*-1,4-diaminocylcohexane, 1,2-bis(4-pyridyl)ethane (BPEA), 1,2-di(4-pyridyl)ethylene (BPEE) and 1,4,8,11-tetraazacyclotetradecane (cyclam) were used as co-crystal formers. This indicates the

formation of a new phase in each of the cases. In order to study the intermolecular interactions and the arrangement of molecules in the material, suitable single crystals were obtained by the slow evaporation method and the crystal structure determined by SXRD. The instrument details of instrument used for determining crystal structures are given in Section 2.6.

Table 3.2: Summary of the results from the search of Cambridge Structural Database (CSD).

functional groups present[b]	raw data[c]			refined data[d]			Range/Å	Mean distance/Å
	No. Of structures	homosynthons	Heterosynthons	No. of structures	homosynthons	heterosynthons		
OH	8009	1023 (13%)	-	3490	316 (9%)	-	2.41-3.04	2.805(2)
OH and N_{arom}	580	62 (11%)	302 (52%)	160	11 (7%)	86 (54%)	2.51-3.07	2.735(3)
OH and $CONH_2$	119	66 (55%) $CONH_2\cdots O{=}CNH_2$	38 (32%) $OH\cdots O{=}CNH_2$	44	11 (32%) $CONH_2\cdots O{=}CNH_2$	26 (76%) $OH\cdots O{=}CNH_2$	2.54-3.03	2.707(3)
		7 (6%) OH···OH	31 (24%) $OH\cdots NH_2CO$		2 (9%) OH···OH	24 (70%) $OH\cdots NH_2CO$	2.62-3.09	2.812(4)
OH and O=C	2592	269 (10%) OH···OH	1136 (44%) OH···O=C	396	26 (7%) OH···OH	166 (42%) OH···O=C	2.42-3.04	2.745(2)
OH and COOH	683	230 (33%) COOH···O=C(OH)	387 (56%) OH···O=C(OH)	86	35 (41%) COOH···O=C(OH)	58 (67%) OH···O=C(OH)	2.38-3.02	2.672(3)
		23 (4%)OH···OH	362 (53%) OH···OHC=O		6 (7%) OH···OH	55 (64%) OH···OHC=O	2.61-3.08	2.812(2)
OH and NH_2	427	28 (7%) OH···OH	179 (42%) $OH\cdots NH_2$	225	13 (6%) OH···OH	101 (64%) $OH\cdots NH_2$	2.56-3.07	2.848(4)

a- The following parameters were used as search criteria: 3D-coordinates determined, only organic crystal structures with R≤7.5% were included in the search while structures with disorder and errors, and polymeric species were excluded. The search was performed on CSD Version 5.33 (November2011) + 2-updates.

b- A search for molecules containing the specified functional group(s) either exclusively or in conjunction with other groups.

c- The raw search results refer to the specified functional group(s) including occurrences where other groups may be present.

d-The refined search results refer to the specified functional group(s) in the absence of other groups in the immediate vicinity.

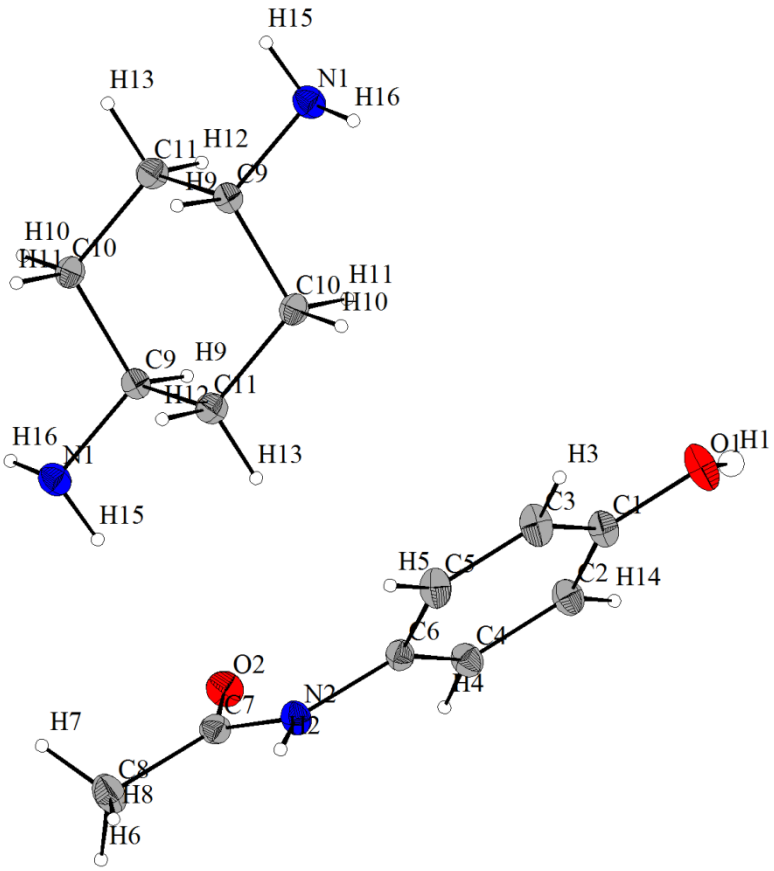

Figure 3.5: ORTEP plot of co-crystal (**1**) (The displacement ellipsoids are drawn at the 50% probability level and atoms in the asymmetric unit are labelled). Key: nitrogen, blue circles; oxygen, red circles; carbon, grey circles; hydrogen, small white circles.

3.3. Results and discussion

3.3.1. Co-crystal (1) [(paracetamol)$_1$-(*trans*-1,4-diaminocylcohexane)$_{0.5}$]

Synthesis of co-crystal (1)

Single crystals of co-crystal (**1**) were obtained by dissolving paracetamol (302 mg, 2.00 mmol) and *trans*-1,4-diaminocyclohexane (114 mg, 1.00 mmol) in 3 mL of methanol. Colourless crystals of (**1**) were obtained after four days when the solution containing PAC/CCF was allowed to stand at room temperature.

The ^{1}H-NMR spectrum on isolated single crystals of co-crystal (**1**) was recorded in DMSO-d$_6$ to confirm the PAC/CCF ratio. ^{1}H chemical shift values are reported on the δ scale. ^{1}H-NMR (300 MHz, DMSO-d$_6$) of the co-crystal (**1**): δ 9.64 (s, 2H), 7.32 and 6.66 (AA′XX′, 2 × 4H), 3.97 (br. s, 6H), 2.45 (m, 2H), 1.97 (s, 6H), 1.68 (m, 4H), 1.00 (m, 4H). The integral values in

the ^{1}H-NMR data suggests that the API and the CCF exists in 2:1 molar ratio. (Appendix A.1.1)

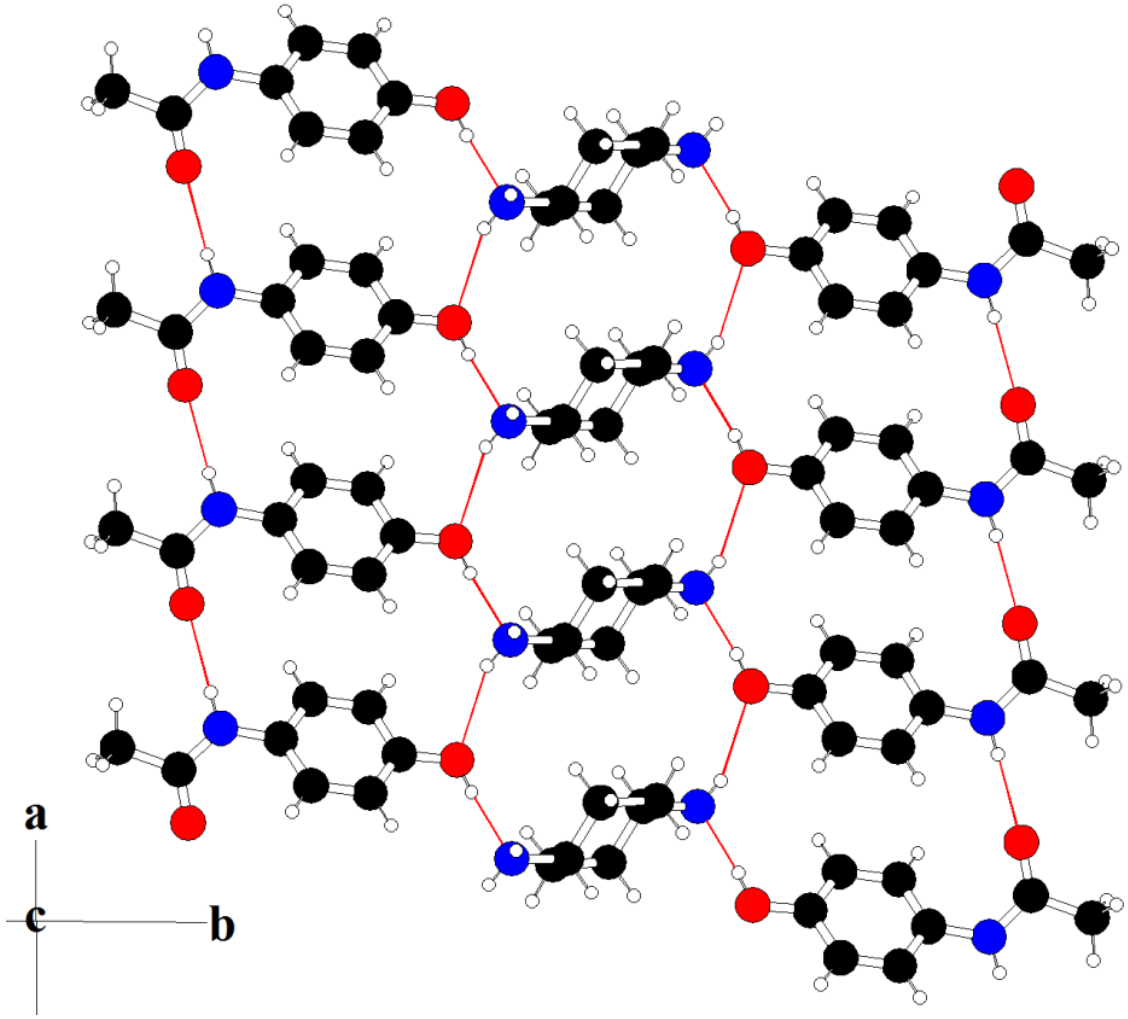

Figure 3.6: The crystal packing arrangement in co-crystal (**1**) viewed along [001].

Crystal structure description of co-crystal (1)

Structural analysis by SXRD revealed the structural features in co-crystal (**1**). Figure 3.5 represents the local co-ordination and atom numbering scheme in (**1**). The asymmetric unit of (**1**) consists of one molecule of paracetamol and half molecule of *trans*-1,4-diaminocyclohexane (Figure 3.5). The crystal structure of (**1**) suggests that the CCF, *trans*-1,4-diaminocylcohexane occupies the inversion centre. (**1**) crystallises in the triclinic crystal system with $\bar{P}1$ as the space group. The full details of the crystallographic information of (**1**) are presented in Table 3.5.

In (**1**), the paracetamol molecules are hydrogen-bonded through N(2)-H(2)···O(2) interactions. These interactions lead to the formation of chains, denoted as **C**(4), extending

infinitely along the *a* crystallographic axis. Two adjacent paracetamol molecules are cross linked by the co-crystal former through O(1)-H(1)···N(1) and N(1)-H(16)···O(1) hydrogen bonding interactions (Figure 3.6). The two adjacent paracetamol molecules and the co-crystal former arrange to form an asymmetric two-dimensional hydrogen-bonded network as shown in Figure 3.6. This asymmetric two dimensional hydrogen-bonded network extends infinitely on both ends of the CCF to form hydrogen-bonded layers of paracetamol and CCF (Figure 3.7). In addition to these hydrogen bonds, several weak and N(1)-H(15)···O(2) interactions between the two-dimensional networks extend the structure into the third dimension.

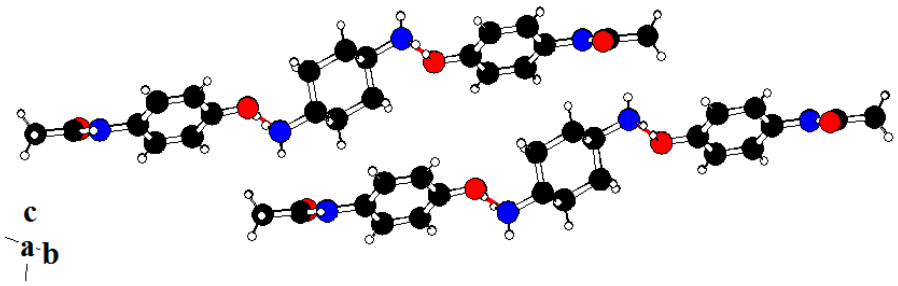

Figure 3.7: Packing arrangement showing hydrogen-bonded layers in co-crystal (**1**).

Table 3.3: Geometric parameters for the hydrogen bonds in co-crystal (**1**)

Hydrogen bond	*d* (H···A)/Å	*d* (D···A)/Å	*θ* (D-H···A)/°	(H···A) vdW cutoff contraction / %
N(2)-H(2)···O(2)	2.06	2.96(2)	174.1	23
O(1)-H(1)···N(1)	1.81	2.68(2)	169.9	33
N(1)-H(16)···O(1)	2.26	3.15(4)	169.9	17
N(1)-H(15)···O(2)	2.32	3.16(5)	158.0	15

A comparison (Figure 3.8) of the simulated powder pattern generated from the single crystal data with the powder pattern of the material obtained from solvent drop grinding experiment indicates that the single crystal is representative of the bulk material.

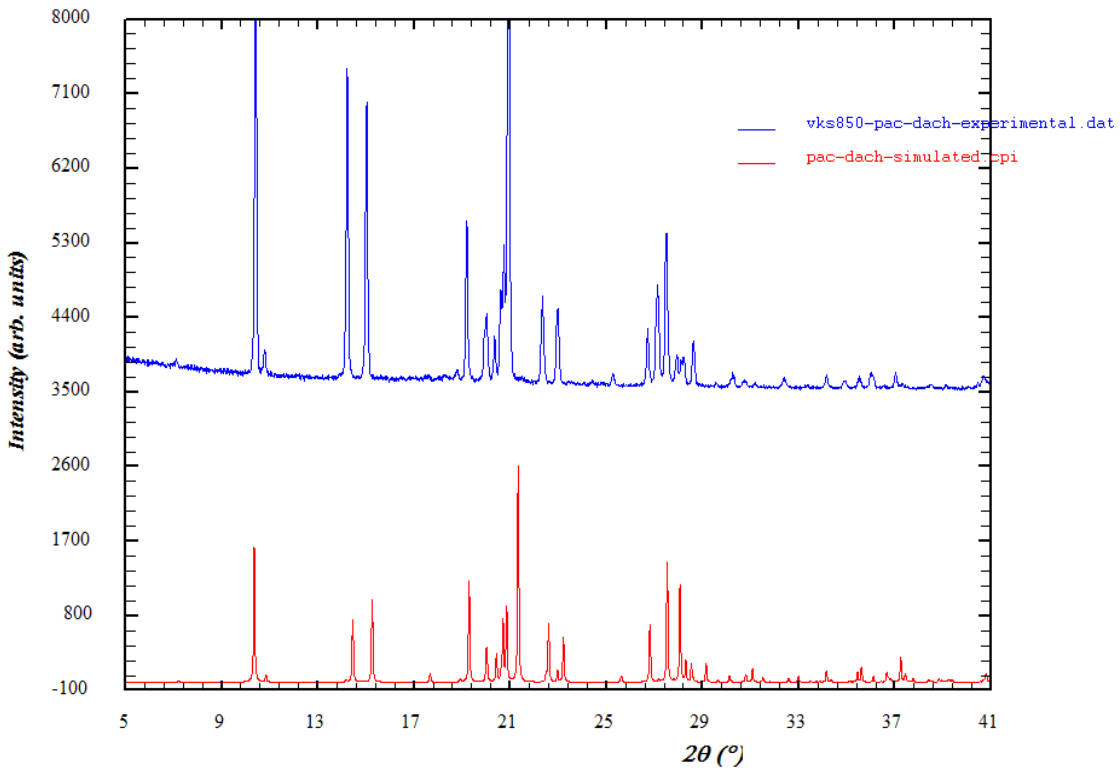

Figure 3.8: Comparison plot of powder X-ray data (blue pattern) *vs* single crystal simulated powder X-ray patter (red) of co-crystal **(1).**

The DSC thermogram of co-crystal (**1**) shows a sharp endotherm with an onset temp of 154.0 °C, corresponding to the melting of the co-crystal (**1**) (Figure 3.9). The thermal events following this could be due to the decomposition of the material. The melting temperature of co-crystal (**1**) is significantly lower than the melting temperature of paracetamol form-I (Figure **3.10**), which melts at 172.1 °C possessing an onset temperature of 168.8 °C. This suggests that the cohesive energy in co-crystals (**1**) are significantly lower when compared to that of paracetamol form-I. This is manifested in terms of comparatively weak hydrogen bonding interactions when compared to paracetamol form-I (Table 3.1and Table 3.3).

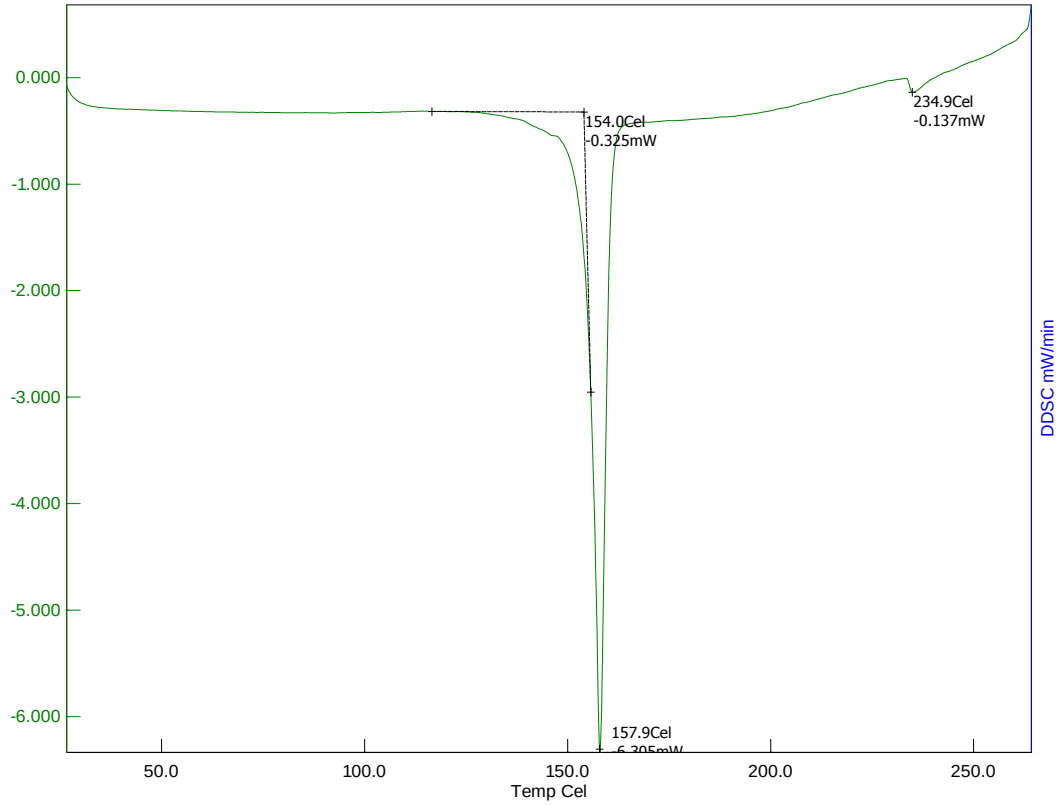

Figure 3.9: DSC of co-crystal (**1**).

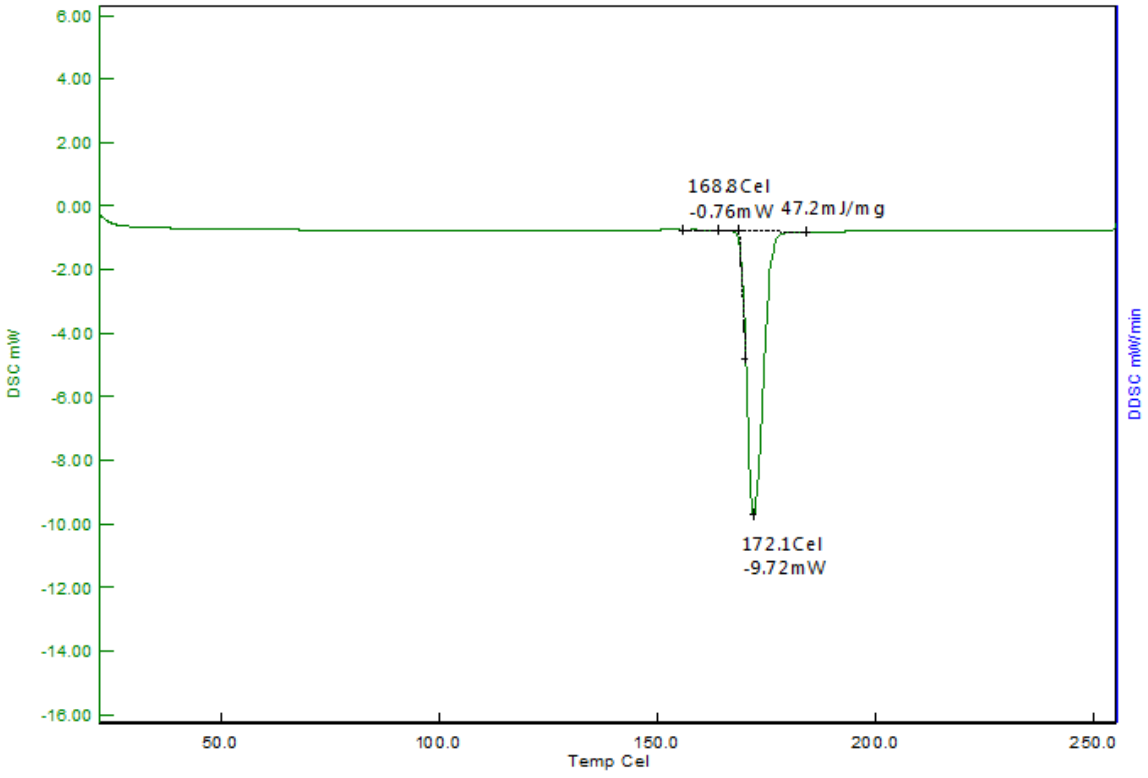

Figure 3.10: DSC of paracetamol form-I.

3.3.2. Co-crystal (2) [(paracetamol)$_{2.0}$-(1,2-di(4-pyridyl)ethylene)$_{1.0}$-(MeOH)$_{1.0}$]

Synthesis of co-crystal (2)

Diffraction quality crystals of co-crystal (**2**) were obtained from a methanol solution containing 2 mmol (302 mg) of paracetamol and 1 mmol of 1,2-di(4-pyridyl)ethylene (182 mg). Pale yellow coloured crystals of co-crystal (**2**) were isolated after five days when the solution was allowed to stand at room temperature for crystallisation.

The ^{1}H NMR spectrum of co-crystal (**2**) indicates the presence of 1 molecule of methanol while the API-CCF ratio is 2:1. δ ^{1}H NMR (300 MHz, DMSO-d_6) of the co-crystal (**2**): 9.65 (s, 2H), 9.16 (br. s, 2H), 8.60 and 7.60 (AA'XX', 2 × 4H), 7.53 (s, 2H), 7.34 and 6.68 (AA'XX', 2 × 4H), 4.13 (s, 1H), 3.17 (s, 3H), 1.97 (s, 6H). (Appendix A.1.2)

Crystal structure description of co-crystal (2)

The asymmetric unit of co-crystal (**2**) contains two molecules of paracetamol, one molecule of 1,2-di(4-pyridyl)ethylene (BPEE) and one molecule of methanol (Figure 3.11). The three components crystallise in a triclinic system with $\bar{P}1$ as the space group. The full crystallographic details are given in Table 3.5.

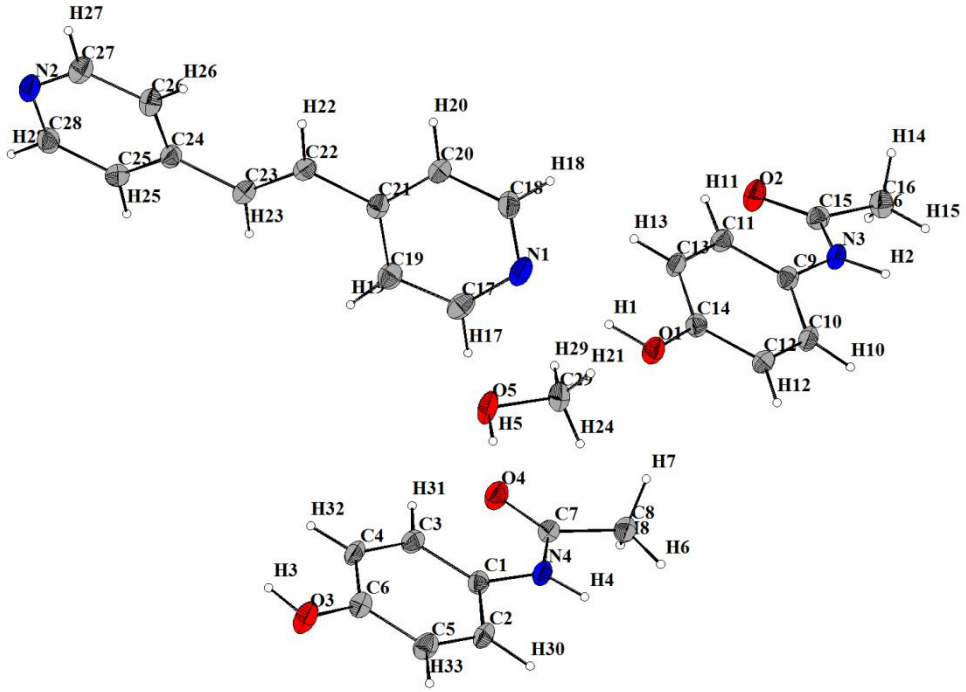

Figure 3.11: ORTEP diagram of co-crystal (**2**).

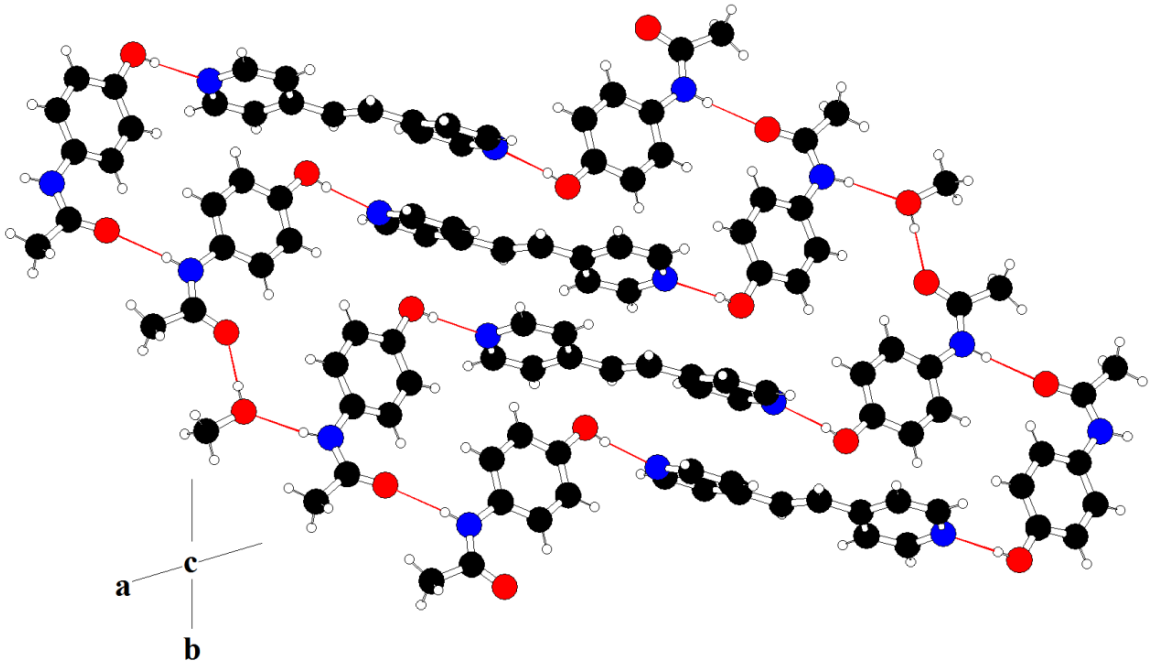

Figure 3.12: Packing arrangement in co-crystal (**2**).

The crystal packing arrangement of co-crystal (**2**) demonstrates that two crystallographically independent paracetamol molecules are linked through N(4)-H(4)···O(2) hydrogen bonding interactions (Figure 3.12). These dimeric paracetamol units are connected by the methanol molecules, the solvent of crystallisation. The methanol molecules act as a bridge between the neighbouring dimeric pairs of paracetamol molecules through N(3)-H(2)···O(5) and O(5)-H(5)···O(4) hydrogen bonding interactions (Figure 3.12). The paracetamol and methanol molecules arrange to form chains propagating infinitely, directed approximately along [$\bar{1}$10] (Figure 3.12). These paracetamol-methanol chains are crosslinked by the co-crystal former 1,2-di(4-pyridyl)ethylene through O(1)-H(1)···N(1) and O(1)-H(3)···N(3) hydrogen bonds (Figure 3.12 and Table 3.4). In addition to the hydrogen bonding interactions, there are strong π-π interactions between the neighbouring aromatic rings of BPEE. These π-π interactions are arranged in a face to face/centre to edge stacking arrangement with a slip angle of 18.2^{o}, possessing a centroid to centroid distance of 3.32 Å. The three components arrange to form a two-dimensional network. Several weak interactions between the 2D networks stabilise the co-crystal to extend the structure into the third dimension. Comparison of the single crystal simulated powder pattern with the powder pattern generated from solvent drop grinding experiment suggests that the crystal analysed is representative of the bulk material (Figure 3.13).

Table 3.4: Geometric Parameters for the hydrogen bonds in co-crystals (**2**)

Hydrogen bond	*d* (H···A)/Å	*d* (D···A)/Å	*θ* (D-H···A)/^{o}	(H···A) vdW cutoff contraction / %
O(1)-H(1)···N(1)	1.85	2.78(6)	177.9	33
N(3)-H(2)···O(5)	1.93	2.83(3)	162.9	29
O(3)-H(3)···N(2)	1.85	2.71(4)	169.8	33
N(4)-H(4)···O(2)	1.99	2.90(7)	173.8	27
O(5)-H(5)···O(4)	1.76	2.72(4)	173.8	35

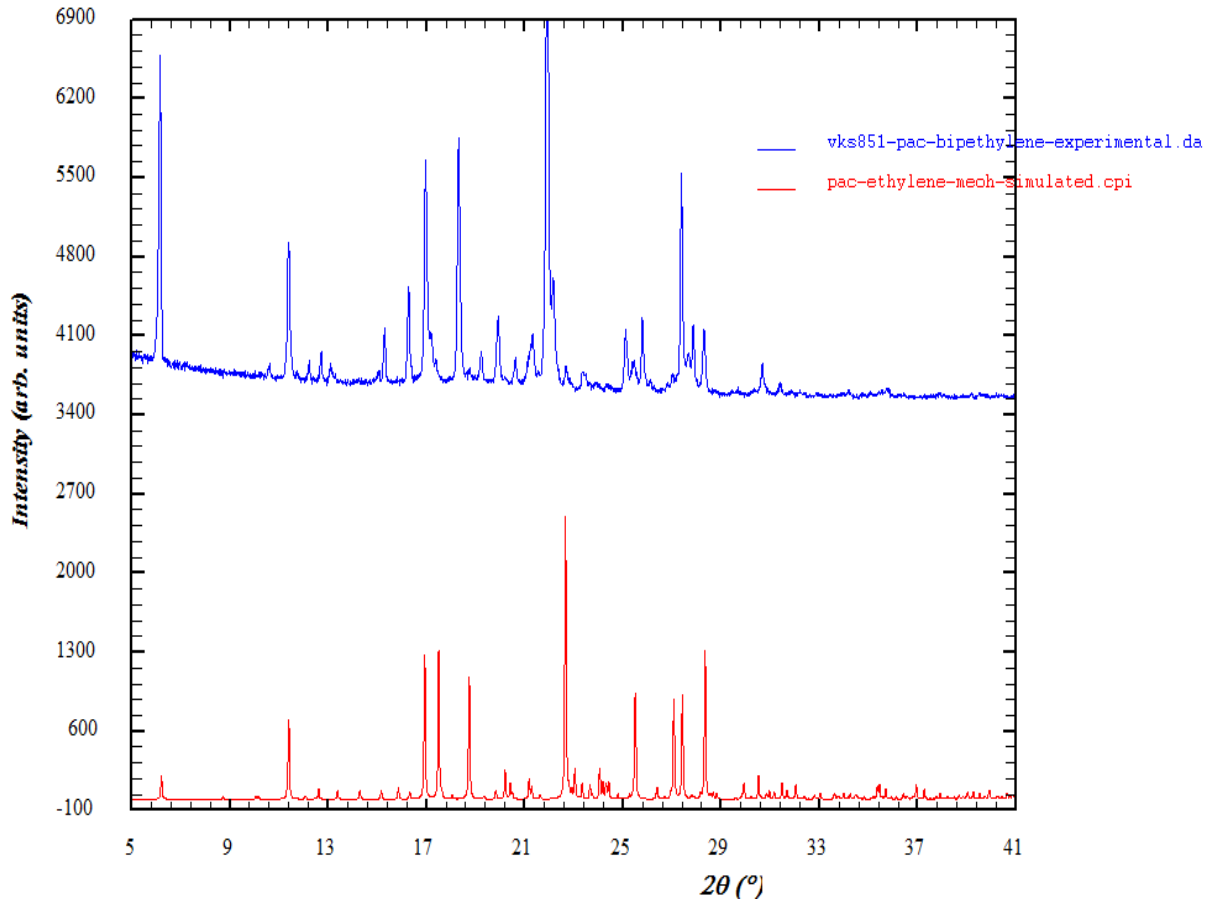

Figure 3.13: Comparison plot of powder X-ray data *vs* single crystal simulated pattern of co-crystal (**2**).

DTA/TGA of co-crystal (2)

The DTA/TG data (Figure 3.14) of co-crystal (**2**) shows a broad endotherm with an onset of 110.9 °C, with a corresponding weight loss of 6.1% in the TG curve. The weight loss in the TG thermogram corresponding to the loss of 1 mole of methanol molecules from the crystal lattice. The endothermic transition in the DTA consists of two peaks at 115.9 °C and 118.0 °C. The first peak at 115.9 °C could be due to the loss of methanol molecules from the crystal lattice; this is immediately followed by the melting of the material at 118.0 °C. The melting at 118.0 °C correlates with the melting of the co-crystal (**2**) as observed in capillary melting experiments. The transitions in the DTA curve following the melting of the material could be due to the decomposition of the material, seen as abrupt weight loss in the TGA curve (Figure 3.14).

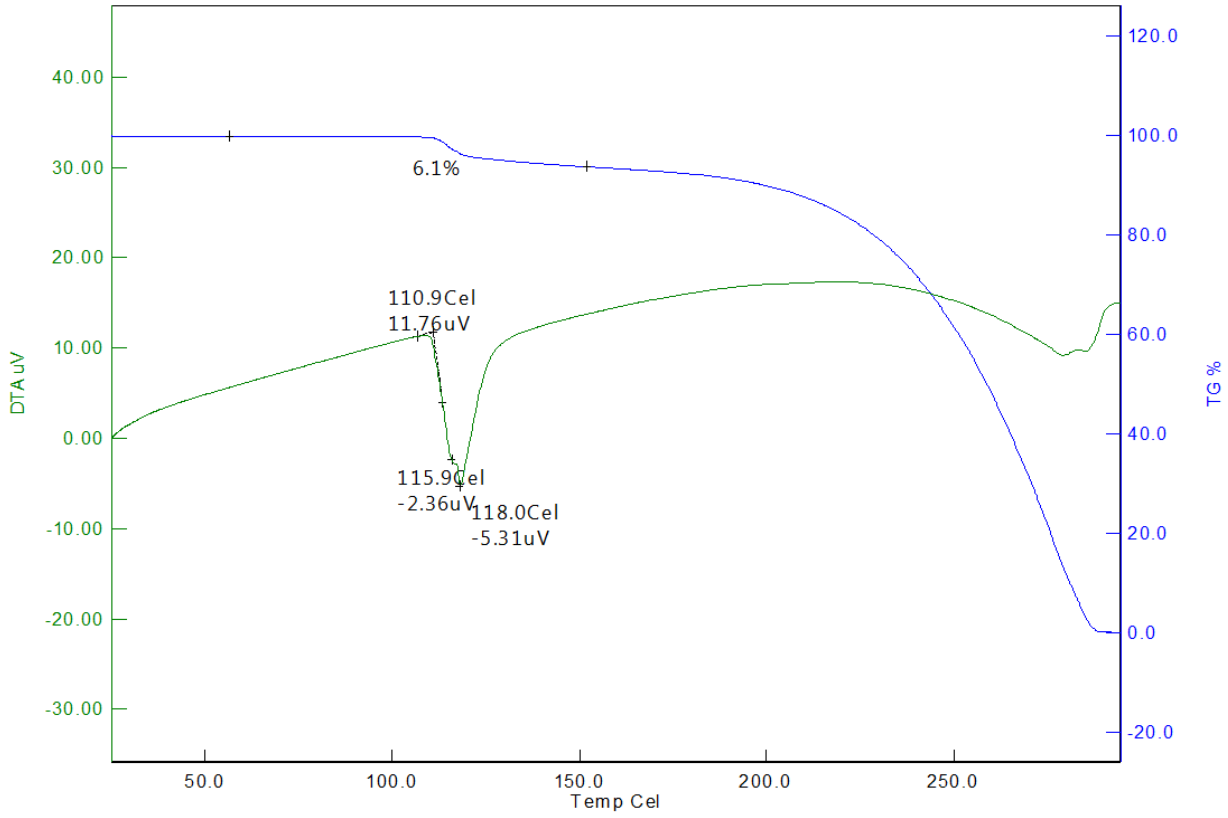

Figure 3.14: DTA/TG data of co-crystal (**2**).

Table 3.5: Crystallographic data of co-crystals (**1**)-(**4**).

	(**1**)	(**2**)	(**3**)	(**4**)
Chemical formula	$C_{11}H_{16}N_2O_2$	$C_{29}H_{32}N_4O_5$	$C_{40}H_{42}N_6O_4$	$C_{43}H_{62}N_8O_{11}$
Formula weight	208.26	516.59	670.8	867.01
Crystal system	Triclinic	triclinic	Triclinic	triclinic
a / Å	5.0174(5)	9.0546(2)	8.9707(4)	9.888(2)
b / Å	8.8907(9)	10.6241(2)	12.8633(6)	14.169(3)
c / Å	12.7562(1)	14.3162(3)	16.8305(2)	16.272(4)
α / °	106.21(4)	82.97(3)	106.06(2)	79.15(2)
β / °	91.40(5)	89.69(3)	95.27(2)	79.09(2)
γ / °	90.15(5)	73.85(3)	95.13(3)	88.40(3)
Space group	$P\bar{1}$	$P\bar{1}$	$P\bar{1}$	$P\bar{1}$
V / Å^3	546.2 (1)	1312.3 (5)	1844.8 (1)	2198.5 (8)
Z	2	2	2	2
$N_{reflection}$/ $N_{parameter}$	4141 / 136	4904 / 343	4389 / 469	10747 / 550
ρ_{calc} / g cm^{-3}	1.266	1.307	1.208	1.310
Radiation type	Mo Kα (λ =0.710173 Å)	Mo Kα (λ =0.710173 Å)	Mo Kα (λ =0.710173 Å)	Mo Kα (λ =0.710173 Å)
T / K	100	100	293	100
θ range/°	2-40	1 – 27	2 – 27	1 – 28
Range of *h*	-8 to 8	-9 to 11	-11 to 11	-12 to 13
Range of *k*	-15 to 15	-17 to 18	-16 to 16	-18 to 18
Range of *l*	-18 to 21	-13 to 11	-16 to 21	-0 to 21
Rmerge	0.019	0.023	0.028	0.097
R_1 / %	3.75	4.18	5.44	4.08
$_wR_2$ / %	4.24	4.34	5.67	4.84
Goodness-of-fit	1.072	1.117	1.102	0.965

3.3.3. Co-crystal (3) [(paracetamol)$_{2.0}$-(1,2-di(4-pyridyl)ethane)$_{2.0}$]

Synthesis of co-crystal (3)

Single crystals of co-crystal (**3**) were isolated after 5 days from a DMSO solution containing a 1:1 molar ratio of paracetamol (151 mg, 1.00 mmol) and 1,2-di(4-pyridyl)ethane (BPEA) (184 mg, 1.00 mmol).

The ^{1}H-NMR data of isolated single crystals of co-crystal (**3**) suggests that the paracetamol and 1,2-di(4-pyridyl)ethane are in a 1:1 mole ratio. ^{1}H-NMR (DMSO-d_6) of co-crystal (**3**): δ 9.66 (s, 2H), 9.15 (s, 2H), 8.44 and 7.25 (AA'XX', 2 × 4H), 7.33 and 7.25 (AA'XX', 2 × 4H), 2.94 (s, 8H), 1.97 (s, 6H). (Appendix A.1.3)

The DSC data (Figure 3.15) of co-crystal (**3**) reveals a sharp endotherm with an onset temperature of 113.7 °C and peak at 116.6 °C, which corresponds to the melting of the compound. The endotherm occurs at a significantly different temperature when compared to the melting temperatures of PAC (168-172 °C) and BPEA (110-112 °C).

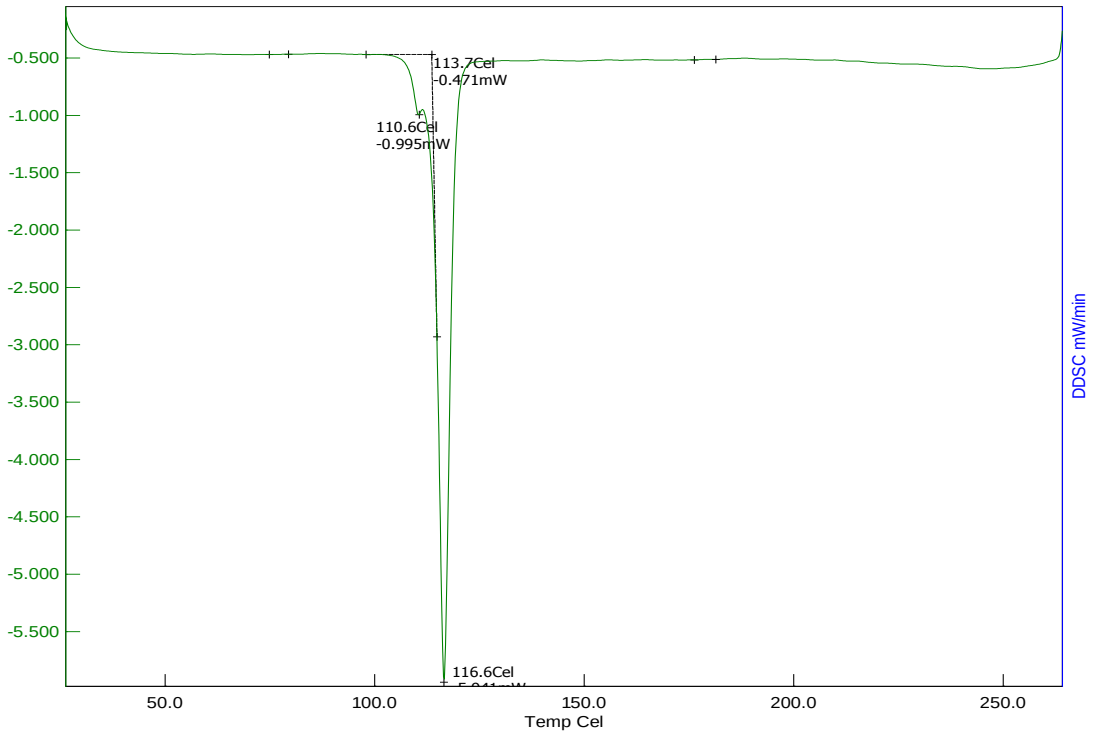

Figure 3.15: DSC of co-crystal (**3**).

Crystal structure description of co-crystal (3)

The co-crystal (**3**) crystallises in triclinic crystal system with four independent molecules in the asymmetric unit, two each of paracetamol and the co-crystal former 1,2-di(4-pyridyl)ethane (Figure 3.16). The CH_2 groups of one of the crystallographically independent BPEA molecules are found to be disordered over two sites and were refined anisotropically with occupancies of 0.47 and 0.53. Analogous to co-crystals (**1**) and (**2**), the phenolic O-H groups of both the paracetamol molecules participate in hydrogen bonding interactions with the co-crystal former through O(1)-H(1)···N(4) and O(3)-H(44)···N(2) interactions. While in co-crystals (**1**) and (**2**) it is only the phenolic O-H group that participates in hydrogen bonding interactions with the CCF, here in co-crystal (**3**), the amidic N-H groups of both the paracetamol molecules also participates in hydrogen bonding interaction with the CCF through N(6)-H(6)···N(3) and N(5)-H(45)···N(1) interactions (Figure 3.17 and Table 3.6). From the crystal packing arrangement it can be noticed that none of the carbonyl groups participate in conventional hydrogen bonding interactions. However, they participate in weak C-H···O interactions with inversion related molecules. The two components in co-crystal (**3**) arrange to produce crystallographically distinct stepped chains of molecules as presented in Figure 3.17. In addition to the conventional hydrogen bonding interactions there are several weak interactions between the one dimensional chains extending the structure into a third dimensional structure.

A comparison (Figure 3.18) of single crystal simulated powder pattern with the experimental powder pattern suggests that the crystal analysed is representative of the bulk sample, as evident from the ^{1}H-NMR data.

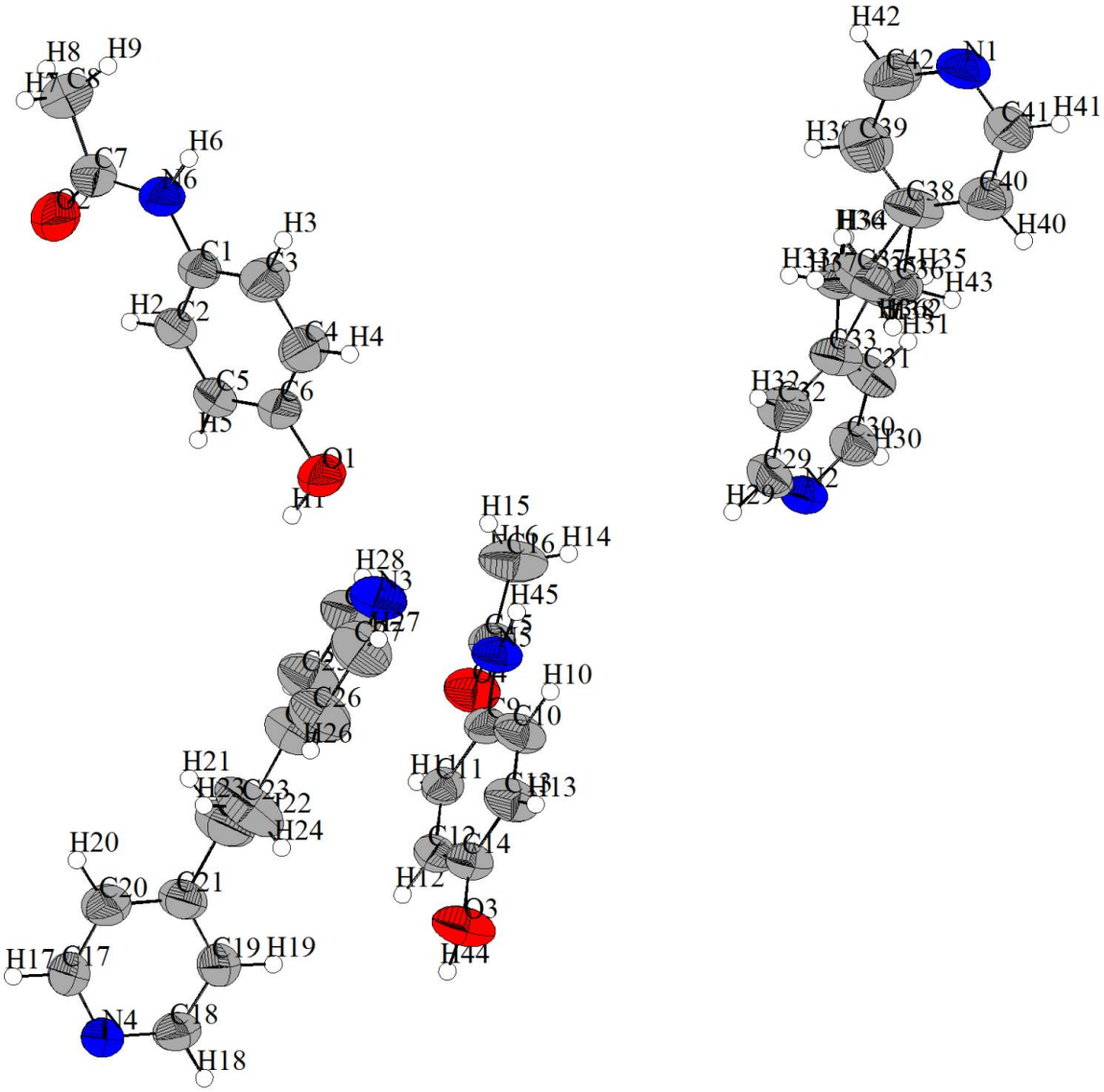

Figure 3.16: ORTEP diagram of co-crystal (**3**).

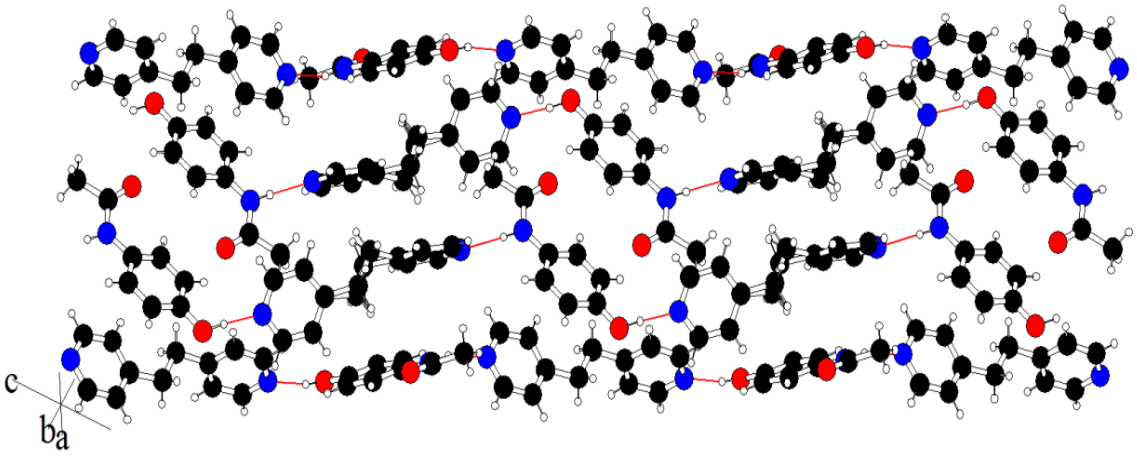

Figure 3.17: Packing arrangement in co-crystal (**3**).

Table 3.6: Geometric Parameters for the hydrogen bonds in co-crystals (**3**)

Hydrogen bond	*d* (H···A)/Å	*d* (D···A)/Å	*θ* (D-H···A)/^{o}	(H···A) vdW cutoff contraction / %
O(1)-H(1)···N(4)	1.75	2.71(2)	166.6	36
N(6)-H(6)···N(3)	2.02	2.99(6)	166.4	26
O(3)-H(44)···N(2)	1.77	2.75(3)	175.8	35
N(5)-H(45)···N(1)	1.98	2.96(4)	175.5	28

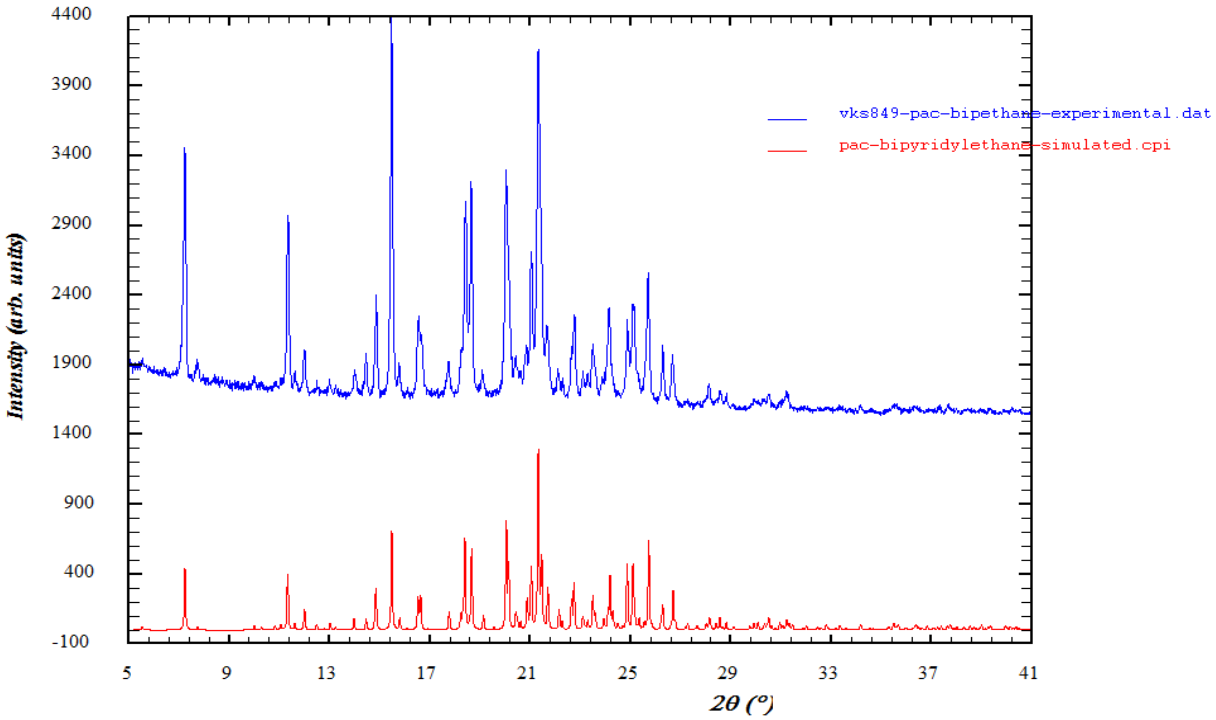

Figure 3.18: Comparison of powder X-ray data (blue pattern) *vs* single crystal simulated patter of co-crystal (**3**) (red pattern).

3.3.4. Co-crystal (4) [(paracetamol)$_{4.0}$-(1,4,8,11-tetraazacyclotetradecane)$_{1.0}$]

Synthesis of co-crystal (4)

Single crystals of co-crystal (**4**) were isolated after three days from a methanolic solution containing 4:1 molar ratio of paracetamol (151 mg, 1.00 mmol) and 1,4,8,11-tetraazacyclotetradecane (50 mg, 0.25 mmol).

The DSC thermogram of co-crystal (**4**) (Figure 3.20) shows an endothermic transition with an onset temp of 124.1 °C, corresponding to the melting of the compound.

Crystal structure description of co-crystal (4)

The asymmetric unit of co-crystal (**4**) consists of four crystallographically independent paracetamol molecules, two cations of 1,4,8,11-tetraazacyclotetradecane (cyclam) occupying inversion centres and a carbonate dianion (Figure 3.20).

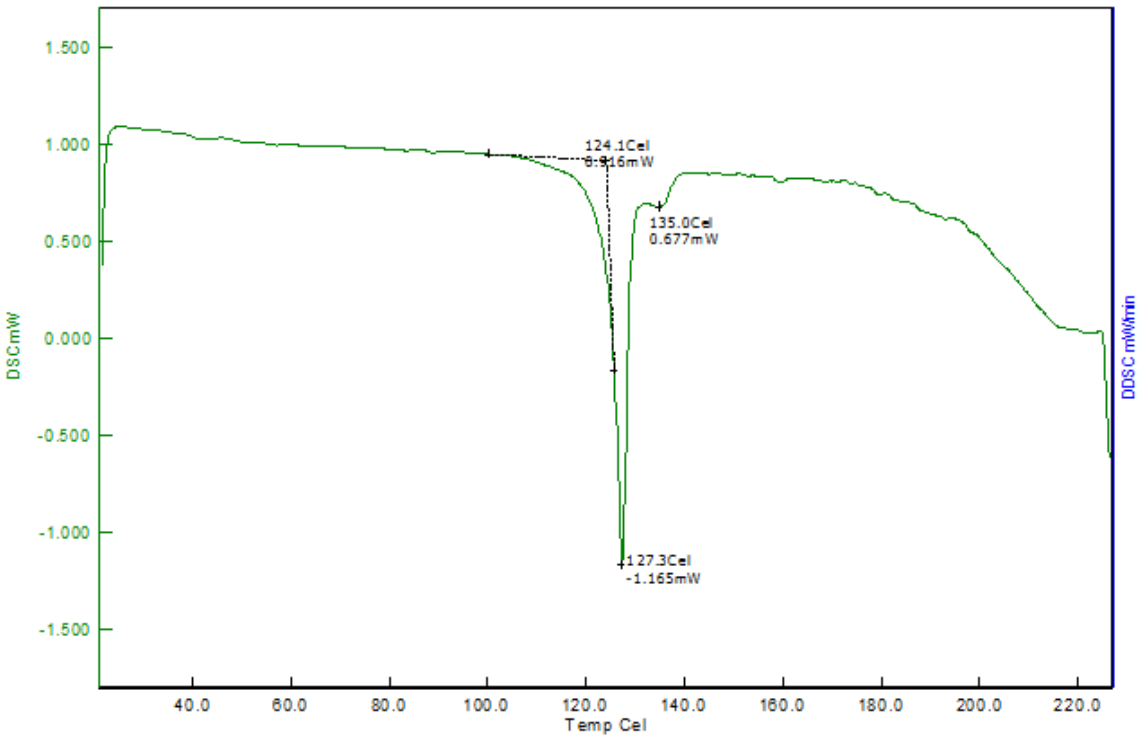

Figure 3.19: DSC of co-crystal (4).

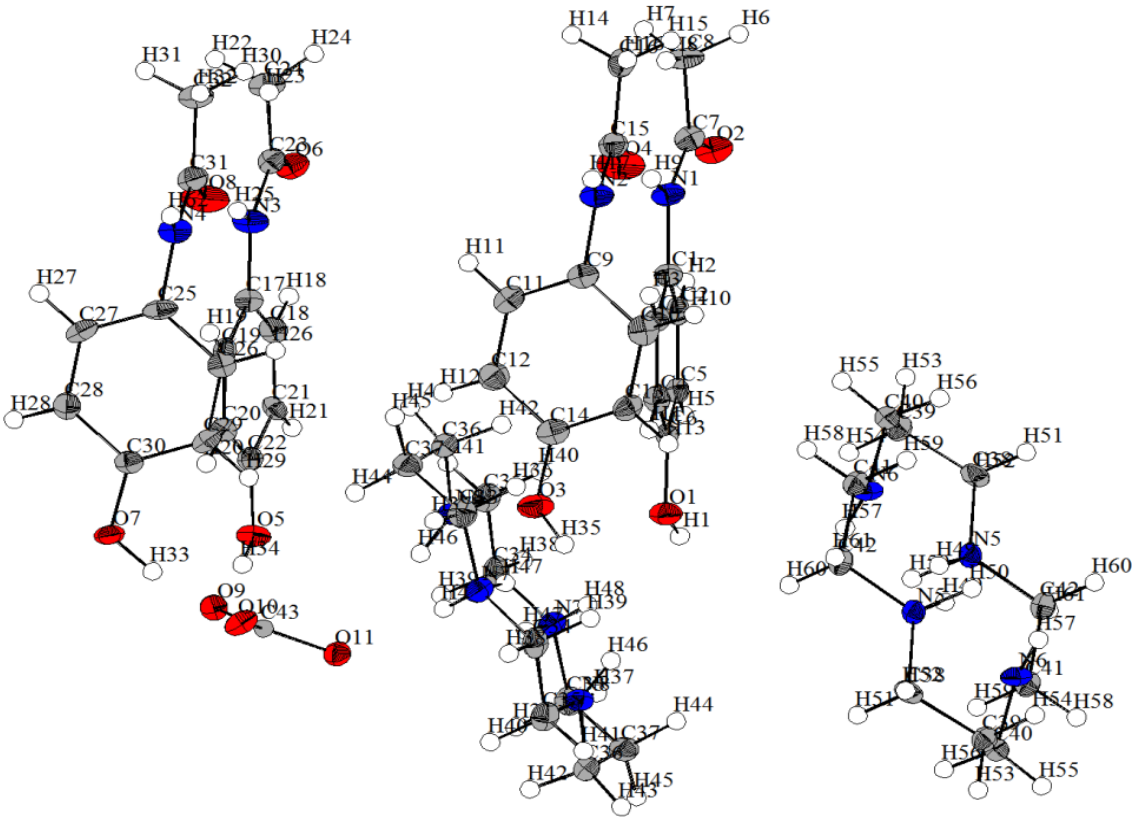

Figure 3.20: ORTEP diagram of co-crystal (**4**).

Two crystallographically independent paracetamol molecules hydrogen bond through N(1)-H(9)···O(4), N(2)-H(17)···O(2) and N(3)-H(25)···O(8), N(4)-H(62)···O(6) hydrogen bonding interactions to form two independent C(9) chains of paracetamol molecules. These chains propagate along [$\bar{1}$00] direction (Figure 3.21).

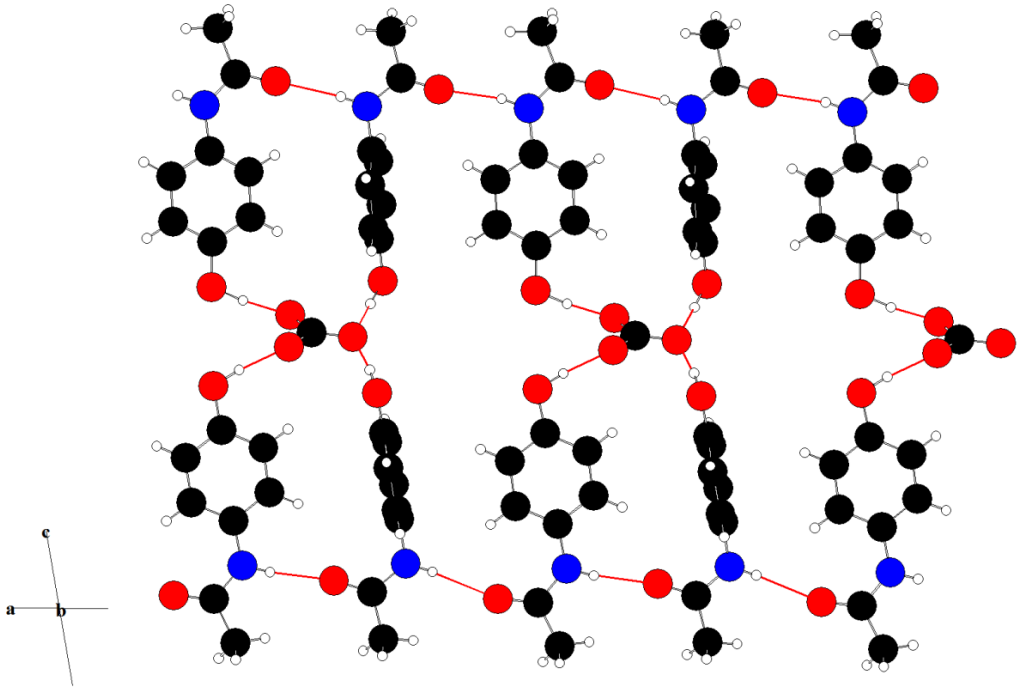

Figure 3.21: Hydrogen binding interactions between paracetamol molecules in co-crystal (**4**).

In addition to the hydrogen bonding interactions, there are π···π interactions acting between each independent paracetamol chains. These interactions are arranged in a perpendicular (T-Shaped) configuration with bonding distances of around 3.693Å-4.204Å. The carbonate dianion is central to the arrangement of the molecules in co-crystal (**4**). Each oxygen atom, while acting as acceptors participates in two hydrogen bonding interactions to cross link the paracetamol chains through O(1)-H(1)···O(11), O(3)-H(35)···O(10) and O(5)-H(34)···O(9), O(7)-H(33)···O(10) hydrogen bonding interactions to form a two-dimensional network as shown in Figure 3.21. In addition, the carbonate dianion also participates in hydrogen bonding interactions with two cyclam cation molecules through $N(7)^{+}$-H(48)···$^{-}$O(11) and $N(5)^{+}$-H(50)···$^{-}$O(9) to form a three dimensional structure. The full crystallographic details and geometric parameters of all the hydrogen bonding interactions of (**4**) are given in Table 3.5 and Table 3.7 respectively. The cyclam molecules do not participate in hydrogen bonding interactions with the paracetamol molecules. The cyclam molecules while hydrogen bonding with the carbonate dianions lie in the spaces created by the two-dimensional network formed between the paracetamol and carbonate dianion molecules (Figure 3.22). Whilst the work on (**4**) was in progress, a crystal structure similar to (**4**) was reported by Vania *et.al.*,[147] However, the reported crystal structure is different form co-crystal (**4**) and is a hydrate form of (**4**). Due to the presence of water molecules in the crystal structure there are additional

hydrogen bonding interactions in the reported structure which is significantly different to (**4**) presented here.

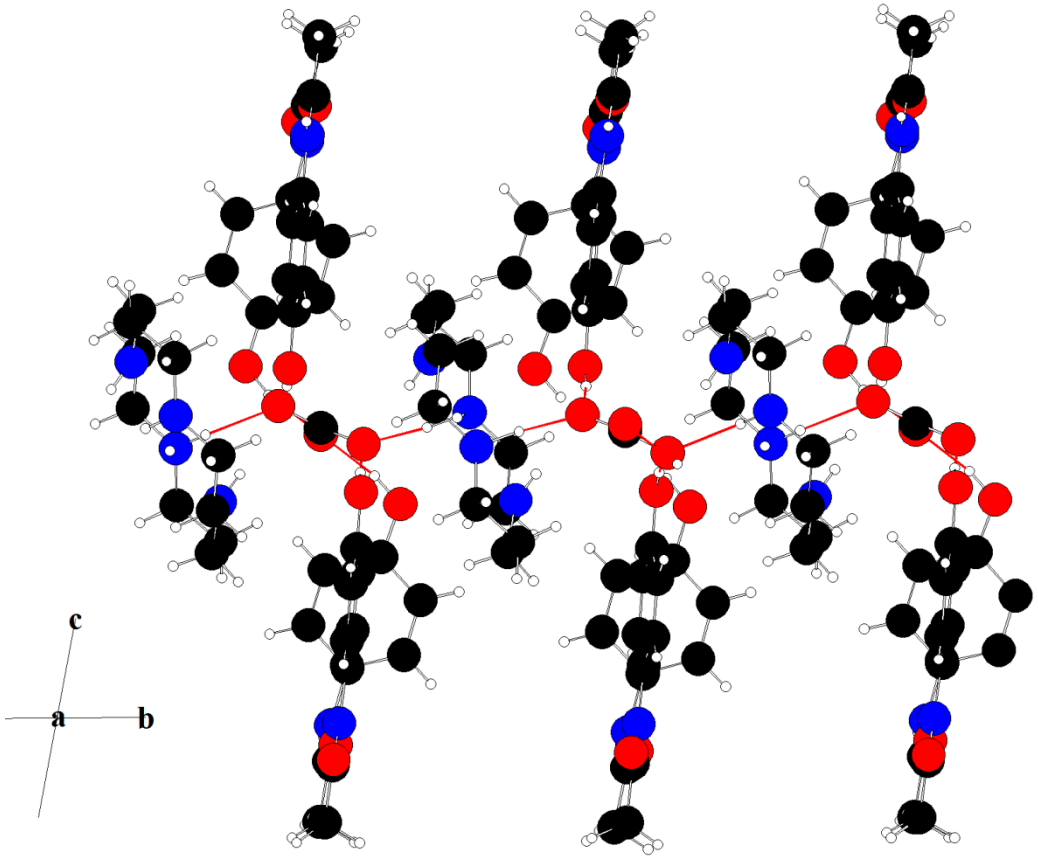

Figure 3.22: Hydrogen bonding interactions between paracetamol and co-crystal former (1,4,8,11-tetraazacyclotetradecan) in co-crystal (**4**).

Table 3.7: Geometric parameters for the hydrogen bonds in co-crystal (**4**)

Hydrogen bond	*d* (H···A)/Å	*d* (D···A)/Å	*θ* (D-H···A)/^{o}	(H···A) vdW cutoff contraction / %
O(1)-H(1)···O(11)	1.53	2.57(7)	172.7	43
N(1)-H(9)···O(4)	1.95	2.81(5)	168.0	28
N(2)-H(17)···O(2)	2.04	2.91(6)	166.8	25
N(3)-H(25)···O(8)	1.97	2.83(7)	173.5	28
O(7)-H(33)···O(10)	1.67	2.60(2)	169.3	39
O(5)-H(34)···O(9)	1.68	2.60(4)	172.3	38
O(3)-H(35)···O(10)	1.67	2.62(5)	166.7	39
N(7)-H(47)···N(8) (intra)	2.13	2.87(7)	124.7	22
$N(7)^{+}$-H(48)···$^{-}$ O(11)	1.88	2.64(8)	146.4	31
N(5)-H(49)···N(6) (intra)	2.22	2.87(4)	132.3	18
$N(5)^{+}$-H(50)···$^{-}$O(9)	1.59	2.65(6)	164.6	42
N(4)-H(62) ···O(6)	2.15	3.02(3)	167.8	21

3.4. Discussion

The molecular structure of paracetamol contains two hydrogen bond donors; the phenolic O-H and the amidic N-H groups and three acceptor groups; the amidic nitrogen, oxygen and phenolic oxygen atoms as shown in Scheme 3.1. During the co-crystal formation these hydrogen bond donor and acceptor groups of paracetamol are in competition with the donor and acceptor groups of different CCF molecules. The resulting structure in most cases is the one that optimizes the donor-acceptor interactions between the paracetamol and the CCF molecules. Considering the hydrogen bonding interactions in paracetamol form-I) it can be noticed that the strong hydrogen bonds in paracetamol form-I are formed between the phenolic O-H and amidic carbonyl groups. These interactions are absent in all the co-crystals (**1**)-(**4**) and are replaced by the O-H···N supramolecular synthon in co-crystals (**1**)-(**3**) and O-H···O interactions in co-crystal (**4**). These interactions between the paracetamol and CCF

molecules operate over similar distances compared to the O-H···O interactions in the paracetamol form-I, suggesting that they are of comparable strength. The argument of comparable strength is supported by the percentage contraction in the H···A van der Waals cut-off and red shift of the ν(D-H) stretching frequencies, measured by infrared spectroscopy (Table 3.8). The IR spectra of paracetamol form-I and co-crystals (**1**)–(**4**) are given in (Appendix A.2.2 to A.2.5)

Table 3.8: Bond stretching frequencies in paracetamol and the four co-crystals, determined by infra-red spectroscopy.

Assignment	pac in gas-phase[148]	pac Form I	(**1**)	(**2**)	**(3)**	**(4)**
ν(O-H) / cm^{-1}	3653	3160	3326	3070	3195	3163
ν(N-H) / cm^{-1}	3465	3324	3326, 3273	3290	3246	3276
$\nu(C\text{-}H)_{aromatic}$ / cm^{-1}	3034	2895	3049	2870	2950	2980
ν(C=O) / cm^{-1}	1721	1651	1636	1653	1673	1653

According to the empirical rules of hydrogen bonding interactions proposed by Etter,[149] the best hydrogen bonding interactions are observed between the best donor and acceptor groups in the system. The geometric and spectroscopic data of hydrogen bonding interactions in co-crystals (**1**) – (**4**) are consistent with the best donor – best acceptor rule. In co-crystals (**1**) – (**4**) the best donor, phenolic O-H is hydrogen-bonded to the best acceptor, resulting in the formation of O−H···N interactions, while in co-crystal (**4**) it results in the formation of O−H···O interactions. Consistent with the other suggestions of Etter *et. al.* all of the remaining proton donors and acceptors also participate in hydrogen bond formation, as evidenced in all the four co-crystals by the N−H···O=C interactions between paracetamol molecules, which are of similar strength to those observed in paracetamol itself. Co-crystal (**2**) has additional hydrogen bonds N−H···O and O−H···O=C due to the incorporation of solvent molecules in the crystal lattice. The hydrogen bonding interactions in co-crystals (**1**) – (**4**) are in accord with the empirical rules proposed by Etter.

Complexes with hydrogen bonds are stabilised by a combination of electrostatic, polarization, induction, and dispersion energy terms. From an electrostatic viewpoint, any hydrogen bonding interaction may be considered to have contributions from interactions between monopoles, dipoles, quadrupoles, etc., each of which has a different characteristic cut-off in

terms of distance. One common means of assigning the character of the hydrogen bond is the contraction, with respect to the sum of the van der Waals radii, of the H···A distance. Proton-centered hydrogen bonds typically exhibit a contraction of between 40 and 55% of the sum of the van der Waals radii.[150] In co-crystals (**1**)−(**4**)the van der Waals cut-off contraction lies for most hydrogen bonds between 20 and 40% (Table 3.3, Table 3.4, Table 3.6, Table 3.7) which suggests these hydrogen bonds may be classed as being of moderate strength in which the electrostatic interaction terms are dominant. In co-crystal (**4**), due to presence of charged species, the van der Waals contraction exceeds 40% in the O−H···O interaction, suggesting that the interaction is strong when compared to other interactions. It has been empirically established that hydrogen bonds become increasingly linear with increasing strength, as linearity optimizes the electrostatic component (dipole−monopole, dipole−dipole) of the interaction. The electrostatic contribution to the intermolecular interaction tends to dominate and imparts directionality on hydrogen bonds. This is particularly significant in short and proton-centered hydrogen-bonds, whose typical angular range is $160 \leq \theta/^{\circ} \leq 180$, but also applies to longer bonds of electrostatic nature. According to Reed *et al.*,[151] charge transfer between donor and acceptor groups has a strong influence on the geometrical and spectral properties of the co-crystals. In particular, in a D−H···A hydrogen bond there is charge transfer from lone pairs or π-molecular orbitals of the electron donor (proton acceptor) to the anti-bonding orbitals of the D−H bond of the electron acceptor (proton donor). An increase of electron density in the anti-bonding orbitals elongates the D−H bond, which causes the red-shift of the D-H stretching frequency. Therefore charge transfer and hence hydrogen bond formation may be inferred from comparison of characteristic vibrational frequencies of a free R-D-H group with that of the same group in the presence of a hydrogen bond acceptor. The characteristic vibrational frequencies of the four co-crystals (**1**)−(**4**) and of crystalline paracetamol form I may be compared with those observed in the gas phase infrared spectrum of paracetamol (Table 3.8). The frequencies of the ν(O−H), ν(N−H), and ν(C=O) stretching vibrations in co-crystals (**1**)−(**4**) and in paracetamol form I are red-shifted by up to 16% relative to the equivalent vibrations in the gas-phase spectrum of paracetamol. From the crystal structure determination, it can be deduced that the lone pair of the nitrogen atom of each of the co-crystal formers (**1**)−(**3**) and the lone pair of the oxygen atom in co-crystal former (**4**) is aligned along the axis of the O−H bond of the hydroxyl group of paracetamol, thereby facilitating charge transfer between the donor and acceptor pair. Therefore, we conclude that both electrostatic and charge transfer terms influence the directional behaviour of the hydrogen bonds in co-crystals (**1**)−(**4**).

In all four co-crystals presented here, the structural and spectroscopic data indicate that the hydrogen bonds formed between the PAC and the CCF are of comparable strength to those originally present in the API. Co-crystals (**1**)−(**3**) studied here have the same, *i.e.* O−H···N supramolecular heterosynthon between the PAC and CCF, while in co-crystal (**4**) there is no direct interaction between the co-former and paracetamol instead the paracetamol molecules are hydrogen-bonded to the carbonate anion through O−H···O synthon. In structure (**3**) in addition to the O−H···N there is a N−H···N supramolecular interaction observed between the PAC and CCF. Our investigations show that difunctional CCFs, able to form chain-like structural motifs through distinct hydrogen bonds, are necessary for co-crystal formation with paracetamol. This is in accordance with previously reported CCFs in multi- component crystalline forms of paracetamol. Although CSD analysis suggests carboxylic acids and amides as potential co-crystal formers, our experiments demonstrate that they are not effective for paracetamol. This may be due to the self-complementary hydrogen bonding nature of these functional groups, which favours homosynthon formation rather than heterosynthon with phenolic O-H group. A hierarchical arrangement between the best donor of paracetamol to the best acceptor in CCF is observed in all the co-crystals presented here and is indeed observed in almost all of the previously reported co-crystal forms of paracetamol. Of the reported co- crystals of paracetamol, only those involving theophylline and bipyridine[152] do not follow the hierarchical arrangement of hydrogen bonding. In the case of the paracetamol-bipyridine co-crystal, strong π−π interactions (at a distance of *ca.* 3.4 Å) between the pyridine moieties of bipyridine stabilize the crystal structure in co-operation with the hydrogen bonds. In the case of the paracetamol-theophylline co-crystal,[152] the best acceptor of theophylline, the imidazole nitrogen atom, does not participate in conventional hydrogen bonds. The two molecules are arranged such that they form flat hydrogen-bonded sheets.

The DSC data of the co-crystals reveal single sharp endotherms at 157.9, 113.1, 116.6, and 124.3 °C for products (**1**)−(**4**) respectively. These endotherms, which correspond to the melting point of the solids, occur at significantly different temperatures to those of paracetamol (168−172 °C) or the co-crystal former (trans-1,4-diaminocyclohexane, 68−72 °C; trans- 1,2-di-(4-pyridyl)-ethylene, 148−152 °C; 1,2-bis(4-pyridyl)-ethane, 110−112 °C; 1,4,8,11-tetraazacyclotetradecane, 185-188 °C), indicating the formation of co-crystals and not simple physical mixtures. All the four co-crystals described here have melting

temperatures reduced from that of paracetamol, suggesting that the cohesive energy of co-crystals (**1**)−(**4**) is reduced from that of pure paracetamol form I.

3.5. Conclusion

Analysis of structural data in the CSD resulted in the identification of a range of potential co-crystal formers which form complementary hydrogen bonding interactions with paracetamol. Subsequent co-crystal screening by solvent-drop grinding in conjunction with high-throughput PXRD led to the discovery of four new co-crystals of paracetamol. The co-crystals (**1**)−(**3**) presented here utilize the O−H···N supramolecular heterosynthon, while co-crystal (**4**) utilises the O−H···O synthon. The ability of phenols to form these hetero and homo synthons is consistent with the results of the analysis of the structural database, suggesting the approach may be applicable to a wider range of phenol derivatives. Comparison of the geometric and spectroscopic parameters of the hydrogen-bonds in co-crystals (**1**)−(**4**) with those for paracetamol reveals that they are of similar strength, irrespective of the chemical identity of the synthon. The study shows that a balance between the retrosynthetic approach (synthon method) and database screening of supramolecular synthons provides a useful approach to the targeted synthesis.

Chapter 4: Hydrogen-Bonded Host-Guest Complexes of Furosemide

4.1. Introduction

Molecular host–guest complexes are those that are composed of two or more molecules or ions that are held together through non-covalent interactions and are arranged in a unique structural relationship. A necessary requirement for a complex to be classified as host-guest complex is that the host and the guest molecules are distinguishable from one another. In the host–guest complexes, the host component is generally the larger molecule and it encompasses or forms an array to include the smaller guest molecules. Based on the arrangement of guest molecules, there are two principal types of host – guest complexes: the tunnel inclusion complexes[153] and the clathrates[154]. In the first type the guests are included in the tunnels between the host molecules and can be in mutual contact with one other, arranged in a head-to-head or head-to-tail orientation. In the second category the guests are in the cages separated from one another by the intervening host molecules. The host molecules are also broadly classified into two main types: (i) those that form complexes by fitting convex guests into the concave cavity of hosts and (ii) those that form lattice inclusion compounds by packing in such a manner as to leave cavities, channels or layers in the crystal structure so as to accommodate various guest molecules. In a host-guest arrangement, the host molecules can interact through directional bonds of various types, of which hydrogen bonding is undoubtedly the most important one. However, host arrangements formed through non-directional forces such as the ubiquitous dispersion forces or van der Waals forces are also known.[155]

The design and synthesis of crystalline molecular complexes that assemble into a host-guest arrangement in the solid-state is an area of intense current interest. A key to controlling the packing arrangement in a crystal lies in controlling the type and orientation of the non-covalent interactions between the components. The strong and directional nature of hydrogen bonds has led to their widespread use in self-assembling systems. In the solid state, rules have been delineated to allow the reasonable prediction of hydrogen-bonding packing patterns in crystals. However, the synthesis of host-guest molecules in the crystalline state based on empirical rules is often frustrating due to the absence of reliable structural paradigms. In the absence of reliable structural parameters, chemists are left with no option but to search for molecular components that persistently form host-guest arrangements in the presence of a variety of guests.

The host-guest complexes discussed in this chapter are the binary molecular complexes of furosemide. The host-guest arrangement of the complexes studied here are derived by analysing their crystal structures. The complexes presented here belong to the class of compounds called crystalline clathrates. According to IUPAC, clathrates are "inclusion compounds in which the guest molecule is in a cage formed by the host molecule or by a lattice of host molecules".[156]

Furosemide (FUR) is a loop diuretic drug, which is widely used in the treatment of congestive heart failure and oedemas arising from cardiac, renal, and hepatic failure.[157] It is a class IV drug according to the biopharmaceutics classification system (BCS) and suffers from both low permeability and low solubility.[158] The low permeability and delivery-related issues have been addressed by a number of approaches, the most recent ones being emulsification and the use of mesoporous materials as carriers.[159] Goud *et al.*[160] used co-crystallisation as their strategy to improve the solubility of furosemide. The formation of co-crystals between furosemide and eight different co-crystal formers (caffeine, urea, *p*-aminobenzoic acid, acetamide, nicotinamide, isonicotinamide, adenine, and cytosine) was reported, with enhanced solubility and dissolution profiles of these materials relative to pure furosemide. However, only two of the compositions (caffeine and cytosine co-crystals) were obtained as single crystals, whereas the crystal structures of the other six co-crystals remained unknown.

The molecular structure of furosemide is shown in Scheme 4.1. The molecular structure gives an indication of the molecule's ability to exhibit conformational polymorphism[161] about its various flexible bonds. The rigid portion of the molecule is the anthranilic acid moiety, and the conformationally flexible portions are the sulfonamide group and the furan ring. The intramolecular N-H···O hydrogen bond renders rigidity to the anthranilic acid moiety; consequently, rotation about the phenyl-carboxylic acid C-C bond is difficult. Sulfonamide and furan ring torsions can result in different conformers in solution, thereby increasing the likelihood of polymorphism in the solid state.

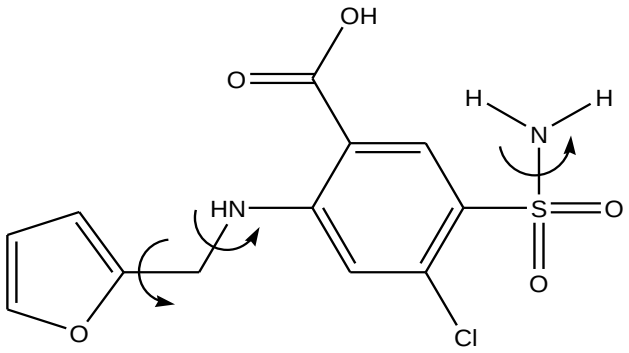

Scheme 4.1: Molecular structure of furosemide. The arrows indicate the conformational flexibility of the molecule along these bonds.

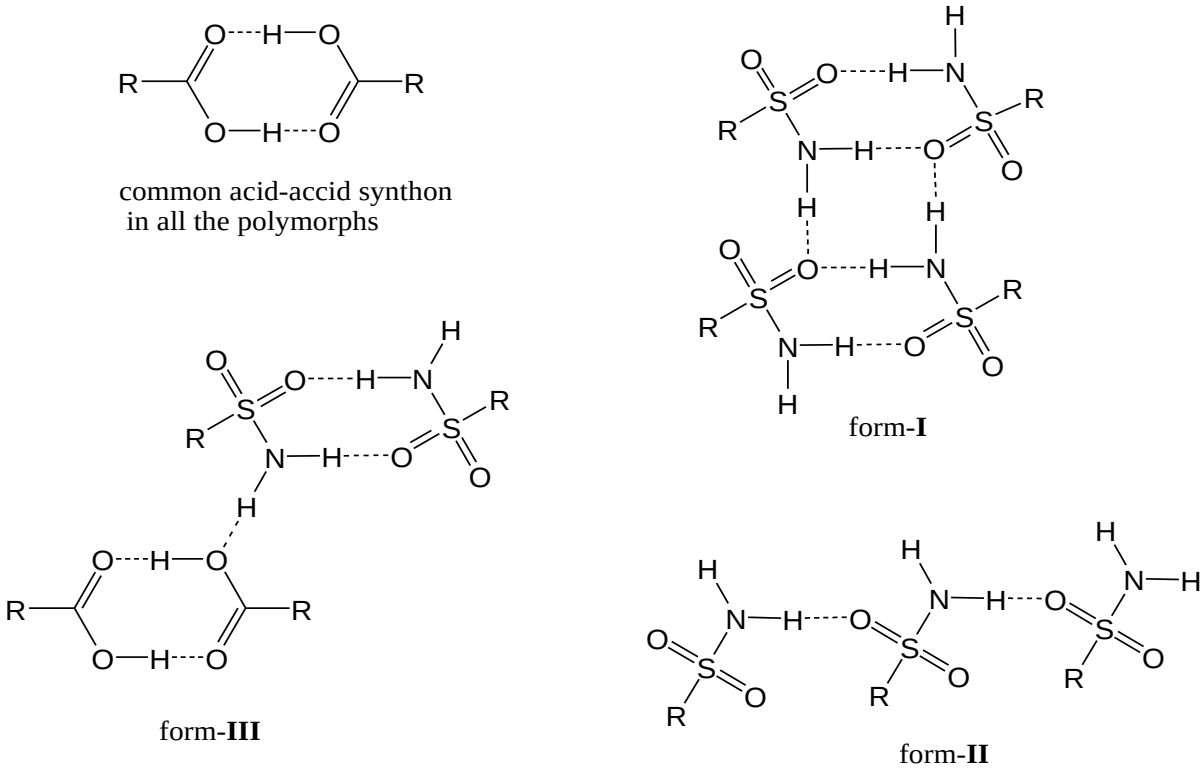

Scheme 4.2: Hydrogen bonding interactions observed in known polymorphic forms of furosemide.

The first crystal structure of furosemide was published in 1978 by Lamotte *et al.*[162] Two other polymorphic crystalline forms of furosemide were reported by Babu *et al.*[163] Matsuda[164] and Ge *et al.*[165] attempted to crystallise several crystalline forms of furosemide. Whilst they were unsuccessful in obtaining the crystal structures of the new crystalline forms, they

characterised three polymorphic forms and two solvates of furosemide by FTIR, terahertz spectroscopy, PXRD and thermal analysis. There are three known forms of furosemide for which crystal structures have been determined. All the three known forms of furosemide contain the acid-acid supramolecular synthon and differ by the hydrogen bonding network formed by the sulphonamide groups (Scheme 4.2). The commonly available crystalline form of furosemide is labelled as form-I and is the thermodynamic stable form. The other two forms of furosemide are metastable and convert to form-I by grinding.

The synthesis of a series of host-guest complexes formed by furosemide. While the host-guest arrangement of the complexes presented is a serendipitous outcome of the synthesis, the design strategy is based on the empirical rules proposed by Margaret Etter.[166] Etter formulated that, in neutral organic compounds, the crystal packing is dependent on the interaction between the best hydrogen bond donor and acceptor groups present in a system in which other possible intermolecular interactions are weak and non-directional. The design strategy is based on what follows from the above rule but on a higher level. It is proposed that that the crystal packing in a system will depend on the charge assisted hydrogen bonding interaction whilst containing other directional hydrogen bonding interactions.

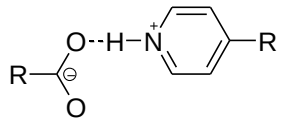

charge assisted O-H---N
supramolecular synthon

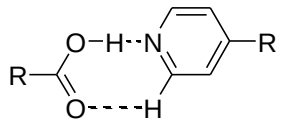

neutral acid-pyridine
supramolecular synthon

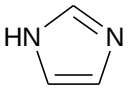

imidazole

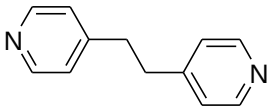

1,2-bis(4-pyridyl) – ethane

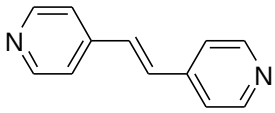

trans-1,4-di(4-pyridyl) – ethylene

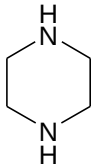

piperazine

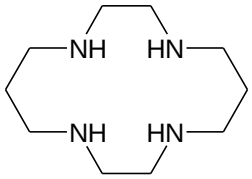

1,4,8,11-tetraazacyclotetradecane

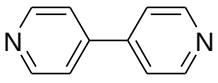

4,4'-bipyridyl

Scheme 4.3: Molecular diagram of the guest molecules and the supramolecular synthons studied here.

Based on the above proposed strategy the six co-crystal formers (Scheme 4.3) were selected for the investigation of the molecular complex formation. Based on the predicted pKa[15] values of the co-formers and furosemide it was anticipated that furosemide will form salts with imidazole (IM), piperazine (PIP) and 1,4,8,11-tetraazacyclotetradecane (cyclam) and co-crystals with 1,2-bis(4-pyridyl)ethane (BPEA), 1,2-di(4-pyridyl)ethylene (BPEE) and 4,4'-bipyridyl (BIPY) molecules. Whilst some of the results presented here are in agreement with this prediction, others do not show proton transfer between the FUR and CCF. The molecular complexes presented here were initially synthesised though solvent drop grinding followed by crystallisation from appropriate solvents through slow solvent evaporation. In the chapter, the term molecular complex is synonymously used to represent salts and co-crystals.

4.2. Results and discussion

4.2.1. Crystal structure description of molecular complex (5) [(furosemide)$_1$-(imidazole)$_1$]

Single crystals of molecular complex (**5**) were obtained by dissolving furosemide and imidazole (1:1) in 2 mL of methanol. Light yellow coloured crystals of (**5**) were isolated within 2 hours. The single crystal structure reveals that (**5**) crystallises in a centrosymmetric space group, $P2_1/C$. The full crystallographic details of (**5**) are presented in Table 4.2.

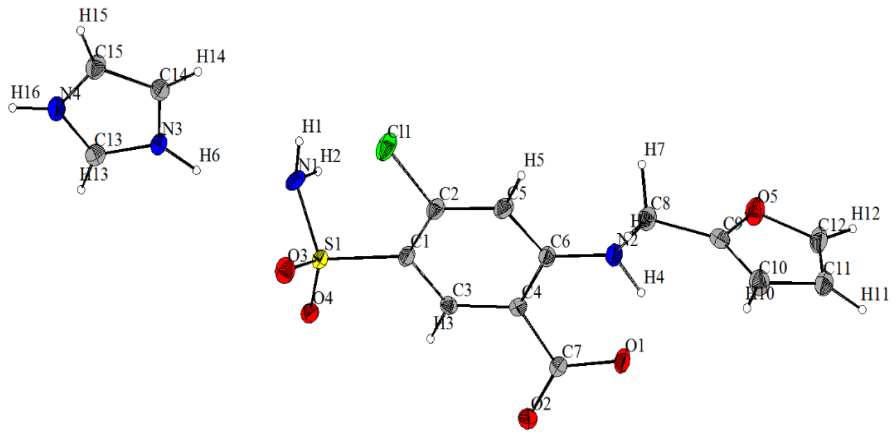

Figure 4.1: ORTEP plot of co-crystal (**5**) (The displacement ellipsoids are drawn at the 50% probability level and atoms in the asymmetric unit are labelled). Key: chlorine, green circles; sulphur, yellow circles; nitrogen, blue circles; oxygen, red circles; carbon, grey circles; hydrogen, small white circles.

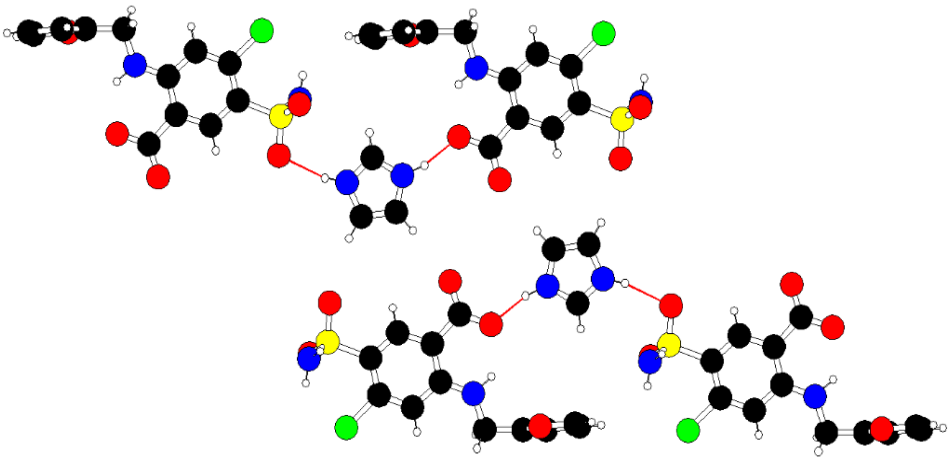

Figure 4.2: Hydrogen bonding interactions between furosemide and imidazole molecules in molecular complex (**5**). Solid red lines represent intermolecular hydrogen bonds. Key: chlorine, green circles; sulphur, yellow circles; nitrogen, blue circles;oxygen, red circles; carbon, grey circles; hydrogen, small white circles.

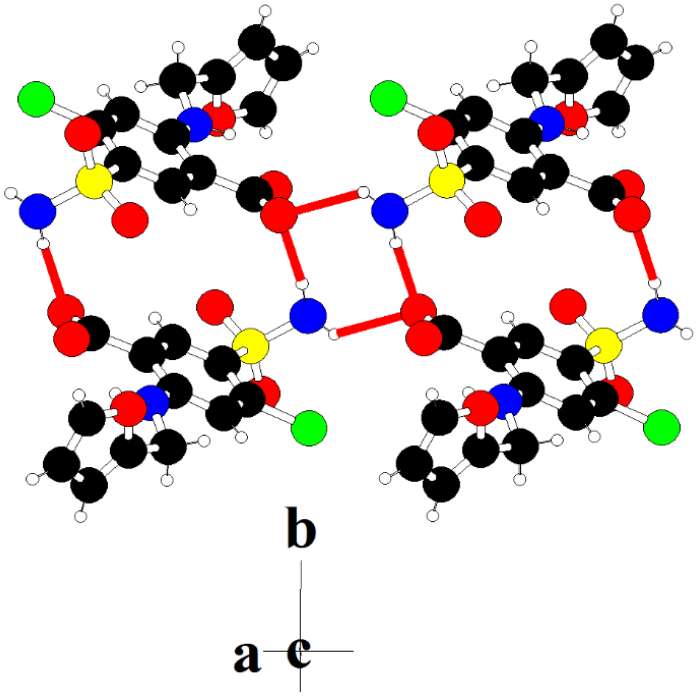

Figure 4.3: Hydrogen bonding interactions between furosemide molecules in molecular complex (**5**).

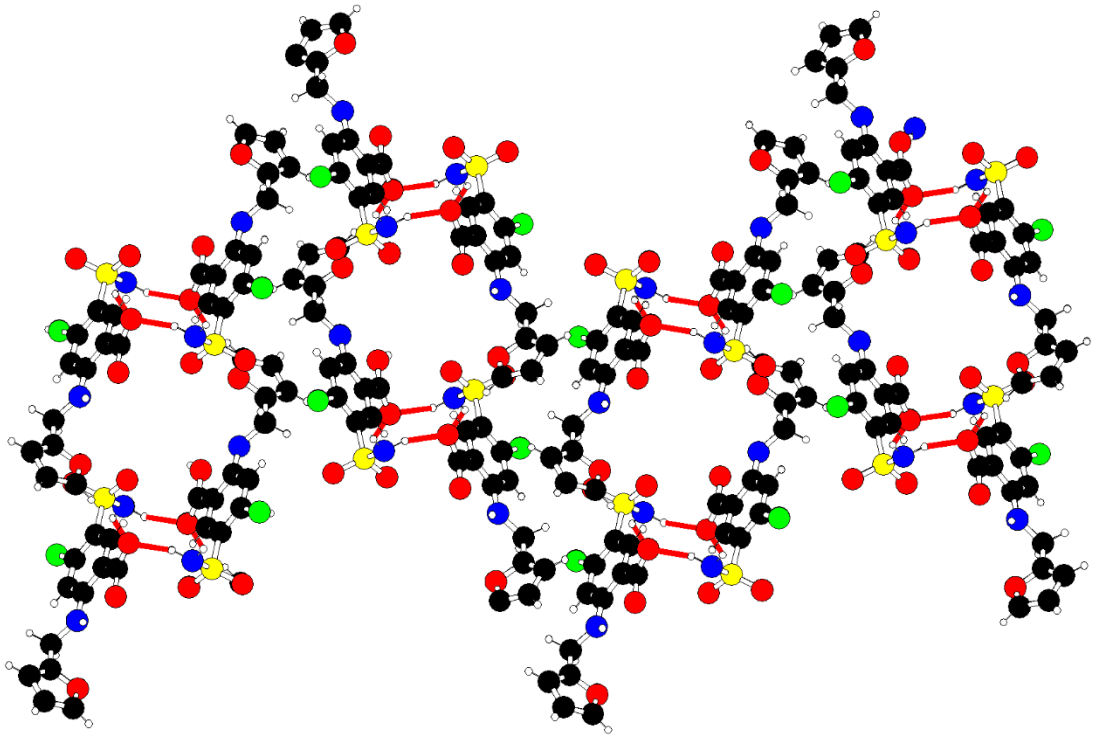

Figure 4.4: Host molecules forming channels in molecular complex (**5**), without the imidazole guest molecules.

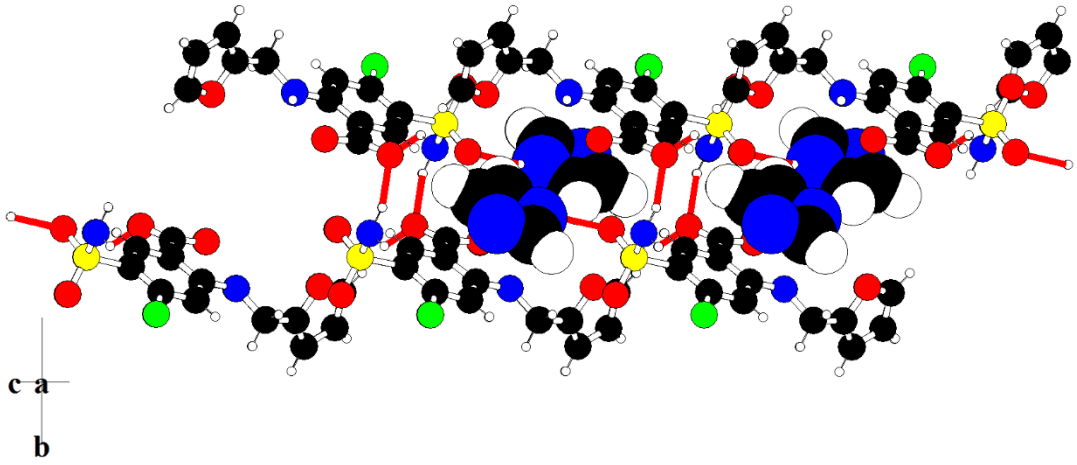

Figure 4.5: Host-guest arrangement in molecular complex (**5**). The imidazole molecules are shown in space fill settings.

The asymmetric unit consists of one molecule each of furosemide and imidazole (**5**) (Figure 4.1). Each furosemide molecule is hydrogen-bonded to two adjacent imidazole molecules

through N^{+}(3)-H(6)···O^{-}(1) and N(4)-H(16)···O(4) hydrogen bonding interactions (Table 4.1) (Figure 4.2). In addition, each furosemide molecule is hydrogen-bonded to two other furosemide molecules through N(1)-H(1)···O(2) and N(1)-H(2)···O(2) hydrogen bonding interactions (Table 4.1) to form a cyclic motif of the type $\mathbf{R}_2^2(4)$, as shown in Figure 4.3. Apart from these hydrogen bonding interactions, one C-H group of the furan ring hydrogen bonds to the carbonyl group of carboxylate anion through C(12)-H(12)···O(2) interactions (Table 4.1). The furosemide molecules assemble to form a host network possessing channels as shown in Figure 4.4. The channels propagate infinitely along the *a* crystallographic axis. These host channels in complex (**5**) are occupied by the imidazole guest molecules. A space-filling representation of the guest molecules occupying the host furosemide channels is shown in Figure 4.5.

The DSC thermogram of complex (**5**) shows a sharp endothermic transition with an onset temp of 201.5 ^{o}C, corresponding to the melting of the compound the molecular complex (Figure 4.6). The transitions following this could be due to the decomposition of the material.

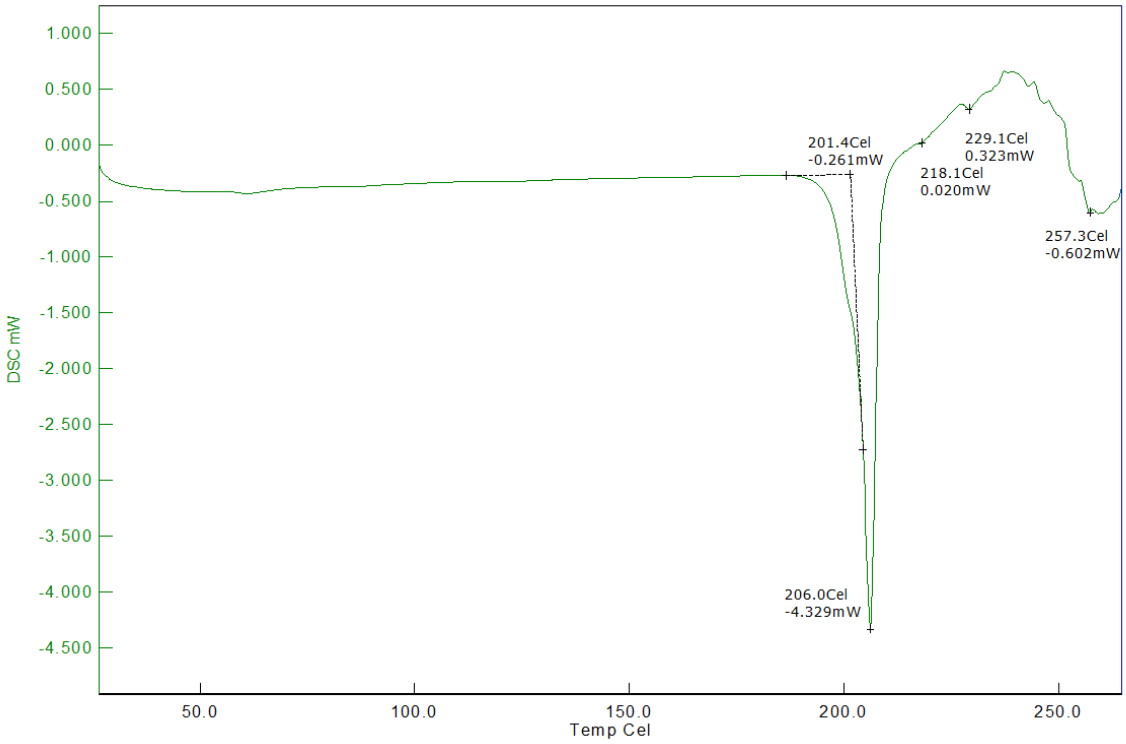

Figure 4.6: DSC of molecular complex (**5**).

4.2.2. Crystal structure description of molecular complex (6) [(furosemide)$_1$-(piperazine)$_1$]

The crystals of molecular complex (**6**) were obtained by slow evaporation from an ethanolic solution containing furosemide and piperazine in a 1:1 mole ratio. Colourless crystals of (**6**) appeared after 2 days. The single crystal structure shows that the asymmetric unit of (**6**) consists of one molecule each of furosemide and piperazine (Figure 4.7).

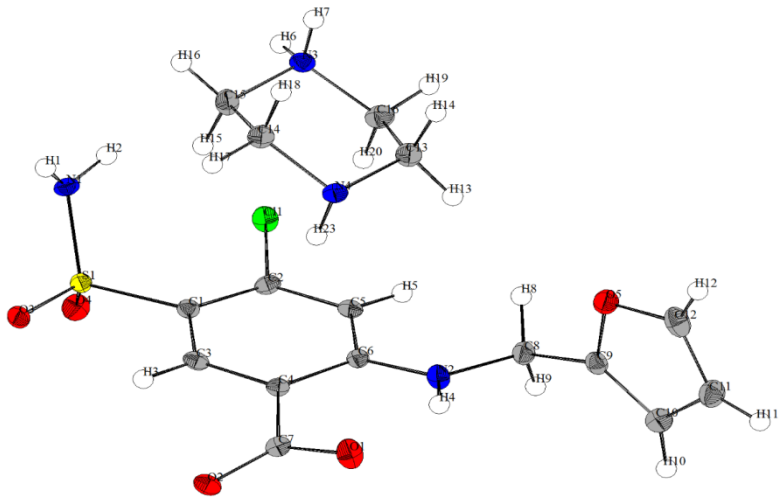

Figure 4.7: ORTEP plot of furosemide – piperazine molecular complex (**6**).

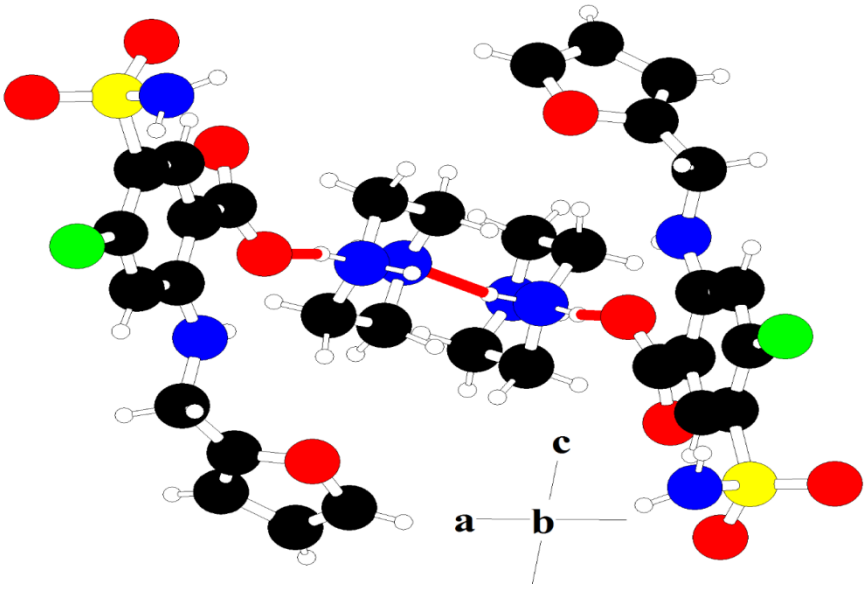

Figure 4.8: Hydrogen bonding interactions between furosemide and piperazine in molecular complex (**6**).

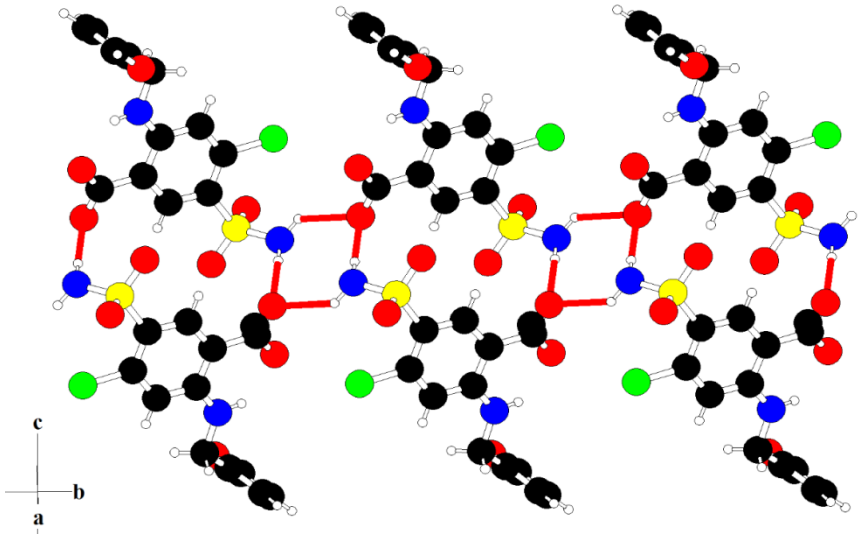

Figure 4.9: Hydrogen bonding interactions between furosemide molecules in molecular complex (**6**).

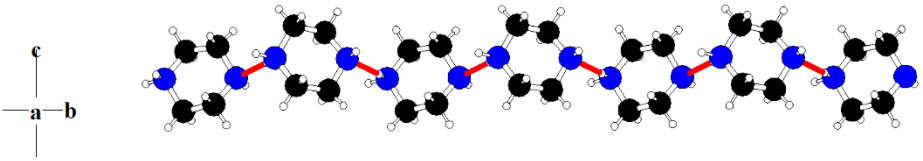

Figure 4.10: Hydrogen bonding interaction between piperazine molecules in molecular complex (**6**).

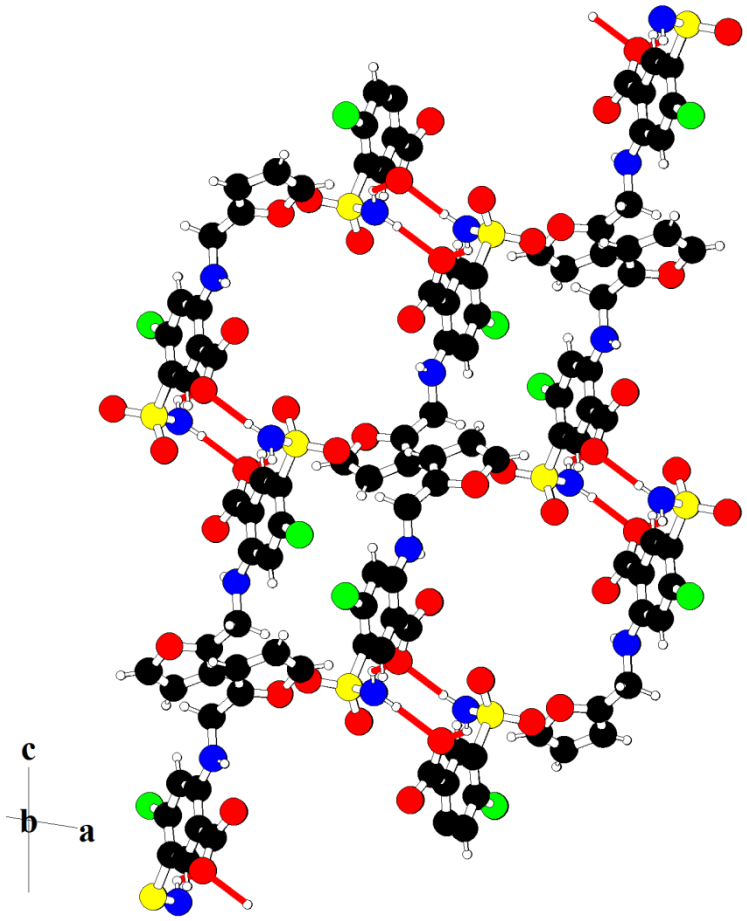

Figure 4.11: Furosemide channels in molecular complex (**6**).

The compound crystallises in the monoclinic crystal system with $P2_1/n$ as the space group. Analogous to the molecular complex (**6**), each furosemide molecule is hydrogen-bonded to two other furosemide molecules through N(1)-H(1)···O(2) and N(1)-H(2)···O(2) hydrogen bonding interactions (Table 4.1) to form a ring motif of the type $\mathbf{R}_2^2(4)$ (Figure 4.9). In addition, similar to complex (**5**), one of the C-H groups of furan also participates in hydrogen bonding interactions with the carbonyl group of the carboxylate anion to form a C(12)-H(12)···O(2) interaction (Table 4.1). The furosemide molecules arrange to form a host network of molecules resulting in channels as shown in Figure 4.11. These channels extend infinitely along the '*b*' crystallographic axis. The channels formed by the furosemide molecules are occupied by the piperazine molecules (Figure 4.12). The piperazine molecules, whilst hydrogen bonding with the furosemide molecules, also hydrogen bond among themselves through N(3)-H(6)···N(1) interactions to form an infinite network of hydrogen-bonded piperazine molecules (Figure 4.10). These interactions extend infinitely along the *b* crystallographic axis. Each piperazine molecule is hydrogen-bonded to the furosemide

molecules through N^{+}(3)-H(6)···O^{-}(1) charge assisted hydrogen bonding interactions (Figure 4.8). The crystal packing arrangement of molecular complex (**6**) is shown in Figure 4.12. The full crystallographic details of (**6**) are given in Table 4.2.

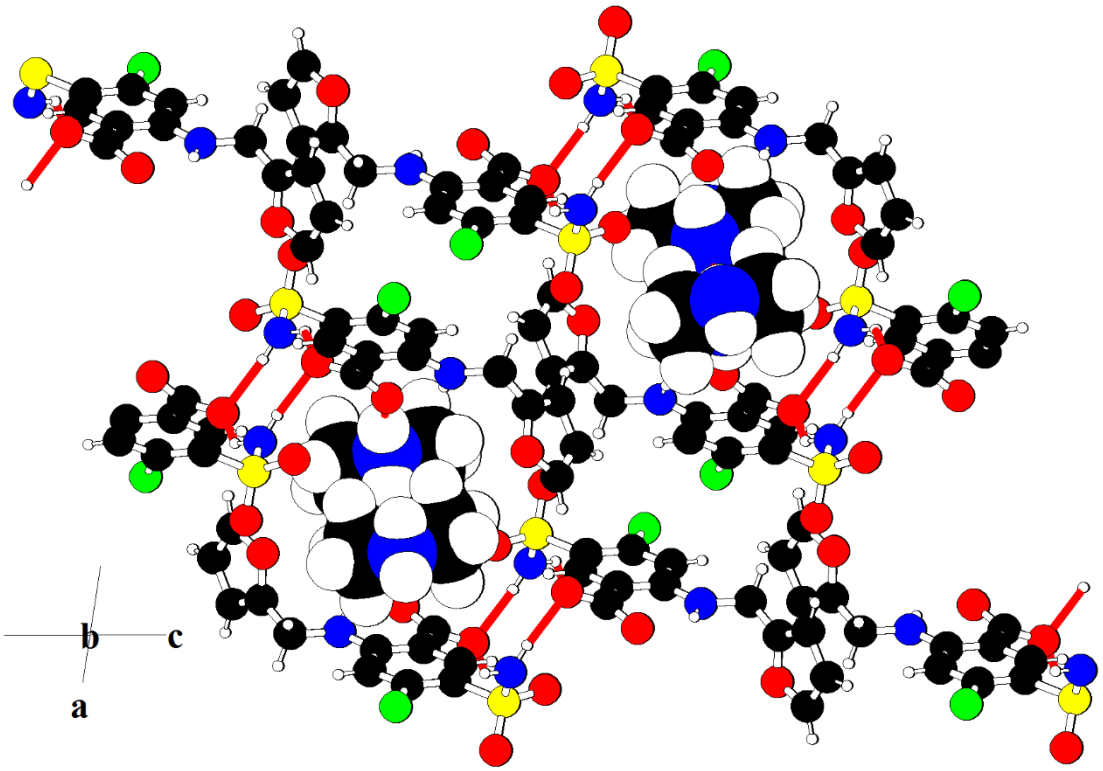

Figure 4.12: Host-guest assembly in molecular complex (6). The guest piperazine molecules are shown in space fill representation.

The DSC thermogram of (**6**) indicates an endothermic transition with an onset temp of 214.5 ^{o}C, corresponding to the melting of the compound (Figure 4.13). Complex (**6**) possesses a significantly different melting temperature compared to the starting materials FUR (220-222 ^{o}C) and PIP (109-110 ^{o}C).

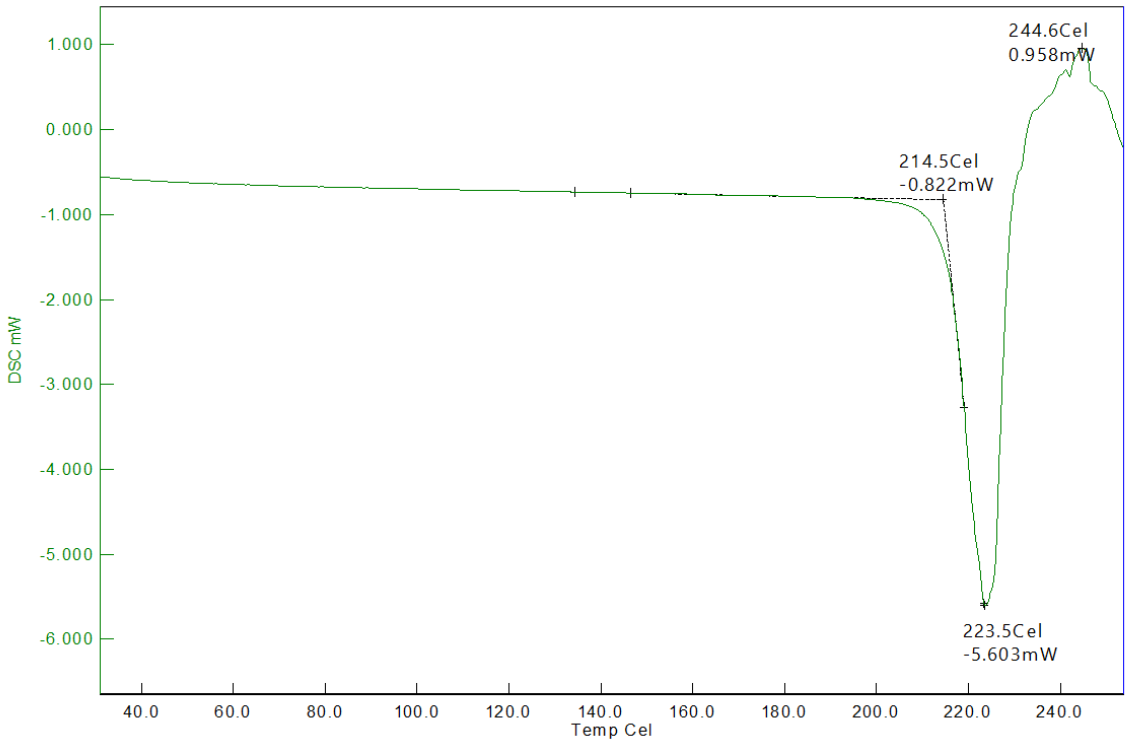

Figure 4.13: DSC of molecular complex (**6**).

4.2.3. Crystal structure description of molecular complex (7) [(furosemide)$_1$-(1,4,8,11-tetraazacyclotetradecane)$_{0.5}$]

Single crystals of molecular complex (**7**) were obtained by slow evaporation from an acetone solution containing furosemide and 1,4,8,11-tetraazacyclotetradecane in a 1:0.5 mole ratio. The crystal structure shows that the molecule crystallises in the $P\bar{1}$ space group. The full crystallographic details of (**7**) are given in Table 4.2. The crystal structure of (**7**) shows that the asymmetric unit consists of one molecule of furosemide and half a molecule of 1,4,8,11-tetraazacyclotetradecane, with 1,4,8,11-tetraazacyclotetradecane molecules possessing an inversion centre (Figure 4.14). Two furosemide and one 1,4,8,11-tetraazacyclotetradecane molecules generate a three component supermolecule stabilised through N^+(3)-H(6)···O^-(1) charge assisted hydrogen bonding interactions (Table 4.1) (Figure 4.15). The crystal structure shows that proton transfer occurs between the furosemide O-H groups to the basic amine nitrogen of cyclam resulting in the formation of a salt (Figure 4.15). Analogous to molecular complexes (**5**) and (**6**), similar hydrogen bonding interactions N(1)-H(1)···O(2) and N(1)-H(2)···O(2) (Table 4.1) are observed between the furosemide molecules resulting in the formation of a ring motif, $\mathbf{R}_2^2(4)$ (Figure 4.16). Whilst all other molecular complexes (**5**) and (**6**) contained hydrogen bonding interactions formed between the C-H of furan and

the carbonyl of furosemide, these interactions are not observed in molecular complex (**7**). However, several weak interactions exist between the furosemide molecules which lead to channels as shown in Figure 4.17. These channels are occupied by the co-former cyclam (Figure 4.18).

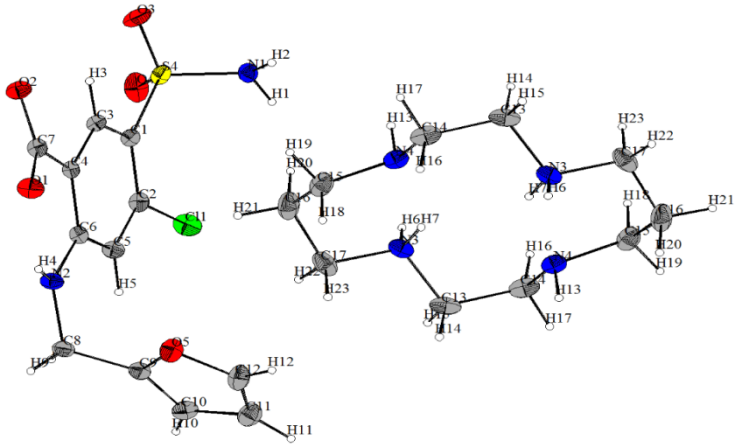

Figure 4.14: ORTEP plot of molecular complex (**7**).

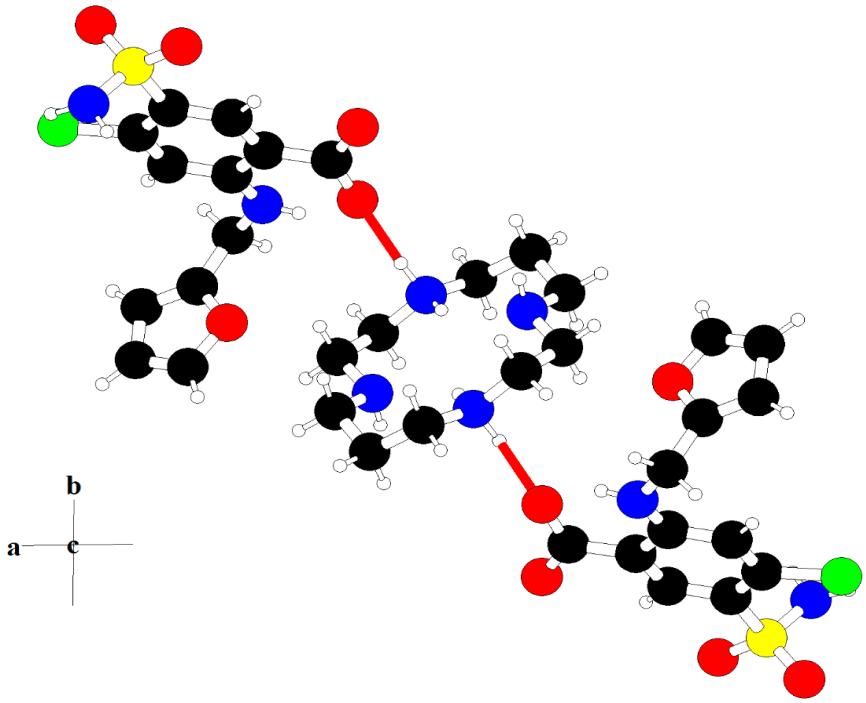

Figure 4.15: Hydrogen bonding interactions between furosemide and 1,4,8,11-tetraazacyclotetradecane in molecular complex (**7**).

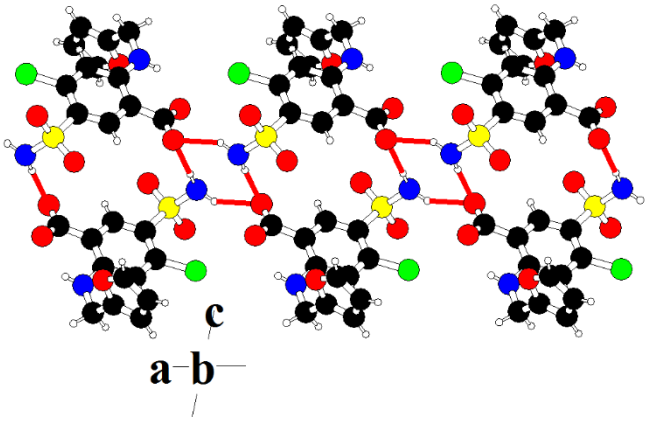

Figure 4.16: Interactions between furosemide molecules in molecular complex (**7**).

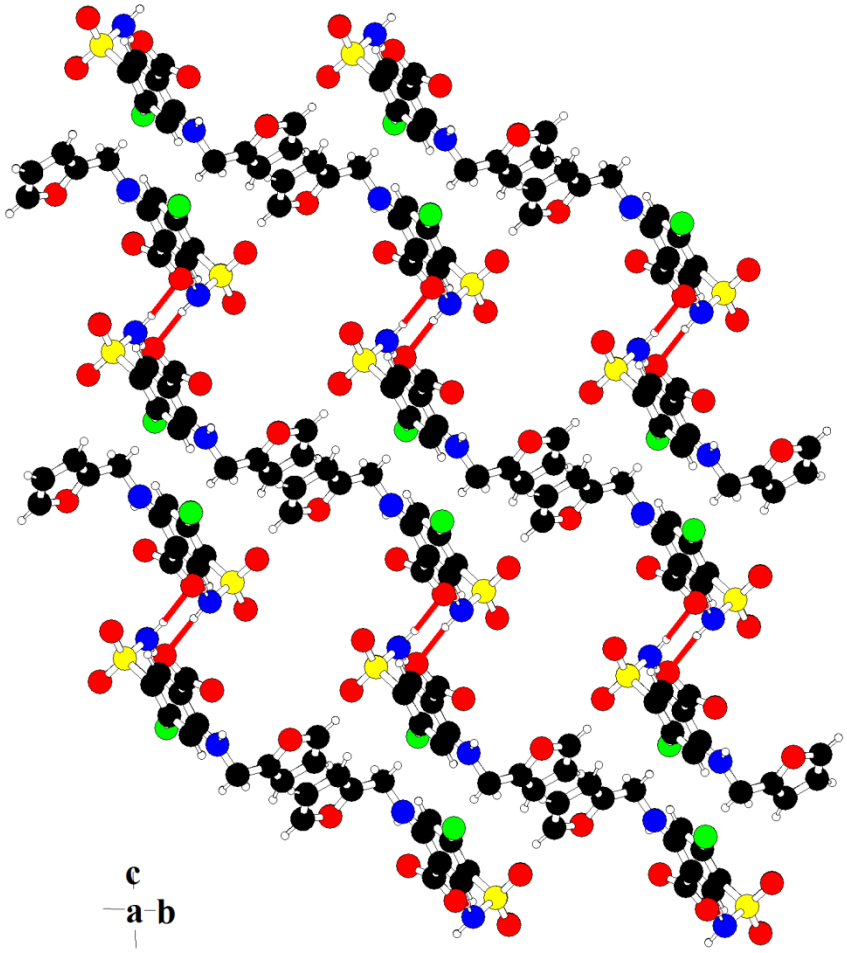

Figure 4.17: Channels formed by furosemide host network in molecular complex (**7**).

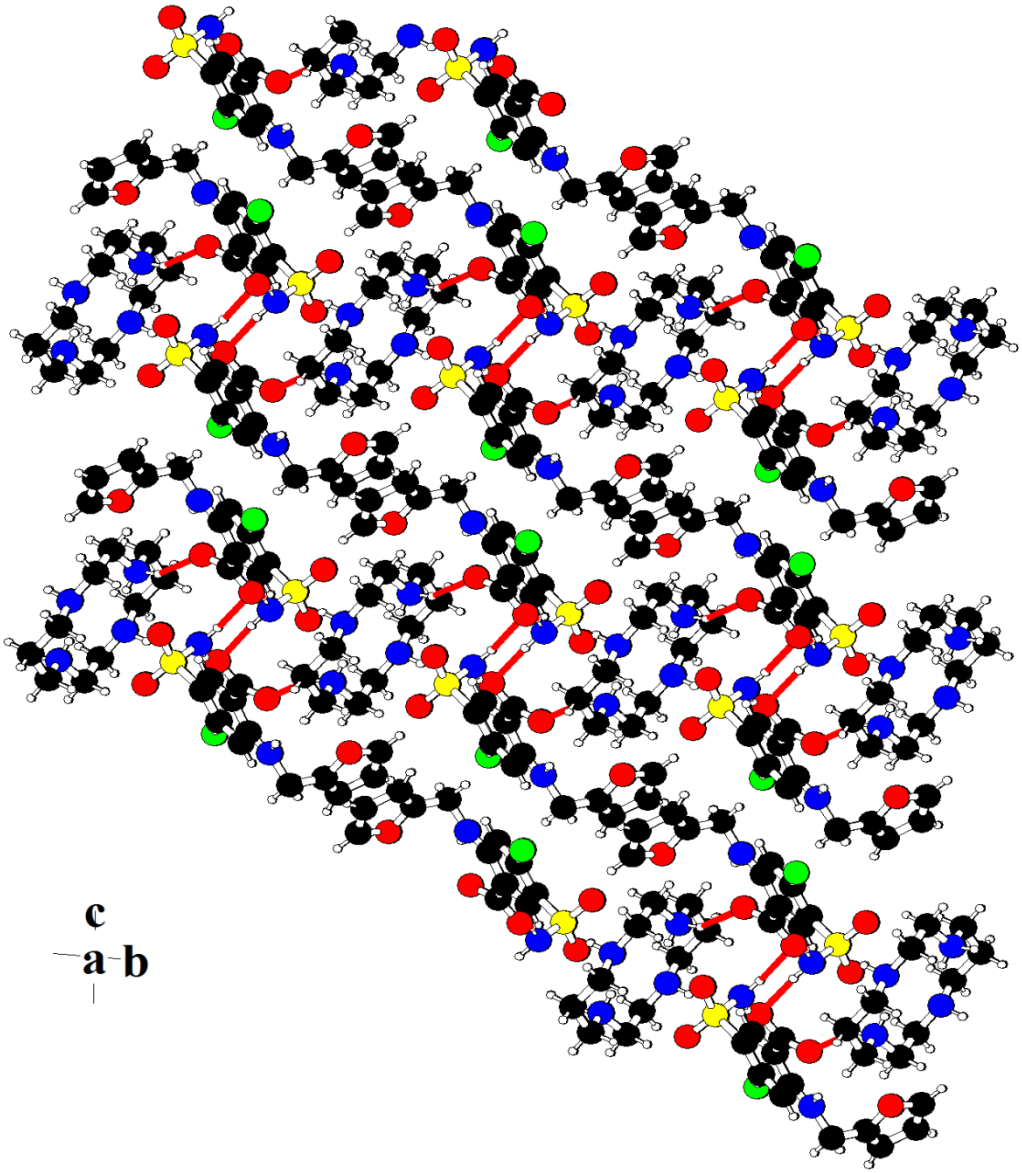

Figure 4.18: Host-guest arrangement in molecular complex (**7**).

The DSC data of the molecular complex (**7**) (Figure 4.19) shows a sharp endothermic transition with an onset temperature of 177.0 ^{o}C, corresponding to the melting of the compound. The transitions following this could probably be due to the decomposition of the material. The melting endotherm of the complex (**7**) is different to the melting points of the starting materials FUR (218-220 ^{o}C) and cyclam (182-186 ^{o}C).

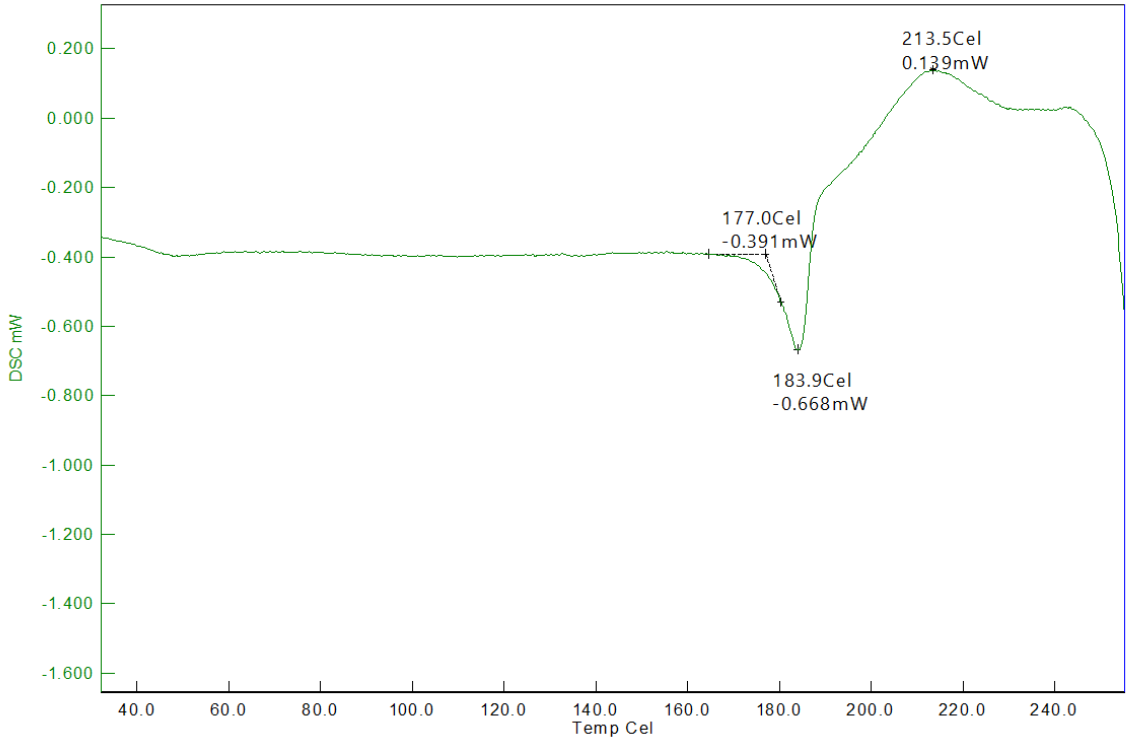

Figure 4.19: DSC of molecular complex (**7**).

4.2.4. Crystal structure description of molecular complex (8) [(furosemide)$_1$-(1,2-bis(4-pyridyl)ethane)$_{0.5}$]

Diffraction quality crystals of molecular complex (**8**) were obtained from a 2-propanol solution containing furosemide and 1,2-bis(4-pyridyl)ethane in 1:0.5 mole ratio. The asymmetric unit of (**8**) consists of one molecule of furosemide and half a molecule of 1,2-bis(4-pyridyl)ethane, with 1,2-bis(4-pyridyl)ethane molecules occupying inversion centre (Figure 4.20). The complex crystallises in a monoclinic crystal system with $P2_1/c$ as the space group. The full crystallographic details of (**8**) are given in Table 4.2. The 1,2-bis(4-pyridyl)ethane molecules and the furosemide molecules are hydrogen-bonded through N^+(3)-H(6)···O^-(1) charge assisted hydrogen bonding interactions (Table 4.1) (Figure 4.22). Analogous to molecular complexes (**5**) and (**6**), the furosemide molecules hydrogen bond through N(1)-H(1)···O(2) and N(1)-H(2)···O(2) interactions (Table 4.1) to form the ring motif, $\mathbf{R}_2^2(4)$ (Figure 4.21). In addition, one of the C-H groups of furosemide also participates in hydrogen bonding interactions with the carbonyl group though C(12)-H(12)···O(2) interactions (Table 4.1). The furosemide molecules arrange to form a network of host molecules containing channels, extending infinitely along the *a* crystallographic axis as show

in Figure 4.23. These channels are occupied by the 1,2-bis(4-pyridyl)ethane molecules resulting in the formation of host-guest assembly as shown in Figure 4.24.

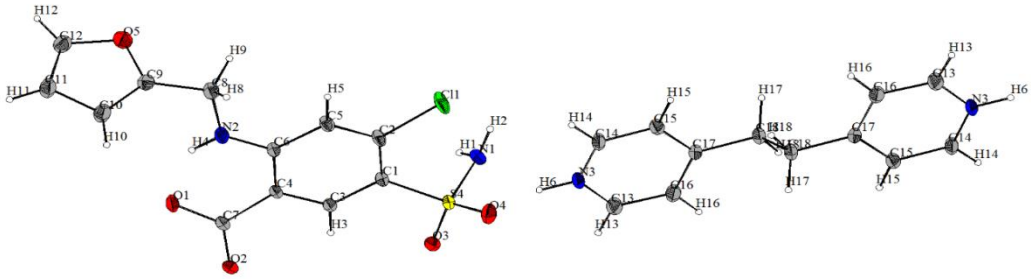

Figure 4.20: ORTEP plot of molecular complex (**8**).

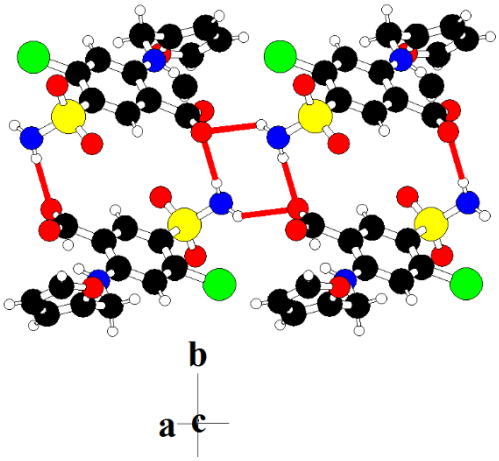

Figure 4.21: Hydrogen bonding interactions between furosemide molecules in molecular complex (**8**).

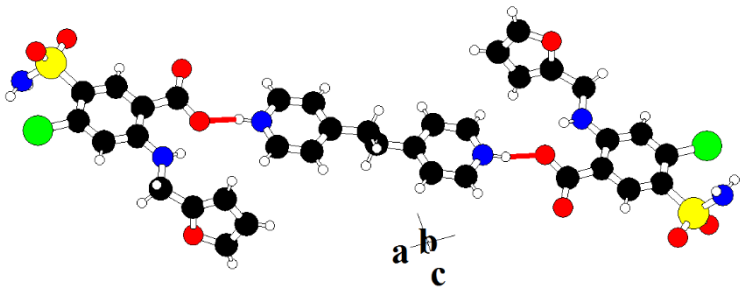

Figure 4.22: Hydrogen bonding interactions between furosemide and 1,2-bis(4-pyridyl)ethane in molecular complex (**8**).

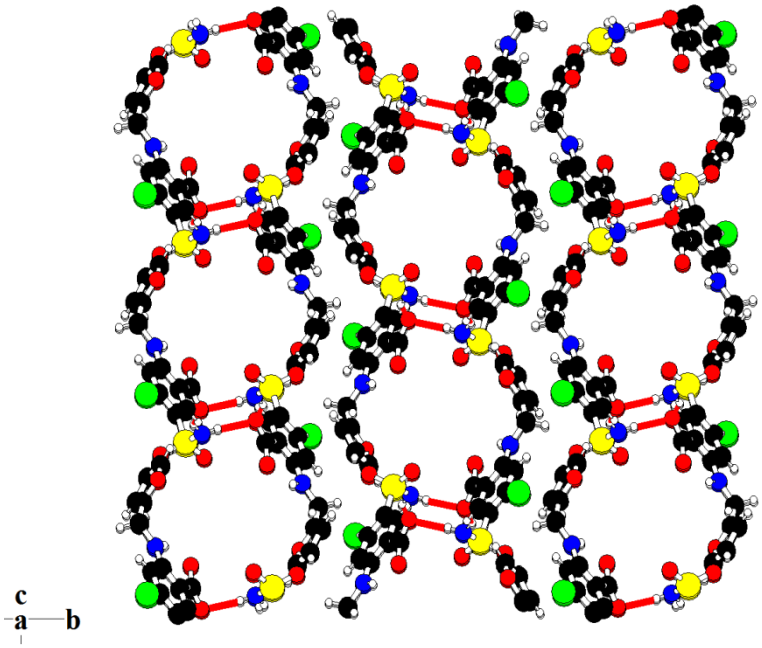

Figure 4.23: Furosemide channels in molecular complex (**8**).

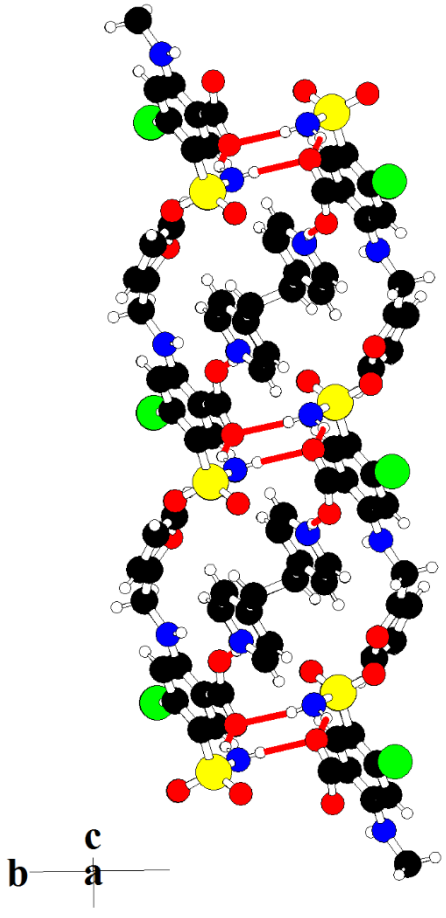

Figure 4.24: Host-guest arrangement in molecular complex (**8**).

The DSC thermogram of the molecular complex (**8**) (Figure 4.25) shows a sharp endothermic transition with an onset temperature of 237.9 ^{o}C and a peak at 242.3 ^{o}C. The endothermic transition matches with the melting of the complex as analysed by a capillary melting experiment. The melting transition is immediately followed by an exothermic transition, which could be due to the decomposition of the material.

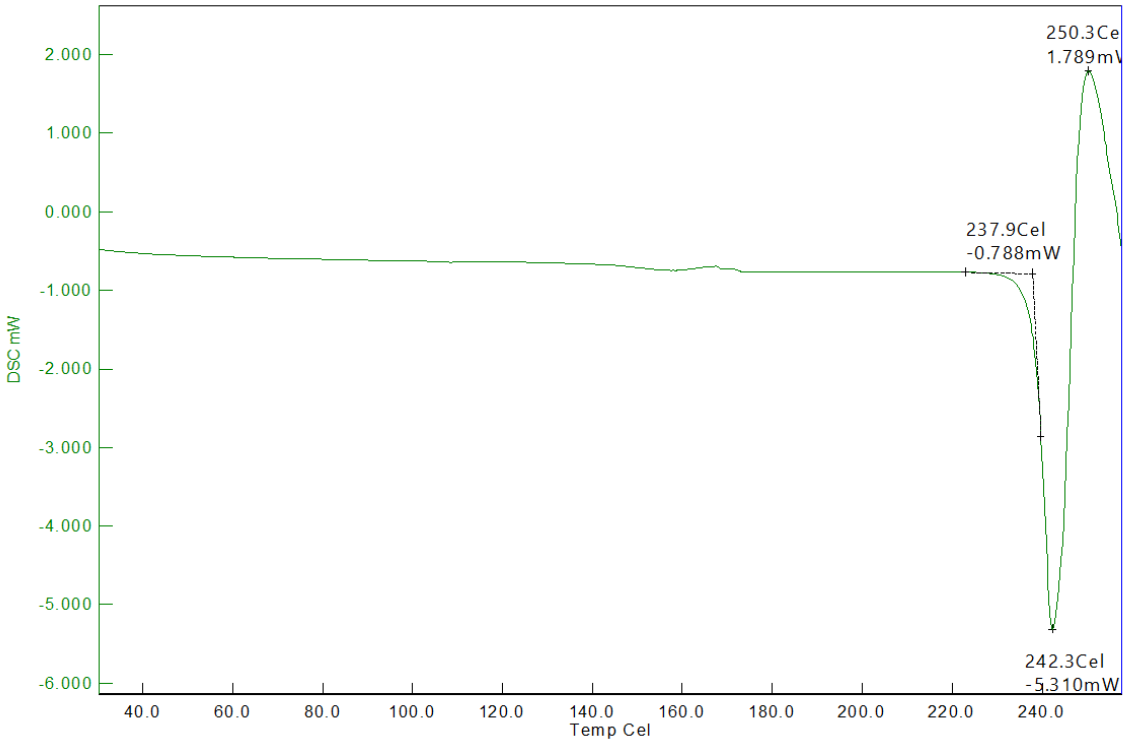

Figure 4.25: DSC of molecular complex (**8**).

Table 4.1: Geometric parameters for the hydrogen bonds in molecular complexes (**5**) – (**10**)

Compound	Hydrogen bond	*d* (H···A)/Å	*d* (D···A)/Å	*θ* (D-H···A)/^{o}
(5)	N^{+}(3)-H(6)···O^{-}(1)	1.70	2.61(2)	164.3
(5)	N(1)-H(1)···O(2)	2.32	2.99(4)	132.6
(5)	N(1)-H(2)···O(2)	1.89	2.83(5)	162.2
(5)	N(2)-H(4)···O(1) (intra)	1.96	2.64(2)	127.9

(5)	C(12)-H(12)···O(2)	2.36	3.3(2)	169.7
(5)	N(4)-H(16)···O(4)	1.97	2.83(6)	164.7
(6)	N^{+}(3)-H(6)···O^{-}(1)	1.67	2.65(3)	165.7
(6)	N(1)-H(1)···O(2)	1.89	2.79(4)	174.9
(6)	N(1)-H(2)···O(2)	2.16	2.88(6)	133.6
(6)	N(2)-H(4)···O(1) (intra)	1.95	2.63(7)	135.6
(6)	C(12)-H(12)···O(2)	2.41	3.33(5)	169.1
(6)	N(3)-H(7)···N(4)	1.93	2.79(3)	158.3
(7)	N^{+}(3)-H(6)···O^{-}(1)	1.86	2.33(3)	148.3
(7)	N(1)-H(1)···O(2)	2.02	2.86(5)	150.8
(7)	N(1)-H(2)···O(2)	1.91	2.84(6)	173.3
(7)	N(2)-H(4)···O(1) (intra)	1.98	2.67(4)	138.6
(7)	N(3)-H(7)···N(4) (intra)	2.22	2.89(2)	140.7
(8)	N^{+}(3)-H(6)···O^{-}(1)	1.67	2.58(2)	167.1
(8)	N(1)-H(1)···O(2)	2.05	2.87(2)	173.8
(8)	N(1)-H(2)···O(2)	2.3	3.0(4)	138.1
(8)	N(2)-H(4)···O(1) (intra)	1.93	2.65(6)	140.7
(8)	C(12)-H(12)···O(2)	2.56	3.49(5)	163.5
(9)	N^{+}(3)-H(6)···O^{-}(1)	1.63	2.54(4)	161.4

(9)	N(1)-H(1)···O(2)	2.06	2.84(7)	175.2
(9)	N(1)-H(2)···O(2)	2.24	2.97(4)	136.7
(9)	N(2)-H(4)···O(1) (intra)	1.94	2.64(4)	137.5
(9)	C(12)-H(12)···O(2)	2.56	3.35(7)	173.7
(10)	N(1)-H(2)···O(3)	2.19	3.0(4)	146.0
(10)	N(2)-H(4)···O(2) (intra)	1.99	2.68(3)	136.7
(10)	O(1)-H(6)···N(3)	1.76	2.60(5)	164.8
(10)	C(13)-H(13)···O(2)	2.44	3.18(6)	130.8
(10)	N(1)-H(1)···O(1)	2.60	3.06(5)	120.6

4.2.5. Crystal structure description of molecular complex (9) [(furosemide)$_1$-(1,2-di(4-pyridyl)ethylene)$_{0.5}$]

The single crystals of molecular complex (**9**) were obtained by slow evaporation from an ethanolic solution containing furosemide and 1,2-di(4-pyridyl)ethylene in a 1:0.5 molar ratio. The crystal structure of (**9**) is isostructural to the molecular complex (**8**). The molecule crystallises in a monoclinic crystal system with $P2_1/c$ as the space group. The asymmetric unit of the molecule consists of one molecule of furosemide and half a molecule of 1,2-di(4-pyridyl)ethylene, with the 1,2-di(4-pyridyl)ethylene occupying the inversion centre (Figure 4.26). The full crystallographic details are given in Table 4.2. The crystal structure shows that there is complete transfer of the furosemide O-H protons to the basic pyridyl nitrogens of 1,2-di(4-pyridyl)ethylene. The N^+-H hydrogen on the 1,2-di(4-pyridinum)ethylene cation was located from difference density map. Two furosemide and one 1,2-di(4-pyridyl)ethylene molecules generate a three component super molecule stabilised through $N^+(3)$-H(6)···$O^-(1)$ charge assisted hydrogen bonding interactions (Table 4.1) (Figure 4.27). Similar to the molecular complex (**8**), the two components furosemide and 1,2-di(4-pyridyl)ethylene arrange to form a host-guest assembly as shown in Figure 4.28 and Figure 4.29, with the

furosemide molecules forming the host network and the 1,2-di(4-pyridyl)ethylene molecules occupying the guest positions.

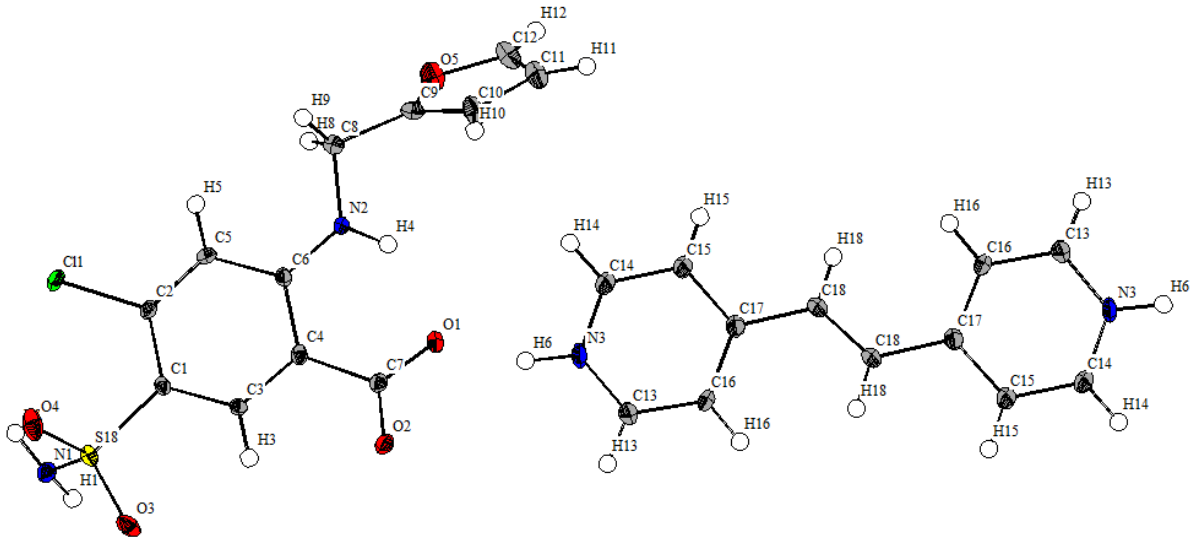

Figure 4.26: ORTEP plot of molecular complex (**9**).

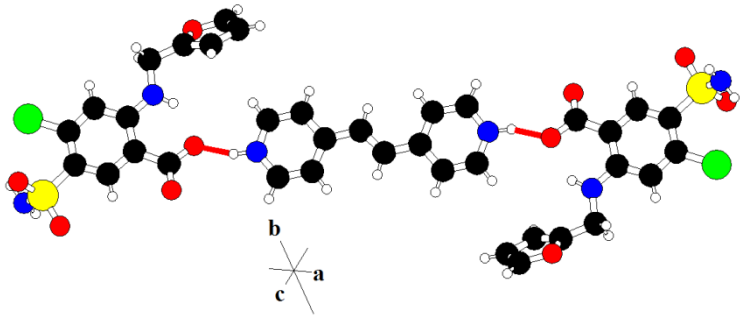

Figure 4.27: Hydrogen bonding interactions between furosemide and 1,2-di(4-pyridyl)ethylene in molecular complex (**9**).

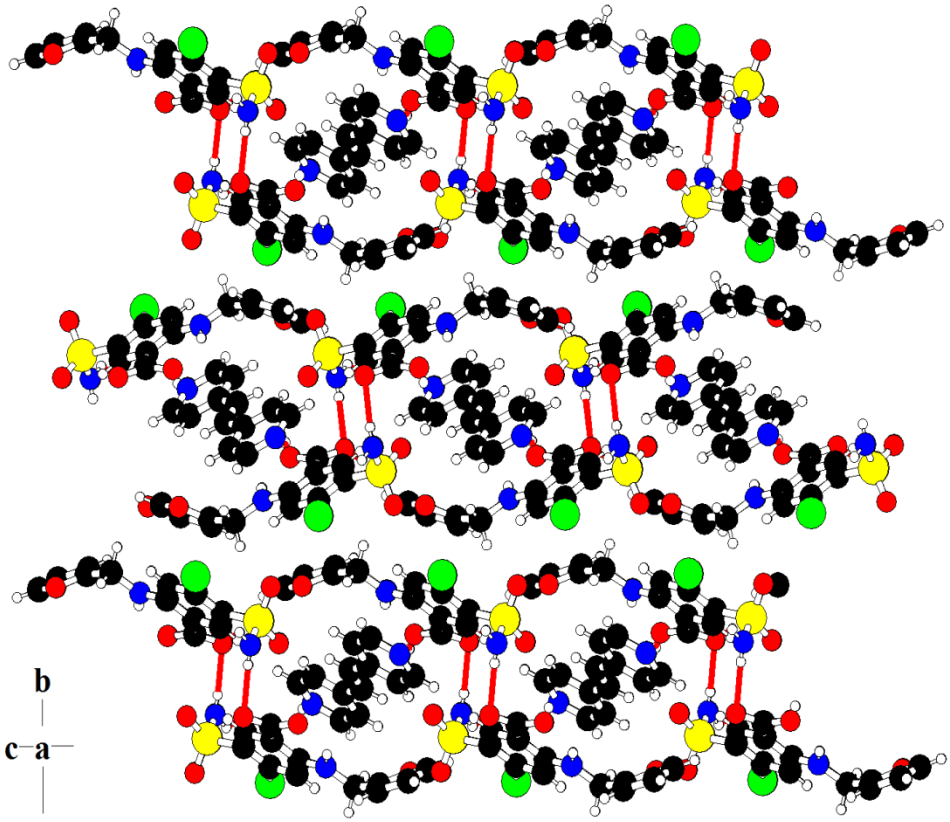

Figure 4.28: Host-guest assembly in molecular complex (**9**).

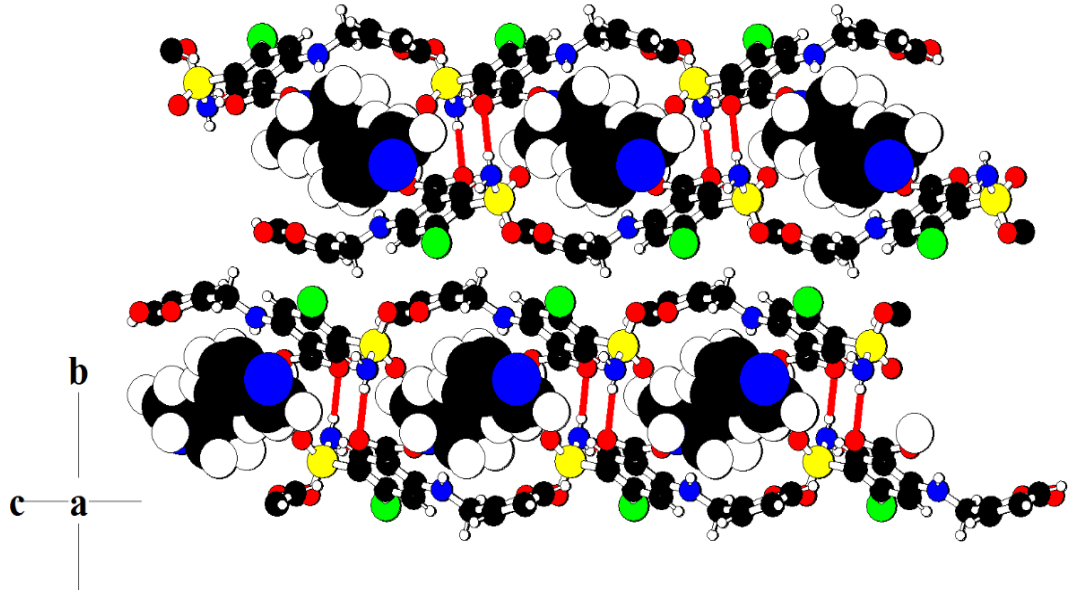

Figure 4.29: Host-guest assembly in molecular complex (**9**).

The molecular complex (**9**) has a higher melting point (DSC endotherm at 246.5 ^{o}C) compared to that of the two starting materials (Figure 4.29).

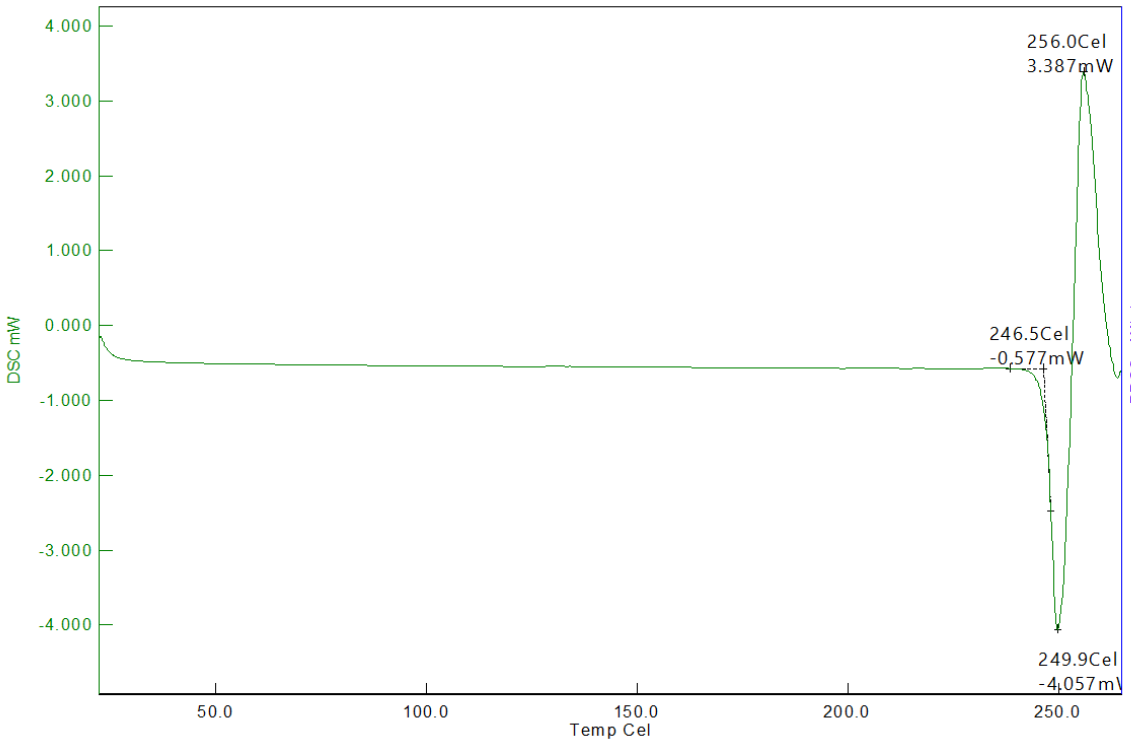

Figure 4.29: DSC of molecular complex (**9**).

4.2.6. Crystal structure description of molecular complex (10) [(furosemide)$_1$-(4,4'-bipyridyl)$_{0.5}$]

The single crystals of co-crystal (**10**) were obtained from a 2-propanol solution containing furosemide and 4,4'-bipyridyl in 1 to 0.5 mole ratio. Pale yellow coloured crystals of co-crystal (**10**) were obtained after 2 days of crystallisation. (**10**) crystallises in monoclinic crystal system with C2/*c* as the space group. The asymmetric unit of (**10**) consists of one molecule of furosemide and half a molecule of 4,4'-bipyridyl (Figure 4.30). The co-crystal former, 4,4'-bipyridyl, holds a crystallographic inversion centre. The two components furosemide and 4,4'-bipyridyl are stabilised through the acid-pyridine supramolecular synthon, while forming the O(1)-H(6)···N(3) and C(13)-H(13)···O(2) hydrogen bonding interactions (Table 4.1) (Figure 4.31). The N-H groups of furosemide hydrogen bond with one of the sulphoxide SO_2 oxygen atoms in the sulphonamide and the oxygen of the O-H groups of acid through N(1)-H(2)···O(3) and N(1)-H(1)···O(1) interactions (Table 4.1) as

shown in Figure 4.32. The furosemide molecules arrange to a network of molecules forming channels extending infinitely along the b crystallographic axis as shown in Figure 4.33. The channels formed by the furosemide molecules are occupied by the guest molecules 4,4'-bipydiyl to form a host-guest assembly as shown in

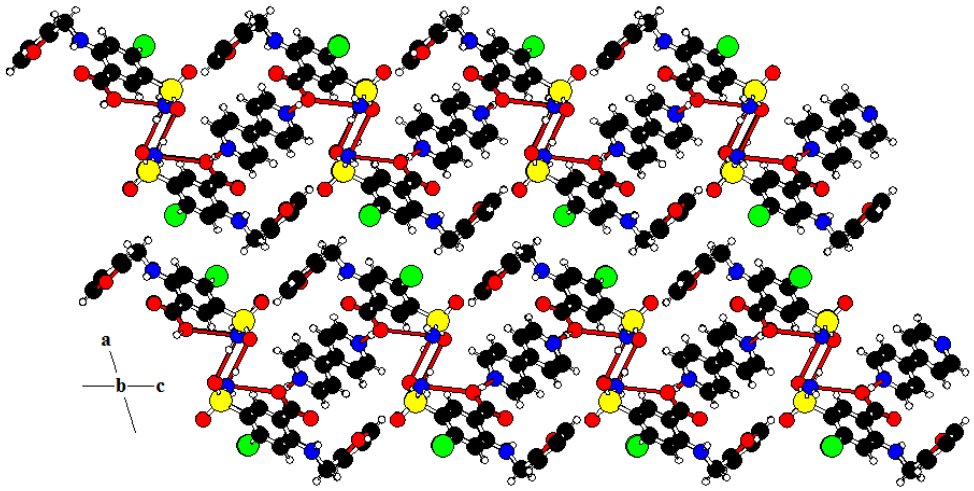

Figure **4.34**. The full crystallographic details of the molecular complex are presented in Table 4.2.

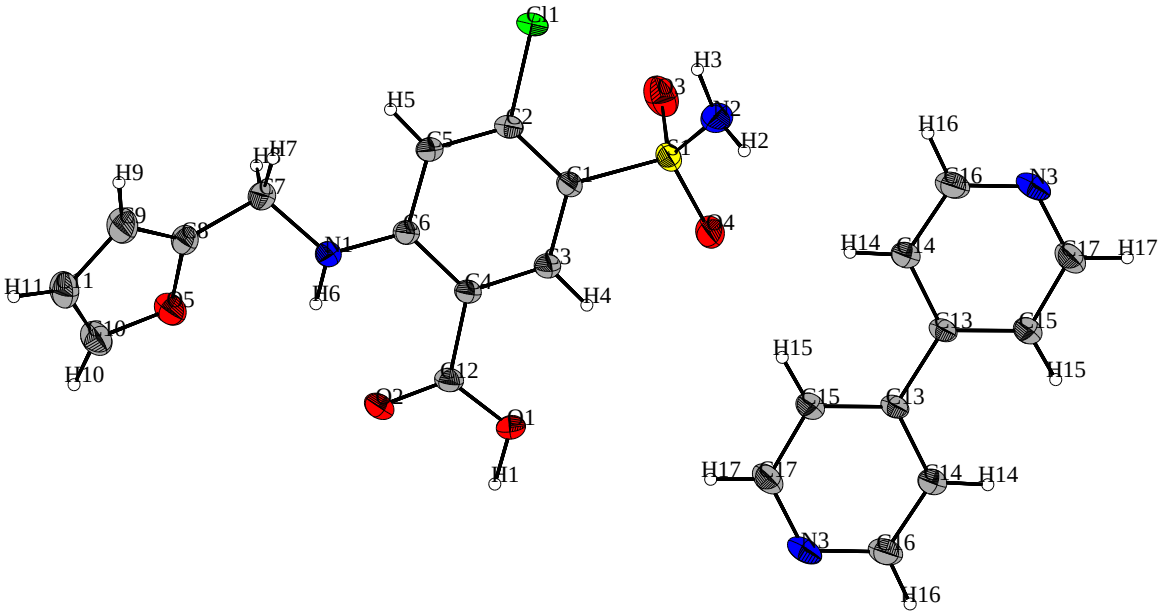

Figure 4.30: ORTEP diagram of co-crystal (**10**).

.

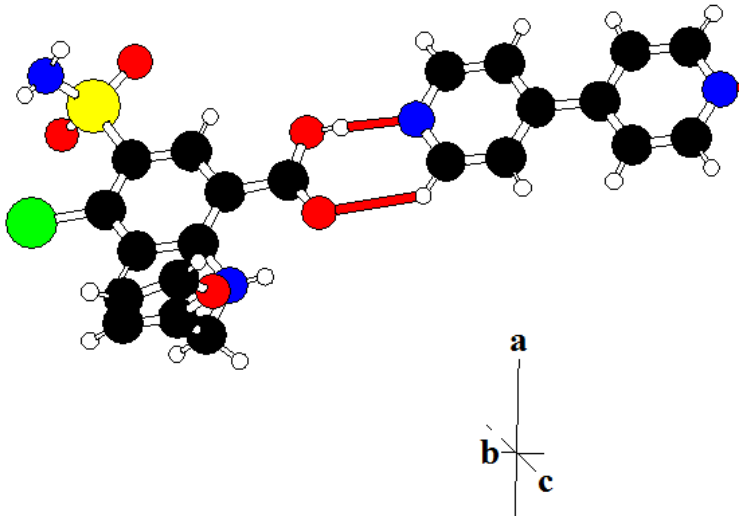

Figure 4.31: Hydrogen bonding interactions between furosemide and 4,4'-bipyridyl. The 4,4'-bipyridyl occupies inversion centre.

.

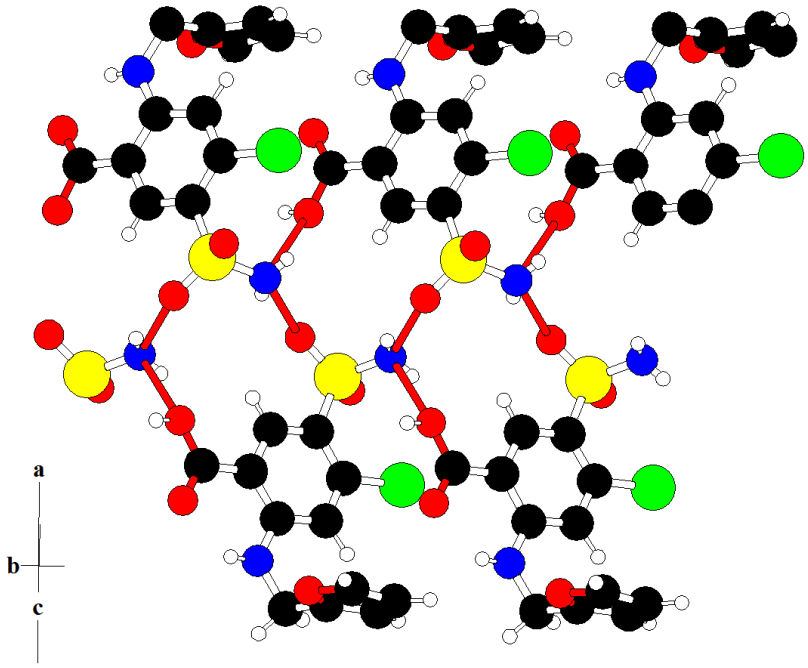

Figure 4.32: Hydrogen bonding interactions between furosemide molecules.

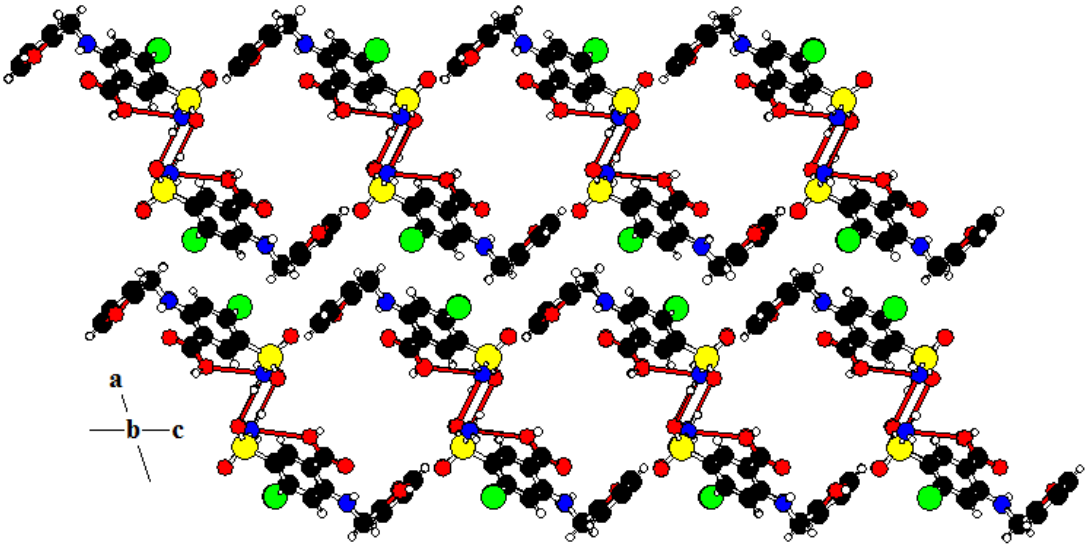

Figure 4.33: Host network: Channels formed by the furosemide molecules.

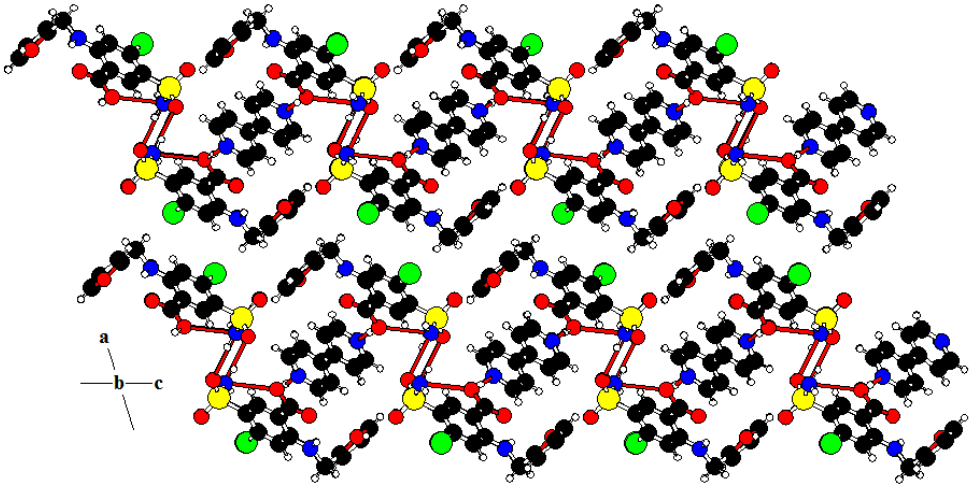

Figure 4.34: Host-guest assembly in co-crystal (**10**).

The DSC thermogram of the co-crystals of molecular complex (**10**) (Figure 4.35) shows a sharp endothermic transition with an onset temperature of 223.4 ^{o}C. The endothermic transition corresponds to the melting of the compound as examined by the capillary melting experiment. The transitions following the melting could be due to the decomposition of the material.

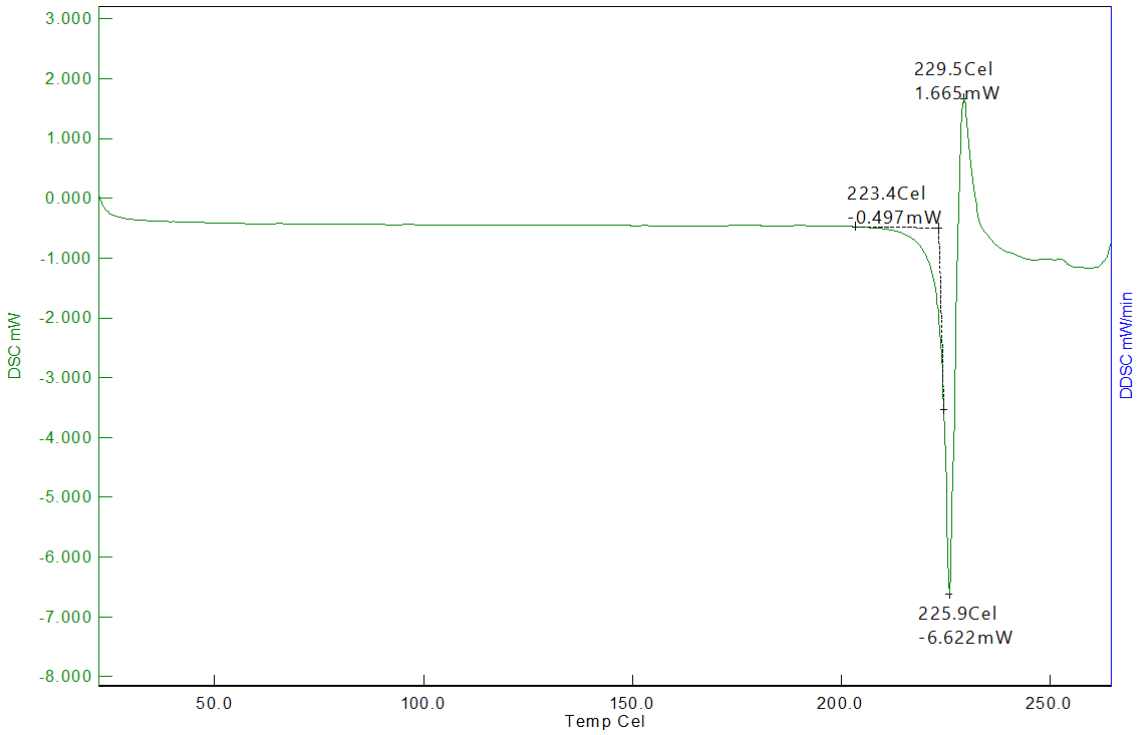

Figure 4.35: DSC thermogram of molecular complex (**10**).

Table 4.2: Crystallographic data of co-crystals (**5**)-(**10**).

	(**5**)	(**6**)	(**7**)	(**8**)	(**9**)	(**10**)
Chemical formula	$C_{15}H_{15}Cl_1N_4O_5S_1$	$C_{16}H_{21}Cl_1N_4O_5S_1$	$C_{17}H_{23}Cl_1N_4O_5S_1$	$C_{18}H_{17}Cl_1N_3O_5S_1$	$C_{18}H_{16}Cl_1N_3O_5S_1$	$C_{17}H_{15}Cl_1N_3O_5S_1$
Formula weight	398.8	416.8	430.9	422.9	421.9	408.8
Crystal system	monoclinic	monoclinic	triclinic	monoclinic	monoclinic	monoclinic
a / Å	8.759(8)	13.19(3)	8.864(9)	9.011(9)	9.0086(6)	26.35(5)
b / Å	21.264(19)	8.764(18)	9.562(10)	20.70(3)	19.7597(12)	6.648(13)
c / Å	9.205(9)	16.08(3)	11.930(15)	9.974(10)	10.0500(7)	21.29(5)

α / °	90	90	93.97(3)	90	90	90
β / °	95.110(17)	98.87(4)	101.61(4)	93.644(17)	94.150(4)	107.61(7)
γ / °	90	90	90.49(2)	90	90	90
Space group	$P2_1/c$	$P2_1/n$	$P\bar{1}$	$P2_1/c$	$P2_1/c$	$C2/c$
V / Å^3	1708.5(3)	1837.4(7)	987.9(2)	1856.2(4)	1784.3(3)	3555.0(13)
Z	4	4	2	4	4	8
$N_{reflection}$/ $N_{parameter}$	2958/235	2914/244	4890/253	4837/253	3303/253	3144/244
ρ_{calc} / g cm^{-3}	1.55	1.51	1.45	1.51	1.57	1.53
Radiation type	Mo Kα (λ =0.710173 Å)	Mo Kα (λ =0.710173 Å)	Mo Kα (λ =0.710173 Å)	Mo Kα (λ =0.710173 Å)	Mo Kα (λ =0.710173 Å)	Mo Kα (λ =0.710173 Å)
T / K	100	100	100	100	100	100
θ range/°	2.9 to 30.1	1.8 to 29.7	1.7 to 33.9	2.2 to 32.1	2.2 to 29.9	2.9 to 30.4
Range of *h*	-12 to 12	-18 to 18	-13 to 13	-13 to 13	-12 to 12	-37 to 35
Range of *k*	0 to 30	0 to 12	-14 to 14	0 to 30	0 to 27	0 to 9
Range of *l*	0 to 12	0 to 22	0 to 18	0 to 14	0 to 14	0 to 25
R_1 / %	4.4	4.1	4.3	3.5	4.7	3.7
$_wR_2$ / %	4.8	4.3	5.5	3.6	5.4	3.9

Goodness -of-fit	1.031	1.113	0.9123	1.102	0.9447	1.123

4.3. Discussion

The molecular structure of furosemide (Scheme 4.1) indicates that the molecule contains four conventional hydrogen bond donor and six conventional hydrogen bond acceptor groups, after taking into consideration that the halogen atom (chlorine) can also act as hydrogen bond acceptor. In addition, furosemide is confomationally flexible along the furanylmethylamino ($-NH-CH_2-C_4H_3O$) and sulfamoyl ($-SO_2-NH_2$) fragments. At the same time, some molecular fragments seem to be very rigid, i.e. the benzene ring, secondary amino group, the carboxylic acid group, the chlorine, as well as the sulphur atoms lie practically in one plane. The conformation of the sulfamoyl and furanylmethylamino fragments can be described by three torsion angles: $C_2-C_1-S_1-N_1$ (τ1), $C_6-N_2-C_8-C_9$ (τ2), and $N_2-C_8-C_9-O_5$ (τ3) (Figure 4.36 for atom numbering). The latter two torsion angles characterize the rotation of the furanylmethylamino fragment along the N_2-C_8 bond and of the furanyl ring along the C_8-C_9 bond. The other important structural feature in the furosemide is the orientation of the NH_2 in relation to the SO_2 in the sulphonamide group. In all the molecular complexes studied here the NH_2 is oriented anti to the SO_2 in the sulphonamide group. The results of the conformational analysis of the furosemide molecule in the crystal structure are summarized in Table 4.3.

Table 4.3: Several torsion angles: τ1 ($C_2-C_1-S_1-N_1$), τ2 ($C_6-N_2-C_8-C_9$), τ3 ($N_2-C_8-C_9-O_5$), and orientation of NH_2 group in the sulfamoyl group characterizing the conformation of the furosemide molecule in different molecular complexes.

Crystal structure	τ1	τ2	τ3	Orientation of NH_2	conformation
Furosemide form-I	163.2(4)	-61.4(6)	-57.6(6)	trans	TG^-G^-anti
Molecular complex (**5**)	-66.0(6)	-172.6(9)	-65.6(2)	trans	G^-TG^{-anti}

Molecular complex (**6**)	-64.6 (3)	164.6(1)	-81.2(5)	trans	$G^{-}TG^{-anti}$
Molecular complex (**7**)	68.2(4)	-69.6(9)	-47.8(8)	trans	$G^{+}G^{-}G^{-anti}$
Molecular complex (**8**)	-65.4(9)	166.2(4)	-107.4(1)	trans	$G^{-}TT^{anti}$
Molecular complex (**9**)	-65.1(5)	176.2(4)	-124.3(6)	trans	$G^{-}TT^{anti}$
Molecular complex (**10**)	64.7(8)	-70.7(8)	-60.1(8)	trans	$G^{+}G^{-}G^{-anti}$

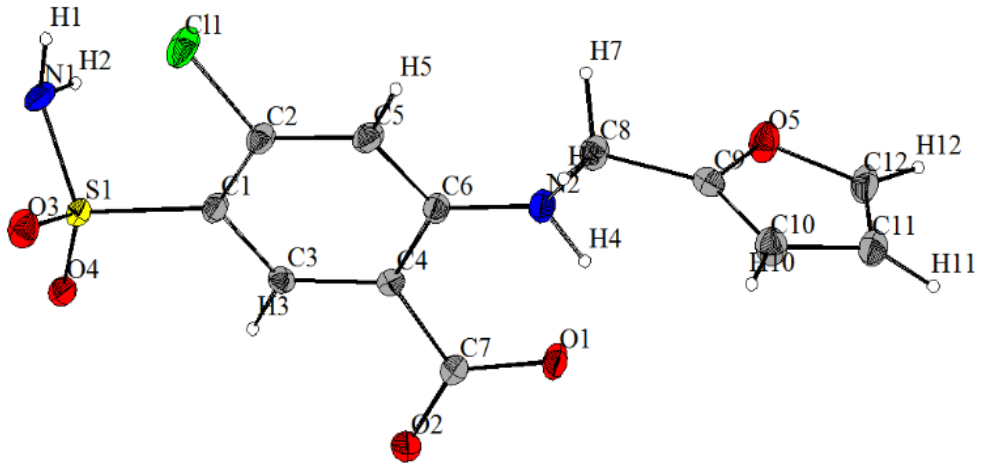

Figure 4.36: ORTEP of furosemide with numbering.

In the molecular complexes presented here the sulfamoyl group adopts either gauche+ or gauche− conformation, with no intermediate *trans* conformation. The furanylmethylamino fragment, when compared to the furosemide form-I adopts *trans* conformation in molecular complexes (**5**), (**6**), (**8**) and (**9**), while being gauche− in (**7**) and (**10**) molecular complexes. All the overlayed conformations of furosemide are shown in Figure 4.37. While the carboxylic acid group in furosemide form-I and in molecular complex (**10**) lie in the plane of the benzene ring, in other molecular complexes presented here the carboxylate anion is slightly twisted with respect to the benzene plane.

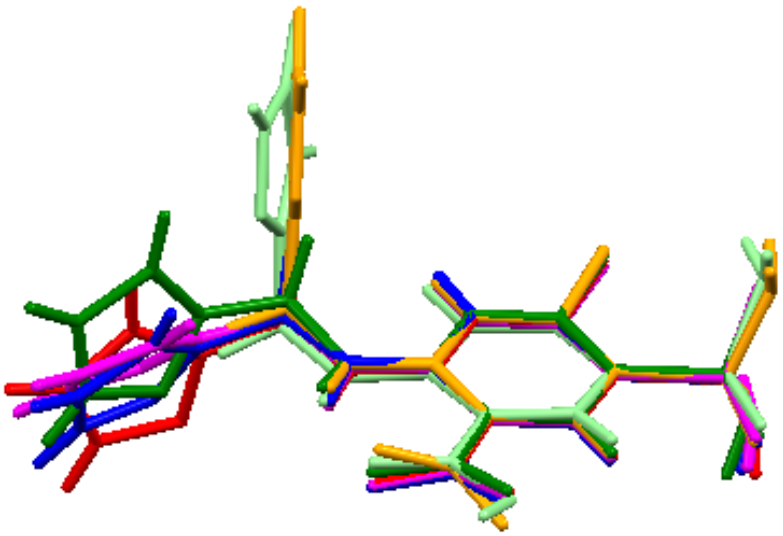

Figure 4.37: Overlaid conformations of furosemide molecules in all the molecular complexes.

A generally accepted guideline[167] for salt formation is that the proton transfer will occur from an acid to a base when the difference in pKa (ΔpKa being the difference between the pKa value of a protonated base and that of the acid) is >3.5, and a neutral co-crystal will form when the ΔpKa < 0. A co-crystal to salt continuum exists between 0 ≤ΔpKa ≤ 3.5. The molecular complexes formed by piperazine, imidazole, 1,4,8,11-tetraazacyclotetradecane are in agreement with the calculated pKa values.[168] Whilst the calculated pKa of values for 1,2-bis(4-pyridyl)ethane, 1,2-di(4-pyridyl)ethylene and 4,4'-bipyridyl fall in the 0 ≤ΔpKa ≤ 3.5 range, salt formation is observed in the single crystal structure when 1,2-bis(4-pyridyl)ethane and 1,2-di(4-pyridyl)ethylene are used as co-formers. However, a neutral molecular complex resulted when 4,4'-bipyridyl is used as the co-crystal former. This suggests that the prediction of the degree of proton transfer in the solid-state form based on the pKa difference remains imprecise and may also show variations with the solvent of crystallisation. The ^{1}H-NMR spectra of the molecular complexes (**6**)-(**10**) are given in Appendices A.1.4 to A.1.8. The ^{1}H-NMR data suggests that the crystal analysed is a representative of the bulk material.

The molecular complexes (**5**) - (**9**) are stabilised through charge transfer hydrogen bonding interactions. The charge separation resulting from the proton transfer leads to the dominance of electrostatic interactions over other noncovalent interactions. The molecular complexes (**5**) to (**9**) exhibit the charge assisted hydrogen bonding interactions. These interactions drive the

molecular complex formation whilst forming other hydrogen bonds between furosemide molecules. The hydrogen bonding interactions observed between the furosemide molecules are different in co-crystal (**10**) when compared to the interactions in molecular complexes (**5**) –(**9**). In molecular complex (**10**), the two components are stabilised through a neutral acid-pyridine heterosynthon. In summary, the molecular complexes (**5**) – (**10**) studied here suggest that the charge transfer hydrogen bonding interactions can be used to control the auxiliary hydrogen bonding interactions. These auxiliary hydrogen bonds between furosemide molecules arrange to form a network of host molecules exhibiting 1D channels. These channels are occupied by the guest (co-crystal former) molecules in all the molecular complexes. The guests molecules studied here vary in size and shape.

4.4. Conclusion

In conclusion, six new host-guest molecular complexes of furosemide with various heterocyclic bases have been synthesised and structurally characterised. It has been demonstrated that the crystal packing arrangement of the molecules is dependent on the dominant intermolecular interaction in the complex. The charge assisted hydrogen bonding interaction is the dominant interaction in the molecular complexes (**5**) to (**9**). This interaction drives the crystal packing arrangement in the complexes to form persistent hydrogen bonding interactions between furosemide molecules. Such persistent hydrogen bonding interactions between furosemide molecules are not observed in molecular complex (**10**), where the two components are stabilised through an acid-pyridine supramolecular synthon. In all the complexes, the two components arrange to form host-guest supramolecular complexes. A detailed conformational analysis of furosemide shows that the molecule can exist in different conformational orientations. This allows the host network formed by the furosemide molecules to accommodate different guests of varying size.

Chapter 5: A Robust Two-Dimensional Hydrogen-Bonded Network for the Predictable Assembly of Ternary Co-crystals.

5.1. Introduction

One of the primary goals of molecular crystal engineering is, given the molecular structure of the constituent components, one should be able to predict the crystal structure.[169] In this context, John Maddox[170] noted that "inability to predict crystal structures from the molecular structures is one of the continuing scandals of modern science". The prediction of crystal structure is of importance since the crystal structure of any material is most arguably the important piece of information that could be obtained about the material, which directly or indirectly determines/influences the properties of the material.[171] A crystal is considered as a supermolecule[172] and, when compared to the molecular structure, represents a higher level of complexity with crystallisation considered as the supramolecular reaction. In order to predict crystal structures on a routine basis, a complete understanding of the synthetic step, the crystallisation process, is required. In the absence of a complete understanding of the crystallisation process, crystal engineers are left with no option but to empirically develop new strategies leading to the prediction of related crystal structures. At present the prediction of crystal structures is done by two methods: (a) computational methods and (b) crystal engineering based methods. Computational methods of crystal structure prediction are precise and deal primarily with known molecular compositions. It usually involves the analysis of molecular recognition features of the constituent molecules in the context of how they generate symmetry operations when optimized to form a close packing structure, thus resulting in the prediction of crystal structure. Usually, by this method a number of possible crystal structures are obtained, with the experimental structure being hidden amongst the other possible structures. The computational method of structure prediction is often inadequate or extremely difficult when (i) the experimental structure is not the thermodynamically stable structure but a higher-energy (metastable) kinetically stabilised structure and (ii) in systems containing flexible molecules with the number of symmetry-independent non-hydrogen atoms >20 and (iii) in systems with Z'>1.

Crystal engineering methods of crystal structure prediction are generally less precise compared to *ab-initio* or force-field methods and are typically restricted to predicting networks of entirely new phases containing known molecules. Crystal engineering based

structure prediction can be done in two ways (i) based on a blueprint obtained rationally or serendipitously[173] and (ii) retro-synthesis based structure prediction. By the first process, the crystal structure of a known compound serves as a blueprint for rational selection and prediction of the packing arrangements in related compounds. The retro-synthesis based strategy involves the identification of a robust combination of supramolecular synthons from CSD analysis that are specific to functional groups. A crystal engineer then seeks to reproduce these supramolecular synthons in a series of related molecules. Both processes involve complete understanding of the delicate intermolecular interactions existing between the component or components. However, the ability to reproduce a set of supramolecular synthons or to synthesise a material based on a blueprint structure occurs only in an ideal situations. Often serious problems arise due to the following reasons:

1. The number of possible supramolecular synthons can increase steeply upon little increase in the molecular functionality.

2. Since the hydrogen bonding/ intermolecular interactions existing between the molecular components are weak the presence of polymorphism[174] cannot be avoided.

3. The most serious problem is the interference from the hydrocarbon residue, which is considered to be a supramolecular functionality and participates in molecular recognition units.

Structure prediction by retro-synthesis based strategies has been limited to the prediction of a supramolecular synthon, with little or no control over the packing arrangements of other functional groups. Prediction of crystal packing arrangements by these methods occurs only in ideal or rare situations. Strategies that overcome the above problems and allow the prediction of space group symmetry, gross structural features, and the prediction of lattice parameters and atomic co-ordinates are of importance in crystal engineering.

In this chapter, the prediction of the space group and crystal packing arrangements in co-crystals uses the crystal engineering method and is based on identifying an *n*-dimensional network and utilising the *n*-dimensional network to predict the space groups and packing arrangements in other co-crystals. The approach in the chapter for the synthesis of *n*-dimensional networks is based on selection of components based on the geometry of the functional groups. The geometry of the functional groups plays important role in the molecule's ability to participate in hydrogen bonding interactions. The identification of a

robust *n*-dimensional network reduces the structure prediction problem of crystal engineering to the 3-*n* dimensions thereby improving the predictability. Whilst robust supramolecular synthons[175] are common between functional groups, robust networks based on combinations of supramolecular synthons are extremely rare: a notable exception being the publications from Ward group,[176] where the robust two-dimensional network utilized ionic interactions.

In addition to crystal structure prediction, one of the challenges of organic crystal engineering is the ability to synthesise higher order crystals. In order to synthesise ternary or higher order co-crystals, a better understanding of the molecular recognition processes is required. Synthesizing higher order co-crystals and understanding molecular recognition processes is absolutely essential if we are to understand the enormously complex and efficient molecular recognition processes in enzyme–coenzyme–substrate complexes.[177] While the number of binary co-crystals are increasing every day, synthesis of ternary or higher order crystals is still challenging and frustrating, with few exceptions.[178] This is largely due to the absence of reliable structural paradigms. Synthesis of ternary or higher order co-crystals is also hampered by the number of possible cross-over reactions and by the solubility of the components. A mixture of several components with quite different solubility profiles could form a co-crystal, but more often than not will only result in the precipitation of the individual component with the lowest solubility. One alternative for this is to select the solvent of crystallisation as one of the components, which has been followed in the work presented here. While there is no agreement between different research groups on what constitutes a component, it is accepted that if there is a crystal engineering aspect attached to how the solvent molecules arrange within the crystal then the solvent molecule can be regarded as a component and the molecular complex termed as ternary or binary co-crystal rather than a co-crystal solvate or solvate.

With the target of identifying a robust two-dimensional network and to synthesise ternary co-crystals, whilst working with furosemide. Furosemide is a conformationally flexible molecule which contains carboxylic acid and sulphonamide in addition to other functional groups. The pseudo-tetrahedral sulphonamide group, unlike the planar carboxylic acid group, provides additional dimensionality for hydrogen bonding interactions.[179] The ability of carboxylic acid groups to form molecular complexes with pyridine functional groups is well known and has been used in many cases.[180] Considering the known ability of carboxylic acids to readily form the acid-pyridine supramolecular heterosynthon, 4,4’-bipyridyl was selected as one of the co-crystal formers (CCF). The strategy for the identification of a robust two-dimensional

network and co-crystal synthesis is based on utilising the geometry of the functional groups present in furosemide, 4,4'-bipyridyl and other ternary components. The results which resulted in positive outcome of mechano-chemical synthesis or co-crystallisation are presented here. All the co-crystals presented here were initially synthesised through mechano-chemical methods and then through crystallisation from solvent.

5.2. Co-crystal (11) [(furosemide)$_1$- (4,4'-bipyridyl)$_{0.5}$]

5.2.1. Synthesis of co-crystal (11)

Considering the molecular symmetry of 4,4'-bipyridyl (Scheme 5.2). Furosemide (33.0 mg, 1 mmol) and 4,4'-bipyridyl (7.8 mg, 0.5 mmol) were ground together with a mortar and pestle in the presence of 20 μL of acetonitrile for 5 minutes. The solvent drop grinding method indicated the formation of a phase different to the starting materials, as analysed by XRPD. Identical amounts of furosemide and 4,4'-bipyridyl were then dissolved in 2 ml of acetonitrile and allowed to crystallise through slow evaporation of solvent. Single crystals of diffraction quality were obtained after 2 days.

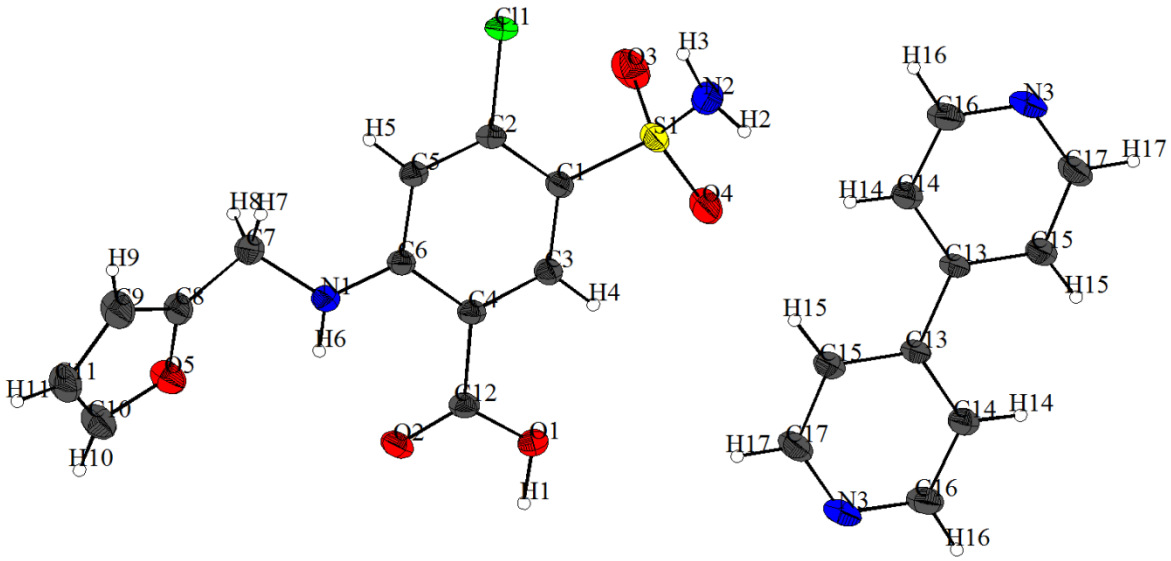

Figure 5.1: ORTEP plot of co-crystal (**11**) showing the atom numbering. (The displacement ellipsoids are drawn at the 50% probability level and atoms in the asymmetric unit are labelled). Key: chlorine, green circle; sulphur, yellow circles; oxygen, red circles; nitrogen, blue circles; carbon, grey circles; hydrogen, small white circles.

5.2.2. Crystal structure of co-crystal (11)

Single crystal data collection followed by structural analysis revealed the structural features in co-crystal (**11**). The asymmetric unit of (**11**) consists of one molecule of furosemide and half molecule of 4,4'-bipyrdiyl (bipy) (Figure 5.1). The compound crystallises in a monoclinic crystal system with $P2_1/n$ as the space group. The full crystallographic details are given in Table 5.1.

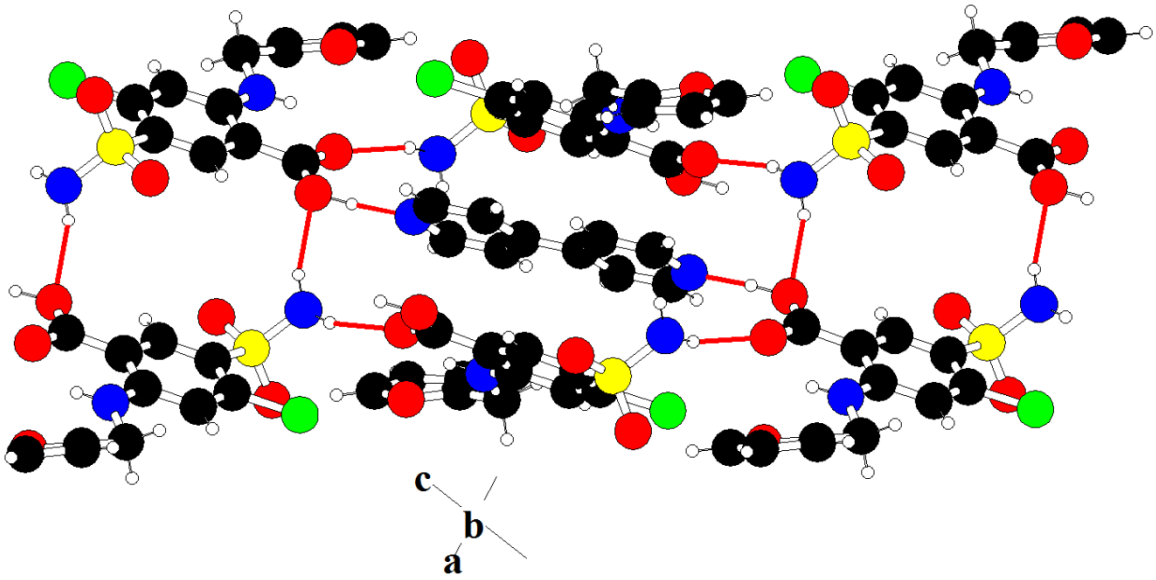

Figure 5.2: Packing arrangement in co-crystal (**11**), viewed along the [010] direction. Solid red lines represent intermolecular hydrogen bonds. Key: chlorine, green circles; sulphur, yellow circles; oxygen, red circles; nitrogen, blue circles; carbon, black circles; hydrogen, small white circles.

The two components in co-crystal (**11**) are held together through O(1)-H(1)···N(3) interactions between the O-H donor group of the carboxylic acid and the pyridyl nitrogen of bipyridyl (Table 5.3). In addition to the O-H···N interactions, the sulphonamide donors of furosemide are hydrogen-bonded to the carboxylic acid acceptors through N(2)-H(2)···O(1) and N(2)-H(3)···O(2) hydrogen bonding interactions (Table 5.3). Two inversion related furosemide molecules, stabilised through N(2)-H(2)···O(1) interactions propagate along the screw axis to generate a host network of furosemide molecules, with the bipy molecules occupying the guest positions (Figure 5.2). The two components arrange to form a three dimensional structure through host-guest as shown in Figure 5.2. The co-crystal (**11**) is a polymorphic form of co-crystal (**10**) presented in section 4.6.2.

Differential Scanning Calorimetry (DSC) of co-crystal (11)

The DSC thermogram of co-crystal (**11**) was obtained by weighing around 5.0 mg of the sample in an aluminium pan and crimping with a pinhole in the lid. The weighed sample was analysed over the temperature range between 25 and 280 °C at a constant heat rate of 10 ^{o}C/min. The thermogram of (**11**) reveals a sharp endotherm at 225.4 ^{o}C with an onset at 222.9 ^{o}C, which corresponds to the melting of (**11**). The melting is followed by decomposition (Figure 5.3).

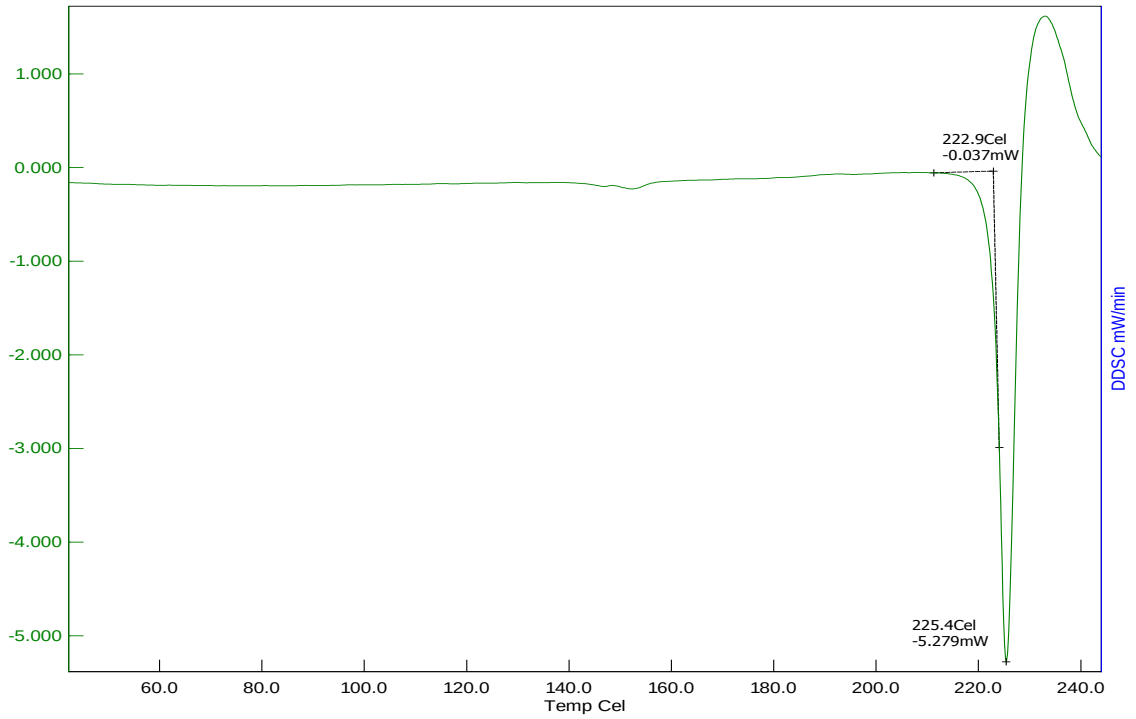

Figure 5.3: DSC thermogram of co-crystal (**11**).

Considering the ditopic acceptor nature of bipyridyl and the ability of the donor groups in furosemide to form a multiple hydrogen bonding interactions, the co-crystal formation was anticipated at a 1:1 molar composition of fus-bipy molecules. However, this was not the case; the two components remained as a physical mixture of the two components at this composition (Figure 5.4).

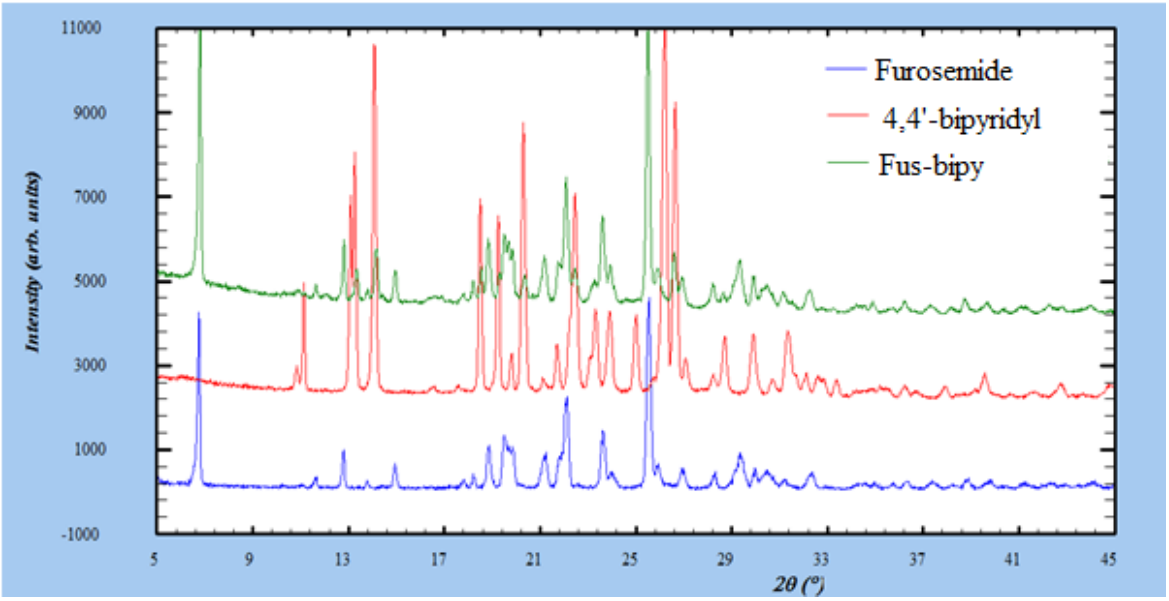

Figure 5.4: Powder X-ray diffraction data illustrating the formation of physical mixture when the composition of fus-bipy was altered to 1:1 molar composition.

This is the starting point for the investigation of ternary co-crystals. Considering the geometry of the functional groups in furosemide and the ability of bipyridyl, to act as ditopic acceptor, by systematically introducing a third component to the fus–bipy (1:1) mixture, it was possible to isolate crystalline phases different from the starting materials. The third component introduced, was altered in terms of the number of hydrogen bond donor and acceptor groups present. Initially dimethyl sulphoxide and methanol were used as the ternary components.

5.3. Co-crystal (12) [(furosemide – bipyridyl – DMSO (1-1-1)]

5.3.1. Crystal structure of co-crystal (12)

Diffraction quality crystals of co-crystal (**12**) were obtained after 5 days when equimolar amounts of furosemide and bipyridyl dissolved in DMSO were allowed to crystallise by slow solvent evaporation. (**12**) crystallises in the space group $P\bar{1}$ (Table 5.1). The asymmetric unit of (**12**) consists of one molecule each of furosemide, bipyridyl and DMSO (Figure 5.5). The DMSO molecule acts as a conventional hydrogen bond acceptor and is hydrogen-bonded to one of the N-H donors of furosemide through N(1)-H(7)···O(6) hydrogen bonding interactions (Figure 5.6), while the other N-H group of furosemide is hydrogen-bonded to one of the pyridyl groups of 4,4'-bipyridyl through N(1)-H(6)···N(3) interactions (Table 5.3). One end of the bipyridyl molecule is hydrogen-bonded to the N-H donor of the sulphonamide

while the other end of bipyridyl participates in the well-known acid-pyridine supramolecular heterosynthon through O(1)-H(1)···N(4) and C(21)-H(21)···O(2) interactions (Table 5.3) (Figure 5.6).

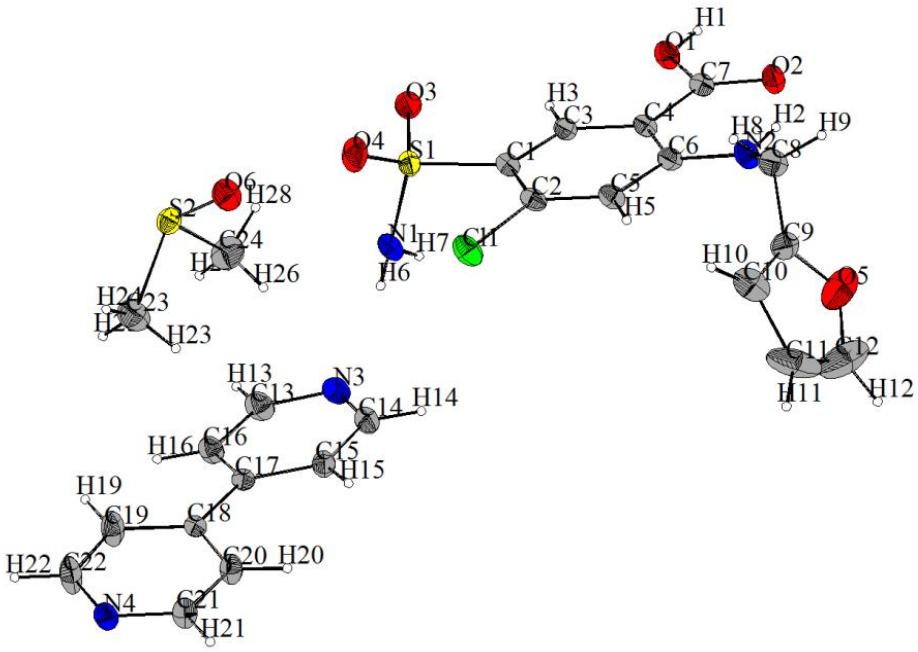

Figure 5.5: ORTEP plot of co-crystal (**12**).

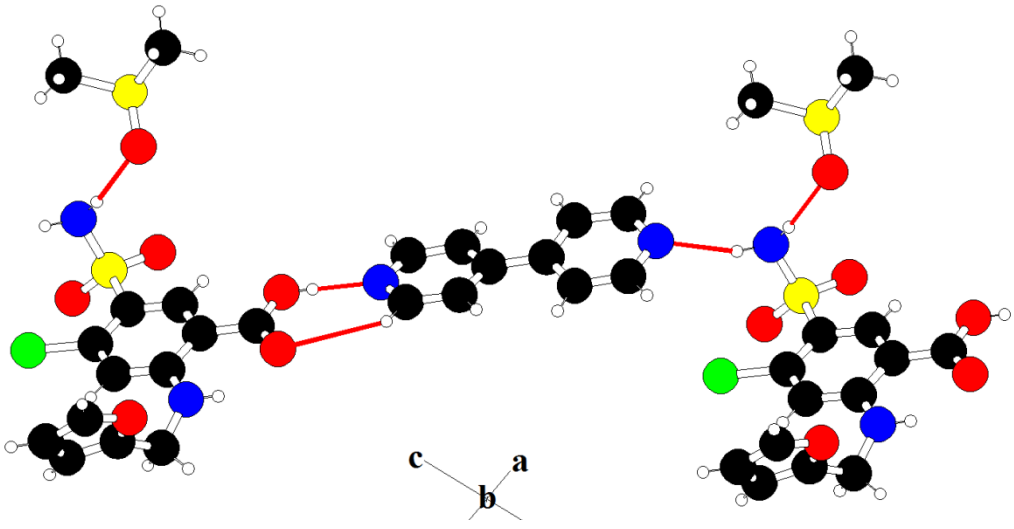

Figure 5.6: Hydrogen bonding interactions in co-crystal (**12**).

Thermal analysis of co-crystal (12)

Single crystals of co-crystal (**12**) were subjected to a combined TGA/DTA (Figure 5.7) analysis. The thermogram indicates an endothermic transition at 117.2 ^{o}C with a weight loss of around 15.2%, which is due to the loss of 1 mole of DMSO molecule in (**12**). This transition is followed by a broad exothermic transition which could be due to the loss of half molecule of 4,4'-bipyridyl. This transition is followed by an endothermic transition, corresponding to the melting of the compound at 217.7 ^{o}C.

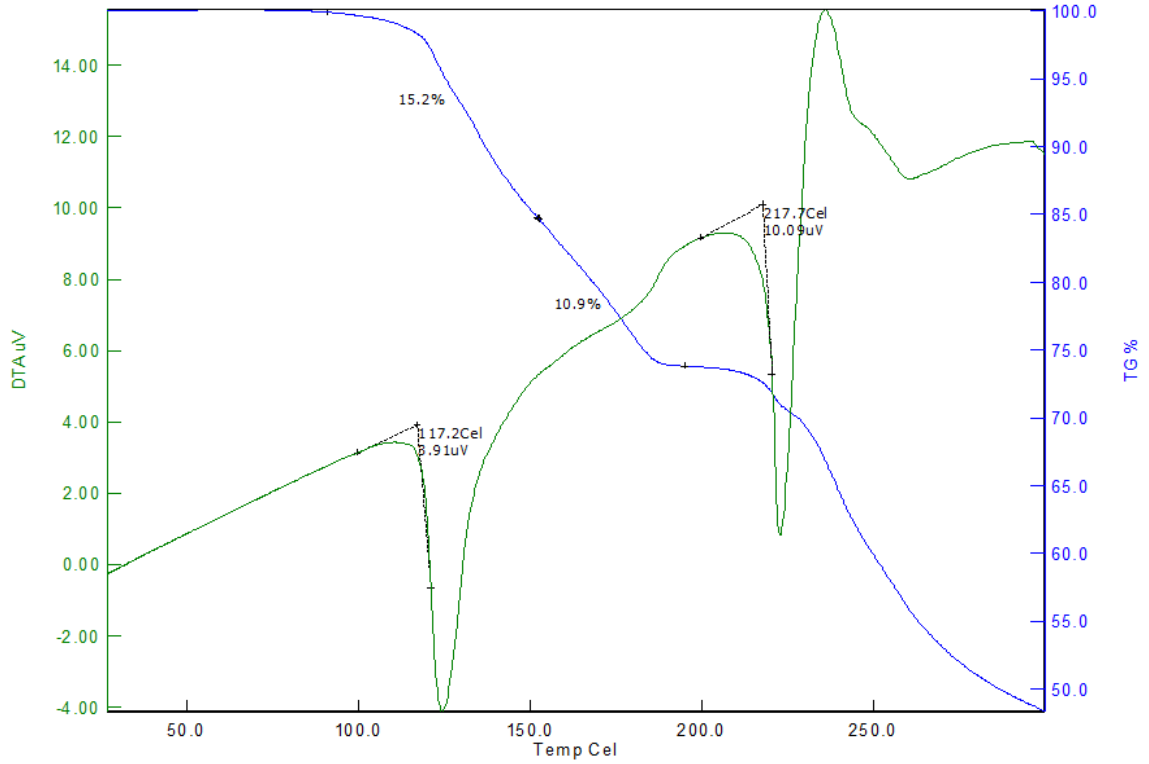

Figure 5.7: DTA/TGA of co-crystal (**12**).

Discussion:

In addition to the conventional hydrogen bonding interactions, the C-H groups of DMSO participate in weak C(24)-H(28)···O(4) interactions with the sulphoxide acceptor groups of furosemide to form a two-dimensional network involving three components. The hydrogen bonds observed between furosemide and other components are in accordance with the principle of hierarchy as proposed by Etter.[181] In addition to the hydrogen bonding interactions, there are π–π interactions between the aromatic moiety of furosemide and one of the pyridyl rings of 4,4'–bipyridyl (Figure 5.8). The two-dimensional network formed by co-crystal (**12**) is shown in Figure 5.9. The interactions between furosemide and the ternary

component propagate along *a* crystallographic axis, while the interactions between furosemide and bipyridyl propagate diagonally in the *ac* plane.

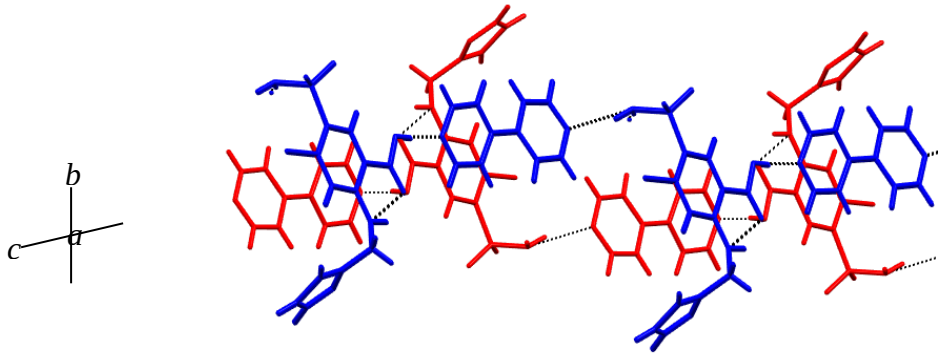

Figure 5.8: π–π interactions between the aromatic moieties of furosemide and bipyridyl in co-crystal (**12**).

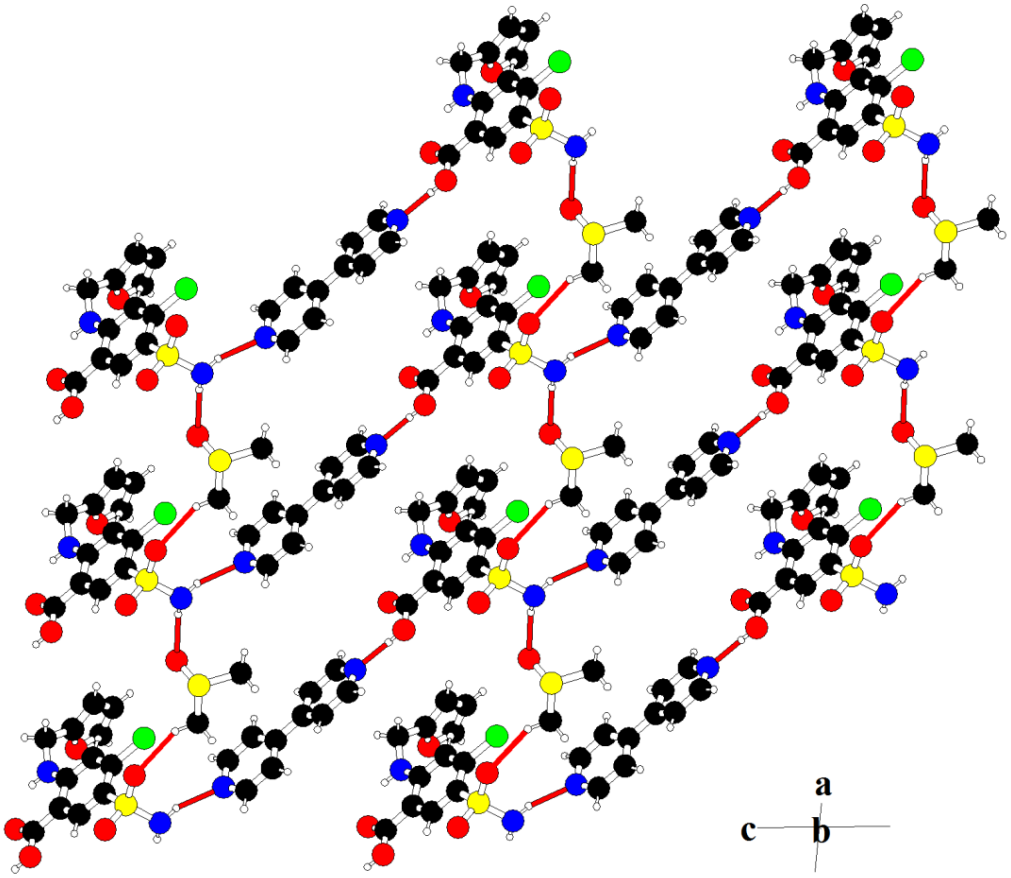

Figure 5.9: The two-dimensional network in co-crystal (**12**) viewed along the [010] direction.

The co-crystal (**12**) crystallises in the $P\bar{1}$ space group while stabilised through an asymmetric two dimensional network. Therefore, upon reproducing the asymmetric two–dimensional network like the one observed in (**12**) one can expect the space group to be unaltered ($P\bar{1}$). The crystal packing arrangement and space group of (**12**) serves as a blueprint for the selection and rational synthesis of other ternary co-crystals presented here. Taking the weak C-H···O interactions between the furosemide and ternary component into consideration, co-crystal formation was anticipated by introducing a ternary component containing functional groups which could act both as a donor and acceptor simultaneously. Alcohols serve as good targets for this purpose. Since the hydrogen bonding interactions between DMSO and furosemide molecules are along *a* crystallographic axis in (**12**), by introducing molecules containing alcohol functional groups as ternary components, co-crystal formation can be anticipated through similar hydrogen binding interactions with a reduced *a* crystallographic axis.

5.4. Co-crystal (13) [(furosemide – bipyridyl – MeOH (1-1-1)]

5.4.1. Synthesis of co-crystal (13)

Furosemide (33.0 mg, 1.0 mmol) and 4,4'-bipyrrdyl (15.6 mg, 1 mmol) were ground together in the presence of 20 µl of methanol using a mortar and pestle. The product obtained from the solvent drop grinding method was dissolved in 2 ml of methanol and allowed to crystallise via slow evaporation of methanol. Single crystals of diffraction quality were isolated from the crystallisation flask after one day and were analysed by single crystal X-ray diffraction.

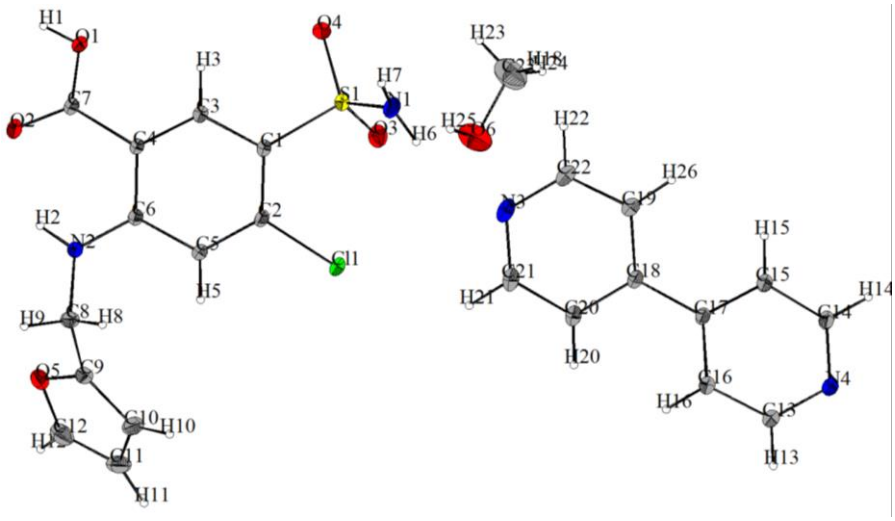

Figure 5.10: ORTEP plot of co-crystal (**13**).

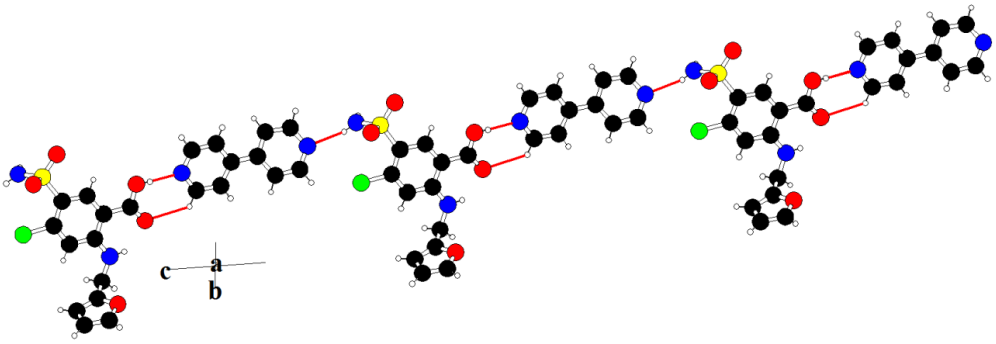

Figure 5.11: Hydrogen bonding interactions between furosemide and bipyridyl in co-crystal (**13**), viewed along the [100] direction.

5.4.2. Crystal structure of co-crystal (13)

Co-crystal (**13**) consists of one molecule each of furosemide, 4,4'-bipyridyl and methanol in the asymmetric unit (Figure 5.10). As expected, based on the blueprint structure (**12**), the three components crystallise in space group $P\bar{1}$ through similar combinations of hydrogen bonding interactions to form an asymmetric two-dimensional network. The full crystallographic details are given in Table 5.1. Analogous to co-crystal (**12**), the *syn* N-H (syn with respect to chlorine) and the carboxylic O-H of furosemide are hydrogen-bonded to the pyridyl nitrogen of bipyridyl through N(1)-H(6)···N(3) and O(1)-H(1)···N(4) hydrogen bonding interactions (Table 5.3), these interactions extend diagonally in the [100] direction (Figure 5.11). These furosemide – bipyridyl aggregates are linked by the methanol molecule through N(1)-H(7)···O(6) and O(6)-H(25)···O(3) hydrogen bonding interactions (Table 5.3), extending infinitely along the *a* crystallographic axis (Figure 5.12). In addition to the hydrogen bonding interactions, there are strong π-π interactions between the aromatic rings of furosemide and bipyridyl as shown in Figure 5.13. These arene–arene interactions are not completely parallel but, as is usual for such systems, are arranged in a slipped face-to-face/ center-to-edge stacking arrangement, with a slip angle of 13.4^{o} (Figure 5.13). The arene – arene interactions of the kind observed here are known to serve as robust supramolecular synthons[182] and are abundant in chemical and biological systems.[183] The π–π interactions interact cooperatively while extending infinitely along the crystallographic *a* axis.[184] In addition to these interactions, the C-H groups of one of the pyridyl moieties of bipyridyl is involved in weak interactions with the furan ring to form perpendicular C-H···π interactions, extending infinitely through the crystallographic *b* axis. These interactions, measured from the center of the furan ring to the C(14) and C(13) carbon atoms, have a distance of 3.332(3)Å and 4.027(2)Å.

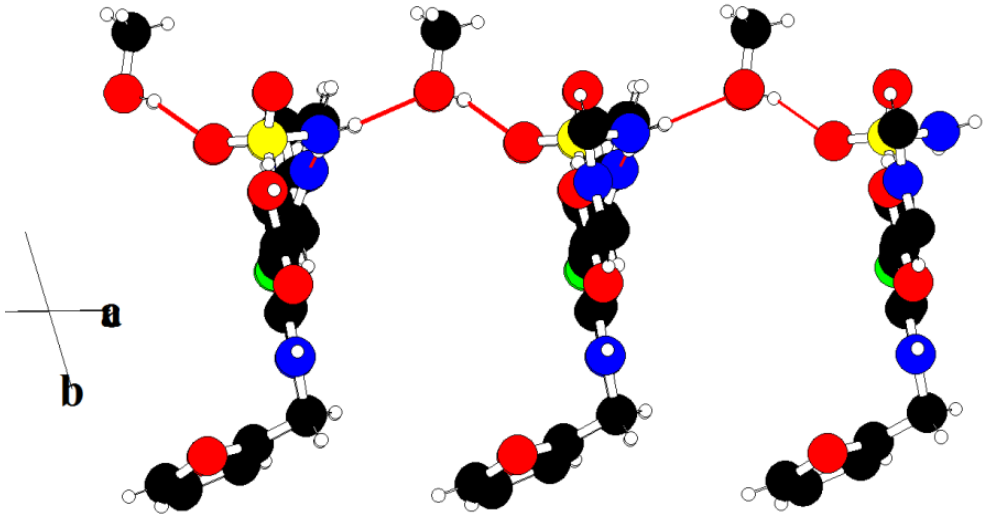

Figure 5.12: Hydrogen bonding interactions in co-crystal (**13**) between the furosemide and ternary component (methanol) extending infinitely along the crystallographic *a* axis.

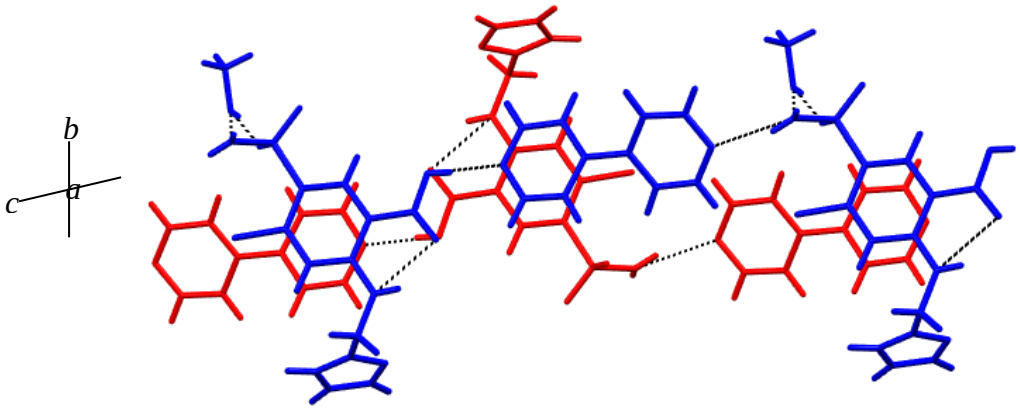

Figure 5.13: π–π interactions between the furosemide and pyridyl moieties in co-crystal (**13**), viewed through crystallographic *a* axis (the dotted black lines represent the hydrogen bonding interactions).

Thermal analysis of co-crystal (13)

The TGA/ DTA of co-crystal (**13**) is shown in Figure 5.14. The thermogram indicates a crystal–crystal phase transition at 103.2 ^{o}C, accompanied by a weight loss of 7.2%, which corresponds to the loss of one mole of methanol. In addition to this, there is a transition at 220.2 ^{o}C with an onset of 219.5 ^{o}C corresponding to the melting of the compound, which is followed by decomposition of the material.

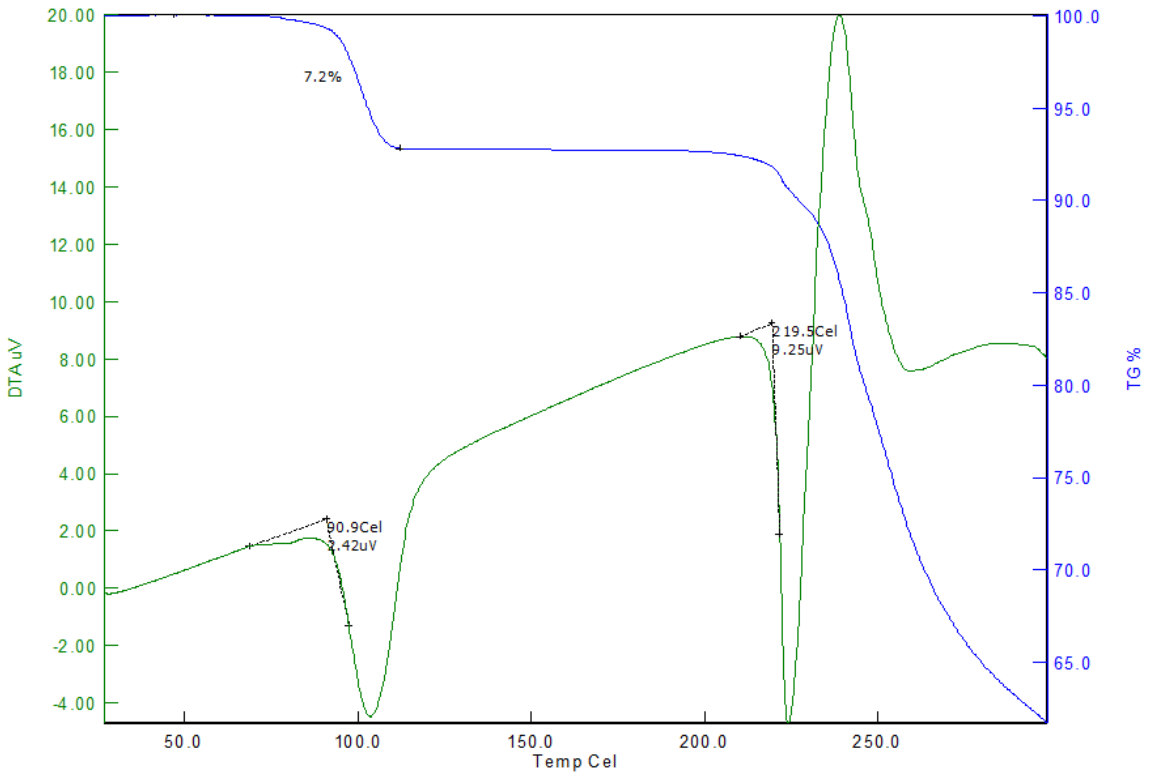

Figure 5.14: TG/ DTA of co-crystal (**13**).

Based on the blue print structure of co-crystal (**12**), it was anticipated that will be a decrease in the *a* crystallographic axis going from (**12**) to (**13**) (Table 5.1), while the interactions between furosemide and ternary component (methanol) are along the crystallographic *a* axis as observed in (**13**). In both ternary co-crystals (**12**) and (**13**), the ternary components DMSO and MeOH have an identical role, acting as a bridge between the furosemide–bipyridyl aggregates. The three components in the two ternary co-crystals (**12**) and (**13**) are stabilised through an asymmetric two-dimensional hydrogen bonding network. The two dimensional network formed by co-crystals (**12**) and (**13**) is shown in Figure 5.9 and Figure 5.15 respectively.

Table 5.1: Crystallographic data of co-crystals (**11**), (**12**), and (**13**).

	(**11**)	(**12**)	(**13**)
Chemical formula	$C_{17}H_{15}Cl_1N_3O_5S$	$C_{24}H_{25}Cl_1N_4O_6S_2$	$C_{24}H_{25}Cl_1N_4O_6S_2$
Formula weight	408.8	565.1	519.0
Crystal system	monoclinic	triclinic	triclinic
a / Å	11.4883(6)	9.7483(4)	7.3552(9)
b / Å	9.6632(5)	10.4805(4)	9.3457(11)
c / Å	16.1106(8)	14.1432(5)	18.124(2)
α / °	90.00	96.253(2)	80.525(6)
β / °	101.252(2)	93.883(2)	82.376(6)
γ / °	90.00	114.448(2)	75.758(6)
Space group	$P2_1/n$	$P\bar{1}$	$P\bar{1}$
V / Å^3	1754.12(16)	1297.39(9)	1185.5(2)
Z	4	2	2
$N_{reflection}/ N_{parameter}$	8688/244	7440 / 334	9112/316
ρ_{calc} / g cm^{-3}	1.548	1.446	1.454
Radiation type	Mo Kα (λ =0.710173 Å)	Mo Kα (λ =0.710173 Å)	Mo Kα (λ =0.710173 Å)
T / K	100	100	100
θ range/°	3 – 44	4 – 34	1 – 40
Range of *h*	-22 – 22	-15 – 15	-12 – 12
Range of *k*	-16 – 18	-16 – 16	-14 – 15
Range of *l*	-31 – 31	-21 – 21	-31 – 31
Rmerge	0.0455	0.0263	0.0305
R_1 / %	4.26516	4.46	4.17
$_wR_2$ / %	4.64728	4.5	4.47
Goodness-of-fit	1.076	1.118	1.077

In co-crystals (**12**) and (**13**), the lattice metrics along the *a* and *c* axis and the angle β between them are dependent on the two-dimensional network. The two dimensional network depends

on the hydrogen bonding interactions and the conformational flexibility of the sulphonamide group.

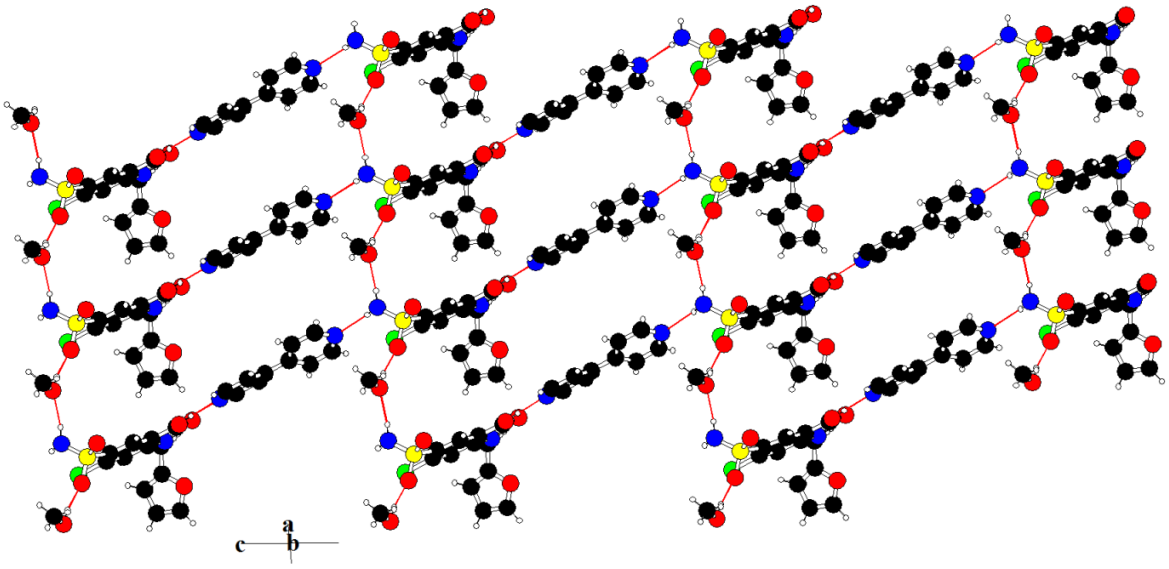

Figure 5.15: Two-dimensional network in co-crystal (**4**).

A careful examination of crystal structures (**12**) and (**13**) suggests that the length of the *b* lattice parameter is determined on the long axis of the furosemide molecules, which is determined by the conformational flexibility of the furosemide molecules. It is important to mention that the dependence of the angles α and γ could not be rationalized based on the structural features observed in ternary co-crystals (**12**) and (**13**). Considering the two-dimensional network observed in co-crystal (**13**), and noticing that the methyl groups of methanol in crystal structure (**13**) are involved only in van der Waals interactions, other alcohol functional group containing compounds (ethanol, 2-propanol, 1-butanol) were used as ternary components.

5.5. Co-crystals (14) [(furosemide – bipyridyl – ethanol (1-1-1)]; (15) [(furosemide – bipyridyl – 2-propanol (1-1-1)]; and (16) [(furosemide – bipyridyl – 1-butanol (1-1-1)]

5.5.1. Mechanochemical synthesis of ternary co-crystals (14), (15), and (16)

Co-crystals (**14**), (**15**) and (**16**) were synthesised mechano-chemically by grinding furosemide (1.00 mmol, 33.0mg) and 4,4'-bipyridyl (1.00 mmol, 15.6mg) separately in the presence of 20 µl of ethanol, 2-propanol, 1-butanol for 2 minutes using a mortar and pestle.

In each case, new polycrystalline materials resulted. Their powder diffraction patterns differ from those of either the starting materials or any known binary phases. It was not possible to

isolate single crystals of co-crystals (**14**), (**15**) and (**16**). Several crystallisation attempts using a 1:1 molar ratio of furosemide and bipyridyl in presence of ethanol, 2-propanol, 1-butanol resulted in the concomitant formation of co-crystals (**10**) (furosemide – bipyridyl (1-0.5)) and (**11**) furosemide – bipyridyl (1-0.5). The two co-crystals (**10**) and (**11**) are co-crystal polymorphs; in this section (**11**) is discussed while (**10**) was discussed in section 4.2.6.

While, it has not been possible to isolate single crystals of ternary co-crystals (**14**), (**15**) and (**16**), evidence for the formation of a ternary co-crystal is obtained by the analysis of powder X-ray diffraction patterns of polycrystalline materials obtained by solvent drop grinding.

Figures 5.16, 5.17 and 5.18 present the powder diffraction patterns of co-crystals (**14**), (**15**) and (**16**) indexed using TOPAS.[185] The unit cell parameters obtained by indexing reflections in co-crystals (14), (15) and (16) and the residual profile fitting parameters obtained by fitting each of the powder patterns are given in Table 5.2.

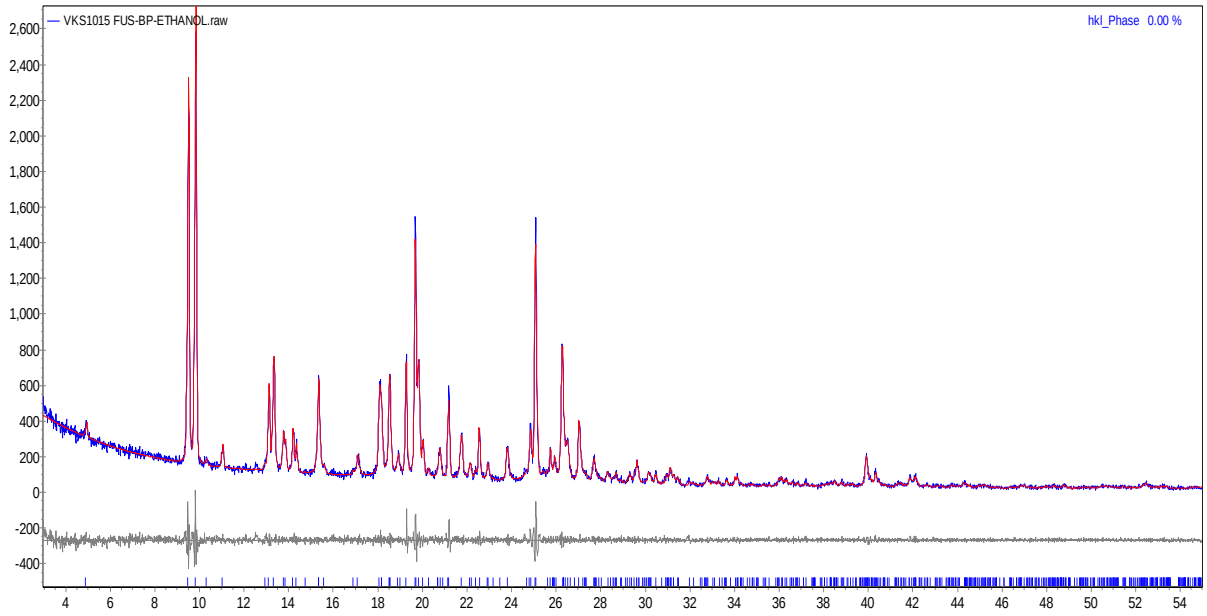

Figure 5.16: Powder X-ray diffraction pattern of co-crystal (**14**) (Furosemide – bipyridyl – ethanol). The blue pattern represents the observed powder profile; the red pattern represents the profile calculated by using the cell parameters obtained by indexing the reflections of co-crystals (**14**); the bottom profile in each of the figures represents the difference between the observed and calculated powder patterns.

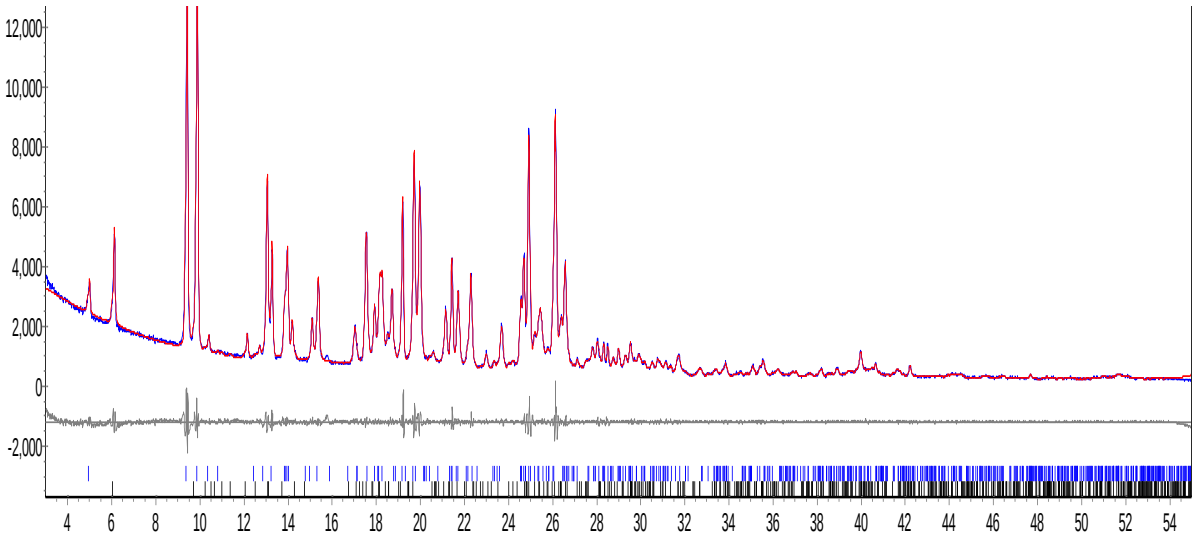

Figure 5.17: Powder X-ray diffraction pattern of co-crystal (**6**) (Furosemide – bipyridyl – 2-propanol). The reflections marked in blue represent the reflection of co-crystal (15) while the reflections marked in black represent the reflections of furosemide form-I.

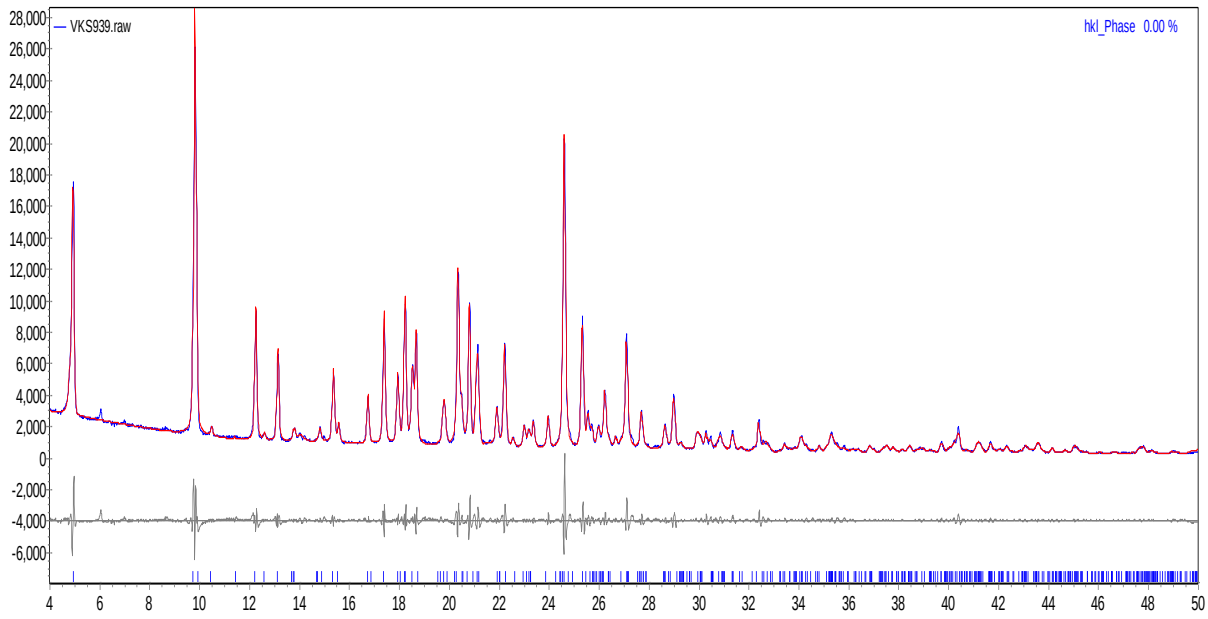

Figure 5.18: Powder X-ray diffraction pattern of co-crystal (**6**) (Furosemide–bipyridyl–1-butanol)

Table 5.2: Unit cell parameters of co-crystals (**14**), (**15**) and (**16**) from powder diffraction pattern.

	(14)	**(15)**	**(16)**
Chemical formula	$C_{24}H_{25}Cl_1N_4O_6S$	$C_{25}H_{27}Cl_1N_4O_6S$	$C_{26}H_{29}Cl_1N_4O_6S$
Formula weight	533.0	547.0	561.0
Crystal system	triclinic	triclinic	triclinic
a / Å	7.193(8)	7.860(5)	7.537(4)
b / Å	9.780(6)	10.001(2)	9.374(3)
c / Å	18.694(2)	18.402(4)	18.282(2)
α / ^{o}	89.88(5)	76.13(1)	81.67(7)
β / ^{o}	75.50(3)	76.56(5)	80.54(5)
γ / ^{o}	73.17(1)	70.94(2)	75.6(3)
Space group	$P\bar{1}$	$P\bar{1}$	$P\bar{1}$
V / Å^3	1208.96(5)	1257.41(2)	1226.57(8)
FOM	7.8	5.5	7.2
R_{wp} / %	8.64	5.62	4.95

Discussion:

The powder diffraction pattern analysis of co-crystals (**14**), (**15**) and (**16**) suggests that the ternary components ethanol, 2-propanol, 1-butanol have identical roles as observed in co-crystal (**12**) and (**13**) i.e. the ternary components acts as a bridge between the furosemide – bipyridyl aggregates and the three components are stabilised through the two-dimensional network observed in co-crystal (**13**). The two-dimensional network common to all the ternary co-crystals is shown in Scheme 5.1.

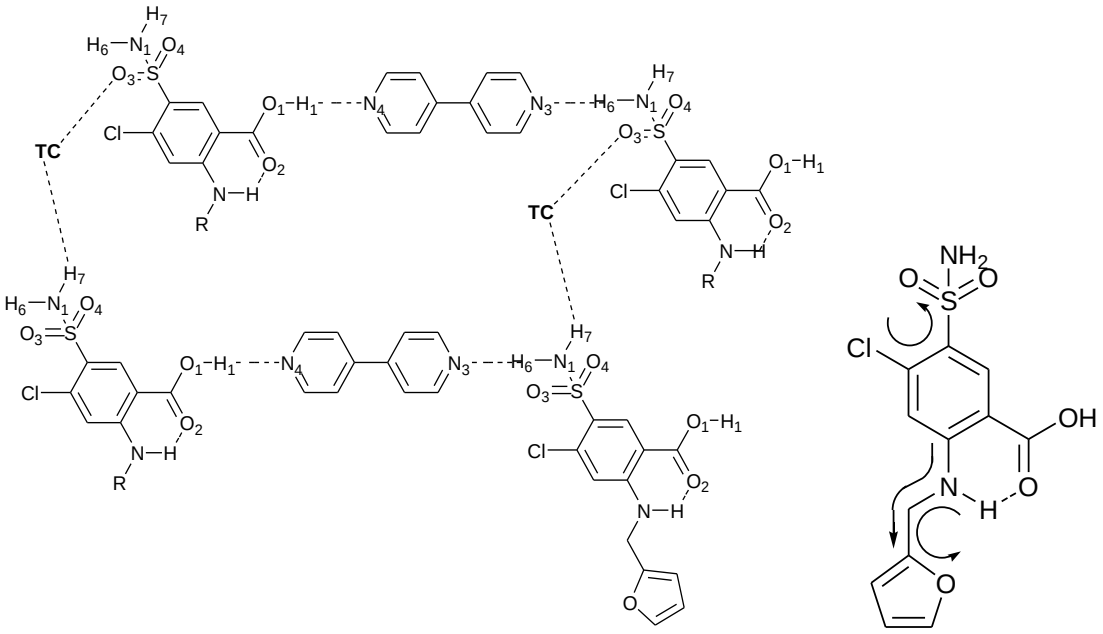

Scheme 5.1: (a) Representation of the two-dimensional network observed in co-crystals (**2**) – (**7**) (Abbreviations: TC – Ternary component (DMSO, DMF, MeOH, EtOH, 2-propanol, 1-butanol), R- Furan ring). (b) conformational flexibility of the furosemide molecules.

Table 5.3: Geometric aspects of co-crystals (**11**), (**12**), (**13**), (**17**), (**18**) and (**19**):

Compound	Hydrogen bond	*d* (H⋯A)/Å	*d* (D⋯A)/Å	*θ* (D-H⋯A)/^{o}	(H⋯A) vdW cutoff contraction / %
11	O(1)-H(1)⋯N(3)	1.57	2.53(2)	166.5	43
	N(2)-H(2)⋯O(1)	2.15	2.97(4)	157.2	21
	N(2)-H(3)⋯O(2)	2.04	1.93(3)	169.2	25
11(intra)	N(1)-H(6)⋯O(2)	2.00	2.67(6)	134.6	26
12	N(1)-H(6)⋯N(3)	2.11	2.99(4)	160.9	23
	N(1)-H(7)⋯O(6)	2.13	2.91(7)	172.0	22
	O(1)-H(1)⋯N(4)	1.75	2.56(3)	174.7	36
	C(24)-H(28)⋯O(4)	2.53	3.38(5)	147.0	7
12	C(23)-H(25)⋯O(3)	2.51	3.40(6)	166.4	8
12(intra)	N(2)-H(2)⋯O(2)	2.00	2.69(7)	139.5	26
13	N(1)-H(6)⋯N(3)	2.18	2.97(8)	162.4	21
	N(1)-H(7)⋯O(6)	2.02	2.89(6)	169.1	26

	O(6)-H(25)···O(3)	1.97	2.77(3)	161.4	27
	O(1)-H(1)···N(4)	1.84	2.62(2)	173.2	33
13(intra)	N(2)-H(2)···O(2)	1.99	2.66(4)	138.5	27
17	O(1)-H(1)···N(4)	1.69	2.60(3)	150.9	38
	N(1)-H(6)···N(3)	1.98	2.91(3)	152.7	28
	N(1)-H(7)···O(6)	2.09	2.93(4)	166.2	23
	O(6)-H(25)···O(3)	2.02	2.78(6)	153.5	26
17(intra)	N(2)-H(2)···O(2)	2.00	2.66(3)	139.8	26
18	O(1)-H(1)···N(3)	1.81	2.62(2)	169.5	34
	N(1)-H(6)···N(4)	2.11	2.97(6)	160.2	23
	O(6)-H(25)···O(4)	1.89	2.75(4)	176.0	30
	N(1)-H(7)···O(6)	2.01	2.88(2)	171.7	26
18(intra)	N(2)-H(2)···O(2)	1.97	2.66(5)	137.1	27
19	O(1)-H(1)···N(4)	1.83	2.61(6)	173.6	33
	N(1)-H(6)···N(3)	2.12	2.92(6)	162.4	23
	N(1)-H(7)···O(6)	2.14	2.95(3)	157.9	21
	O(6)-H(25)···O(3)	1.87	2.70(4)	173.6	31
19(intra)	N(2)-H(2)···O(2)	2.02	2.65(2)	138.1	26

The discovery of the asymmetric two-dimensional hydrogen-bonded network (Scheme 5.1) in all the ternary co-crystals, allowed for the prediction of space group and gross structural features in related compounds from their molecular structure, the π–π interactions between aromatic moieties of furosemide and bipyridyl play significant role in stabilising the crystal structures. In addition, to the space group and gross structural features the lattice metrics *a*, *b*, *c* and *β* are depended on the structural features discussed earlier.

To predict the crystal packing arrangement in other ternary co-crystals and to test the robustness of the two-dimensional network, the compounds ethylene glycol, 1,4-butanediol and hydroquinone were used as ternary components (Scheme 5.2). The ternary components ethylene glycol, 1,4-butanediol and hydroquinone selected possess mirror planes in their molecular structure. With no chiral centres in the molecular structures of any of the components, the number of possible space groups reduces to $P\bar{1}$, based on the asymmetric two-dimensional network.

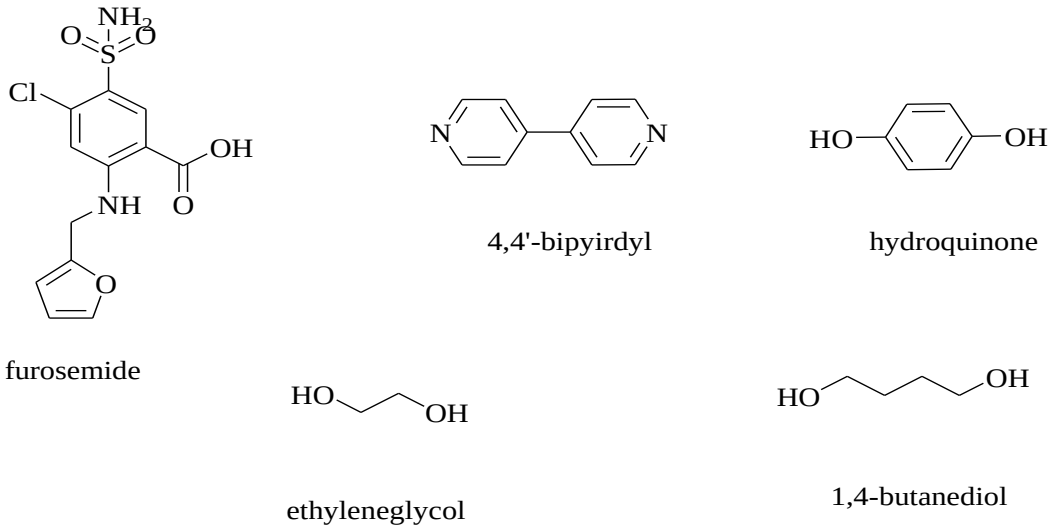

Scheme 5.2: Molecules used for the prediction of crystal structures.

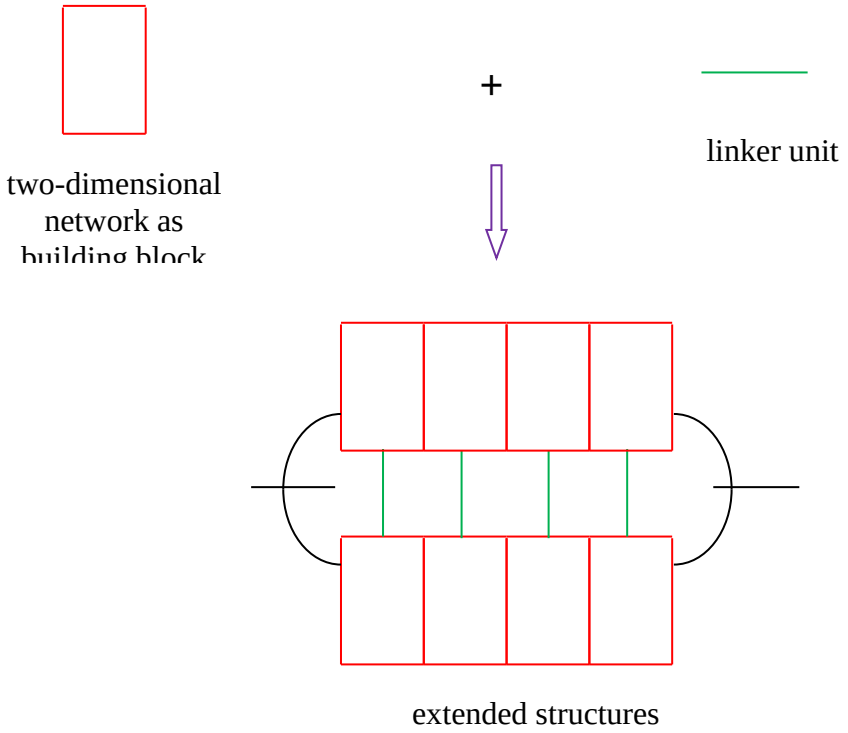

Scheme 5.3: Two-dimensional network as building block and the corresponding extended solids network.

Based on the molecular structure of the three components, the asymmetric two-dimensional network and the π–π interactions between furosemide – bipyridyl aggregates observed in co-

crystals (**13**), one can predict the formation of extended solids, crystallised through the robust two-dimensional network discovered earlier. A pictorial representation of the extended solids is shown in Scheme 5.3.

5.6. Co-crystals (17) [(furosemide – 4,4'-bipyridyl – ethylene glycol (1-1-0.5))]; (18) [(furosemide – 4,4'-bipyridyl – 1,4-butanediol (1-1-0.5))]; (19) [(furosemide – 4,4'-bipyridyl – hydroquinone (1-1-0.5))]

Mechanochemical synthesis of co-crystals (17), (18), (19)

Co-crystals (**17**) and (**18**) were synthesised by grinding furosemide (1mmol, 33.0mg) and 4,4'-bipyridyl (1mmol, 15.6mg) in the presence of 10µl of ethylene glycol and 1,4-butanediol respectively for 5 minutes. Co-crystal (**19**) (furosemide – 4,4'-bipyridyl – hydroquinone (1-1-0.5)) is synthesised by grinding furosemide (1mmol, 33.0mg), 4,4'-bipyridyl (1mmol, 15.6mg) and hydroquinone (0.5mmol, 5.5mg) in presence of 20µl of acetonitrile for 3 minutes using a mortar and pestle.

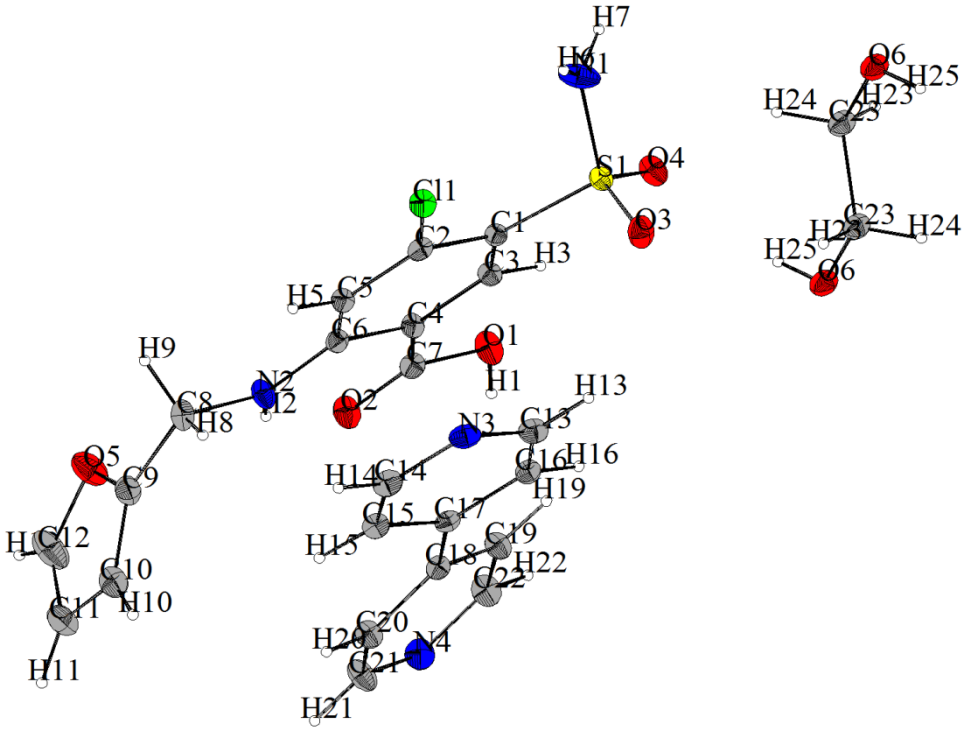

Figure 5.19: ORTEP picture of co-crystal (**17**) (furosemide – bipyridyl – ethylene glycol) (1-1-0.5).

Crystallisation of co-crystals (17), (18) and (19)

Diffraction quality crystals of co-crystals (**17**) and (**18**) were obtained by dissolving 1-1 molar amounts of furosemide (1 mmol, 33.0 mg) and 4,4'-bipyridyl (1 mmol, 15.6 mg) in 2.0 ml of ethylene glycol and 2.0 ml of 1,4-butanediol respectively and allowing them crystallise through slow evaporation. Single crystals of co-crystals (**17**) and (**18)** were obtained after 6 days. Crystals of co-crystal (**19**) (furosemide – 4,4'-bipyridyl – hydroquinone (1-1-0.5)) are synthesised by dissolving furosemide (1mmol, 33.0mg), 4,4'-bipyridyl (1mmol, 15.6mg) and hydroquinone (0.5mmol, 5.5mg) in 3ml of acetonitrile and allowing them to crystallise through slow evaporation of solvent. Single crystals of co-crystal (**19**) were isolated from the crystallisation flask after 4 days.

5.6.1. Crystal structure of co-crystal (17) [(furosemide – 4,4'-bipyridyl – ethylene glycol (1-1-0.5))]

The crystal structure analysis reveals the structural features in co-crystal (**17**). As anticipated, the asymmetric unit of (**17**) consists of one molecule each of furosemide and 4,4'-bipyridyl and half a molecule of ethylene glycol (Figure 5.19). The three components, as predicted crystallise in the space group $P\bar{1}$ and are stabilised through the asymmetric two-dimensional hydrogen-bonded network. The full crystallographic details are given in Table 5.4.

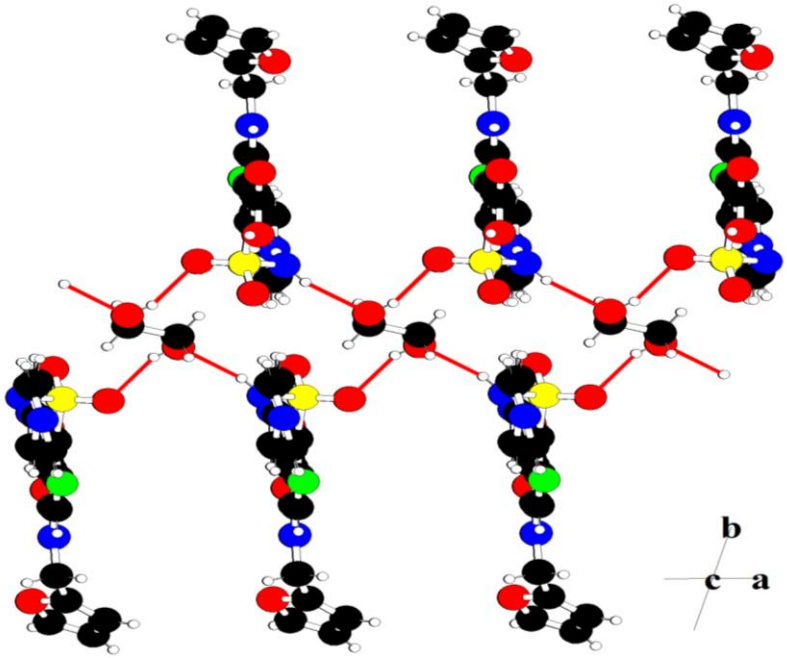

Figure 5.20: Interactions between furosemide and ternary component ethylene glycol in co-crystal (**17**) viewed along the [001] direction.

Analogous to other ternary co-crystals, the *anti* N-H and *syn* S=O (*syn* and *anti* with respect to chlorine) of furosemide are hydrogen-bonded to the acceptor and donor groups of ternary components through N(1)-H(7)···O(6) and O(6)-H(25)···O(3) hydrogen bonding interactions (Table 5.3) (Figure 5.20). Similar to other ternary co-crystals the hydrogen bonding interactions between furosemide and the ternary component, in this case ethylene glycol, extend along the *a* crystallographic axis, since ethylene glycol possess and inversion center, similar hydrogen bonding interactions extend on the other end of the molecule (Figure 5.20). In addition to these interactions, one end of the bipyridyl is hydrogen-bonded to the *syn* N-H of furosemide through N(1)-H(6)···N(3) interactions while the other end of bipyridyl participates in an acid pyridine supramolecular heterosynthon through O(1)-H(1)···N(4) and C(22)-H(22)···O(2) interactions (Table 5.3) (Figure 5.21). While the hydrogen bonding interactions between the furosemide and the bipyridyl molecules are common in all the ternary co-crystals, these interactions in co-crystal (**17**) propagate almost parallel to the *c* crystallographic axis as shown in Figure 5.21. The three components arrange *via* the two dimensional network as shown in Figure 5.22. In addition to the hydrogen bonding interactions, there are strong π–π (3.362(2)Å and 3.285(4)Å) (Figure 5.23) interactions between the aromatic moieties of furosemide and bipyridyl. Analogous to other ternary co-crystals the π–π interactions between the aromatic moieties of furosemide and bipyridyl are arranged in a slipped offset face-to-face/ center-to-edge fashion with a slip angle of 5.87°.

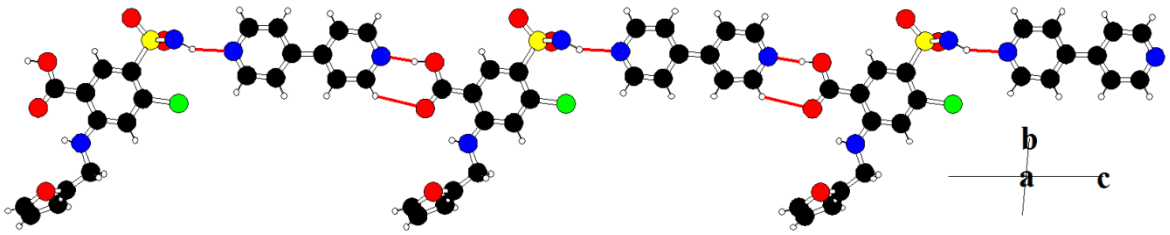

Figure 5.21: Interactions between furosemide and bipyridyl molecules in co-crystal (**17**) viewed along the [100] direction.

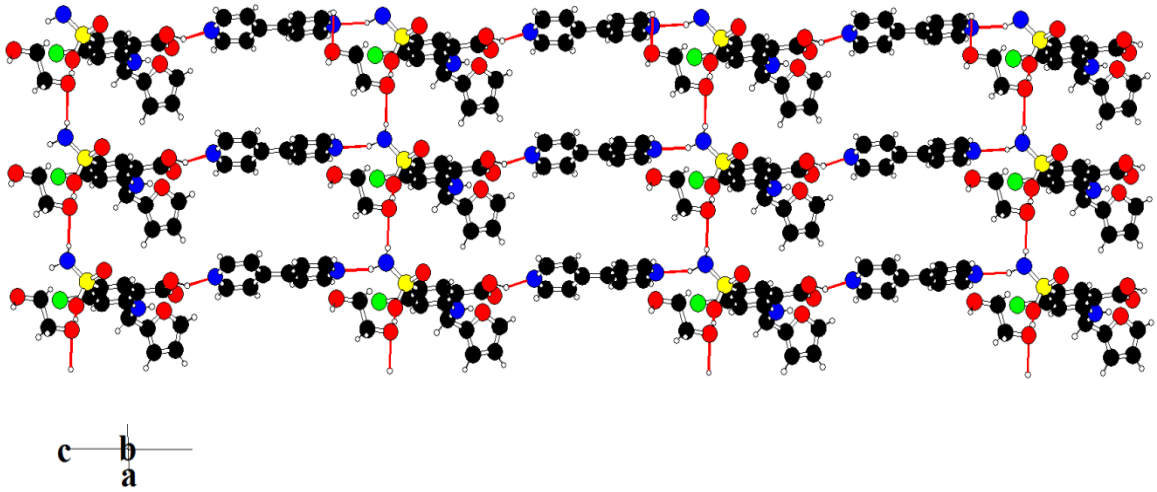

Figure 5.22: Two-dimensional network formed by the three components in co-crystal (**17**), viewed along the [010] direction.

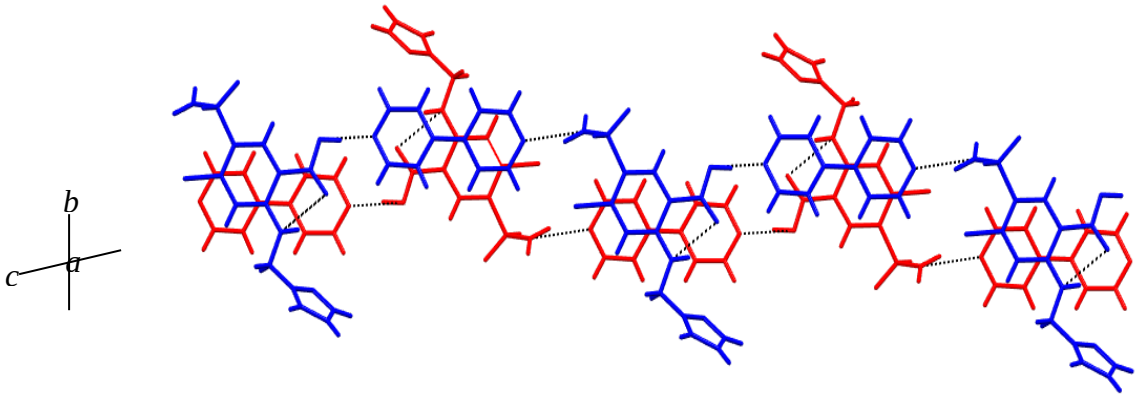

Figure 5.23: π–π interactions in co-crystal (**17**).

Thermal analysis of co-crystal (17)

The TGA/ DTA analysis of co-crystal (**17**) indicate a broad transition with an onset at 69.8^{o}C, corresponding to a weight loss of around 4.9%. This transition and the corresponding weight loss are due to evaporation of surface bound ethylene glycol molecules, which is the solvent of crystallisation. This transition is followed by a transition at 116.3^{o}C, with an onset of 110.0^{o}C, with a corresponding weight loss of 6.5%. This transition and the corresponding weight loss are equal to the loss of half molecule of lattice bound ethylene glycol molecule. This is followed by a transition in the DTA curve at 220.5 ^{o}C with an onset at 216.8 ^{o}C, which is due to the melting of the compound. This transition is immediately followed by decomposition. The DTA/ TGA thermograms of (**17**) are indicated in Figure 5.24.

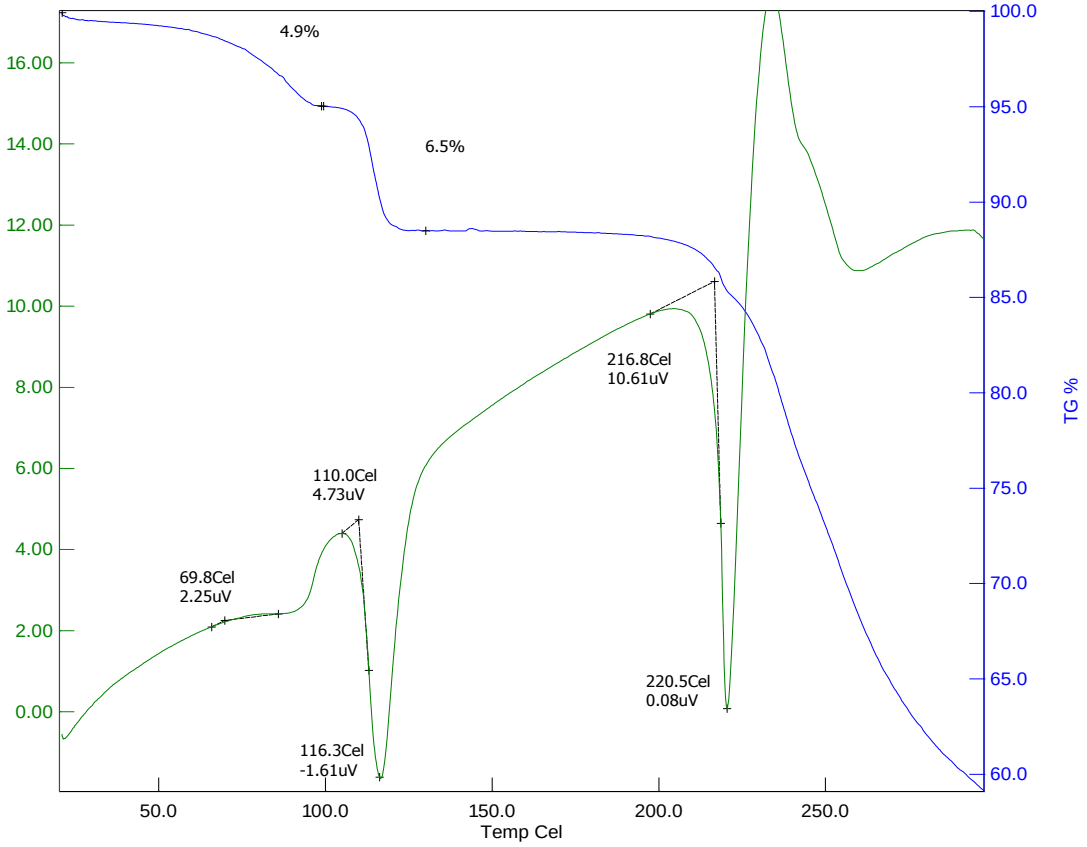

Figure 5.24: TG/DTA of co-crystal (**17**).

5.6.2. Crystal structure of co-crystal (18) [(furosemide – 4,4'-bipyridyl – 1,4-butanediol (1-1-0.5))]

The single crystal X-ray diffraction analysis of co-crystal (**18**) reveals that the asymmetric unit of (**18**) consist of one molecule each of furosemide, 4,4'-bipyridyl and half molecule of 1,4-butanediol (Figure 5.25).

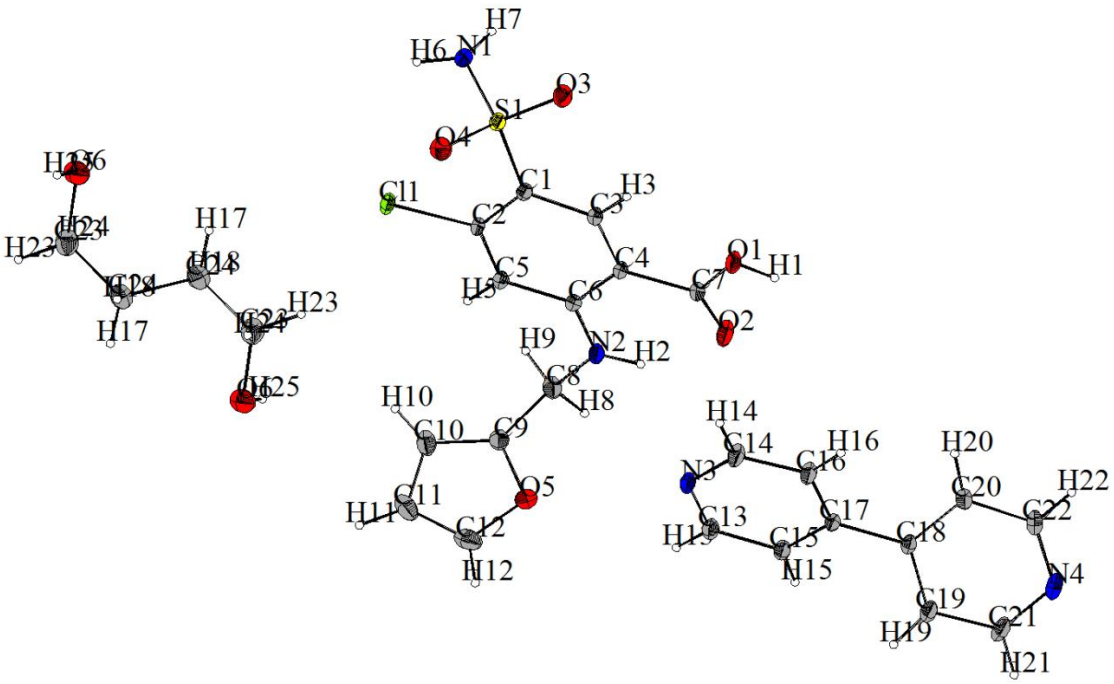

Figure 5.25: ORTEP plot of Co-crystal (**18**).

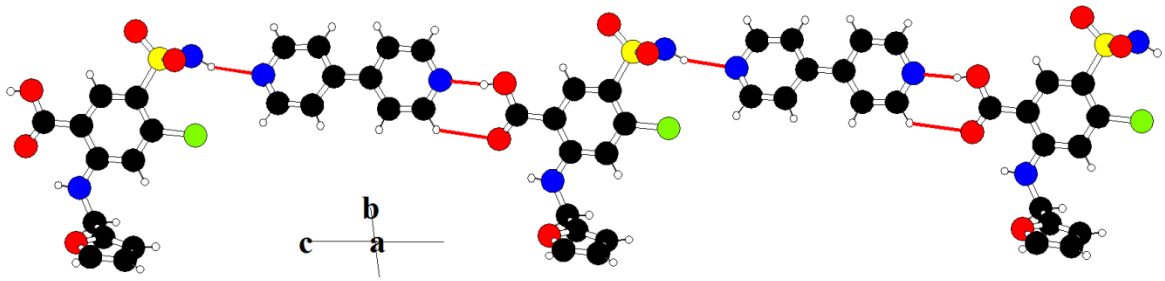

Figure 5.26: Hydrogen bonding arrangement between furosemide and bipyridyl molecules in co-crystal (**18**) along the [010] direction.

The arrangement of the three components in (**18**) is similar to that observed in other ternary co-crystals. The three components in (**18**) are arranged *via* the asymmetric two dimensional hydrogen-bonded network while crystallizing in space group $P\bar{1}$. The full crystallographic details are given in Table 5.4. The *syn* N-H (with respect to chlorine) and the carboxylic O-H

are hydrogen-bonded to the pyridyl nitrogen's of 4,4,'-bipyridyl through O(1)-H(1)···N(4) and N(1)-H(6)···N(3) interactions (Table 5.3) (Figure 5.26), the *anti* N-H of furosemide is hydrogen-bonded to the oxygen of the 1,4-butanediol to form N(1)-H(7)···O(6) hydrogen bonds, while the O-H group of 1,4-butanediol is hydrogen-bonded to the of the sulphoxide group of furosemide though O(6)-H(25)···O(3) interactions (Table 5.3) (Figure 5.27). Analogous to co-crystal (**17**), since the ternary component 1,4-butanediol contains an inversion centre in its molecular structure, the three components crystallise with the 1,4-butanediol possessing an inversion centre, with the two-dimensional network extending on the other end of the molecule. Analogous to other ternary co-crystals the π–π interactions between the aromatic moieties of furosemide and bipyridyl are arranged in a slipped offset face-to-face/ centre-to-edge fashion with a slip angle of 7.82^{o} (Figure 5.28). The two-dimensional network in co-crystal (**18**) is similar to the two-dimensional network observed in co-crystal (**13**). The two-dimensional network extends diagonally in the [010] direction as shown in Figure 5.29.

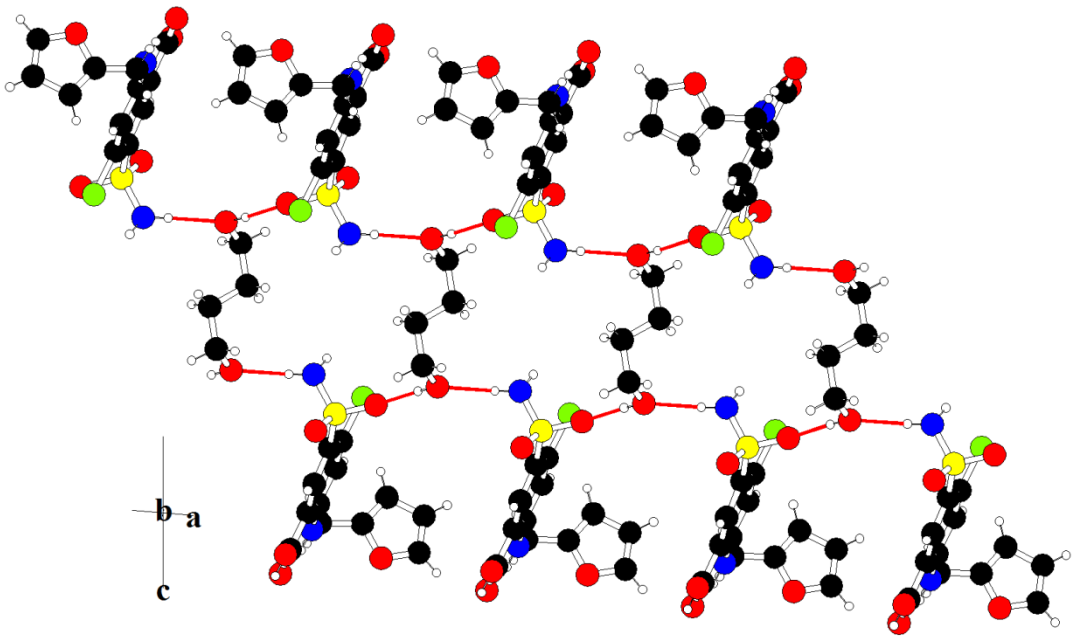

Figure 5.27: Packing arrangement in co-crystal (**18**) along the [010] direction.

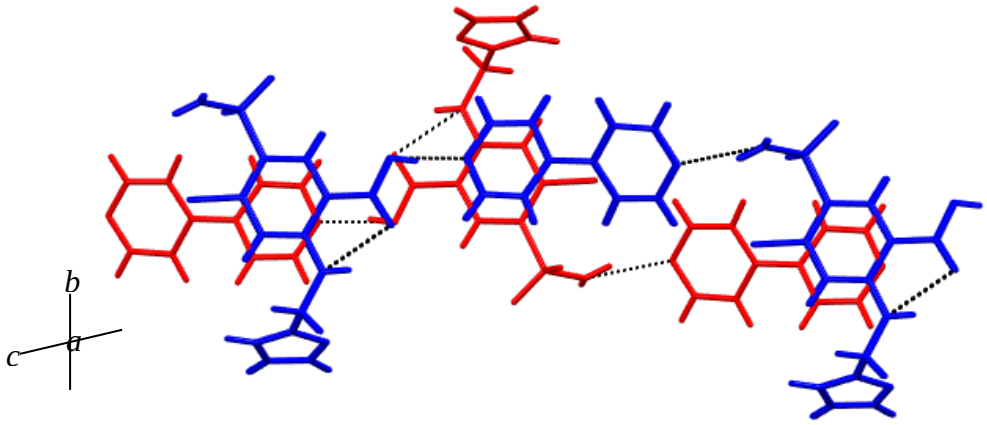

Figure 5.28: π–π interactions between aromatic moieties of furosemide and bipyridyl in co-crystal (**18**).

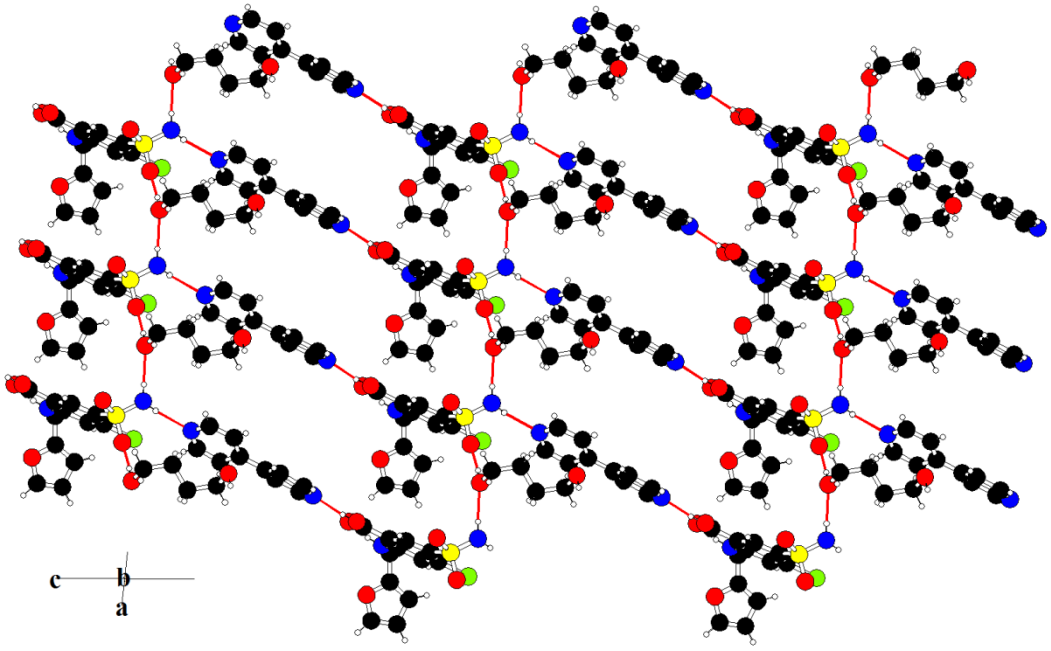

Figure 5.29: two-dimensional pattern in co-crystal (**18**) viewed along the [010] direction.

DTA/TGA of co-crystal (18)

The TGA/ DTA thermogram of co-crystal (**18**) are shown in Figure 5.30. The DTA thermogram indicates a transition at around 100.1^{o}C, with a corresponding weight loss of 8.85% in the TG curve. This corresponds to the loss of half mole of 1,4-butanediol from the crystal lattice. In addition to this the DTA shows transitions at 159.4^{o}C followed by transition corresponding to the melting of the material at 207.2^{o}C which is followed by decomposition of the material.

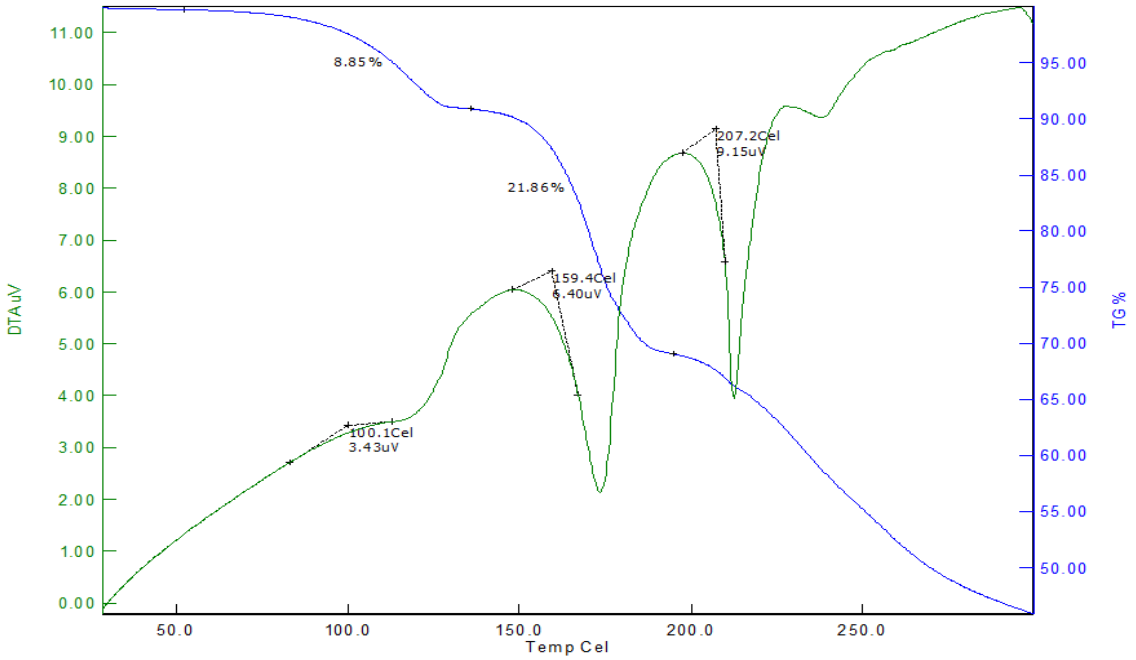

Figure 5.30: DTA/TGA of co-crystal (**18**).

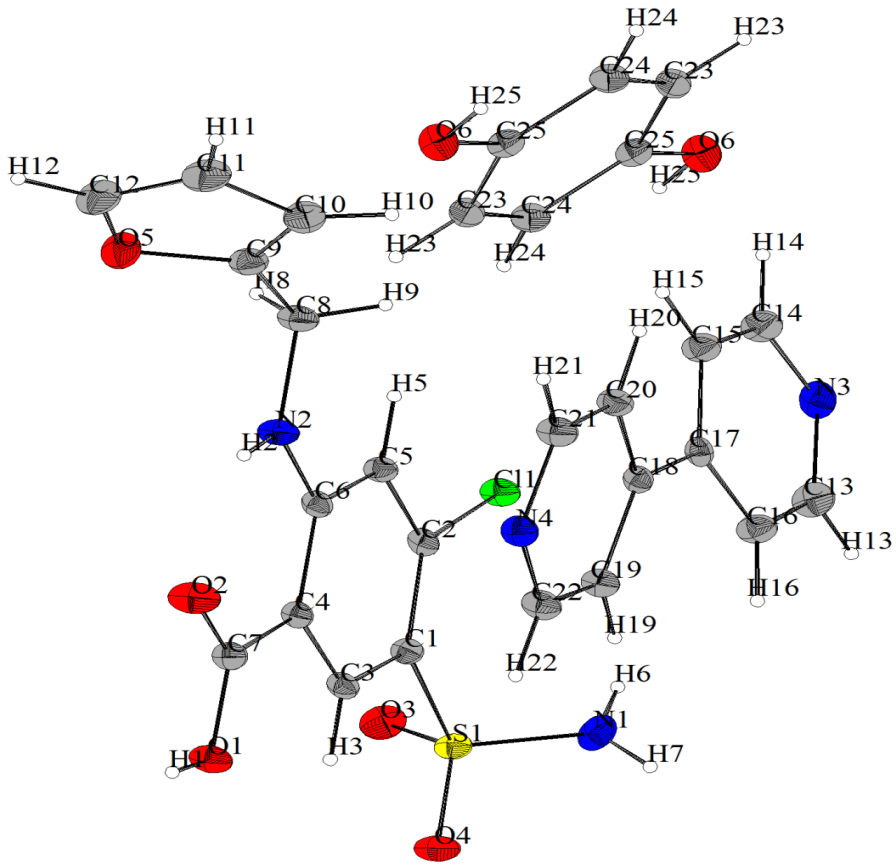

Figure 5.31: ORTEP picture of co-crystal (**19**).

5.6.3. Crystal structure of co-crystal (19) [(furosemide – 4,4'-bipyridyl – hydroquinone (1-1-0.5))]

The ternary co-crystal (**19**) contains one molecule each of furosemide, 4,4'-bipyridyl and half molecules of hydroquinone in the asymmetric unit (Figure 5.31). The three components stabilised through the two–dimensional network (Figure 5.35) and π–π interactions (Figure 5.32) crystallise in $P\bar{1}$ space group (Table 5.4). Analogous to co-crystals (**11**)–(**18**), the bipyridyl molecule links two furosemide molecules through acid–pyridine and pyridine–amine supramolecular synthons (Figure 5.33) to form parallely arranged furosemide – bipyridyl aggregates. These furosemide bipyridyl aggregates are linked through N(1)-H(7)···O(6) and O(6)-H(25)···O(3) hydrogen bonding interactions (Table 5.3) formed by the hydroxyl group of hydroquinone (Figure 5.34). The ternary component, hydroquinone holds an inversion centre thereby allowing the non-covalent interactions to extend on the other end of the molecule (Figure 5.34). The π–π interactions in co-crystal (**19**) are analogous to other ternary co-crystals, arranged in a offset face–to–face / center–to–edge fashion with a slip angle of 12.7 °.

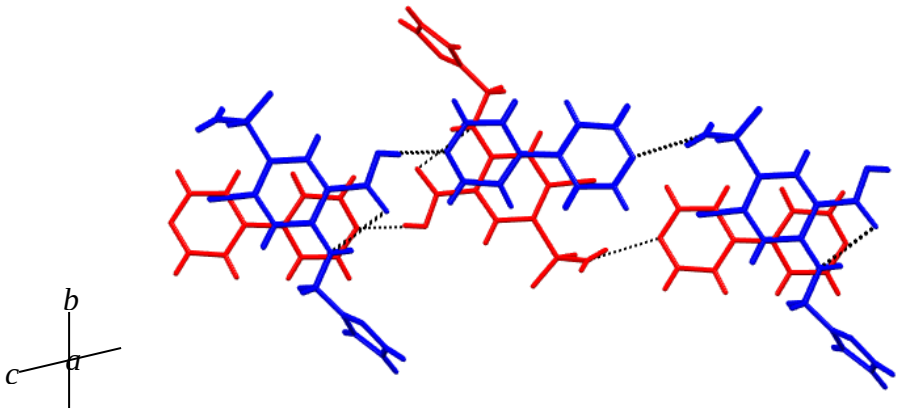

Figure 5.32: π – π interactions in co-crystal (**19**).

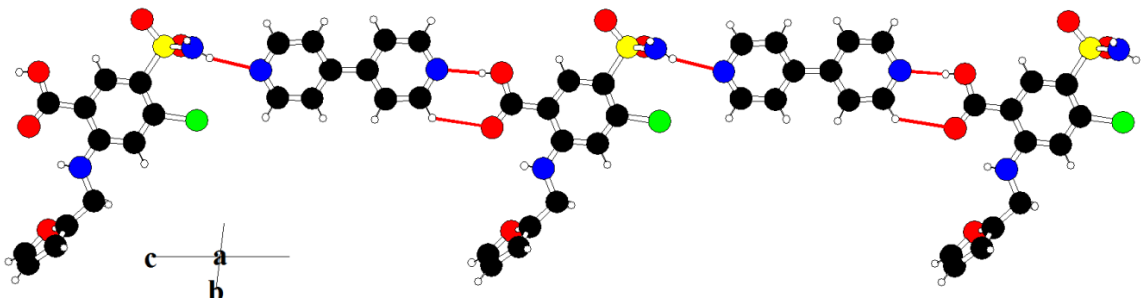

Figure 5.33: Interactions between furosemide and bipyridyl in co-crystal (**19**) viewed along the [100] direction.

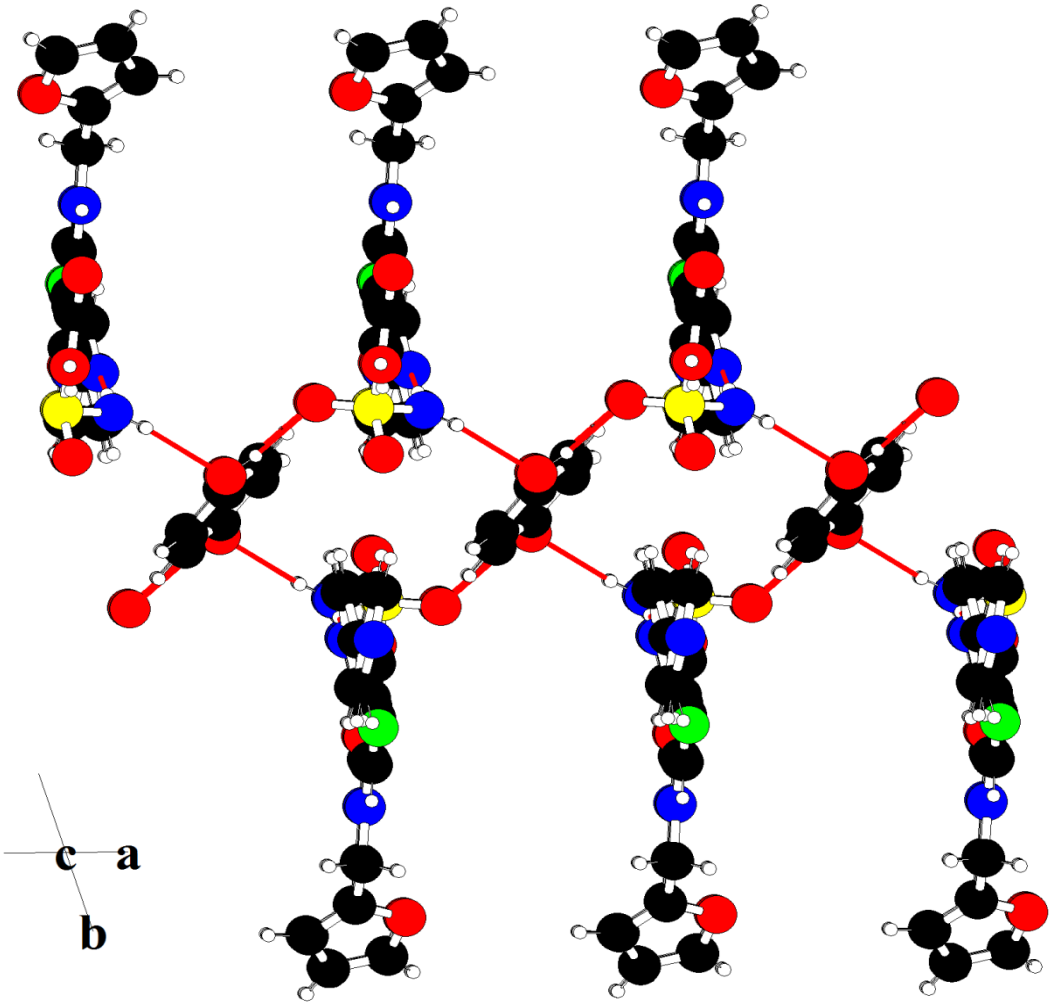

Figure 5.34: Interactions between furosemide and hydroquinone in co-crystal (**19**) viewed along the [001] direction.

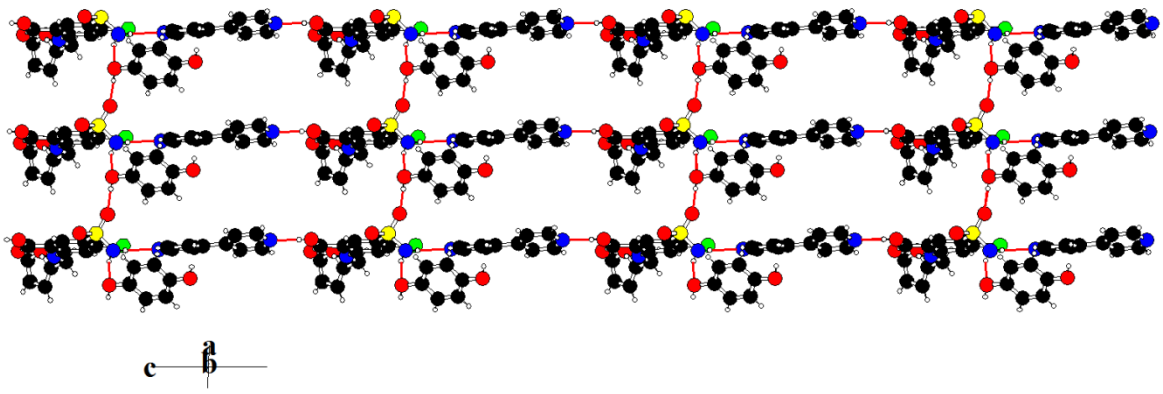

Figure 5.35: Two-dimensional hydrogen-bonded network observed in co-crystal (**19**) viewed along the [010] direction.

DSC of co-crystal (19)

The DSC thermogram of co-crystal (**19**) was performed using 6.152 mg of the sample. The thermogram of (**19**) reveals a sharp endotherm at 210.8 ^{o}C with an onset at 207.4 ^{o}C, which corresponds to the melting of (**19**). The melting temperature of (**19**) is significantly diferent to the melting temperature of the other two components (4,4'-bipyridyl (112-114 ^{o}C); hydroquinone (170-172 ^{o}C)) . The DSC thermogram shows that the melting of (**19**) is followed by decomposition (Figure 5.36).

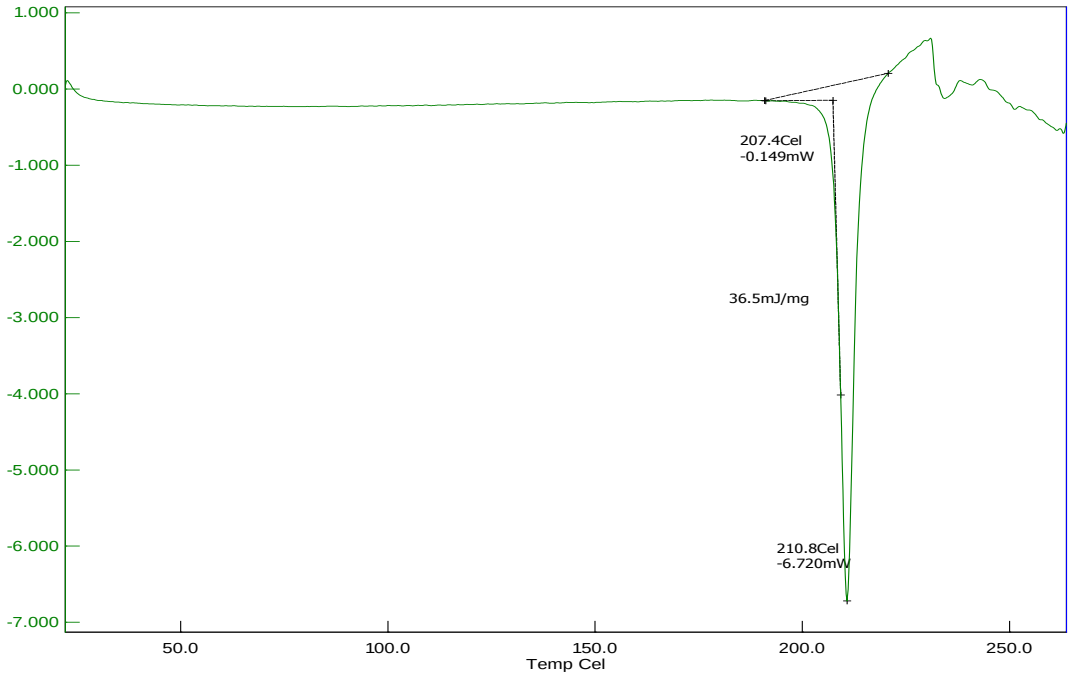

Figure 5.36: DSC of co-crystal (**19**).

Table 5.4: Crystallographic Data of co-crystals (**9**), (**10**) and (**11**)

	(**9**)	(**10**)	(**11**)
Chemical formula	$C_{24}H_{25}Cl_1N_4O_6S_2$	$C_{24}H_{25}Cl_1N_4O_6S_2$	$C_{24}H_{25}Cl_1N_4O_6S_2$
Formula weight	518.0	532.0	542.0
Crystal system	Triclinic	Triclinic	Triclinic
a / Å	6.7510(5)	7.3972(7)	6.9302(4)
b / Å	9.5719(6)	9.3373(8)	9.9356(6)
c / Å	18.6178(13)	18.1141(16)	18.6298(11)

α / °	84.977(4)	80.504(4)	83.633(3)
β / °	89.783(4)	82.039(4)	89.624(3)
γ / °	73.488(4)	75.173(4)	72.794(3)
Space group	$P\bar{1}$	$P\bar{1}$	$P\bar{1}$
V / Å^3	1148.76(14)	1186.81(19)	1217.34(13)
Z	2	2	2
$N_{reflection}$/ $N_{parameter}$	6368/319	7624/325	5405/334
ρ_{calc} / g cm^{-3}	1.497	1.489	1.479
Radiation type	Mo Kα (λ =0.710173 Å)	Mo Kα (λ =0.710173 Å)	Mo Kα (λ =0.710173 Å)
T / K	100	100	100
θ range/°	1 – 34	1 – 37	1 – 29
Range of *h*	-10 – 10	-12 – 12	-9 – 9
Range of *k*	-14 – 14	-15 – 12	-13 – 12
Range of *l*	0 – 29	-30 – 30	-24 – 25
Rmerge	0.0360	0.0399	0.0239
R_1 / %	6.73	3.76	4.36
$_wR_2$ / %	6.40	4.22	3.66
Goodness-of-fit	0.965	1.030	1.098

5.7. Conclusion

In theory an attempted co-crystallisation of molecules containing sulphonamide, carboxylic acid, halogen, furan, pyridine, sulphoxide and hydroxyl functional groups could result in the formation of several products stabilised through a plethora of intermolecular interactions. These functional groups are known to participate in various heteromeric and homomeric interactions. However, in the study presented here it has been shown that the supramolecular reaction between furosemide, 4,4'-bipyridyl and DMSO resulted in the formation of a solid stabilised through an infinitely arranged two-dimensional network as observed in co-crystal (**12**). The space group and the arrangement of the components in co-crystal (**12**) served as a blueprint for the selection and synthesis of co-crystals (**13**)–(**16**). Crystal structure determination of co-crystal (**13**) and powder pattern indexing of co-crystals (**14**)–(**16**)

suggests that the three components in (**14**)–(**16**) are stabilised through an analogous asymmetric two-dimensional hydrogen-bonded network. The discovery of the asymmetric robust-two dimensional network in ternary co-crystals allowed for the prediction of space group symmetry and gross structural features in ternary co-crystals (**17**)–(**19**). Prediction of gross structural features and space group symmetry in (**17**)–(**19**) at this level of accuracy is unprecedented in organic crystal engineering. We have obtained eight new molecular complexes, seven of which involve three components, that are constructed using the identical supramolecular synthons involving (a) acid–pyridine, (b) amine–pyridine, (c) arene–arene, (d) amine–sulphoxide in co-crystal (**12**) while (d) amine – hydroxyl and (e) hydroxyl–sulphoxide in ternary co-crystals (**13**)–(**19**). The supramolecular reaction involving the above supramolecular synthons results in the formation of a high yielding product stabilised through a robust asymmetric two-dimensional hydrogen-bonded network, can be classified as a high-yielding supramolecular reaction.[186] Here, robust is defined as the ability of the asymmetric two-dimensional hydrogen-bonded network to maintain its dimensionality and general structural features when changes occur in the ancillary functional groups. We have shown that the robust two-dimensional network serves as a building block for the synthesis of extended solids (**17**)–(**19**). Extended solids are common in metal-organic frameworks, wherein a polyvalent metal ion acts as an effective multi-dimensional hub, between which organic linkers are connected to form a three dimensional structure. In such solids, the metal-coordination bonds stabilize the crystal structures. While, extended solids formed through metal-organic frameworks are common, there are very few examples of rationally synthesised extended solids stabilised though ionic interactions between organic components. To the best of our knowledge, there are no examples of extended solids in the literature stabilised through neutral hydrogen bonding interactions, especially in cases containing three or more components. While the geometry of all the functional groups are important, the pseudo–tetrahedral shaped sulphonamide group is central to all the ternary co-crystals, the three components hydrogen bond by exploiting the pseudo–tetrahedral geometry of the sulphonamide group, based on this we can also conclude that it is essential for all of the donors of furosemide to participate in hydrogen bonding interactions. The π–π interactions play a significant role in the assembly of the molecules. While in co-crystal (**11**) the bipyridyl molecule crystallises by occupying the inversion centre, in all other ternary co-crystals it acts as a ditopic hydrogen bond acceptor by bridging between the furosemide molecules leading to the formation of the asymmetric two-dimensional network. Finally it can be concluded that solid state architectures formed by neutral hydrogen bonding interactions can be predicted by

crystal engineering methods. Identifying such robust hydrogen bonding networks formed by different combinations of supramolecular synthons is crucial for effective crystal engineering. It has been shown a robust two–dimensional network can serve as a supramolecular module[187] or synthon for directing the assembly of the components in three dimensions. The results presented here show that the synthesis of two–dimensional networks through hydrogen bonding requires the presence of polyvalent functional groups with three or more hydrogen bonding functionalities. The robust two–dimensional hydrogen-bonded networks of the type presented here can be considered to be crucial for nano-structural elements.[188] The results presented here also indicate that physical mixtures of two components can be used for the synthesis of ternary co-crystals.

Chapter 6: Conclusions and Further Work

6.1. Conclusions

In the thesis presented here the co-crystallisation of two APIs, paracetamol and furosemide are discussed. Co-crystals are molecular complexes containing two or more components in the crystal lattice. All the co-crystals presented in the thesis are synthesized by mechanochemical and crystallisation methods. The co-crystals are then analysed by X-ray diffraction to understand the intermolecular interactions. The following conclusion are drawn from the work presented here.

6.1.1. Molecular complexes of paracetamol

In chapter 3 the co-crystals of paracetamol are described. The strongest hydrogen bonding interactions in paracetamol are formed between the phenolic O-H and the amidic oxygen to form O-H···O=C interactions. In co-crystals (**1**)–(**3**), these interactions are replaced by the O-H···N interactions while in co-crystal (**4**) they are replaced by the O-H···O between the PAC and CCF. The interactions observed in (**1**)–(**4**) are in accordance with the empirical rules followed by Etter. The hierarchical arrangement between the best donors to the best acceptors is in agreement with all the previous reported multi-component crystalline forms of paracetamol. In addition to the best donor to best acceptor interactions there are additional hydrogen bonds in each of the molecular complexes. Co-crystal (**2**) has additional N−H···O and O−H···O=C interactions due to the incorporation of solvent molecules in the crystal lattice. In (**3**), there are N−H···N interactions between the API and CCF. In (**4**), the paracetamol molecules are hydrogen bonded to the carbonate anion through O−H···O synthon. The cyclam molecules in (**4**) does not participate in hydrogen bonding interactions with the paracetamol molecules and acts as a spacer between the pair of paracetamol and carboxylate chains.

The results presented in chapter 3 suggest that difunctional CCFs are necessary for co-crystal formation with paracetamol. While CSD analysis suggests that the carboxylic acids and amide groups containing molecules as potential co-crystal formers, the experimental results suggest that these are not effective. The study shows that a balance between the retrosynthetic approach (synthon method) and database guided co-crystal screening of supramolecular synthons provides a useful approach to the targeted co-crystal synthesis.

6.1.2. Molecular complexes of furosemide

Furosemide is a loop diuretic drug, and suffers from both low permeability and solubility. To understand the intermolecular interactions and to rationally predict the crystal packing arrangements a series of molecular complexes of furosemide were synthesized and presented in chapter 4. The study demonstrates that the crystal packing arrangement of the furosemide complexes is dependent on the dominant intermolecular interaction in the complex. The charge assisted hydrogen bonding interaction (Scheme 6.1(a)) is the dominant interaction in the molecular complexes (**5**) to (**9**) and drives the crystal packing arrangement leading to the formation of isostructural host-guest complexes, thereby allowing to rationally predict the crystal packing arrangement of other complexes. However, such persistent crystal packing arrangement was not observed in complex (**10**), where the two components are stabilised through a neutral acid-pyridine supramolecular synthon (Scheme 6.1(b)). The results show that subtle change in the dominant intermolecular interaction can alter the packing arrangement significantly.

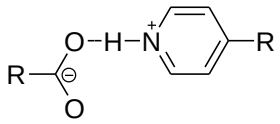

(a) charge assisted O-H---N supramolecular synthon

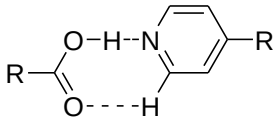

(b) neutral acid-pyridine supramolecular synthon

Scheme 6.1: Supramolecular synthons studied in chapter 4. The dotted lines indicate hydrogen bonding interactions

6.1.3. Proton transfer

The empirical rule for proton transfer based on the pKa values suggests that proton transfer will occur from acid to base when the difference in pKa (ΔpK_a = p*K*a(base) - p*K*a(acid)) is > 3.5. In the six molecular complexes studies in chapter 4, proton transfer was found to occur in complexes (**5**)–(**9**). Based on the results observed in complexes (**8**) and (**9**) it could be predicted that molecular complex (**10**) would be stabilised through charge transfer interaction. However, this was not the case; the two components in (**10**) are held together through neutral acid-pyridine heterosynthon when crystallised under similar solvent and temperature conditions. There is no question that further work is required on this aspect, with a wider range of pH levels and co-molecules, whilst controlling other experimental

conditions. However these limited results add another set of examples that call into question the robustness of the pKa rule.

6.1.4. The asymmetric two-dimensional hydrogen bonded network

In chapter 4, it was shown that the charge assisted hydrogen bonding interaction drives the crystal packing. In chapter 5 the work on predicting the crystal packing arrangement was further extended whilst working with furosemide. In theory an attempted co-crystallization of FUR, BIPY and DMSO could result in the formation of several products stabilised through a plethora of intermolecular interactions. However, the study shows that the supramolecular reaction between furosemide, 4,4'-bipyridyl and DMSO results in the formation of a solid stabilised through an infinitely arranged two-dimensional network as observed in co-crystal (**12**).

The space group and the crystal packing arrangement in co-crystal (**12**) served as a blueprint for the selection and synthesis of other ternary co-crystals (**13**)–(**16**). Crystal structure determination of co-crystal (**13**) and powder pattern indexing of co-crystals (**14**)–(**16**) suggests that the three components in (**14**)–(**16**) are stabilised through an analogous asymmetric two-dimensional hydrogen-bonded network (Scheme 6.2). The discovery of the asymmetric robust-two dimensional network in ternary co-crystals allowed for the prediction of space group symmetry and gross structural features in other ternary co-crystals (**17**)–(**19**). The pseudo-tetrahedral shape of the sulphonamide group and the planarity of the carboxylic acid groups are central to all of the ternary co-crystals presented in chapter 5. The study demonstrates that networks that can maintain their dimensionality and integrity when changes occur in the ancillary functional groups provide a degree of predictability in the crystal packing arrangements in the solid state. Identification of similar robust *n*-dimensional networks may therefore offer a means of improving the effectiveness of crystal engineering. The study also shows that physical mixtures of components can be used for the synthesis of new higher order co-crystals.

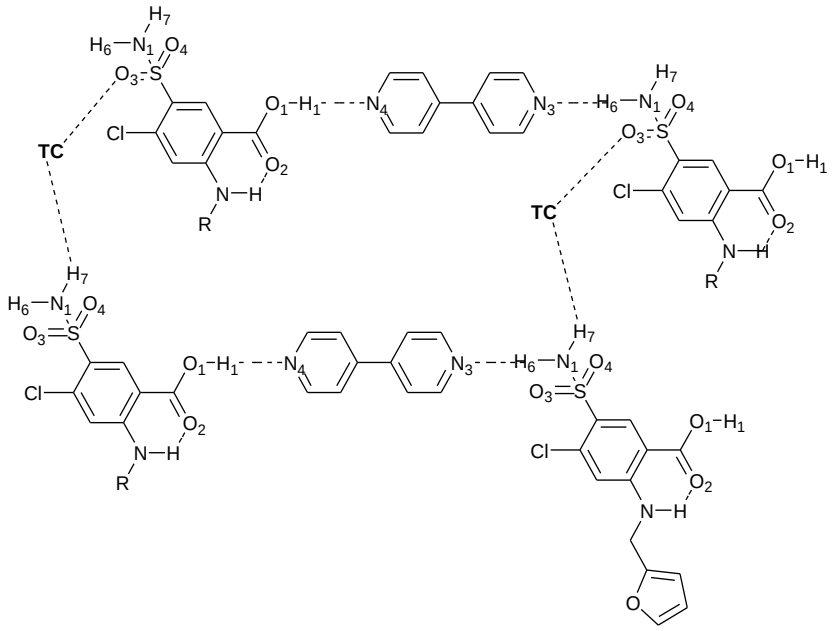

Scheme 6.2: Schematic illustration of the two-dimensional network observed in all ternary co-crystals (**12**)–(**19**). R = furfuryl group, TC = ternary component (DMSO; MeOH; ethanol; 2-propanol; 1-butanol; ethylene glycol; 1,4-butanediol; hydroquinone). The dotted lines indicate hydrogen bonding interactions.

6.2. Further work

The compounds presented in the thesis are fully characterised. However, given further time and extensive investigation, other novel co-crystals of paracetamol or related molecules can be produced by utilizing the robust O-H···N supramolecular synthon identified in Chapter 3. The work on co-crystals of paracetamol can be extended for the synthesis of other ternary co-crystals. The understanding of intermolecular interactions in co-crystal (**2**) serves as a good starting point for this purpose. It can be anticipated that other ternary co-crystals can be synthesised by replacing the methanol in (**2**) with other hydroxyl group containing molecules.

Furosemide is a diuretic drug with low permeability and water solubility, the CCFs used in molecular complexes (**5**) and (**6**) belong to the class of materials categorised as generally recognised as safe (GRAS). The complexes (**5**) and (**6**) can serve as an alternative for oral dosage of furosemide. However, further work is necessary to study the stability, bioavailability and dissolution profiles of these molecular complexes. In addition, the charge assisted hydrogen bonding interaction can be used as a rationale for the synthesis of other molecular complexes whilst using GRAS listed CCFs.

The synthesis of ternary or higher order crystals remains to be a challenge in organic crystal engineering. The robust 2-D network identified in chapter 5 can serve as a rationale for the synthesis of ternary co-crystals in molecules containing similar functional groups.

6.3. Concluding remarks.

The prediction of crystal packing arrangements of a molecular complex from the molecular structure under a defined set of conditions remains a challenge in organic crystal engineering. The work presented here identifies empirical based strategies to predict the crystal packing arrangements in molecular complexes of active pharmaceutical ingredients. One such strategy is based on utilizing the dominant hydrogen bonding interaction in molecular complexes, i.e. the charge-assisted hydrogen bonding interactions. The other is based on identifying robust supramolecular synthons which lead to the formation of extended motifs in molecular complexes. The two strategies were found to be promising to make reasonable predictions on the likely molecular association and packing of molecular complexes in the families of compounds presented here.

[1] (a) G. C. Maitland, M. Rigby, E. B. Smith, W. A. Wakeham, *Intermolecular Forces. Their Origin and Determination*, Clarendon, Press, Oxford, **1981**; (b) J. Israelachvili, *Intermolecular and surface forces*, 2nd ed., Academic Press, Amsterdam, **1992**; (c) A. J. Stone, *The Theory of Intermolecular Forces*, Clarendon Press, Oxford, **1996**.

[2] G. A. Jeffrey, *An Introduction to Hydrogen Bonding*, Oxford University Press, USA, 1st edition, 1997.

[3] P. Gilli, V. Bertolasi, V. Ferretti, G. Gilli, *J. Am. Chem. Soc.* **1994**, 116**,** 909.

[4] A. Werner, *Liebigs Ann. Chem.*, **1902**, 322, 261

[5] A. Hantzsch, *Ber. Dtsch.Chem.Ges.*, **1910**, 43, 3049.

[6] P. Pfeiffer, *Berichte der deutschen chemischen Gesellschaft*, 1914, **47**, 1580.

[7] W. M. Latimer and W. H. Rodebush, *J. Am. Chem. Soc.* **1920**, 42, 1419.

[8] M. L. Huggins, *J. Phys. Chem.* **1922**, 26, 601.

[9] C. C. Andersen, O. Hassel, *Z. Kristallogr.*, **1926**, 123**,** 151.

[10] B. Sterling, Hendricks, *J. Am. Chem. Soc.*, **1928**, 50, 2455.

[11] L. Pauling, *The nature of the Chemical Bond.* Cornell University Press, NY, **1939**.

[12] (a) D. B. Amabilino, J. F. Stoddart, *Chem. Rev.* **1995**, 95, 2725; (b) P. R. Ashton, I. Baxter, M. C. T. Fyfe, F. M. Raymo, N. Spencer, J. F. Stoddart, A. J. P. White, D. J. Williams, *J. Am. Chem. Soc.* **1998**, 120, 2297.

[13] D. J. Sutor, *Nature*, **1962**, 195, 68–9.

[14] P. Metrangolo, G. Resnati, Halogen *bonding - Fundamentals and applications*: Springer, **2007**.

[15] J. D. Dunitz, R. Taylor, *Eur. J. Chem.* **1997**, 3, 89.

[16] G. R. Desiraju, R. Parthasarathy, *J. Am. Chem. Soc.* **1989**, 111, 8725.

[17] V. R. Pedireddi, D. S. Reddy, B. S. Goud, D. C. Craig, A. D. Rae, G. R. Desiraju, *J. Chem. Soc. Perkin Trans.* **1993**, 2, 2353.

[18] T. Bui, S. Dahaoui, C. Lecomte, G. R. Desiraju, E. Espinosa, *Angew. Chem. Int. Ed.*, **2009**, 48, 3838.

[19] B. K. Saha, R. K. R. Jetti, L. S. Reddy, S. Aitipamula, A. Nangia, *Cryst. Growth Des.* **2005**, **5**, 887.

[20] F. Ponzini, R. Zagha, K. Hardcastle, J. S. Siegel, *Angew. Chem. Int. Ed.*, **2000**, 13, 2323.

[21] C. A. Hunter, J. K. M. Sanders, *J. Am. Chem. Soc.* **1990,** 112 (14), 5525.

[22] (a) M. O. Sinnokrot, C. D. Sherrill, *J. Phys. Chem. A*, **2003**, 107, 8377; (b) M. O. Sinnokrot, C. D. Sherrill, *J. Phys. Chem. A*, **2004**, 108, 10200.

[23] E. G. Hohenstein, J. Duan, C. D. Sherrill, *J. Am. Chem. Soc.*, **2011**, 133, 13244.

[24] (a) H. Mansikkamki, M. Nissinen, K. Rissanen, *Angew. Chem. Int. Ed.*, **2004**, 43, 1243.; (b) S. E. Snyder, P. I. Volkers, D. A. Engebretson, W. Lee, W. H. Pirkle, J. R. Carey, *Org. Lett.* **2007**, 9, 2341; (c) N. F. She, M. Gao, X. G. Meng, G. F. Yang, J. A. A.W. Elemans, A. X. Wu, L. Isaacs, *J. Am. Chem. Soc.* **2009**, 131, 11695.

[25] E. J. Corey, *Pure Appl. Chem.* **1967**, 14, 19.

[26] (a) G. R. Desiraju, *Crystal Engineering. The Design of Organic Solids,* Elsevier, Amsterdam, **1989;** (b) G. R. Desiraju, *Angew. Chem.. Int. Ed. Engl.*, **1995**, 34, 2311.; (c) G. R. Desiraju, *Angew. Chem. Int. Ed.*, **2007**, 46, 8342.

[27] (a) M. C. Etter. *Acc. Chem. res.* **1990**, 23,120.; (b) M. C. Etter, J. C. MacDonald, J. Bernstein, *Acta Crystallogr. Sect. B*, **1990**, 46, 256.; (c) M. C. Etter, *J. Phys. Chem.* **1991**, 95, 4601.; (d) J. Berstein, R. E. Davis, L. Shimoni, N. Chang, *Angew. Chem. Int. Ed. Engl.* **1995**, 34, 1555.

[28] G. R. Desiraju, *Crystal Engineering: The Design of Organic Solids*; Elsevier: New York, **1989**.

[29] R. Pepinsky, *Phys. Rev.*,**1955**, 100, 971.

[30] G. M. J. Schmidt, *Pure Appl. Chem*, **1971**, 27, 647.

[31] Thomas, J. M. *Phil. Trans. R. Soc. Lond. A*, **1974**, 277, 251.

[32] J.-M. Lehn, *Angew. Chem. Int. Ed.* **1988**, 27, 89.

[33] J. D. Dunitz, *Pure Appl. Chem*, 63, **1991**, 177.

[34] J. S. Moor, S. Lee, *Chem. Ind.* **1994**, 556.

[35] (a) C. B. Aakeroy, A. M. Beatty, *Aust. J. Chem.* 2001, **54,** 409.; (b) M. W. Hosseini, *CrystEngComm.* **2004**, 6, 318.; (c) L. MacGillivray, *CrystEngComm.* 2004, **6,** 77.; (d) L. Brammer, *Chem. Soc. Rev.* **2004**, 33, 476.; (e) M.W. Hosseini, *CrystEngComm*. 2004, **6**, 318.; (f) L. R. MacGillivray, *CrystEngComm.* **2004**, 6, 77.; (g) L. Brammer, *Chem. Soc. Rev.* **2004**, 33, 476.; (h) D. L. Caulder, K. N. Raymond, *Acc. Chem. Res.* **1999**, 32, 975.; (i) D. N. Reinhoudt, M. Crego-Calama, *Science*, **2002**, 295, 2403.; (j) J.-M. Lehn, *Science* **2002**, 295, 2400.

[36] D. Wiechert, D. Mootz, T. Dahlems, *J. Am. Chem. Soc*., **1997**, 119, 12665.

[37] C. B. Aakeroy, A. M. Beatty, B. A. Helfrich, *J. Am. Chem. Soc.* **2002**, 124, 14425.

[38] C. B. Aakeroy, A. M. Beatty, B. A. Helfrich, *Angew. Chem. Int. Ed.* **2001**, 40**,** 3240.

[39] (a) M.C. Etter, G. M. Frankenbach, *Chem. Mater.*, **1989**, 1, 10. (b) M. C. Etter, *Acc. Chem. Res.*, **1990**, 23**,**120.

[40] R. Melendez, A. D. Hamilton, *Top. Curr. Chem.*, **1998**, 198, 97.

[41] T. W. Panunto, Z. Urbanczyk-Lipkowska, R. Johnson, M. C. Etter, *J. Am. Chem. Soc.* **1987**, *109*, 7786.

[42] M. W. Hosseini, R. Ruppert, P. Schaeffer, A. De Cian, J. Fischer, *J. Chem. Soc., Chem. Commun.* **1994**, 2135.

[43] (a) J. M. Lehn, M. Mascal, A. DeCian, J. Fischer, J. *J. Chem. Soc., Perkin Trans.* **1992**, *2*461.; (b) J. M. Lehn, M. Mascal, A. DeCian, J. J. Fisher, *J. Chem. Soc., Chem. Commun.* **1990**, 479.

[44] D. J. Duchamp, R. E. Marsh, *Acta Crystallogr.*, **1969**, B25, 5.

[45] S. V. Kolotuchin, E. E. Fenlon, S. R. Wilson, C. J. Loweth, S. C. Zimmerman, S. C. *Angew. Chem., Int. Ed. Engl.* **1995**, 34, 2654.

[46] S. V. Kolotuchin, P. A. Thiessen, E. E. Fenlon, S. R. Wilson, C. J. Loweth, S. C. Zimmerman, *Chem. Eur. J.* **1999**, 5, 2537.

[47] B. Gong, C. Zheng, E. Skrzypczak-Jankun, Y. Yan, J. Zhang *J. Am. Chem. Soc.* **1998**, 120, 11194.

[48] O. Ermer, *J. Am. Chem. Soc.* **1988**, 110, 3747.

[49] O. Ermer, *Angew. Chem., Int. Ed. Engl.* **1988**, 27, 829.

[50] M. J. Zaworotko, *Chem. Soc. Rev.*, **1994**,23, 283.

[51] O. Ermer, A. Eling, *J. Chem. Soc., Perkin Trans.* **1994**, 2, 925.

[52] J. W. Steed and J. L. Atwood, Supramolecular Chemistry, 2nd Edition, Wiley publication, **2009**, page 3.

[53] L. C. Fetterly, ‘‘*Organic adducts’’, in Non-Stoichiometric Compounds*, edited by L. Mandelcorn, pp. 491–567, Academic Press, New York etc, **1964**.

[54] H. M. Powell, *‘‘Clathrates’’, in Non-Stoichiometric Compounds*, edited by L. Mandelcorn, pp. 438–490, Academic Press, New York, **1964**.

[55] (a) A. E. Smith, *J. Chem. Phys.*, **1950**, 18, 150. (b) A. E. Smith, *Acta Cryst.*, **1952**, 5, 224.

[56] H. U. Lenne, H. C. Mez, W. Schlenk, *Chem. Ber.*, **1968**, 101, 2435.

[57] H. U. Lenne, H. C. Mez, W. Schlenk, *Liebigs Ann. Chem.*, **1970**, 732, 70.

[58] H. U. Lenne, *Acta Cryst.*, **1954**, **7**, 1.

[59] H. Bekkum, J. D. Remijnse, B. M. Wepster, *J. Chem. Soc. Chem. Comm.*, **1967**, 67.

[60] (a) W. Schlenk, *Ann.*,**1951**, 573, 142.; (b) W. Schlenk, *Liebigs Ann. Chem.*, **1949**, 565, 204.

[61] M. Simard, D. Su, J. D. Wuest, *J. Am. Chem. Soc.* **1991**, 113, 4696.

[62] (a) R. Bishop, *Synlett*, **1999**, 1351.; (b) A. T. Ung, R. Bishop, D. C. Craig, I. G. Dance, M. L. Scudder, *J. Chem. Soc., Perkin Trans.* **1992**, 2, 861.

[63] (a) M. Valık, B. Dolensky, H. Petrıckova, V. Kral, *Chem. Commun.* **2002**, 67**,** 609.; (b) C. Pardo, E. Sesmilo, E. Gutierrez-Puebla, A. Monge, J. Elguero, A. Fruchier, *J. Org. Chem.* **2001**, 66, 1607.; (b) J. Kagan, S. Y. Chen, D. A. Agdeppa, W. H. Watson, V. Zabel, *Tetrahedron Lett.* **1977**, 51, 4469.; (c) J. D. Field, P. Turner, M. M. Harding, T. Hatzikominos, L. Kim, *New J. Chem.* **2002**, 26, 720.; (d) M. C. Kimber, A. C. Try, L. Painter, M. M. Harding, P. Turner, *J. Org. Chem.* **2000**, 65, 3042.; (e) A. C. Try, L. Painter, M. M. Harding, *Tetrahedron Lett*, **1998**, 39, 9809.; (f) X. Shi, B. Miller, *J. Org. Chem.* **1995**, 60, 5714.

[64] F. Tomislav, A. V. Trask, W. Jones, W. D. S. Motherwell, *Angew. Chem. Int. Ed.*, **2006**, 45, 7546.

[65] D. E. Palin, H. M. Powell, *J. Chem. Soc.*,**1948**, 815.

[66] J. S. Buck, W. S. Ide. *J. Am. Chem. Soc.*, **1931**, 53**,** 2784.

[67] J. S. Anderson, *Nature*, **1937**, 140, 583.

[68] S. A. Remyga, R. M. Myasnikova, A. I. Kitaigorodski, *Zh. Strukt. Khim.*, **1969**, 10, 1131.

[69] J. N. Van Niekerk, D. H. Saunder, *Acta Crystallogr*, **1948**, 1, 44.

[70] B. Hall, J. P. Devlin. *J Phys Chem.*, **1948**, 71, 465.

[71] F. Wohler, *Annalen*, **1884**, 51, 153.

[72] A. R. Ling, J. L. Baker, *J. Chem. Soc.*, **1893**, 63, 1314.

[73] A. Bond, *Cryst. Eng. Comm.*, **2007**, 9, 833.

[74] C. B. Aakeroy, D. J. Salamon, *Cryst. Eng. Comm.*, **2005**, 7, 439.

[75] B. R. Bhogala, A. Nangia, *New J. Chem.*, **2008**, 32, 800.

[76] G. P. Stahly, *Cryst. Growth Des.*, **2007**, 7, 1007.

[77] S. L. Childs, K. I. Hardcastle, *Cryst. Growth Des.*, **2007**, **7**, 1291.

[78] W. Jones, W. Motherwell, W. D. Trask, *A. V. MRS Bull*, **2006**, 341, 875.

[79] P. Vishweshwar, J. A. McMohan, M. J. Zaworotko, *J. Pharm. Sci.*, **2006**, 95, 499.

[80] (a) I. D. H. Oswald, D. R. Allan, P. A. McGregor, W. D. S. Motherwell, S. Parsons, C. R. Pulham, *Acta Crystallogr., Sect. B*, **2002**, 58, 1057.; (b) O. Almarsson, M. J. Zaworotko, *Chem. Commun.* **2004**, 188, 1889.; (c) B. Rodriguez-Spong, C. P. Price, A. Jayasankar, A. J.

Matzger, N. Rodrıguez-Hornedo, *Adv. Drug Delivery Rev.* **2004**, 56, 241.; (d) N. Blagden, M. Matas, P. T. Gavan, P. York, *Adv. Drug. Delivery Rev.* **2007**, 59, 617.

[81] (a) C. B. Aakeroy, D. J. Salmon, *CrystEngComm*, **2005**, 7, 439.; (b) G. R. Desiraju, *Angew. Chem., Int. Ed. Engl.* **1995**, 34, 2311. (b) T. Steiner, *Angew. Chem., Int. Ed.* **2002**, 41, 48.; (c) C. B. Aakeroy, N. Schultheiss, Assembly of Molecular Solids via Non-covalent Interactions, In *Making Crystals by Design-from Molecules to Molecular Materials, Methods, Techniques, Applications*; F. Grepioni, D. Braga, Eds.; Wiley-VCH: Weinheim, Germany, **2007**.; (d) T. R. Shattock, K. K. Arora, P. Vishweshwar, M. J. Zaworotko, *Cryst. Growth Des.* **2009**, 8, 4533.

[82] (a) G. Kartum, W. Vogel, K. Andrussov, *Dissociation Constants of Organic Acids in Aqueous Solution*; Butterworth & Co. Publishers: London, **1961**.; (b) C. B. Aakeroy, J. Desper, J. F. Urbina, *Chem. Commun.* **2005**, 2820.; (c) S. L. Childs, G. P. Stahly, A. Park, *Mol. Pharmaceutics*, **2007**, 4, 323.

[83] N. Issa, P G. Karamertzanis, G. W. A. Welch, S. L. Price, *Cryst. Growth Des*, 2009, ***9***, 442.

[84] B. Rodriguez-Spong, P. Zocharski, **2003**, AAPS J. **5**: Abstract M1298.

[85] A. Trask, W. Jones, "*Crystal engineering of organic cocrystals by the solid state grinding approach*." *Top. Curr. Chem.*, **1967**, 254, 41.

[86] Z. Wang, J. Chen, T. Lu, *Cryst. Growth Des.*, **2012**, 12**,** 4562.

[87] A. V. Katdare, J. F. Bavitz, *Drug Dev. Ind. Pharm.* **1984**, 10, 789.

[88] (a) A. V. Katdare, J. A. Ryan, J. F. Bavitz, D. M. Erb, J. K. Guillory, *Mikrochim. Acta (Wien)*, **1986**, 3, 1. (b) T. Hu, S. Wang, T. Chen, S. Lin, *J. Pharm. Sci.*, **2002**, 91, 1351.; (c) S. Basavoju, D. Bostrom, S. Velaga, *AAPS Annual Meeting and Exposition*, San Antonio, TX, USA, **2006**. (d) W. Chongcharoen, S. R. Byrn, N. Sutanthavibul, *J. Pharm. Sci.* **2008**, 97**,** 473.; (e) S. Roy, N. R. Goud, N. J. Babu, J. Iqbal, A. K. Kruthiventi, A. Nangia, *Crystal Growth & Design*, **2008**, 8, 12.

[89] Y. Matsuda, R. Akazawa, *Journal of Pharmacy and Pharmacology*, 1994, 46, 162.

[90] B. Rodriguez-Spong, **2005**, *Enhancing the Pharmaceutical Behavior of Poorly Soluble Drugs Through the Formation of Cocrystals and Mesophases*, Ph.D. Thesis, University of Michigan.

[91]J. F. Remenar, S. L. Morissette, *J. Am. Chem. Soc.*, **1984**, 125**,** 8456.

[92] D. P. McNamara, S. L. Childs, J. Giordano, A. Iarriccio, J. Cassidy, M. S. Shet, R. Mannion, E. Donnell, A. Park, *Pharm. Res.*, **2006**, 23, 1888.

[93] A. Bak, A. Gore, E. Yanez, M. Stanton, S. Tufekcic, R. Syed, A. Akrami, M. Rose, S. Surapaneni, T. Bostick, A. King, S. Neervannan, D. Ostovic, A. Koparkar, *J. Pharm. Sci.,* **2008**, 97, 3942.

[94] P. Sanphui, S. Sudalai Kumar, A. Nangia, *Cryst. Growth Des.* **2012**, 12, 4588.

[95] N. J. Babu, A. Nangia, *Cryst. Growth Des.* **2011**, 11, 2662.

[96] B. C. Hancock, S. L. Shamblin, G. Zografi, *Pharm. Res.* **1995**, 12, 799.

[97] (a) P. H. Stahl, C. G. Wermuth, *Handbook of Pharmaceutical Salts: Properties, Selection and Use*; Helvetica Chimica Acta: Zurich, **2002**.; (b) C. H. Gu, D. J. W. Grant, *Handbook of Experimental Pharmacology: Stereochemical Aspects of Drug Action and Disposition*; Eichelbaum, M.; Testa, B.; Somogyi, A. Eds.; Springer: Berlin, **2003**.

[98] J. Galcera, E. Molins, *Cryst. Growth Des.*, **2009**, 9, 327.

[99] B. Y. Shekunov, P. York, *J. Cryst. Growth*, **2000**, 211, 122.

[100] S. R. Vippagunta, H. G. Brittain, D. J. W. Grant, *Adv. Drug Delivery Rev.* **2001**, 48, 3.

[101] J. Haleblian, W. C. McCrone, *J. Pharm. Sci.* **1969**, 58, 911.

[102] A. P. Simonelli, S. C. Mehta, W. I. Higuchi, *J. Pharm. Sci.*, **1970**, 59, 633.

[103] W. C. Mc. Crone, In Physics and Chemistry of the Organic Solid State; Fox, D.; Labes, M. M.; Weissberger, A., Eds.; Wiley Interscience: New York, **1965**, 2, 725.

[104] S. Khoshkhoo, J. Anwar, *J. Phys. D: Appl. Phys.*, **1993**, 26, 90.

[105] (a) N. Kaneniwa, M. Otsuka, T. Hayashi, *Chem. Pharm. Bull.*, **1985**, 33, 3447-3455 (b) N. Kaneniwa, J. Ichikawa, T. Matsumoto, *Chem. Pharm. Bull.*, **1988**, 36, 1063.

[106] Letter from Abbott Laboratories to healthcare providers. http://www.fda.gov/medwatch/safety/1998/norvir.htm

[107] B. Y. Shekunov, P. York, *J. Cryst. Growth*, **2000**, 211, 122.

[108] S. C. Stinson, Chiral Drugs. *Chem. Eng. News,* **1993**, 71, 38

[109] S. R. Byrn, *J. Pharm. Sci.*, **1976**, 65, 1.

[110] (a) P. Vishweshwar, J. A. McMahon, M. Oliveira, M. L. Peterson, M. J. Zaworotko, *J. Am. Chem. Soc.* **2005**, 127**,** 16802.; (b) X. Cui, A. L. Rohl, A. Shtukenberg, B. Kahr, *J. Am. Chem. Soc.* **2013**, 135**,** 3395.

[111] N. Rodriguez-Hornedo, D. Murphy, *J. Pharm. Sci.*, **1999**, 88, 651.

[112] M. C. Etter, *J. Phys Chem*. **1991**, 95, 4601.

[113] M. C. Etter, S. M. Reutzel, C. G. Choo, *J. Am. Chem. Soc.* **1993**, 115, 4411. (b) W. H. Ojala, M. C. Etter, *J. Am. Chem. Soc.* **1992,** 114, 10228.

[114] R. P. Rastogi and N. B. Singh, *Journal of physical chemistry*, **1966,** *70*, 3315, *(b)* R. P. Rastogi and N. B. Singh, *The Journal of Physical Chemistry*, ***1968***, 79, 4446, *(c)* R. P. Rastogi and B. L. Dubey, *J. Am. Chem. Soc*., **1967,** 200, 2465.

[115](a) F. Tomislav, *chem. Soc. Rev.*, **2012**, 41, 3493–3510 (b) M. D. Eddleston, M. Arhangelskis, F. Tomislav and W. Jones, *Chem. Commun.*, **2012,** 48, 11340–11342.

[116] DIFFRAC.SUITE EVA phase analysis software, BRUKER XRD Software, Version 2, 2013, BRUKER AXS.

[117] *TOPAS version 3*, Bruker-AXS Inc. Madison, Wisconsin, USA (**1999**).

[118] Laue, M., Friedrich, W. and Knipping, P, *Bavarian Academy of Sciences*, **1912**.

119 Bragg, W.H., *Nature*, **1912**, 90, 219. (b) Bragg, W.L. *Proceedings of the Cambridge Philosophical Society*, **1913**, 17, 43-57.

[120] A. L. Patterson, *Z. Krist.*, **1935**, A90 . 517.

[121] A. L. Patterson, *Phys. Rev.*, **1934**, 46 , 372.

[122] A. L. Patterson, *Acta Cryst.* , **1949**, 2, 339

[123] D. Harker, and J. S. Kasper. *Acta Cryst.*, **1948**, 1, 70.

[124] D. Harker, and J. S. Kasper., *J. Chem. Phys*., **1947**, 15 , 882.

[125] H. Hauptman, J. Karle, *Solution of the phase problem. I. The Centrosymmetric Crystal*. American Crystallograohic Association Moonograph No. 3: New York (**1953**).

[126] J. Karle, *International Tables of Crystallography*, Volume-IV, **1974**, 339-358.

[127] . D. Sayre, *Acta Cryst.*, **1952**, 5, 68.

[128] J. P. Glusker, M. Lewis, M. Rossi, *Crystal structure analysis for chemists and biologists*, WILEY-VCH, August 1994.

[129] *APEX-2 software*, Version 1.27; Bruker AXS Inc.: Madison, Wisconsin, USA, **2005**. (33)

[130] SADABS: *Area-Detector Absorption Correction; Siemens Industrial Automation*, Inc.: Madison, WI, **1996**.

[131] G. M. Sheldrick, *Acta Crystallogr., Sect. A*, **2008**, 64, 112.

[132] P. W. Betteridge, J. R. Carruthers, R. I. Cooper, K. Prout, D. J. Watkin, *J. Appl. Crystallogr.* **2003**, 36, 1487.

[133] F. H. Allen, *Acta Cryst., B*, **2002**, 58, 380–388.

[134] (a) RCSB Protein Data Bank: http://www.rcsb.org/pdb; (b) Inorganic Crystal Structure Database: http://www.fiz-karlsruhe.de/icsd.html; (c) Nucleic Acid Database: http://www.ndbserver.rutgers.edu; (d) Crystallography Open Database: http://www.crystallography.net.

[135] CSD-Version5.33 (November2011)+2updates. This version is used in the database search.

[136] I. J. Bruno, J. C. Cole, P. R. Edgington, M. Kessler, C. F. McCrae, P. McCabe, J. Pearson and R. Taylor, New software for searching the Cambridge Structural Database and visualising crystal structures, *Acta Cryst. B*, **2002**, B58, 389–397.

[137] (a) Garekani, H.A., Ford, J.L., Rubinstein, M.H., Rajabi-Siahboomi, A.R., *Int. J. Pharm.* **1999**, *187*, 77–89. (b) Nichols, G.; Frampton, C. S. *J. Pharm. Sci.* **1998**, *87* (6), 684-693. (c) DiMartino, P.; Guyot-Hermann, A. M.; Conflant, P.; Drache, M.; Guyot, J. C. *Int. J. Pharm.* **1996**, *128* (1-2), 1-8.

[138] (a) L. H. Thomas, C. Wales, L. Zhao, C. C. Wilson, *Cryst. Growth Des*. **2011**, *11*, 1450–1452. (b) Al-Zoubi, N.; Malamataris, S. *Int. J. Pharm.* **2003**, *260* (1), 123-135. (c) Al-Zoubi, N.; Kachrimanis, K.; Malamataris, S. *Eur. J. Pharm. Sci.* **2002**, *17* (1-2), 13-21.

[139] Nichols, G.; Frampton, C. S. *J. Pharm. Sci*. **1998**, *87*, 684–693.

[140] Haisa, M., Kashino, S., Maeda, H.,. *Acta Crystallogr. B*30, **1974**, 2510–2512.

[141] Al-Zoubi, N., Kachrimanis, K., Malamataris, S., *Euro. J. Pharm. Sci.* **2002a** 17, 13–21. (b) Al-Zoubi, N., Malamataris, S., *Int. J. Pharm.* **2003.** 260, 123–135. (c) Mikhailenko, M., *J. Cryst. Growth*. **2004.** 265, 616–618.

[142] L. H. Thomas, C. Wales, L. Zhao, and C. C. Wilson, *Cryst. Growth Des.* **2011**, 11, 1450–1452.

[143] Burger, A., *Acta Pharm. Technol.* **1982.** 28, 1–20.

[144] Perrin, M-A; Neumann, M. A.; Elmaleh, H.; Zaska, L. *Chem. Commun.* **2009,** 3181.

[145] (a) Oswald, I. D. H.; Allan, D. R.; McGregor, P. A.; Motherwell, W. D. S; Parsons, S.; Pulham, C. R.. *Acta Crystallogr. Sect. B* **2002,** 58, 1057. (b) André, V.; Piedade, M. F. M; da; Duarte, M. T.. *CrystEngComm* **2012**, 14, 5005. (c) Vrcelj, R. M.; Clark, N. I. B.; Kennedy, A. R.; Sheen, D. B.; Shepherd, E. E. A.; Sherwood, J. N. *J. Pharm. Sci.* **2003**, 92, 2069. (d) Oswald, I. D. H.; Motherwell, W. D. S; Parsons, S.; Pulham, C. R. *Acta Crystallogr. Sect. E* **2002**, 58, O1290.; (e) Oswald, I. D. H..; Pulham, C. R. *CrystEngComm*, **2008**, 10, 1114.
(e) Childs, S. L.; Stahly, G. P.; Park, A. *Mol. Pharmaceutics* **2007**, 4, 323.

[146] Karki, S.; Friscic, T.; Fabian, L.; Laity, P. R.; Day, G. M; Jones, W. *Adv. Mater*. **2009**, 21, 3905.

[147] Vania Andre, M. Teresa Duarte, *CrystEngComm*, **2012**, 14, 5005.

[148] NIST Standard Reference Database 35, NIST/EPA Gas-Phase Infrared Database; National Institute of Standards and Technology: Gaithersburg, MD.

[149] Etter, M. C. *Acc. Chem. Res*. **1990**, 23, 120.

[150] Gilli, G.; Gilli, P. *The Nature of the Hydrogen Bond Outline of a Comprehensive Hydrogen Bond Theory*; Oxford University Press: Oxford, **2009**.

[151] Reed, A. E.; Curtiss, L. A.; Weinhold, F. *Chem. Rev.* **1988**, 88, 899.

[152] Karki, S.; Friscic, T.; Fabian, L.; Laity, P. R.; Day, G. M; Jones, W. *Adv. Mater.* **2009**, 21, 3905.

[153] L. C. Fetterly, *Organic adducts in Non-Stoichiometric Compounds*, edited by L. Mandelcorn, Academic Press, New York, **1964**.

[154] H. M. Powell, *Clathrates in Non-Stoichiometric Compounds*, edited by L. Mandelcorn, Academic Press, New York, **1964**.

[155] D. E. Palin, H. M. Powell, *J. Chem. Soc.*,**1948**, 815.

[156] IUPAC. Compendium of Chemical Terminology, 2nd ed. (the "Gold Book"). Compiled by A. D. McNaught and A. Wilkinson. Blackwell Scientific Publications, Oxford (**1997**)

[157] Granero, G. E.; Longhi, M. R.; Mora, M. J.; Junginger, H. E.; Midha, K. K.; Shah, V. P.; Stavchansky, S.; Dressman, J. B.; Barends, D. M. *J. Pharm. Sci.* **2010**, 99 (6), 2544.

[158] Lindenberg, M.; Kopp, S.; Dressman, J. B. *Eur. J. Pharm. Biopharm.* **2004**, 58 (2), 265.

[159] (a) Ambrogi, V.; Perioli, L.; Pagano, C.; Latterini, L.; Marmottini, F.; Ricci, M.; Rossi, C. *Microporous Mesoporous Mater*. **2012**, 147 (1), 343. (b) Ambrogi, V.; Perioli, L.; Pagano, C.; Marmottini, F.; Ricci, M.; Sagnella, A.; Rossi, C. *Eur. J. Pharm. Sci*. **2012**, 46 (1−2), 43. (c) Zvonar, A.; Berginc, K.; Kristl, A.; Gasperlin, M. *Int. J. Pharm*. **2010**, 388 (1−2), 151.

[160] Goud, N. R.; Gangavaram, S.; Suresh, K.; Pal, S.; Manjunatha, S. G.; Nambiar, S.; Nangia, A. *J. Pharm. Sci*. **2012**, 101 (2), 664.

[161] (a) Corradini, P. *Chem. Ind.* **1973**, 55, 122. (b) Bernstein, J. Conformational Polymorphism. In Organic Solid State Chemistry; Desiraju, G. R., Ed.; Elsevier: Amsterdam, **1987**, pp. 471-518.

[162] Lamotte, J.; Campsteyn, H.; Dupont, L.; Vermeire, M. *Acta Crystallogr. B*, **1978**, 34, 1657−1661.

[163] Babu, N. J.; Cherukuvada, S.; Thakuria, R.; Nangia, A. *Cryst. Growth Des.* **2010**, 10 (4), 1979−1989.

[164] Matsuda, Y.; Tatsumi, E. *Int. J. Pharm.* **1990,** 60, 11 −26.

[165] Ge, M.; Liu, G.; Ma, S.; Wang, W. Bull. *Korean Chem. Soc.* **2009**, 30 (10), 2265 .

[166] Ambrogi, V.; Perioli, L.; Pagano, C.; Latterini, L.; Marmottini, F.; Ricci, M.; Rossi, C. *Microporous Mesoporous Mater*. **2012**, 147 (1), 343.

[167] Johnson, S. L.; Rumon, K. A. *J. Phys. Chem.* **1965**, 69, 74.

[168] The SPARC program (http://archemcalc.com/sparc) uses computational algorithms based on fundamental chemical structure theory to estimate a variety of reactivity parameters. For some examples of the use of the SPARC program for pKa calculations, see (a) Hilal, S. H.; Karickhoff, S. W.; Carreira, L. A. *Quant. Struct. Act. Rel*. **1995**, 14, 348. (b) Hilal, S. H.; Carreira, L. A.; Baughman, G. L.; Karickhoff, S. W.; Melton, C. M. *J. Phys. Org. Chem.* **1994**, 7, 122.

169. (a)G. R. Desiraju, *Crystal Engineering: The Design of Organic Solids*, Elsevier, Amsterdam, **1989**; (b) P. Ball, *Nature*, **1996**, 381, 648; (c) A. Gavezzotti, *Acc. Chem. Res*, **1994**, 27, 309; (d) G. R. Desiraju, *Science*, **1997**, 278, 404.

170. (a) J. Maddox, *Nature*, **1988**, 201, 335;

171. S. L. Price, Adv. Drug Delivery Rev, **2004**, 56, 301.

172. (a) J. D. Dunitz, *Pure Appl. Chem.* **1991**, 63, 177. (b) G. R. Desiraju, *Perspectives in Supramolecular Chemistry, The Crystal as a Supermolecular Entity*, Vol. 2, Wiley, Chichester, **1996**.

173. Zaworotko, M. J. *Chem. Soc. Rev.* **1994**, 283.

174. Dunitz, J. D.; Bernstein, J. *Acc. Chem. Res.* **1995**, 28, 193.

175. (a) J. A. Bis, M. J. Zaworotko, *Crystal Growth & Design,* Vol. 5, No. 3, 1169-1179*;* (b) K. Paisner, L. N. Zakharov, K. M. Doxsee, Crystal Growth & Design, Vol. 10, No. 8, 3757 – 3762; (c) S. Palacin, D. N. Chin, E. E. Simanek, J. C. MacDonald, G. M. Whitesides, M. T. McBride, G. T. R. Palmore, *J. Am. Chem. Soc.* **1997,** 119, 11807-11816. (d) Mujeeb Khan, Volker Enkelmann, and Gunther Brunklaus, *Crystal Growth & Design*, **2009**, 9, 2354 – 2362; (e) D. Cincic, T. Friscic, W. Jones, *Chem. Mater.* **2008,** 20, 6623–6626; (f) S. V. Lindeman, J. Hecht, J. K. Kochi, *J. Am. Chem. Soc.* **2003**, 125, 11597-11606; (g) J. Zheng, P. E. Constantinou, C. Micheel, A. P. Alivisatos, R. A. Kiehl, N. C. Seeman, Nano Lett., **2006,** 6, 1502-1504; (h) S. R. Perumalla, E. Suresh, V. R. Pedireddi, Angew. Chem. Int. Ed. **2005**, 44, 7752 –7757;

176. (a) V. A. Russell, C. C. Evans, W. Li, M. D. Ward, *Science* **1997,** 276, 575; (b) K. T. Holman, A. M. Pivovar, M. D. Ward, *Science* **2001,** 294, 1907.

177. (a) J. D. Dunitz, A. Gavezzotti, Angew. Chem. Int. Ed. **2005**, 44, 1766 – 1787. (b) M. Nomura, V. A. Erdmann, Nature **1970**, 228.

178. a) F. Tomislav, A. V. Trask, W. Jones, W. D. S. Motherwell, *Angew. Chem. Int. Ed.*, **2006**, 45, 7546; (b) C. B. Aakeröy, A. M. Beatty, B. A. Helfrich, *Angew. Chem. Int. Ed.*, **2001**, 40, 3240; (c) B. R. Bhogala, S. Basavoju, A. Nangia, *CrystEngComm*, **2005**, **7**, 551; (d)

K. Sada, K. Inoue, T. Tanaka, A. Epergyes, A. Tanaka, N. Tohnai, A. Matsumoto, M. Miyata, *Angew. Chem. Int. Ed.*, **2005**, 44, 7059; (f) J. Adisoejoso, K. Tahara, S. Okuhata, S. Lei, Y. Tobe, S. D. Feyter. *Angew. Chem. Int. Ed.*, **2009**, 48, 7353. (g) R. Natarajan, G. Magro, L. N. Bridgland, A. Sirikulkajorn, S. Narayanan, L. E. Ryan, M. F. Haddow, A. G. Orpen, J. P. H. Charmant, A. J. Hudson, A. P. Davis, *Angew. Chem. Int. Ed.* **2011**, 50, 11386 –11390.

179. B. Gong, C. Zheng, E. Skrzypczak-Jankun, Y. Yan, and J. Zhang, *J. Am. Chem. Soc.* **1998,** 120, 11194-11195.

180. (a) B. R. Bhogala, P. Vishweshwar, A. Nangia, *Cryst. Growth Des.* **2002**, 2, 325; (b) B. R. Bhogala, S. Basavoju, A. Nangia, *Cryst. Growth Des.* **2005**, 5, 1683; (c) N. Shan, A. D. Bond, W. Jones, *New J. Chem.* **2003**, 27, 365; (d) R. D. B. Walsh, M. W. Bradner, S. Fleischman, L. A. Morales, B. Moulton, N. Rodrıguez-Hornedo, M. J. Zaworotko, *Chem.Commun.* **2003**, 186; (e) B. R. Bhogala, A. Nangia, *Cryst. Growth Des.* **2003**, *3*, 547; (f) O. Almarsson, M. J. Zaworotko, *Chem. Commun.* **2004**, 1889; (g) C. B. Aakeroy, D. J. Salmon, *CrystEngComm* **2005**, 7, 439; (h) C. V. K. Sharma, G. A. Broker, G. J. Szulczewski, R. D. Rogers, *Chem. Commun.* **2000**, 1023; (i) M. Tomura, Y. Yamashita, *Chem. Lett.* **2001**, 532; (j) N. Shan, E. Batchelor, W. Jones, *Tetrahedron Lett.* **2002**, 43, 8721; (k) B. Olenik, T. Smolka, R. Boese, R. Sustmann, *Cryst.Growth Des.* **2003**, 3, 183; (l) A. D. Bond, *Chem. Commun.* **2003**, 250; (m) S. Varughese, V. R. Pedireddi, *Chem. Eur. J.* **2006**, *12*, 1597; (n) M. Du, Z. H. Zhang, X. J. Zhao, H. Cai, *Cryst. Growth Des.* **2006**, 6, 114; (o) C. M. Grossel, A. N. Dwyer, M. B. Hursthouse, J. B. Orton, *CrystEngComm* **2006**, 8, 123; (p) B. R. Bhogala, A. Nangia, *New J. Chem.* **2008**, *32*, 800; (q) R. Santra, N. Ghosh, K. Biradha, *New J. Chem.* **2008**, 32, 1673;

181. (a) M. C. Etter, G. M. Frankenbach, *Chem. Mater.* **1989**, 1, 10; (b) M. C. Etter, *Acc. Chem. Res.* **1990**, 23, 120.

182. (a) C. Dai, P. Nguyen, T. B. Marder, A. J. Scott, W. Clegg, C. Viney, *Chem. Commun.*, **1999**, 2493; (b) F. Ponzini, R. Zagha, K. Hardcastle, J. S. Siegel, *Angew. Chem. Int. Ed.*, **2000**, 39, 13; (c) B. Sarma, L. S. Reddy, A. Nangia, *Crystal Growth & Design,* **2006**, 8, 12; (d) M. Gdaniec, W. Jankowski, M. J. Milewska, T. Połonski, *Angew. Chem. Int. Ed.* **2003**, 42, 3903 –3906;

183. L. M. Salonen, M. Ellermann, F. Diederich, *Angew. Chem. Int. Ed.* **2011**, 50, 4808.

184. L. J. Prins, D. N. Reinhoudt, P. Timmerman, Angew. Chem. Int. Ed. **2001**, 40, 2382 – 2426.

185. Reference for TOPAS

186. C. B. Aakeroy, A. M. Beatty, B. A. Helfrich, *J. Am. Chem. Soc.* **2002**, 124, 14425-14432

187. V. A. Russell and M. D. Ward, *Chem. Mater.* **1996**, 8, 1654.

188. V. A. Russell, M. D. Ward, *Chem. Mater.* **1996,** 8, 1654-1666.